2018-04-10

Targeting Drug Resistance In HCV NS3/4A Protease: Mechanisms And Inhibitor Design Strategies

Ashley N. Matthew
University of Massachusetts Medical School

TARGETING DRUG RESISTANCE IN HCV NS3/4A PROTEASE: MECHANISMS AND INHIBITOR DESIGN STRATEGIES

A Dissertation Presented

By

ASHLEY NICOLE MATTHEW

Submitted to the Faculty of the
University of Massachusetts Graduate School of Biomedical Sciences, Worcester
in partial fulfillment of the requirements for the degree of

DOCTOR OF PHILOSOPHY

APRIL 10th, 2018

MD/PHD PROGRAM

TARGETING DRUG RESISTANCE IN HCV NS3/4A PROTEASE:
MECHANISMS AND INHIBITOR DESIGN STRATEGIES

A Dissertation Presented By

ASHLEY NICOLE MATTHEW

This work was undertaken in the Graduate School of Biomedical Sciences

MD/PHD PROGRAM

The signatures of the Dissertation Defense Committee signify completion and approval as to style and content of the Dissertation

_____
Celia A. Schiffer, Ph.D., Thesis Advisor

_____
Paul Thompson, Ph.D., Member of Committee

_____
William Royer, Ph.D., Member of Committee

_____
Kendall Knight, Ph.D., Member of Committee

_____
Stefan Sarafianos, Ph.D., Member of Committee

The signature of the Chair of the Committee signifies that the written dissertation meets the requirements of the Dissertation Committee

_____
Daniel Bolon, Ph.D, Chair of Committee

The signature of the Dean of the Graduate School of Biomedical Sciences signifies that the student has met all graduation requirements of the School.

_____
Kendall Knight, Ph.D.
Dean of the Graduate School of Biomedical Sciences

APRIL 10th, 2018

TABLE OF CONTENTS

Page #

ABSTRACT

The Hepatitis C virus (HCV) NS3/4A protease inhibitors (PIs) have become a mainstay of newer all-oral combination therapies. Despite improvements in potency of this inhibitor class, drug resistance remains a problem with the rapid emergence of resistance-associated substitutions (RASs). In this thesis I elucidate the molecular mechanisms of drug resistance for PIs against a resistant variant and apply insights toward the design of inhibitors with improved resistance profiles using structural, biochemical and computational techniques. Newer generation PIs retain high potency against most single substitutions in the protease active site by stacking on the catalytic triad. I investigated the molecular mechanisms of resistance against the Y56H/D168A variant. My analysis revealed that the Y56H substitution disrupts these inhibitors' favorable stacking interactions with the catalytic residue His57.

To further address the impact of drug resistance, I designed new inhibitors that minimize contact with known drug resistance residues that are unessential in substrate recognition. The initially designed inhibitors exhibited flatter resistance profiles than the newer generation PIs but lost potency against the D168A variant. Finally, I designed inhibitors to extend into the substrate envelope (SE) and successfully regained potency against RAS variants maintaining a flat profile. These inhibitors both pack well in the enzyme and fit within the SE. Together these studies elucidate the molecular mechanisms of PI resistance and highlight the importance of substrate recognition in inhibitor design. The insights from this thesis provide strategies toward the development of diverse NS3/4A PIs that may one day lead to the eradication of HCV.

DEDICATION

“For he will command his angels concerning you
to guard you in all your ways.”

Psalms 91:11

In loving memory

of my dear cousin

Trenaya L. Johnson

and my beautiful baby

brother, Kearns Louis-Jean

May you both continue

to serve as my guardian angels.

I love you both

and miss you dearly.

Rest in Peace.

“Hey, Black Child”

Hey Black Child
Do you know who you are
Who you really are
Do you know you can be
What you want to be
If you try to be
What you can be

Hey Black Child
Do you know where you are going
Where you're really going
Do you know you can learn
What you want to learn
If you try to learn
What you can learn

Hey Black Child
Do you know you are strong
I mean really strong
Do you know you can do
What you want to do
If you try to do
What you can do

Hey Black Child
Be what you can be
Learn what you must learn
Do what you can do
And tomorrow your nation
Will be what you want it to be

By: Countee Cullen

To my fellow minorities and other marginalized groups, please know that you can and shall succeed! My hope is this work serves as an affirmation and confirmation that you all can have the highest aspirations and success in all facets of life.

ACKNOWLEDGEMENTS

“Do not be anxious about anything, but in everything by prayer and supplication with thanksgiving let your requests be made known to God.”

Philippians 4:6

First and foremost, all glory and honor be unto God. For without Him, none of this would be possible. Graduate school is an arduous process and requires much emotional, mental and spiritual support. I have many people that I owe my sincerest gratitude to, because it takes a village to successfully complete a Doctorate of Philosophy degree. While I may not list all of you here, please know that to anyone who had a hand in my success, I thank you for your support, kindness and generosity you have shown me over the years.

I am forever grateful to my mentor Dr. Celia Schiffer. Thank you for taking a chance and allowing me to join your lab without any hesitation. Your constant support, guidance, kindness, mentorship and love are only a tiny part of the recipe that makes you one of the best mentors at UMMS and beyond. I wish everyone could experience the joys of having you as a mentor and true friend. I know that I am fortunate and will never forget all that you have done for me. Thank you to my little sister Naomi Schiffer for your love and support. I would like to thank Dr. Nese Kurt Yilmaz for always believing in me and providing experimental and writing support. You have truly showed me how to be a great scientist and for that I am forever grateful. To Ellen Nalivaika, I am so grateful for the emotional support you provided and our friendship that has blossomed over

the years. Through all of trials and tribulations I have faced, you were always there for me even when I needed a shoulder to cry on. For that, I thank you. My sincerest thanks to Dr. Akbar Ali. Thank you for pushing me to be the scientist I am. It was a pleasure to work with you and I'm grateful for the wonderful scientific endeavors we embarked on together.

Thank you to my Qualifying Exam Committee (QEC), Thesis Research Advisory Committee (TRAC) and Dissertation Exam Committee (DEC) members: Dr. Daniel Bolon, Dr. Paul Thompson, Dr. William Royer, Dr. Kendall Knight, Dr. David Lambright, and Dr. Stefan Sarafianos. I appreciate the generous amount of time that you put into helping me accomplish my thesis goals. I am grateful for your scientific and emotional support that you have given me over the years. You all helped me evolve into a scientist and I now feel confident that I can tackle my future scientific endeavors.

I am truly grateful for all of the members of my lab past and present. Shurong Hou, Gordon Lockbaum, Florian Leidner, Anne Jecrois, Jacqueto Zephyr, Mina Henes, Klajdi Kosovrasti, Dr. Tania Silvas, Dr. Linah Rusere, and Dr. Jennifer Timm, I will miss seeing your faces every day. There was never a dull moment with any of you and you made life in lab a lot easier. Please know that I believe that you all are amazing scientists, and are going to do wonderful things in the future. To our joint laboratory family, Dr. Brian Kelch, Janelle Hayes, Nick Stone, Dr. Christl Gaubitz, Brendan Page, Dr. Caroline Duffy, Dr. Brendan Hilbert, and

Dr. William Royer, thank you for all of your scientific input. Your help was invaluable and I enjoyed our weekly joint lab meetings.

I am thankful to many members in the UMMS community. I thank the entire Biochemistry and Molecular Pharmacology department: faculty, students, admins and staff. I truly believe that we have the best department on campus. Many of you made my days a lot brighter and enjoyable. Dr. Kendall Knight, thank you for having an open door policy with me. Your mentorship and friendship mean so much to me. To the staff in the GSBS office, Anne Michelson, Annette Stratton, Barbara Bucciaglia, and Mindy Donovan, thank you for always welcoming me when I'd stop by numerous times. Thank you for always being my cheerleaders. Dr. Mary Ellen Lane, thank you for always being there for me when I have needed you. You are an asset to UMMS and I am so happy that you are the new Dean of GSBS. To my UMASS friends/family (in no particular order): Dr. Waldo Zamor, Dr. Milka Koupenova-Zamor, Dr. Josiah Bote, Dr. Kevin Abraham, Dr. Elizabeth Ojukwu, Dr. Racquel Wells, Dr. Lauren Powell (Dr. Boo), Dr. Rand Nashi, Dr. Khanh Pham, Dr. Jose Mercado-Matos, Oghomwen Igiesuorobo, Paul Charles, Dr. Aneth Laban, Pamela Cote, Ms. Linhelle Charles, Robert Layne and MD/PhD cohort. You all mean the world to me and I'm so happy that I chose to come to UMASS. You all have touched my life in some way and I thank you all for the tremendous support that you have provided and the lifetime of friendship that I have gained!

To my best friend in graduate school, Ciearra Smith, I want you to know how proud of you I am. You are a great scientist and awesome friend. I thank you and Joshua Stacker for always being there for me. I know you meet friends in graduate school, but I'm also happy that I have gained a new sister. My sincerest thank you to my undergraduate best friends, Tatiana Zague and Dr. Ganiat Animashawun. Thank you for late night calls, constant support and staying the course with me. To my boyfriend Gerald "JG" Smith, thank you for your friendship and support. I am so grateful for you and love you dearly.

I must take a moment to acknowledge and thank my wonderful family. The MD/PhD takes many years and you have always been so patient with me. Mommy (Lena Matthew), Daddy (Edward Matthew), Alan Washington, Deniece Bushell, Edward Matthew, Trenez Johnson (my boo boo), Victor Bushell, Ylva Almgren, Dr. Babafemi Onabanjo, Washington and Matthew extended families, I thank you all for your prayers, motivation, inspiration and unwavering support. I love you all so very much. Last but far from least, I thank my bestest friend, my twin sister Asia Matthew-Onabanjo. You have been a blessing to me since I was born. I am so proud of the woman you are becoming. Even in the face of adversity, you always rise to the occasion. You are the reason I always give my very best, and I aspire to be like you. I cannot wait to see all the amazing things you do in this lifetime. Stay the course boo boo, you got this!

LIST OF TABLES

Page #

LIST OF FIGURES AND SCHEMES

Page #

LIST OF THIRD PARTY COPYRIGHTED MATERIAL

Figure 1.1: Adapted from Nature Reviews Microbiology, volume 5, issue 6, pages 453–463. Darius Moradpour, François Penin and Charles M. Rice. Replication of hepatitis c virus. Copyright 2007, with permission from Nature Publishing Group (License Number: 4306041070299).

List of Symbols, Abbreviation or Nomenclature

Å	Angstrom
ADME	Absorption, Distribution, Metabolism, Excretion
AU	Asymmetric Unit
CD81	Tetraspanin
CDI	Carbonyldiimidazole
Cryo-EM	Cryoelectron Microscopy
DAA	Direct–Acting Antiviral
DBI	Dibromoisocyanuric Acid
DBU	1,8-Diazabicyclo[5.4.0]undec-7-ene
DCE	Dichloroethane
DIEA	N,N-Diisopropylethylamine
DMAP	4-Dimethylaminopyridine
DMF	Dimethylformamide
DOE	Department of Energy
DTT	Dithiothreitol
EC50	Half Maximal Effective Concentration
ESI	Electrospray Ionization
EtOAC	Ethyl Acetate
Fab	Fragment Antibody
FC	Fold Change
FDA	Food and Drug Administration
ΔG	Change in Gibbs Free Energy
GT	Genotype
GZR	Grazoprevir
h	Hour
HATU	(1-[Bis(dimethylamino)methylene]-1H-1,2,3-triazolo[4,5-b]pyridinium 3-oxid hexafluorophosphate)
HCC	Hepatocellular Carcinoma
HCV	Hepatitis C virus
HIV	Human Immunodeficiency Virus
HPLC	High-Performance Liquid Chromatography
HRMS	High Resolution Mass Spectrometry
IFE	Inner Filter Effect
IPTG	Isopropyl β-D-1-thiogalactopyranoside
K	Kelvin
Ki	Inhibition Constant

LDAO	Lauryldimethylamine Oxide
m/z	Mass to Charge Ratio
MAV	Mitochondrial Antiviral-Signaling Protein
MD	Molecular Dynamics
MWCO	Molecular Weight Cut Off
NMP	N-Methyl-2-pyrrolidone
NMR	Nuclear Magnetic Resonance
OD600	Optical Density (measured at a wavelength of 600 nm)
PDB	Protein Data Bank
PEG-IFN	Pegylated Interferon
PI	Protease Inhibitor
RAS	Resistance Associated Substitution
RAV	Resistance Associated Variant
RB	Resuspension Buffer
RBV	Ribavirin
RCM	Ring Closing Metathesis
RdRp	RNA Dependent RNA Polymerase
RMSD	Root Mean Square Deviation
RT	Room Temperature
SAR	Structure Activity Relationship
SBDD	Structure–Based Drug Design
SE	Substrate Envelope
SOC	Standard of Care
SR-B1	Scavenger Receptor Class B Type 1
SVR	Sustained Virological Rate
TB	Terrific Broth
THF	Tetrahydrofuran
TLC	Thin Layer Chromatography
TRIF	TIR-domain-containing adapter-inducing interferon-β
UV	Ultraviolet
vdW	van der Waals
Vo	Initial Velocity
WNV	West Nile Virus
WT	Wildtype

Chapter I

Introduction

1.1 Hepatitis C Virus Epidemiology

Hepatitis C virus (HCV) is a global epidemic estimated to chronically infect over 71 million people worldwide.[1] HCV is the leading cause of chronic liver disease, which often progresses to cirrhosis or becomes malignantly transformed to hepatocellular carcinoma (HCC).[1] This virus has been termed “the silent killer” as a majority of patients are often asymptomatic and their infection goes decades without detection.[2] In fact, over 80% of infected patients will develop chronic liver disease.[3] HCV was primarily transmitted through contact with blood products.[4] However, injection drug use has become the principal form of transmission with the incidence of intravenous drug injection on a steep rise.[5]

Patients infected with HCV have a heterogeneous population of viral species known as quasispecies due to low fidelity of the RNA-dependent RNA polymerase. In addition to quasispecies contributing to the viral genetic diversity, HCV can also be classified into seven known genotypes (GT1-7) and multiple subtypes (a, b, c etc.).[6-8] Genotypes differ at the nucleotide level by greater than 30% and subtypes differ by 20-25%.[9] GT1 and GT3 are the most prevalent accounting for 46% and 30% of global infections, respectively.[6,7] GT1 infections predominately occur in North America and Europe while GT3 infections are common in South-East Asia. Other genotypes, though less common, also have distinct global distributions. GT2 viruses predominate in sub-Saharan Africa while GT4 viruses account for infections in the Middle East, Egypt and Central Africa. GT5 viruses are endemic to South Africa, GT6 in Asia and GT7 in Central

Africa.[10] Thus, the genetic and global diversity of HCV infection has presented a challenge toward the treatment of patients infected with HCV.

1.2 Hepatitis C Viral Proteins and Life Cycle

HCV is a hepacivirus of the Flaviviridae family with an enveloped positive single-stranded RNA genome that is approximately 9.6-kb in size. The genome is composed of an open reading frame that encodes a long polyprotein precursor consisting of ~3000 amino acids.[11] The 5' untranslated region of the HCV genome contains an internal ribosome entry site that provides access to the host replication machinery for viral protein synthesis.[12,13] The polyprotein precursor is cleaved by cellular and viral proteases into structural (Core, E1, E2), p7 and non-structural (NS2, NS3, NS4A, NS4B, NS5A, NS5B) proteins (**Figure 1.1**). These viral proteins are necessary for viral processes including entry, uncoating, translation, replication, viral assembly and release.

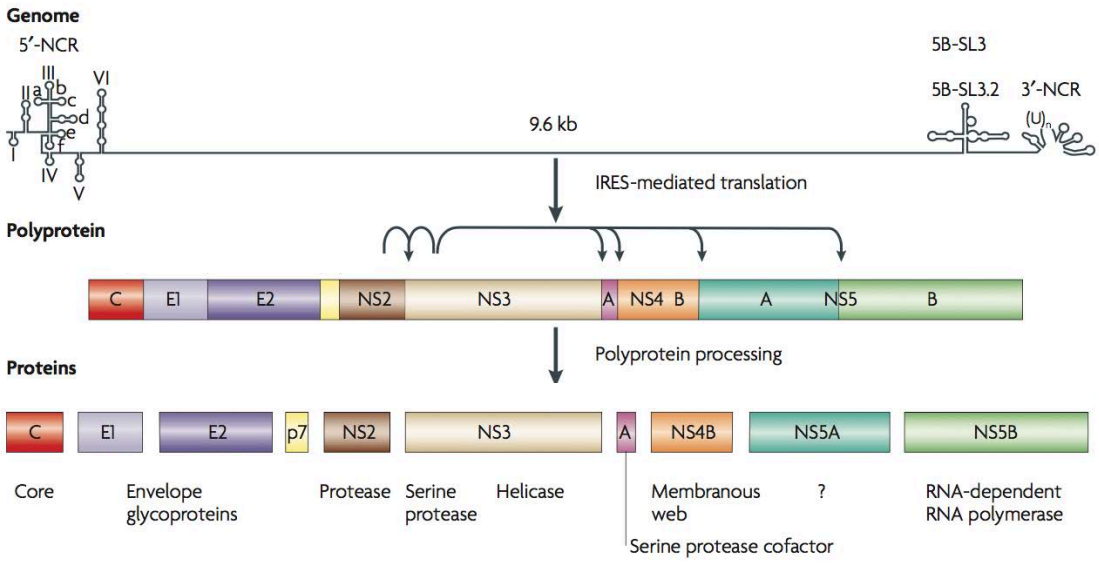

Figure 1.1: HCV genome and processing of the polyprotein.
The HCV genome is 9.6 kb in length and consists of a 5' IRES and 3' UTR. The positive stranded RNA genome is translated into a long polyprotein that is cleaved by host and viral proteases into structural and functional components. Arrows above the polyprotein indicate cleavage by the NS2 and NS3/4A proteases. The structural proteins include the core, envelope and P7 proteins. NS3, NS4A, NS4B, NS5A and NS5B represent the functional proteins that perform integral steps in the viral lifecycle that are necessary for replication and viral maturation.[14]

The core protein is an RNA binding protein that forms the viral nucleocapsid.[15] E1 and E2 are envelope glycoproteins that are responsible for viral entry into the hepatocyte. The elusive P7 protein is a 63 amino acid viroporin that forms a membrane ion channel implicated in viral particle formation and release.[16] The non-structural proteins form the viral replication machinery. They also help assemble and release the virus for subsequent rounds of infection. NS2 is a cysteine protease responsible for cleaving the NS2/NS3 junction. Though less understood, NS2 has also been implicated in viral assembly and release.[11] NS3 is a multifunctional protein with both a protease and helicase domain that facilitates polyprotein cleavage, ATP-dependent RNA unwinding, and evasion of host innate immune function. NS4A is a small cofactor that contributes one beta strand to the N-terminal NS3 protease domain localizing and stabilizing NS3 to the ER membrane and enhancing proteolytic activity.[11] NS4B serves as a membrane anchor through formation of the membranous web, which is a scaffold for the replication complex.[11] The RNA binding protein, NS5A is a phosphoprotein that is responsible for viral assembly. NS5B is the RNA-dependent RNA polymerase (RdRp) which replicates the HCV genome.[11]

In the HCV viral lifecycle, circulating viral particles enter hepatocytes through interactions of envelope proteins E1 and E2 with cell surface receptors including Tetraspanin (CD81), and Scavenger receptor class B type I (SR-B1).[17] Other factors also mediate fusion including LDL receptor, claudin-1 and occludin.[14,18]

Once a successful fusion event occurs, HCV enters the hepatocyte via clatherin-mediated endocytosis and the RNA genome is released into the cytoplasm due to pH dependent membrane fusion.[19] Host cell replication machinery then translates the positive sense RNA into the long polyprotein precursor. Cellular proteases and viral proteases NS2 and NS3/4A proteolytically cleave the polyprotein into functional components.[20] Once translation of the essential proteins is complete, the viral replication complex forms consisting of viral proteins, cellular machinery and nascent RNA strands.[14] Replication occurs in a two-step process: (1) Positive sense RNA template is used to synthesize negative sense RNA. (2) Negative sense RNA then serves as template for the production of positive-sense RNA that is used for RNA replication, translated into protein or packaged into new viral particles.[21] Finally, the viral genome will be packaged into viral particles forming mature virions, which will be trafficked through the secretory pathway and released for subsequent rounds of infection.[14] These steps are crucial to HCV pathogenesis and pharmaceutical companies have developed inhibitors that target essential proteins in the viral life cycle.

1.3 Direct-Acting Antivirals against Hepatitis C Virus

In the last 5-7 years the advent of direct–acting antivirals (DAAs) against HCV proteins NS3/4A, NS5A and NS5B has remarkably improved therapeutic options and treatment outcomes for HCV-infected patients.[22,23] Prior to their development, the standard of care (SOC) for HCV treatment was a combination

of peg-interferon α (Peg-IFN) and ribavirin (RBV). Interferons are a class of cytokines that are secreted by the host innate immune system in response to viral infection.[24] Ribavirin, a purine analogue, though the mechanism of action is not well understood, is believed to promote hypermutation of the RNA genome and inhibit nucleoside biosynthesis as well as other processes that are necessary for viral replication.[25] The Peg-IFN/RBV combination therapy only resulted in a sustained virological response (SVR: the standard indication of cure from infection), of less than 50% in GT1 and slightly higher in other genotypes.[26] Peg-IFN had to be administered via intravenous injection once a week over the course of up to 72 weeks. In addition to poor efficacy, treatment with Peg-IFN caused severe side effects resulting in low tolerability.[27,28] Thus, pharmaceutical companies made a significant effort to develop robust small molecule DAAs against essential proteins in the HCV viral life cycle to overcome the challenges with this non-specific combination therapy.

The first DAAs approved for triple combination therapy with peg-IFN and RBV were NS3/4A protease inhibitors (PIs) telaprevir and boceprevir.[29,30] These inhibitors prevent cleavage of the HCV polyprotein, which is a crucial step in viral replication and maturation. The use of telaprevir and boceprevir to treat HCV infection was a major turning point in anti-HCV development as these drugs significantly increased the SVR to 60-75% in GT1 infected patients.[31-37] However, these first generation DAAs lacked efficacy, tolerability due to severe side effects and required a long duration of treatment (approximately 48 weeks).[38]

We have recently moved toward an era of all-oral IFN-free combination therapy with shorter treatment duration. In fact, the U.S. FDA has approved six new all-oral combination therapies: (1) harvoni® (sofosbuvir/ledipasvir),[39] (2) viekira pak™ (ombitasvir/paritaprevir/ritonavir/dasabuvir),[40] (3) zepatier® (elbasvir/grazoprevir),[41] and (4) epclusa® (sofosbuvir/velpatasvir),[42] (5) vosevi® (sofosbuvir/velpatasvir/voxilaprevir)[43] and (6) mavyret™ (glecaprevir/pibrentasvir).[44,45] Each combination therapy includes small molecule inhibitors that target specific protein in the viral life cycle. Sofosbuvir is nucleotide NS5B inhibitor that gets incorporated into the nascent RNA chain, which induces a chain termination event that prevents active transcription.[46] Dasabuvir is a non-nucleotide NS5B inhibitor that allosterically binds to the polymerase preventing conformational changes that are necessary for viral RNA replication.[47,48] NS5A inhibitors, ledipasvir, ombitasvir, elbasvir, velpatasvir, and pibrentasvir, block RNA replication and virion assembly/release.[49] Paritaprevir, grazoprevir, voxilaprevir and glecaprevir are newer generation NS3/4A PIs. The use of DAA-based combination therapies has increased SVR response to almost 100% in GT1 infections.[50] Of note, the two most recent combinations have pan-genotypic activity, including against GT3, a major milestone in HCV therapeutics.[51] Newer generation inhibitors and various combinations improved SVR rates across all genotypes to greater than 83%.[52] For many patients the new DAA combination therapies have reduced the treatment duration from twenty-four to eight weeks.

Through all of these advances, the NS3/4A PIs have become a critical component in DAA-based combination therapy.

1.4 NS3 Bifunctional Protein and Protease Architecture

The 631 amino acid NS3 protein is a bifunctional enzyme consisting of an N-terminal protease domain and a C-terminal super family II DEAD-box helicase domain (**Figure 1.2**).[11,53] Each domain is essential for viral replication, responsible for a crucial step in the viral life cycle. The protease domain forms a heterodimer with NS4A, a 54-residue protein, which significantly improves catalytic efficiency.[11,54] The NS3 protease is responsible for viral processing and escape from host immune system. The latter function is mediated via cleavage of TRIF or MAV adaptor proteins that play a role in the host's virus-induced signaling pathways.[55,56] The helicase domain unwinds RNA duplexes during viral replication. While both domains of the NS3 can function independently, studies have shown that two domains together are optimal for catalytic efficiency.[57-59]

The first crystal structures of the NS3 protease domain were solved in 1996, providing insights on this target's druggability.[60,61] The protease domain is a chymotrypsin-like serine protease with the canonical catalytic triad residues Asp81, His57 and Ser139.[14] The N-terminal domain is composed of 8 beta strands (one from the NS4A cofactor) and the C-terminal domain has a conventional six-stranded beta barrel, which together form a double barrel fold architecture.[11,60,61] The C-terminal beta barrel domain contains a tetrahedrally

coordinated zinc ion that is necessary for the structural integrity of the protease.[60,61] In fact, this metal ion is located over 20 angstroms away from the catalytic triad residues, which explains its structural role over a functional role in enzyme catalysis. In contrast to other proteases in the chymotrypsin family, the NS3 protease lacks several loops that are responsible for a well-defined substrate-binding pocket.[11] Thus, the substrate-binding groove is quite shallow and solvent exposed[62] (**Figure 1.2**) – a true challenge in early drug design efforts.

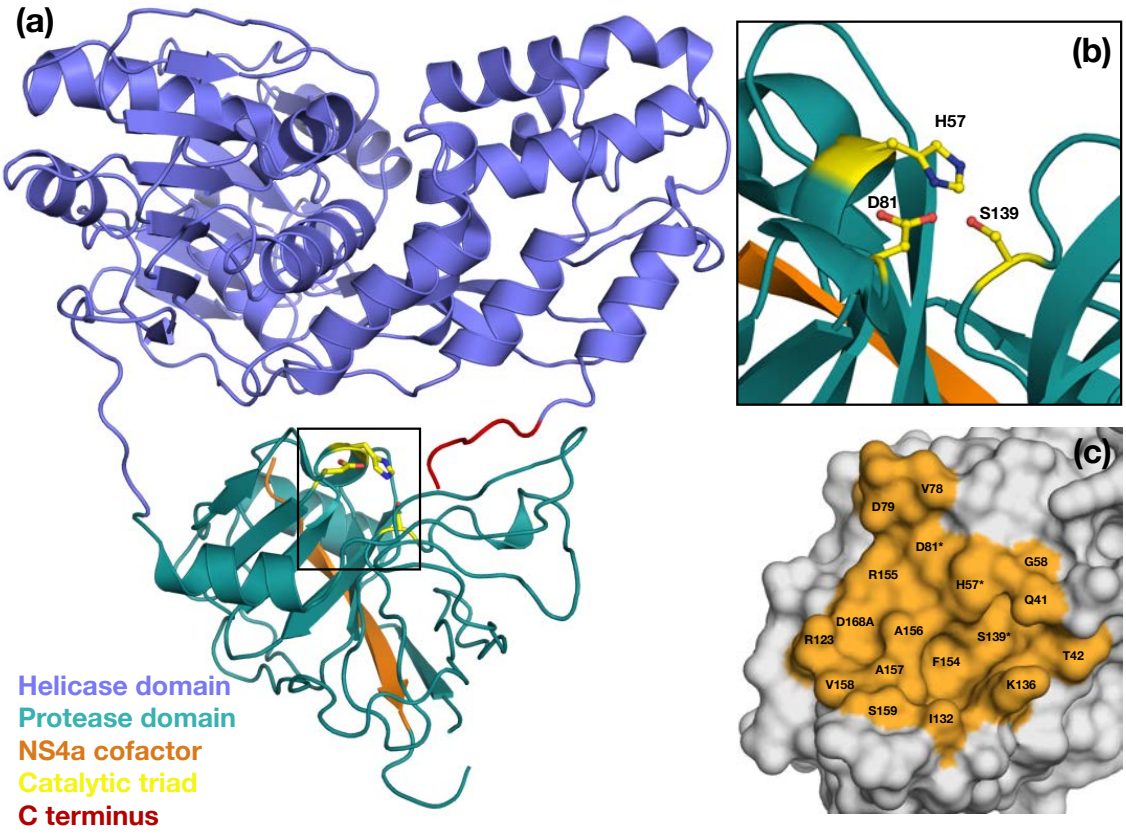

Figure 1.2: Structure of NS3/4A protein and substrate binding pocket.
(a) The NS3/4A protease consists of an N-terminal protease domain (green) and a C-terminal helicase domain (purple). The protease domain is stabilized by the essential NS4A cofactor, which forms one of the N-terminal beta sheets (orange). (b) The NS3/4A is a serine protease with the canonical catalytic triad residues His57, Asp81 and Ser139, shown as yellow sticks. (c) Surface representation of the NS3/4A protease domain highlighting the shallow, solvent exposed binding groove (orange) which hampered early drug discovery efforts. The * indicates the catalytic residues (PDB ID: 3M5L).

1.5 Small Molecule Inhibition of HCV NS3/4A Protease

A major turning point in HCV PI development occurred in 1998, when the N-terminal cleavage product, DDIVPC-OH, of the NS3/4A substrate was identified as a weak competitive inhibitor.[63,64] Pharmaceutical companies exploited this hexapeptide scaffold using structure-based drug design (SBDD)[65-67], which led to the development of the first-in-class NS3/4A PI ciluprevir (BILN-2061) (**Figure 1.3**). BILN-2061 is a macrocyclic inhibitor that exhibited subnanomolar activity against GT1 and an excellent pharmacokinetics profile.[68] Given the excellent profile of this inhibitor, BILN-2061 was advanced to human clinical trials demonstrating the ability to reduce the HCV viral titer in infected patients by up to 3 logs after a 1-2 day administration.[69] Unfortunately, BILN-2061 was discontinued due to severe cardiotoxcity. Nevertheless, this proof-of-concept drug demonstrated that HCV NS3/4A PIs could be potent antivirals used toward the eradication of HCV infection.

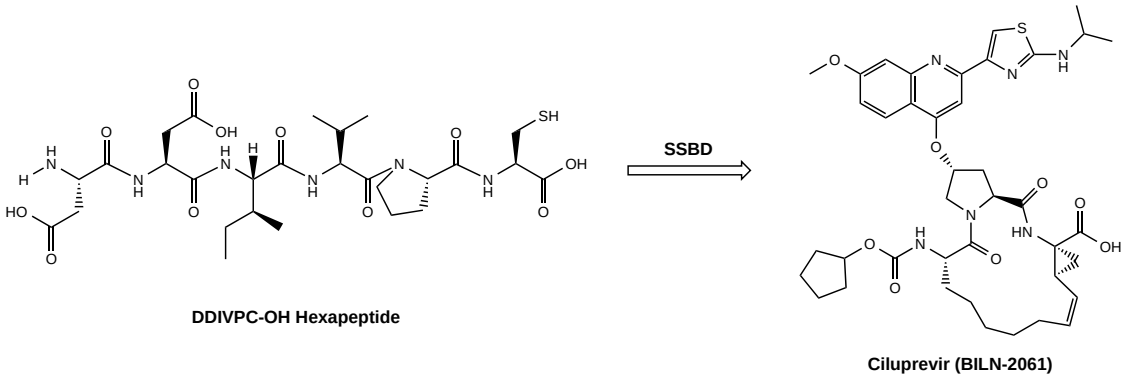

Figure 1.3: Development of proof-of-concept drug ciluprevir.
The N-terminal substrate cleavage product, hexapeptide DDIVPC-OH, was identified as a weak competitive inhibitor of the NS3/4A protease. Structure-based drug design and extrapolation of the hexapeptide scaffold led to the discovery and development of ciluprevir – the first PI in the NS3/4A PI drug class. This drug was discontinued due to its cardiotoxicity.

Two different classes of NS3/4A PIs have been developed over the course of 20 years including: (1) covalent, and (2) non-covalent inhibitors (**Figure 1.4**). Optimization of the scaffold and SBDD resulted in modified peptidomimetics that share a common scaffold spanning the P4–P1' positions.[70-77] All HCV NS3/4A peptidomimetics contain a P1' ketoamide or sulfonamide, P1 cysteine mimic, a P2 proline, P3 moiety, and a P4 or P5 capping group. The first FDA approved PIs were linear inhibitors telaprevir and boceprevir with a ketoamide warhead that forms a reversible covalent bond with the catalytic residue Ser139. However, these inhibitors were not as potent as other inhibitors that were being developed in parallel by other pharmaceutical companies. Moreover, resistance was clinically observed within two weeks of administration with these drugs. In particular, resistance substitutions R155K/T and V36M/S were seen in patients as well as double substitution variants R155K/V36M.[78,79]

More potent and promising inhibitors incorporated a similar scaffold as BILN-2061, a P1–P3 macrocyclic inhibitor with a large P2 moiety. The introduction of a large heterocyclic moiety attached to the P2 proline, significantly improved the potency of the competitive inhibitors.[67,80] The non-covalent competitive inhibitor class share a common P3–P1' peptidic core, and are either linear or macrocyclic; the macrocycle is located either between P1–P3 or P2–P4 moieties. The linear competitive inhibitors include asunaprevir,[81] sovaprevir,[82] and faldaprevir.[83] Asunaprevir was recently approved in Japan as a treatment option for GT1 infection.[84] Simeprevir[85] and danoprevir[86] are P1–P3 macrocyclic inhibitors.

Simeprevir is U.S. FDA-approved to treat GT1 infections.[87] The P2–P4 macrocylic inhibitors include vaniprevir, which was developed by Merck and is also approved for treatment of GT1 in Japan.[88] These inhibitors had improved activity profiles against wildtype GT1 but were highly susceptible to resistance substitutions at residues Arg155, Ala156, and Asp168 – the three most common resistance sites in the protease active site.[89,90] Moreover, these inhibitors lacked activity against other HCV genotypes, a necessary benchmark to meet in anti-HCV development.

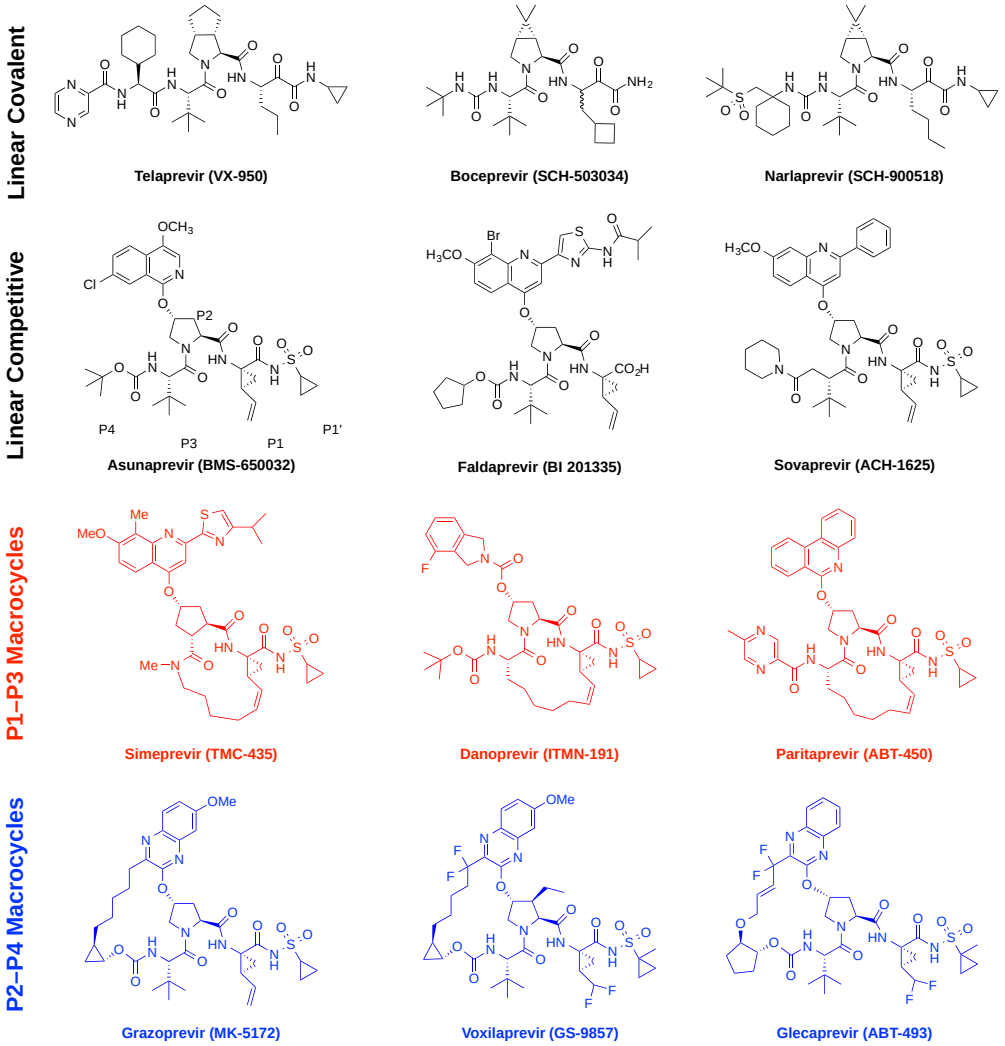

Figure 1.4: 2D chemical structures of NS3/4A protease inhibitors.
There are two inhibitor drugs classes, covalent and non-covalent. The covalent inhibitors are the linear ketoamide drug class. Non-covalent inhibitors can be subdivided into the two groups including linear and macrocyclic. The macrocycle is either located between the P1–P3 positions of the scaffold or P2–P4. The canonical nomenclature for drug moiety positioning is indicated using asunaprevir.

1.6 Development of Pan-genotypic Protease Inhibitors

Toward the development of a pan-genotypic inhibitor, AbbVie introduced paritaprevir, a potent P1–P3 macrocyclic inhibitor with promising activity against the NS3/4A target. In a 3-day monotherapy study with co-administration of ritonavir, an average decrease of 4 $\log_{10}$ in HCV viral RNA was observed at the end of the dosing period.[91] Paritaprevir also had cross-genotypic activity with inhibition observed against GTs 1, 4 and 6.[91] However, paritaprevir exhibited reduced efficacy against the GT3 replicon. The most common single substitution variants selected for in patients were R155K and D168V.[92] Double substitution variants including Y56H/D168A have been observed in clinical samples as well.[93,94] Despite the emergence of resistance, paritaprevir was FDA-approved in 2014 in combination with an NS5A and NS5B inhibitor for the treatment of GT1 infection.

At this time, Merck developed grazoprevir (MK-5172), a very potent P2–P4 macrocyclic inhibitor. It was one of the first PIs to exhibit an excellent activity profile against some common single substitution variants as well as cross-genotypic activity (excluding GT3 – a hard to treat variant).[95,96] In 2016, grazoprevir gained FDA approval in combination with NS5A inhibitor elbasvir for the treatment of GT1 and GT4 infections. This was the first all-oral PI containing regimen with FDA-approval to treat a non GT1 HCV infection, marking a critical turning point in PI development. Grazoprevir demonstrated sub-nanomolar to single digit nanomolar activity against GTs 1, 2, 4, 5, and 6 in antiviral assays

(EC_{50} < 4 nM).[97] However, like paritaprevir antiviral activity of grazoprevir against the GT3 variant was reduced by at least two orders of magnitude.[97] Grazoprevir had improved activity against resistant variant R155K but was highly or moderately susceptible to A156T or D168A, respectively. Moreover, double substitution (Y56H/D168A) and triple substitution variants (Y56H/A156T/D168A/N) were observed in clinical studies.[92,94,97,98]

The success of grazoprevir scaffold led to the development of PIs voxilaprevir and glecaprevir. In 2017, the first pan-genotypic combination therapies consisting of these inhibitors were FDA-approved for the treatment of GT1-6, a major milestone in anti-HCV research.[99,100] Interestingly, voxilaprevir and glecaprevir are structurally similar to grazoprevir with minor modifications to the scaffold (**Figure 1.5**). These inhibitors showed excellent potency against all GTs and have activity against common resistance associated substitutions (RASs) including D168A and R155K. However, like grazoprevir, they are highly susceptible to the A156T variant. Additionally, though limited clinical data exist, double substitutions have been selected for in *in vitro* assays including A156V/D168V, Y56H/Q168R and other combinations of active and distal site substitutions.[51]

All the aforementioned NS3/4A PIs exploit critical interactions within the protease active site that enhance the potency of these inhibitors. However, many of these interactions are not essential for substrate recognition, and substitutions

in the NS3/4A protein for most inhibitors are detrimental to potency resulting in drug resistance. Thus coupling our understanding of substrate recognition and the molecular underpinnings of drug resistance is necessary for the successful development of novel PIs with improved resistance profiles.

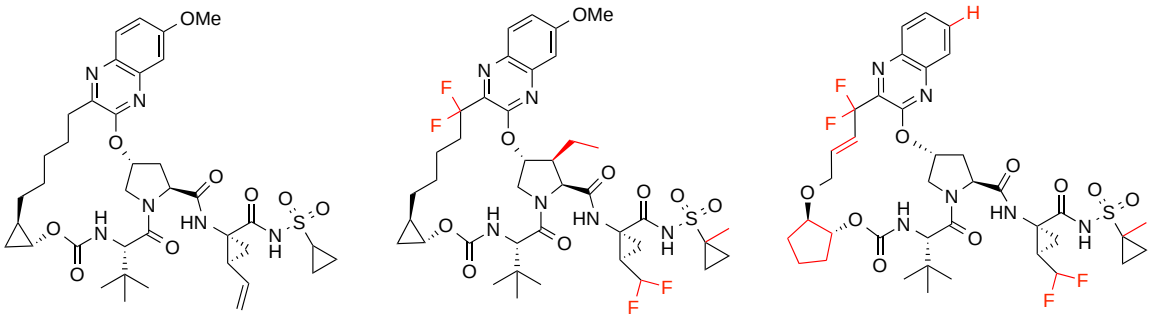

Figure 1.5: 2D chemical structure of grazoprevir and similar P2–P4 macrocyclic inhibitors.
Modifications of grazoprevir scaffold led to development of newer generation PIs voxilaprevir and glecaprevir. Differences in chemical structure are highlighted in red. These minor modifications led the identification of PIs with pan-genotypic activity and lower susceptibility to single site substitutions.

1.7 Substrate Recognition and Protease Inhibitor Resistance

The NS3/4A viral substrates share little sequence homology except a cysteine at P1 and an acid at P6 (**Table 1.1**).[101] Insights from HIV-1 protease, another viral protease with highly diverse substrates, revealed that substrates are recognized by the consensus volume that they occupy in the protease active site, termed the *substrate envelope* (SE) (**Figure 1.6**).[102] High-resolution crystal structures of substrate-protease complexes showed that HCV substrates also occupy a similar volume in the protease active site.[90,101] This consensus volume or SE is the basis of molecular recognition for the NS3/4A protease substrates. It is well established that in the NS3/4A protease, drug resistance substitutions occur where inhibitors protrude outside of the SE and contact residues unessential in substrate recognition.[89]

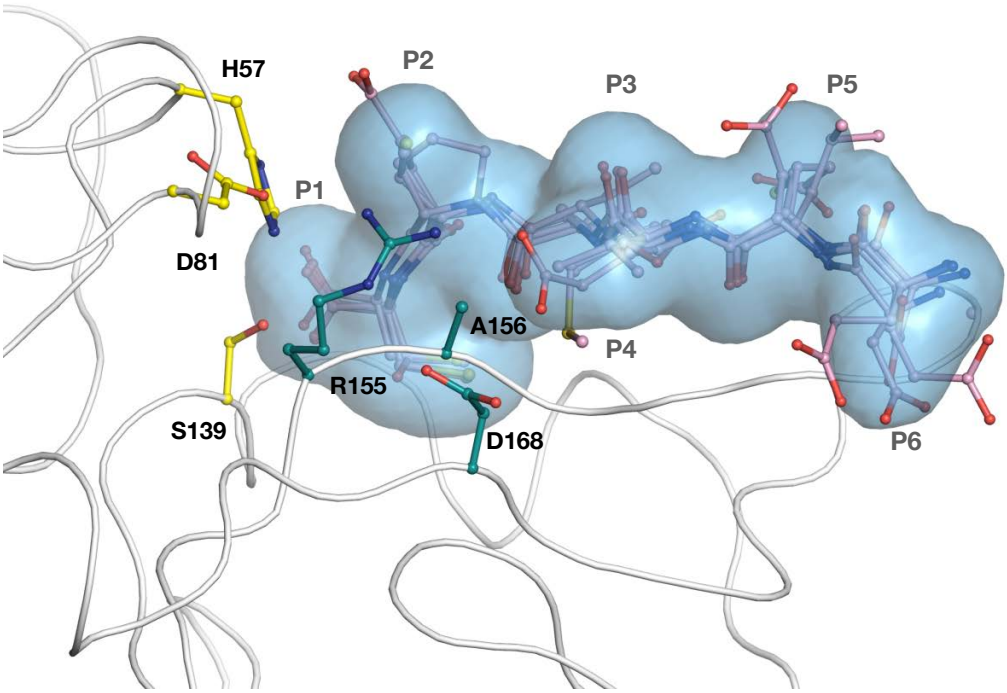

Figure 1.6: Superposition of NS3/4A substrates in the substrate envelope. The NS3/4A substrates (pink) occupy a consensus volume in the protease active site known as the substrate envelope (blue). The NS3/4A protease is shown as a smooth ribbon. The catalytic triad and residues that commonly mutate to confer resistance are shown as yellow and green sticks, respectively.

Table 1.1: Amino acid sequence of NS3/4A protease substrates for GT1

Substrate	Amino Acid at Position:									
	P6	P5	P4	P3	P2	P1	P1’	P2’	P3’	P4'
3-4A	D	L	E	V	V	T	S	T	W	L
4A/4B	D	E	M	E	E	C	S	Q	H	S
4B/5A	E	C	T	T	P	C	S	G	S	V
5A/5B	E	D	V	V	C	C	S	M	S	L
TRIF	$P_{(8)}$[a]	S	S	T	P	C	S	A	H	W
MAVS	E	R	E	V	P	C	H	R	P	Y

[a]The TRIF substrate has a polyproline sequence consisting of 8 proline residues.

Drug resistance results from a loss of inhibitor binding affinity while maintaining substrate processing. The NS5B RNA-dependent RNA polymerase has low fidelity resulting in one substitution per 10^3 – 10^7 nucleotides, which equates to one error per round of genome replication.[103] Thus, due to the large error rate, patients infected with HCV develop a heterogeneous population of viral species known as quasispecies. The P2 moieties of most protease inhibitors protrude beyond the substrate envelope and contact the S2 subsite residues Arg155, Ala156 and Asp168 (**Figure 1.7**).[89] The residues Arg155, Ala156, and Asp168, where the most common drug resistance substitutions occur, are located around the active site. In the inhibitor-bound state, HCV NS3/4A protease has an extensive active site electrostatic network that spans the catalytic triad residues His57 and Asp81 all the way to residues Arg155, Asp168 and Arg123. Residues Arg155 and Asp168, located beyond the substrate envelope, form a salt bridge that is critical to inhibitor binding and disrupted upon substitution at either residue (**Figure 1.7**).

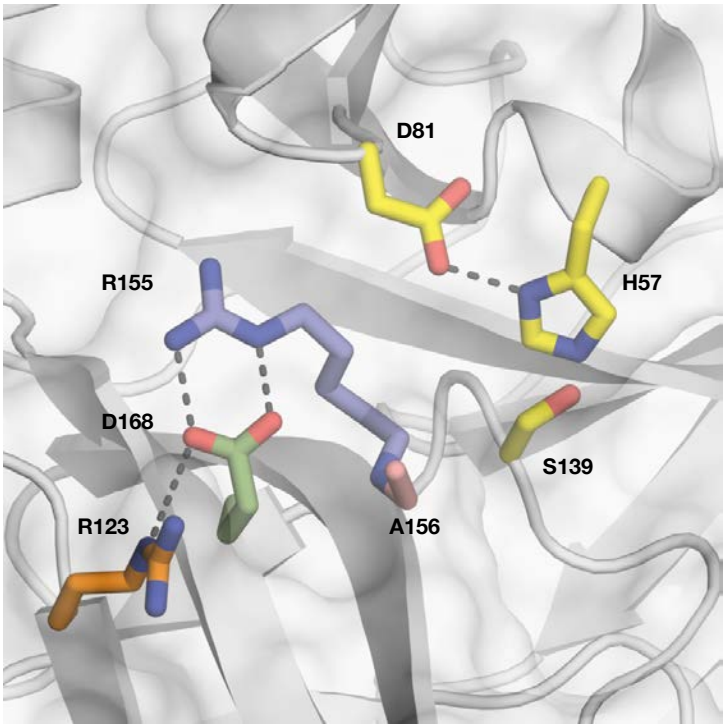

Figure 1.7: Location of common resistance substitutions in the protease active site and the electrostatic network.
The most common sites where substitutions occur that confer resistance to NS3/4A protease inhibitors are Arg155, Ala156 and Asp168 shown in blue, red and greens sticks, respectively. Arg123 is a residue that is variable in GT3 and forms part of the electrostatic network in GT1. The electrostatic network is highlighted by gray dashes. The catalytic triad residues His57, Asp81 and Ser139 are shown as yellow sticks.

1.8 Mechanisms of Resistance for Single Substitutions

The NS3/4A protease inhibitors are highly effective drugs with the ability to rapidly reduce the HCV viral titer in infected patients.[45,104,105] However, most NS3/4A protease inhibitors are highly susceptible to single site substitutions R155K, A156T and D168A. We have shown that the resistance profile of PIs largely depends on how the PIs protrude beyond the substrate envelope,[89,90] which is largely determined by the identity of their P2 moiety and macrocycle location.[106] High-resolution crystal structures of protease inhibitors bound to WT and substituted proteases allowed us to elucidate the molecular basis of resistance against single substitution protease variants.[89] Residues Arg155 and Asp168, located in the S2 subsite, form a critical salt bridge that provides additional hydrophobic surface necessary for inhibitor binding. This salt bridge stabilizes Arg155 in a conformation that allows efficient inhibitor binding. Disruption of this electrostatic network as a result of substitutions at Arg155 or Asp168 underlies the mechanism of resistance for most NS3/4A protease inhibitors.

Residue Arg155 often mutates to a lysine (R155K) to confer resistance. Danoprevir, asunaprevir, and many older generation protease inhibitors have large P2 moieties that predominately bind on the S2 subsite residues (**Figure 1.8**). The guanidinium group of Arg155 makes favorable cation−π interactions with the P2 heterocyclic moiety of these NS3/4A protease inhibitors. Thus, when Arg155 mutates to a lysine residue, inhibitors lose the ability to bind efficiently.

Substitutions at Asp168 cause resistance due to indirect structural effects and changes in electrostatics. Asp168 is a pivotal drug resistance residue as most PIs are susceptible to substitutions at Asp168, which are often present in patients who fail therapy.[107] Notably, the polymorphism Gln168 at this position underlies reduced efficacy of PIs against GT3.[108] We and others have shown structurally that loss in hydrophobic interactions and the hydrogen bond network with Arg155, as a result of substitutions at Asp168 are responsible for reduced inhibitor potency.[89,109,110] However, the introduction of the quinoxaline moiety at the P2 position of the inhibitor scaffold, led to the development of grazoprevir, a compound with a distinct resistance profile relative to inhibitors that primarily interact with S2 subsite residues.

The P2 quinoxaline of grazoprevir binds uniquely in the protease active site, making hydrophobic interactions with the catalytic triad residues His57 and Asp81 (**Figure 1.8**).[89] In fact, the P2 quinoxaline moiety of grazoprevir avoids direct interactions with Arg155 and Asp168, minimizing susceptibility to resistance due to substitutions at these residues. In the case of grazoprevir, although the P2 moiety protrudes outside the substrate envelope,[89] it stacks against the invariant catalytic triad, which is one strategy that can be used to avoid drug resistance.

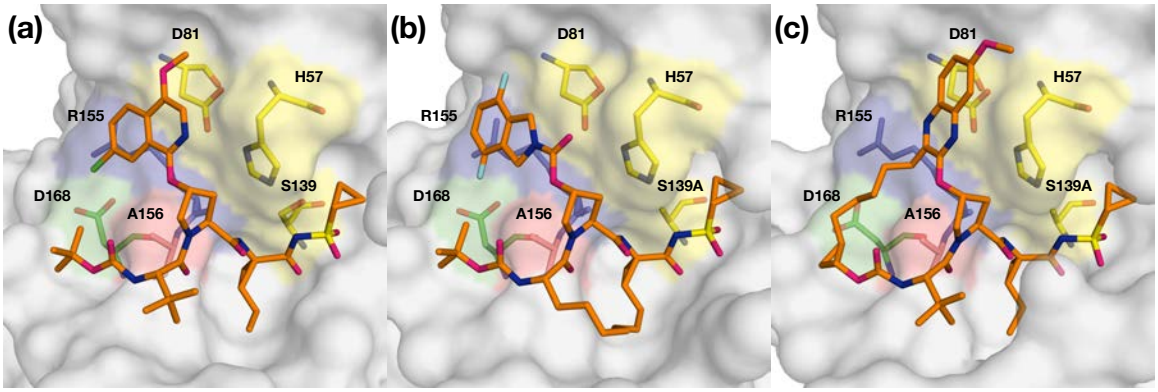

Figure 1.8: The binding mode of NS3/4A PIs.
Surface view of PIs bound to the NS3/4A active site. (a) asunaprevir, (b) danoprevir, and (c) grazoprevir. The catalytic triad is shown in yellow and drug resistance residues Ala156, Arg155, and Asp168 are shown in blue, red and green, respectively. Many of the current inhibitors in clinical development have large P2 groups that contact residues in the S2 subsite, which mutate to confer resistance. Structural analysis revealed that inhibitors have different binding modes underlying reduced inhibitor potency against resistant associated substitutions. The P2 isoindoline group of danoprevir occupies two conformations in the protease active site. (PDB IDs: 4WF8, 3M5L, and 3SUD, respectively).

Even with this unique binding mode, grazoprevir is not immune to resistance. Grazoprevir is highly susceptible to substitutions at Ala156 due to the location of the macrocycle – a major structural feature that impacts PI resistance profiles.[106] Inhibitors with a P2–P4 macrocycle like grazoprevir are susceptible to Ala156 mutations as a change to a larger residue results in steric clash with the macrocycle.[89,111] We rationalized that changing the macrocycle location could improve activity against the A156T variant. Indeed, we have shown 5172-mcP1P3, a P1–P3 macrocyclic analogue of grazoprevir, is less susceptible to Ala156 mutations and has an improved resistance profile.[106] The unique binding mode of grazoprevir is conserved in the P1–P3 macrocyclic analogue (**Figure 1.9**).[111] 5172-mcP1P3 is less susceptible to drug resistance because the P2 group is less constrained than in grazoprevir. Thus, designing inhibitors with modified P2 quinoxalines similar to 5172-mcP1P3 is a strategy that can be employed to develop more robust NS3/4A inhibitors.

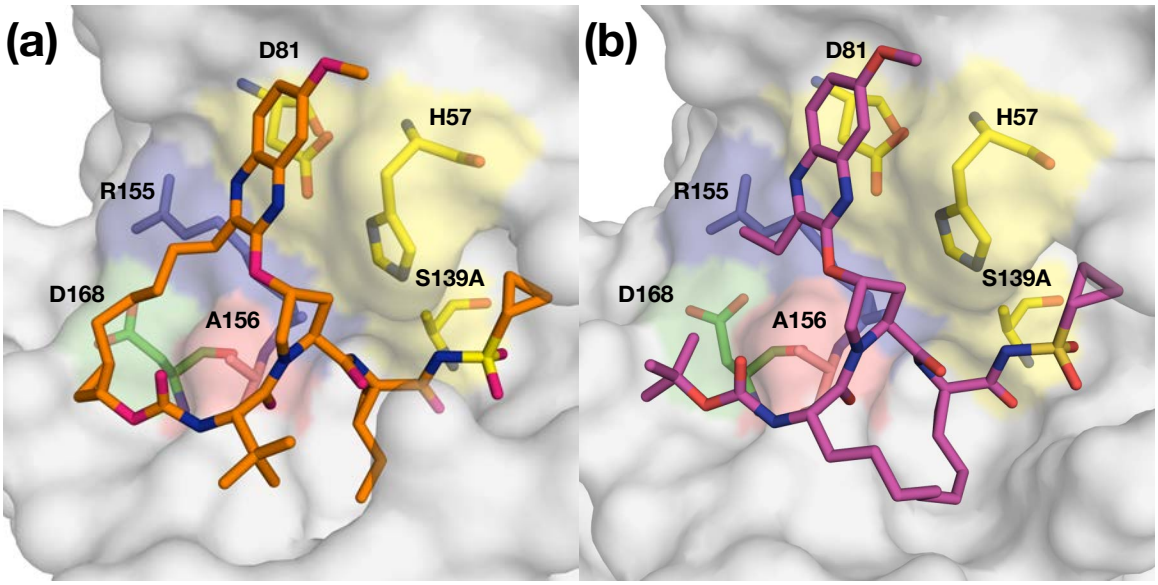

Figure 1.9: Binding conformation of grazoprevir and 5172-mcP1P3 in the active site of wild-type NS3/4A protease.
(a) Grazoprevir and (b) P1–P3 analog 5172mc-P1P3 bind similarly in the protease active site whereby the P2 quinoxaline moiety makes strong interactions with the catalytic residues, minimizing contact with known residues that mutate to confer resistance. The catalytic triad is highlighted in yellow, and drug resistance residues Arg155, Ala156, and Asp168 are shown in blue, red, and green, respectively. (PDB IDs: 3SUD and 5EPN, respectively).

1.9 Emergence of double substitution variants

Newer generation PIs have significantly improved activity against single site substitutions in the protease. However the emergence of multi-substituted variants has become a new problem in PI advancement. Often times, double substitution variants include an Asp168 substitution, such as R155K/D168A, A156T/D168A, Y56H/D168A and Y56H/D168V proteases. Acquisition of an additional substitution may give rise to new viral variants with substitutions that are often not seen alone, as in the case with Y56 and A156 substitutions. One key clinically relevant protease variant is Y56H/D168A, often present in patients who fail therapy with the newer generation PIs.[92,94,98] Grazoprevir and paritaprevir are highly susceptible to this signature variant and exhibit over 500-fold loss in potency.[92,97,112] While the molecular basis of drug resistance caused by single-site RASs has been well characterized, the impact of clinically relevant NS3/4A protease double substitutions on inhibitor binding and the mechanisms of drug resistance remain largely unexplored.[89,90,111] Though the Y56H/D168A variant has been hypothesized to cause resistance due to reduced hydrophobic contacts of the inhibitor P2 moiety with the NS3/4A protease, this alone does not explain the significant loss in potency.[97] Moreover, considering the similarity in the inhibitor scaffolds of the most recently FDA-approved PIs and modes of action, there is a danger that these newly emerging variants may be cross-drug resistant and patients may not respond to any current treatment option. Thus, elucidating the molecular mechanisms of resistance for PIs against these multi-

substituted variants and diversifying our PI arsenal is necessary for the elaboration of next-generation PIs.

1.10 Scope of Thesis

This thesis attempts to understand mechanisms of drug resistance against NS3/4A PIs and develop design strategies to improve PI resistance profiles. It is paramount to elucidate mechanisms of drug resistance against HCV PIs as insights can provide new approaches toward the development of novel antivirals. The newest anti-HCV therapeutics available for the treatment of HCV infection are FDA-approved PIs voxilaprevir and glecaprevir. The development of these pan-genotypic inhibitors was a major achievement in anti-HCV therapeutics. However, one threat to the clinical effectiveness of HCV NS3/4A PIs is the emergence of double substitution variants that confer resistance to these new drugs. In Chapter II, I elucidate the structural and dynamic mechanisms of resistance of PIs against the highly resistant Y56H/D168A variant – identifying a novel mechanism of resistance.

At the conception of this research, the current FDA-approved pan-genotypic NS3/4A PIs were in their infancy. A major goal in the field was to develop robust inhibitors with improved activity against resistance associated single substitutions in the protease active site, including D168A. Grazoprevir was a promising drug but still moderately susceptible to Asp168 and highly susceptible to Ala156 substitutions. To further improve the resistance profile, I explored structure-

activity relationship and used insights from previous structural studies to design novel inhibitors. Chapter III demonstrates that P1–P3 macrocyclic inhibitors based on the grazoprevir scaffold with modified quinoxaline moieties have improved activity against single RASs. Chapter IV highlights the importance of substrate recognition in inhibitor design by use of the substrate envelope to further improve resistance profiles. The designed inhibitors leveraged evolutionarily constrained locations in the protease active site, including the invariant catalytic triad and the substrate envelope. Together these studies highlight the importance of substrate recognition in inhibitor design, elucidate the molecular mechanism of resistance of PIs against multi-substituted variants and provide strategies toward the development of diverse NS3/4A PIs that may one day lead to the eradication of HCV.

Chapter II

Clinical signature variant of HCV NS3/4A protease uses a new mechanism to confer resistance

Preface

Chapter II is a collaborative study that has been submitted for publication.

Matthew, A. N.; Leidner, F.; Newton, A.; Petropoulos, C. J.; Huang, W.; Ali, A.; Kurt Yilmaz, N.; Schiffer, C. A. Clinical signature variant of HCV NS3/4A protease uses a new mechanism to confer resistance.

Contributions from Ashley N. Matthew:

I devised the concept of this manuscript. I performed the cloning, protein expression, purification of GT1a, single and double substitution proteases for this study. I performed all enzyme inhibitor studies and analysis of the biochemical data for this study. I solved three structures for this study and analyzed them with assistance from C.A.S. and N.K.Y. I created most of the figures and tables for this study. I analyzed and wrote the manuscript with guidance from Celia A. Schiffer, Nese Kurt Yilmaz and Florian Leidner.

2.1 Abstract

The development of direct-acting antivirals is a major milestone in the treatment of hepatitis C virus (HCV) infections. The HCV NS3/4A protease inhibitors (PIs) are a mainstay of recent all-oral combination therapies. Despite significant progress, drug resistance remains a problem with the emergence of resistance-associated substitutions causing treatment failure. Newer generation PIs such as grazoprevir and paritaprevir retain high potency against most single substitutions in the protease in part by stacking on the invariant catalytic triad. The evolutionarily conserved catalytic residues cannot mutate without compromising enzymatic activity, an advantage exploited by all recent HCV PIs. Nevertheless, double substitution variants, notably Y56H/D168A have emerged in patients who fail therapy with a PI-containing regimen. The molecular mechanism by which Asp168 substitutions confer resistance has been extensively characterized. However, for this newly emerging clinically relevant variant with an additional mutation at Tyr56, mechanism of resistance is unknown. Here, we elucidate the molecular mechanism of resistance against the Y56H/D168A protease variant, for a series of PIs (grazoprevir and 4 analogs, paritaprevir, and danoprevir), through inhibition assays, co-complex crystal structures and molecular dynamics simulations. The PIs had varying degrees of susceptibility to Y56H/D168A, with those stacking on the catalytic His57 losing the most potency. Structural and dynamic analyses revealed that the Y56H substitution disrupts these inhibitors' favorable stacking interactions with the

neighboring catalytic His57, while still maintaining substrate turnover. Thus we uncovered a new mechanism of resistance used by the Y56H/D168A variant where substitutions at neighboring residues disrupt interactions of the catalytic residue with inhibitors.

2.2 Introduction

Hepatitis C virus (HCV) is a global threat infecting over 150 million people worldwide.[7] Over 80% of individuals infected with HCV develop chronic liver disease, which often progresses to cirrhosis or becomes malignantly transformed to hepatocellular carcinoma.[1] Prior to the introduction of direct-acting antivirals (DAAs), the standard of care for HCV infection consisted of pegylated interferon alpha and ribavirin.[113] This treatment resulted in a sustained virological response (SVR; the standard indication of cure from infection), of less than 50% against genotype 1 (GT1) and had low tolerability due to severe side effects.[114] Fortunately, in the last several years the advent of DAAs against essential viral proteins NS3/4A, NS5A and NS5B has significantly improved therapeutic options and treatment outcomes for patients infected with HCV.[23,115]

HCV is a highly diverse virus with seven known genotypes (GT1–7) and multiple subtypes.[6-8] Patients infected with HCV develop a heterogeneous population of viral species known as quasispecies due to low fidelity of the RNA-dependent RNA polymerase.[116,117] The genetic diversity both among genotypes and within a viral population presents a challenge in the treatment of HCV

infections. The six U.S. FDA approved all-oral combination therapies have varied effectiveness, and especially the earlier therapies can fail against certain genotypes.[115] Newer generation inhibitors and various combinations have improved SVR rates across all genotypes to greater than 83%.[52] The two most recent combination therapies approved in 2017 by the FDA, Vosevi and Mavyret, have pan-genotypic activity, a major milestone in HCV treatment.[43,118] While the treatment options for HCV infection have significantly improved, one major threat to the clinical effectiveness of all anti-HCV drug classes is the emergence of resistance-associated substitutions (RASs) in target proteins.[51,107,112,119]

RASs often weaken inhibitor binding resulting in reduced activity against the target enzyme. The HCV NS3/4A protease inhibitors (PIs) are highly effective drugs with the ability to rapidly reduce the HCV viral titer in infected patients but are susceptible to RASs around the protease active site.[45,105] There are currently five FDA-approved protease inhibitors: simeprevir,[85] paritaprevir (ABT-450),[91] grazoprevir (MK-5172),[120] glecaprevir[51] and voxilaprevir.[121] All of these PIs incorporate large heterocyclic moieties at the P2 position to achieve high potency. However, this large P2 moiety often renders PIs susceptible to RASs, particularly at residues Arg155, Ala156, and Asp168. We have shown that the resistance profile of PIs largely depends on how the PIs protrude beyond the substrate envelope,[89,90] which is largely determined by the identity of their P2 moiety and macrocycle location.[106] Substitutions typically occur at residues that interact with PIs beyond the substrate envelope, preserving substrate recognition

and turnover while disrupting inhibitor binding. Two such residues are Arg155 and Asp168 located in the S2 subsite, which form a critical electronic network that provides a surface essential for inhibitor binding but not for substrate recognition. Our previous crystal structures revealed that disruption of this electrostatic network as a result of substitutions at either Arg155 or Asp168 underlies the mechanism of resistance for earlier generation NS3/4A PIs.[89,109]

Grazoprevir (MK-5172) is a highly potent P2–P4 macrocyclic inhibitor with cross-genotypic activity but reduced potency against GT3, a difficult to treat HCV variant.[96] Grazoprevir was the first inhibitor with a unique binding mode whereby the P2 quinoxaline moiety, which still protrudes beyond the substrate envelope, stacks on the residues of the invariant catalytic triad. The catalytic residues cannot mutate without compromising substrate recognition and turnover, avoiding resistance. Robustness of grazoprevir against resistance prompted this binding mode to be exploited by all newer generation inhibitors including glecaprevir and voxilaprevir, which share a similar scaffold to grazoprevir. This binding mode also minimizes interactions with S2 subsite residues that typically mutate to confer resistance (**Figure 2.1**)[89] and thus reduces grazoprevir's susceptibility to substitutions at residue Arg155. However, grazoprevir is still moderately susceptible to substitutions at Asp168 due to the packing of the P2–P4 macrocycle.

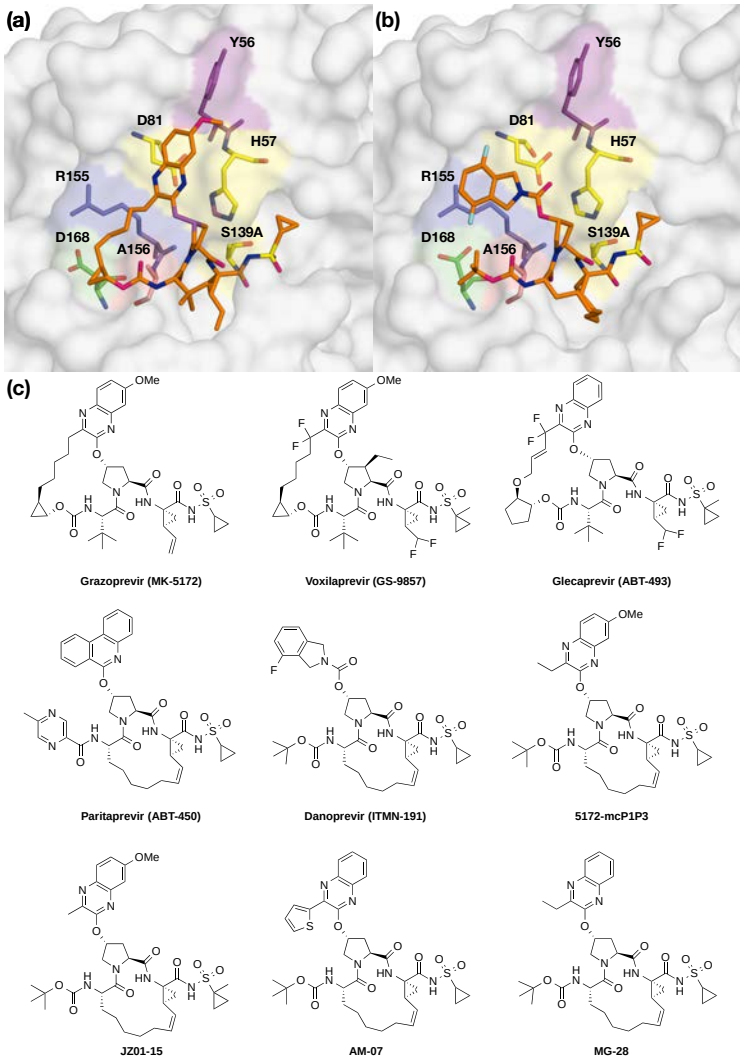

Figure 2.1: The binding mode of NS3/4A protease inhibitors, location of residues that mutate to confer resistance and 2D chemical structure of NS3/4A protease inhibitors.

Surface view of NS3/4A protease inhibitors (a) grazoprevir and (b) danoprevir bound to the active site. Danoprevir's P2 isoindoline moiety occupies two conformations in the protease active site. The catalytic triad is shown in yellow and drug resistance residues Tyr56, Arg155, Ala156, and Asp168 are shown in magenta, blue, red and green, respectively. Residues Tyr56 and Asp168 are located almost 15 Å apart in the protease active site. (c) Grazoprevir, voxilaprevir, glecaprevir and paritaprevir are approved by the FDA. Danoprevir was in clinical development. All other inhibitors were synthesized in house as P1–P3 macrocyclic analogs of grazoprevir.

In fact, most PIs are susceptible to substitutions at Asp168, which are often present in patients who fail therapy.[107] Notably, the polymorphism Gln168 at this position underlies reduced efficacy of PIs against GT3.[122] Glecaprevir and voxilaprevir have improved resistance profiles against D168A and are active against GT3, but like grazoprevir are highly susceptible to substitutions at Ala156[51] due to van der Waals clashes with their P2–P4 macrocycles.[106,111] Unfortunately, even with the newest combinations some patients still fail therapy, with more than one RAS detected in the infecting viral population.[41] The emergence of such double and sometimes triple-site RAS variants in clinic is threatening the effectiveness of current anti-HCV therapies.[98]

While the molecular basis of drug resistance caused by single-site RASs has been well characterized,[89,90,111,123] the impact of clinically relevant NS3/4A protease double substitutions on inhibitor binding and the mechanisms of drug resistance remain largely unexplored. One key clinically relevant protease variant is Y56H/D168A, often present in patients who fail therapy with the newer generation PIs. Grazoprevir and paritaprevir are highly susceptible to this signature variant and exhibit over 500-fold loss in potency.[92,97,112] Substitutions at Tyr56 rarely occur alone, but are becoming common in combination with substitutions at Asp168. These residues are not in physical contact, with Tyr56 located next to the catalytic His57, approximately 15 Å away from residue Asp168. Nevertheless, co-evolution of these two sites results in a detrimental loss of potency for all PIs. The molecular mechanism underlying high-level

resistance of PIs against the Y56H/D168A double substitution variant is unknown.

To elucidate the molecular mechanism of resistance for PIs against the Y56H/D168A NS3/4A protease variant, we used a multi-disciplinary approach involving enzyme inhibition and antiviral assays, co-crystal structures, and molecular dynamics simulations. A panel of 7 NS3/4A PIs (grazoprevir and 4 analogs, paritaprevir, and danoprevir) with varying macrocycle locations and P2 binding modes were tested for enzyme inhibition and antiviral potency. To tease out the impact of individual substitutions, the double substitution variant was compared to both single substitutions and wild-type GT1a NS3/4A protease. While all inhibitors were 3–10 orders of magnitude less active against the Y56H/D168A NS3/4A protease variant, the potency loss was exacerbated for PIs that stack on the catalytic triad, including grazoprevir. Crystal structures and dynamic analysis of grazoprevir bound to protease variants revealed that this resistance is largely due to the Y56H substitution disrupting the favorable stacking interactions with the neighboring catalytic residue His57. Thus, in addition to the loss of the ionic network due to D168A substitution,[89,109] decreased direct interactions with catalytic His57 underlie resistance against this double substitution variant. To prevent such mechanisms of clinically relevant resistance a novel strategy of inhibitor design limiting interactions with Tyr56 while still maintaining stacking against the catalytic residues is warranted.

2.3 Results

2.3.1 Inhibitors are highly susceptible to the Y56H/D168A NS3/4A variant

Enzyme inhibition and replicon potency of HCV NS3/4A PIs correlate closely with efficacy in the clinic, as does loss of potency due to site-specific substitutions. As Y56H and D168A substitutions have been selected in clinic together under the selective pressure of PIs, these two substitutions may have interdependent effects in conferring resistance. Thus to determine the impact of Y56H/D168A and potential interdependency of these substitutions, enzyme inhibition and replicon assays were performed against WT (GT-1a), Y56H, D168A and the double substitution variant for a panel of diverse NS3/4A PIs (**Figure 2.1** and **Tables 2.1, 2.2**). This panel included FDA-approved inhibitors (grazoprevir, paritaprevir), P1–P3 macrocyclic analogs of grazoprevir (5172-mcP1P3, JZ01-15, AM-07, MG-28) and danoprevir (**Figure 2.1**). The inhibitors were selected to test the role of the macrocycle (P1–P3 versus P2–P4) and the packing of the P2 moiety on susceptibility to these substitutions.

All seven inhibitors were potent against WT with inhibition constants (*K*i) ranging from 0.2–7.2 nM, (**Figure 2.2A** and **Table 2.1**), in agreement with previous reports.[124] Similarly, in replicon assays, all inhibitors exhibited sub-nanomolar to 1.4 nM potency against WT HCV (**Figure 2.2B** and **Table 2.2**). Relative to WT protease, all PIs lost potency against the D168A variant, as has

been observed for NS3/4A inhibitors.[96,108] However, the potency losses varied significantly from 14- to 1800-fold, with the thiophene substituted P1–P3 macrocyclic analog AM-07 losing the most potency and danoprevir exhibiting a 200-fold reduction in potency in enzyme inhibition assays. As we previously reported,[124] grazoprevir exhibited > 200-fold lower potency against the D168A variant in enzyme inhibition assays but was still one of the most potent inhibitors against this drug resistant protease variant (K_i =49.1 nM). The P1–P3 macrocyclic inhibitors JZ01-15 and 5172-mcP1P3 (with a methyl and ethyl substituted quinoxaline, respectively) exhibited lower potency against WT protease compared to grazoprevir but were less susceptible to the D168A variant, resulting in an inhibition constant similar to grazoprevir (K_i = 52 and 82.4 nM, respectively). Similar trends were observed in replicon assays with inhibitors losing 10- to 124-fold in potency compared to WT. Grazoprevir was over 100-fold less potent against the D168A variant (EC_{50} = 26.8 nM). Interestingly, JZ01-15 exhibited the best activity against the D168A variant in replicon assays with EC_{50} below 5 nM (EC_{50} = 4.8 nM). Thus the P1–P3 macrocyclic inhibitor with a small methyl substitution on the P2 quinoxaline showed a much flatter resistance profile and was less susceptible to D168A substitution.

The impact of Y56H on inhibition by NS3/4A PIs has not been well characterized, as this substitution is rarely observed alone. Enzyme inhibition assays on our panel of PIs showed that all inhibitors except danoprevir were susceptible to the Y56H substitution, exhibiting reduced potency ranging from

29–177 fold. The antiviral activities closely correlated with enzyme inhibition assays with inhibitors losing 51–138 fold in potency. In contrast, danoprevir, whose P2 isoindoline moiety does not stack on the catalytic triad,[89] maintained potency similar to WT (K_i = 1 nM, EC_{50} = 0.57 nM) against the Y56H variant (K_i = 3 nM, EC_{50} = 6.2 nM).

The potency loss of PIs against Y56H variant could be due to disruption of Tyr56 residue's direct interactions with the P2 quinoxaline. To isolate the effect of direct hydrophobic interactions of the methoxy group at the 7-position of the P2 quinoxaline with the Tyr56 residue, we tested MG-28, which lacks this substituent. MG-28 is an analog of 5172-mcP1P3 and differs only at this position. MG-28 was more susceptible to the Y56H substitution compared to 5172-mcP1P3 (K_i = 205 nM compared with 101 nM). While 5172-mcP1P3 was more potent against WT protease, fold-changes against Y56H variant were comparable regardless of the presence of this group (31 and 29 fold), also for a very close analog (JZ01-15, 30-fold). Thus loss of direct hydrophobic interactions with Tyr56 does not underlie susceptibility to the Y56H substitution, suggesting another mechanism of resistance.

All inhibitors were highly susceptible to the Y56H/D168A variant with enzyme inhibition constants in the mid-nanomolar to micromolar range (K_i = 500 nM – 2 μM). In fact, all inhibitors exhibited a greater than 200-fold loss in potency relative to WT protease. Danoprevir was 500-fold less potent against the Y56H/D168A

protease (K_i = 520 nM). However, most of this potency loss is due to the D168A substitution (K_i = 199 nM) with only an additional 2.5-fold reduction in potency with Y56H. The same trend was observed for danoprevir in replicon assays (D168A EC_{50} = 50.6 nM, Y56H/D168A EC_{50} = 136 nM). In contrast, grazoprevir and paritaprevir were highly susceptible to the Y56H/D168A protease showing 2500-fold and 8500-fold lower potency, respectively compared to WT. The replicon assays correlated with enzyme potency, with grazoprevir and paritaprevir exhibiting 1923- and 2941-fold lower potency against the Y56H/D168A variant. JZ01-15 and 5172-mcP1P3 exhibited a relatively flatter resistance profile, losing 200-400 fold in enzyme inhibition assays. In fact, of the inhibitors with a P2 quinoxaline moiety, JZ01-15 was the only compound with measurable activity against the double substitution variant in replicon assays (EC_{50} = 231 nM). Thus, although the extent of the loss of potency was dependent on the particular inhibitor, the Y56H/D168A variant was detrimental to potency against all the inhibitors.

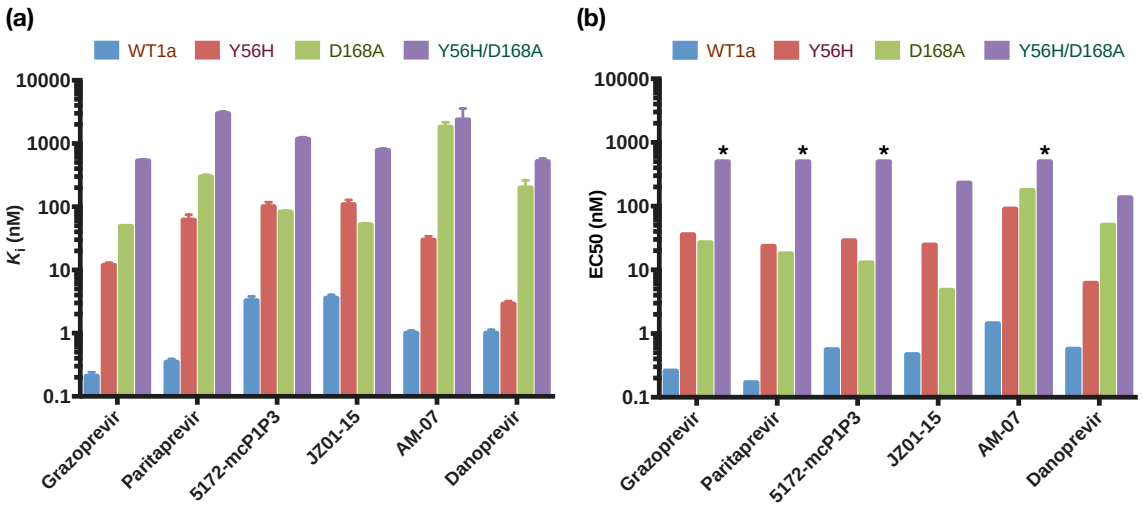

Figure 2.2: In vitro resistance profile of NS3/4A protease inhibitors.
(a) Enzyme inhibition constants (against protease domain) and (b) replicon-based half maximal effective concentrations for WT HCV NS3/4A and drug-resistant variants Y56H, D168A and Y56H/D168A. All inhibitors lost activity against the Y56H/D168A protease variant. * Indicates EC_{50} value greater than 500 nM.

Table 2.1: Inhibitory activity against GT1a HCV NS3/4A protease and drug resistant variants with fold changes with respect to GT1a wild-type, and the Michaelis-Menten constants (K_m) of the protease variants.

Inhibitor	***K*i (nM) (Fold change)**			
	GT1a WT	**Y56H**	**D168A**	**Y56H/D168A**
Grazoprevir	0.21 ± 0.03	11.9 ± 1.1 (57)	49.1 ± 1.6 (234)	531.7 ± 29.7 (2532)
Paritaprevir	0.35 ± 0.04	61.8 ± 13.1 (177)	297 ± 23 (849)	2974 ± 230 (8497)
5172-mcP1P3	3.29 ± 0.52	101 ± 17 (31)	82.4 ± 4.4 (25)	1179 ± 73 (358)
JZ01-15	3.60 ± 0.44	109 ± 19 (30)	52.0 ± 2.4 (14)	784 ± 50 (218)
AM-07	1.0 ± 0.1	29.7 ± 4.2 (29)	1823 ± 347 (1770)	2375 ± 1200 (2306)
MG-28	7.18 ± 1.02	205 ± 33 (29)	190 ± 13 (26)	1773 ± 394 (247)
Danoprevir	1.0 ± 0.1	2.9 ± 0.3 (3)	199 ± 64 (199)	520.3 ± 58.0 (520)
	K_m (µM)			
	7.9 ± 1.2	5.3 ± 0.5	1.3 ± 0.1	3.2 ± 0.4

Table 2.2: Antiviral activity against wild-type GT1a HCV and drug resistant variants, with fold changes with respect to wild-type.

Inhibitor	Replicon EC_{50} (nM) (Fold change)			
	GT1a	**Y56H**	**D168A**	**Y56H/D168A**
Grazoprevir	0.26	35.8 (138)	26.8 (103)	>500 (1923)
Paritaprevir	0.17	23.5 (138)	17.9 (105)	>500 (2941)
5172-mcP1P3	0.56	28.7 (51)	12.9 (23)	>500 (893)
JZ01-15	0.47	24.6 (52)	4.8 (10)	231 (491)
AM-07	1.43	90.6 (63)	177.7 (124)	>500 (350)
Danoprevir	0.57	6.2 (11)	50.6 (89)	136 (239)

2.3.2 Double mutant cycle analysis reveals interdependency of Tyr56 and Asp168 for most PIs

To delineate whether or not there is an interdependency between the two sites of mutation on the loss of inhibitor potency against the double substitution variant Y56H/D168A, the free energy of binding, ΔG (**Table 2.3**), was calculated for each inhibitor from the experimentally measured inhibition constants (**Table 2.1**). If the change in binding free energy (ΔΔG) to the double mutant relative to WT is equal to the sum of the free energy changes to each single mutant, then the substitutions are additive. If not, then the substitutions are coupled or interdependent in conferring resistance. This type of analysis is referred to as a double mutant cycle.[125] The double mutant cycle analysis revealed that the substitutions were not additive but coupled for most of the inhibitors with the exception of danoprevir (difference in ΔΔG only ~0.06 kcal/mol) (**Figure 2.3**), which does not stack on the catalytic residues. The interdependency was most pronounced in other inhibitors with differences in ΔΔG for the double mutant compared to sum of the single mutants of 0.45 kcal/mol for 5172-mcP1P3 and JZ01-15, and 1–2 kcals/mol for grazoprevir, paritaprevir and AM-07. Surprisingly, the substitutions were negatively coupled, with the two changes together having less impact on inhibitor binding than what would be predicted by the simple addition of each independently.

Table 2.3: Gibbs free energy of binding against HCV NS3/4A protease and drug resistant variants, calculated from the enzyme inhibition constants in Table S1.

Inhibitor	ΔG (kcal/mol)			
	GT1a	Y56H	D168A	Y56H/D168A
Grazoprevir	-12.97 ± 0.08	-10.62 ± 0.05	-9.79 ± 0.02	-8.41 ± 0.03
Paritaprevir	-12.67 ± 0.07	-9.66 ± 0.12	-8.75 ± 0.05	-7.40 ± 0.05
5172-mcP1P3	-11.37 ± 0.09	-9.37 ± 0.10	-9.49 ± 0.03	-7.94 ± 0.04
JZ01-15	-11.31 ± 0.07	-9.33 ± 0.10	-9.76 ± 0.03	-8.18 ± 0.04
AM-07	-12.04 ± 0.07	-10.08 ± 0.08	-7.69 ± 0.11	-7.54 ± 0.29
Danoprevir	-12.06 ± 0.06	-11.44 ± 0.06	-8.98 ± 0.19	-8.42 ± 0.06

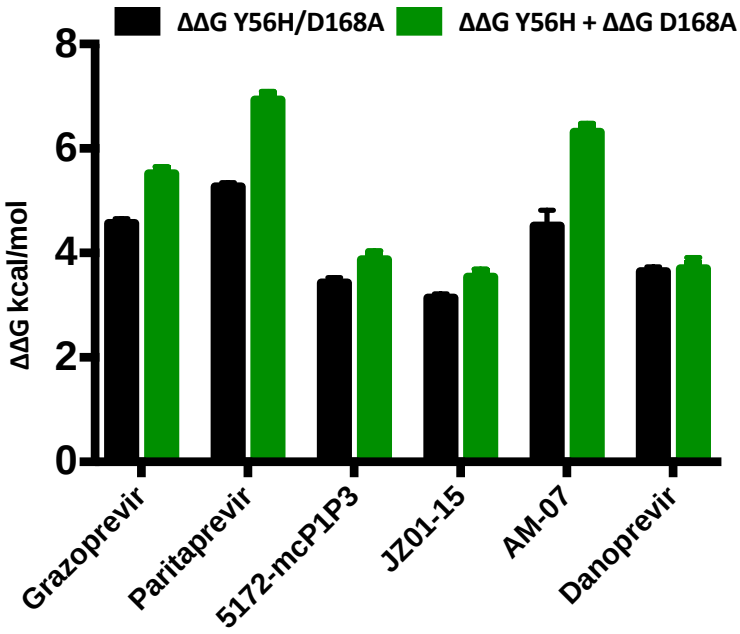

Figure 2.3: Double mutant cycle analysis of NS3/4A protease inhibitors. ΔΔG for each inhibitor used in the enzyme inhibition assay against the Y56H/D168A double substitution (black) and the sum of each single substitution (green). The substitutions Y56H and D168A show a coupled effect for grazoprevir, paritaprevir and AM-07. However, these substitutions are additive for danoprevir and to a lesser extent for 5172-mcP1P3 and JZ01-15.

2.3.3 Crystal structures of protease-inhibitor complexes

As danoprevir and grazoprevir represent the extremes of whether or not the impact of Y56H and D168A are additive or coupled, high-resolution crystal structures were determined of these inhibitors bound to Y56H/D168A and Y56H protease variants. The structures had resolutions ranging from 1.2–1.9 Å, and complemented our previously determined structures of danoprevir (PDB ID: 3M5L and 3SU1 for WT, and D168A respectively) and grazoprevir (3SUD and 3SUF for WT and D168A respectively).[89] In total three new structures of danoprevir–Y56H, danoprevir–Y56H/D168A and grazoprevir–Y56H were determined, but the grazoprevir–Y56H/D168A complex failed to crystalize despite extensive crystallization efforts (**Table 2.4**). These are the first co-crystal structures of NS3/4A PIs bound to either Y56H or the double substitution Y56H/D168A variant. These high-resolution structures afforded us atomic level details of protein-inhibitor interactions to elucidate the structural mechanism of resistance for NS3/4A PIs against the Y56H/D168A protease variant.

Table 2.4. X-ray data collection and crystallographic refinement statistics.

	Y56H-grazoprevir	**Y56H-danoprevir**	**Y56H/D168A-danoprevir**
PDB code	6C2M	6C2O	6C2N
Resolution	1.86 Å	1.18 Å	1.80 Å
Space group	$P2_1$	$P2_12_12_1$	$P2_12_12_1$
Twin Law	h,-k,-h-l		
Twin Fraction	0.26		
Molecules in AU[a]	4	1	1
Cell dimensions:			
a (Å)	56.6	55.4	60
b (Å)	103.3	59.0	55.4
c (Å)	74.0	60.0	58.9
β (°)	90	90	90
Completeness (%)	96.0	99.8	96.4
Total reflections	208132	528153	139059
Unique reflections	63506	65383	18030
Average I/σ	11.4	18.5	17.8
Redundancy	3.3	8.1	7.7
R_{sym} (%)[b]	6.6 (28.1)	6.9 (41.1)	9.8 (29.9)
RMSD[c] in:			
Bond lengths (Å)	0.005	0.015	0.009
Bond angles (°)	0.9	1.9	1.3
R_{factor} (%)[d]	18.1	12.3	16.2
R_{free} (%)[e]	22.4	14.4	19.0

[a]AU, asymmetric unit.
[b]$R_{sym} = \Sigma \mid I - \langle I \rangle \mid / \Sigma I$, where I = observed intensity, $\langle I \rangle$ = average intensity over symmetry equivalent; values in parentheses are for the highest resolution shell.
[c]RMSD, root mean square deviation.
[d]$R_{factor} = \Sigma \mid\mid F_o \mid - \mid F_c \mid\mid / \Sigma \mid F_o \mid$.
[e]R_{free} was calculated from 5% of reflections, chosen randomly, which were omitted from the refinement process.

2.3.4 Danoprevir resistance to the Y56H/D168A variant is solely due to the D168A substitution

Danoprevir is a P1–P3 macrocyclic NS3/4A inhibitor with an isoindoline P2 group. We previously elucidated the resistance mechanisms of this inhibitor against RASs by analyzing high-resolution crystal structures of danoprevir bound to WT and mutant proteases.[25] Comparing the structures of danoprevir bound to WT and Y56H proteases revealed that the binding mode and active site residues Arg155 and Asp168 are unchanged (**Figure 2.4A**). These results reinforced the inhibition data indicating danoprevir is not susceptible to Y56H, likely because the molecular contacts needed for efficient inhibitor binding are unaltered. In contrast, D168A substitution (**Figure 2.5**) resulted in a 0.8 Å shift of the Arg155 side chain away from residue Asp168, disrupting the cation-π interaction critical for danoprevir binding. Superposition of the D168A- and Y56H/D168A-protease structures showed that the active sites are almost identical (**Figure 2.4B**), in agreement with no further significant loss due to addition of Y56H and lack of coupling between the two substitutions for this inhibitor. Thus the D168A substitution alone underlies danoprevir resistance against the Y56H/D168A protease variant.

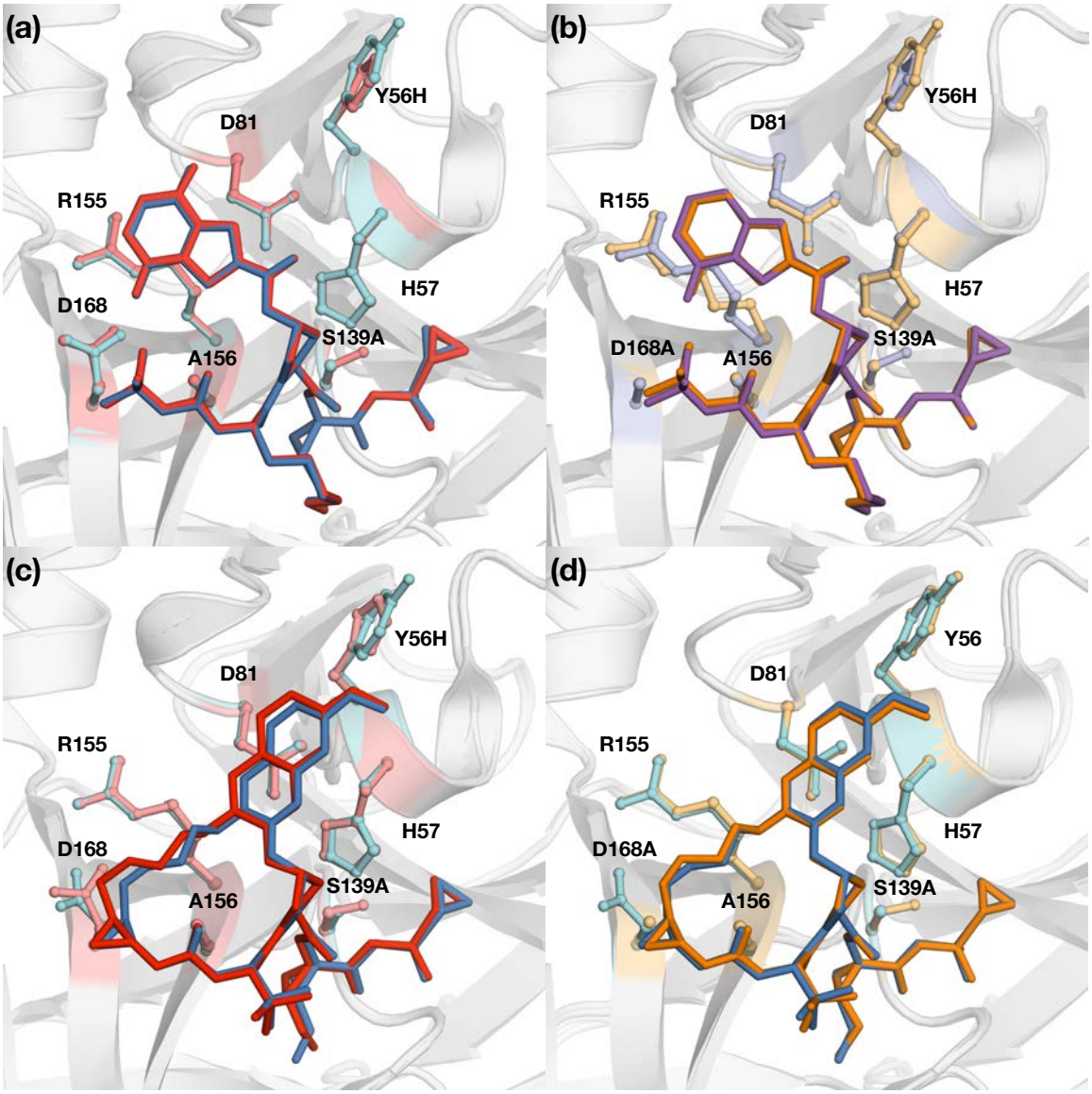

Figure 2.4: Crystal structures of danoprevir and grazoprevir bound to WT and mutant proteases.
Superposition of danoprevir bound to (a) WT (blue) and Y56H (red) and (b) D168A (orange) and Y56H/D168A (purple) proteases. Superposition of grazoprevir bound to (c) WT (blue) and Y56H (red) and (d) D168A (orange) proteases. Danoprevir's P2 isoindoline moiety occupies two conformations in the protease active site. Drug resistance residues and the catalytic triad residues His57, Asp81 and S139A are shown in sticks.

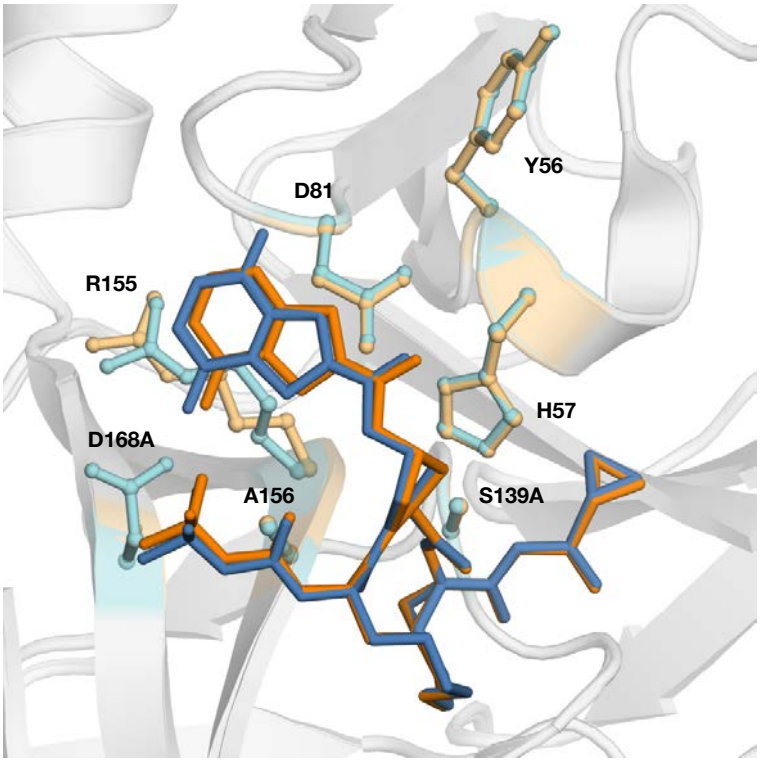

Figure 2.5: Crystal structure of danoprevir bound to WT and D168A HCV NS3/4A proteases.
Superposition of danoprevir bound to WT (blue) and D168A (orange) proteases. Danoprevir's P2 isoindoline moiety occupies two conformations in the protease active site. Drug resistance residues and the catalytic triad residues (His57, Asp81 and S139A) are shown as sticks.

To assess the molecular details of inhibitor packing, van der Waals (vdW) contact energies were calculated for danoprevir and protease active site for each crystal structure. Total vdW contact energies were conserved between WT and Y56H proteases (–83.6 and –82.6 kcal/mol, respectively) as well as D168A and Y56H/D168A proteases (–81.0 and –81.7 kcal/mol, respectively). Compared to WT protease, Y56H contact energy landscape was highly conserved (**Figure 2.6**), but disrupted in the D168A and Y56H/D168A complexes with reduced interactions in the S2-subsite around residue Asp168. Thus, structural changes due to substitution at residue Asp168 underlie resistance to the Y56H/D168A variant for danoprevir, which is expected to be valid for other inhibitors that primarily interact with S2 subsite residues.

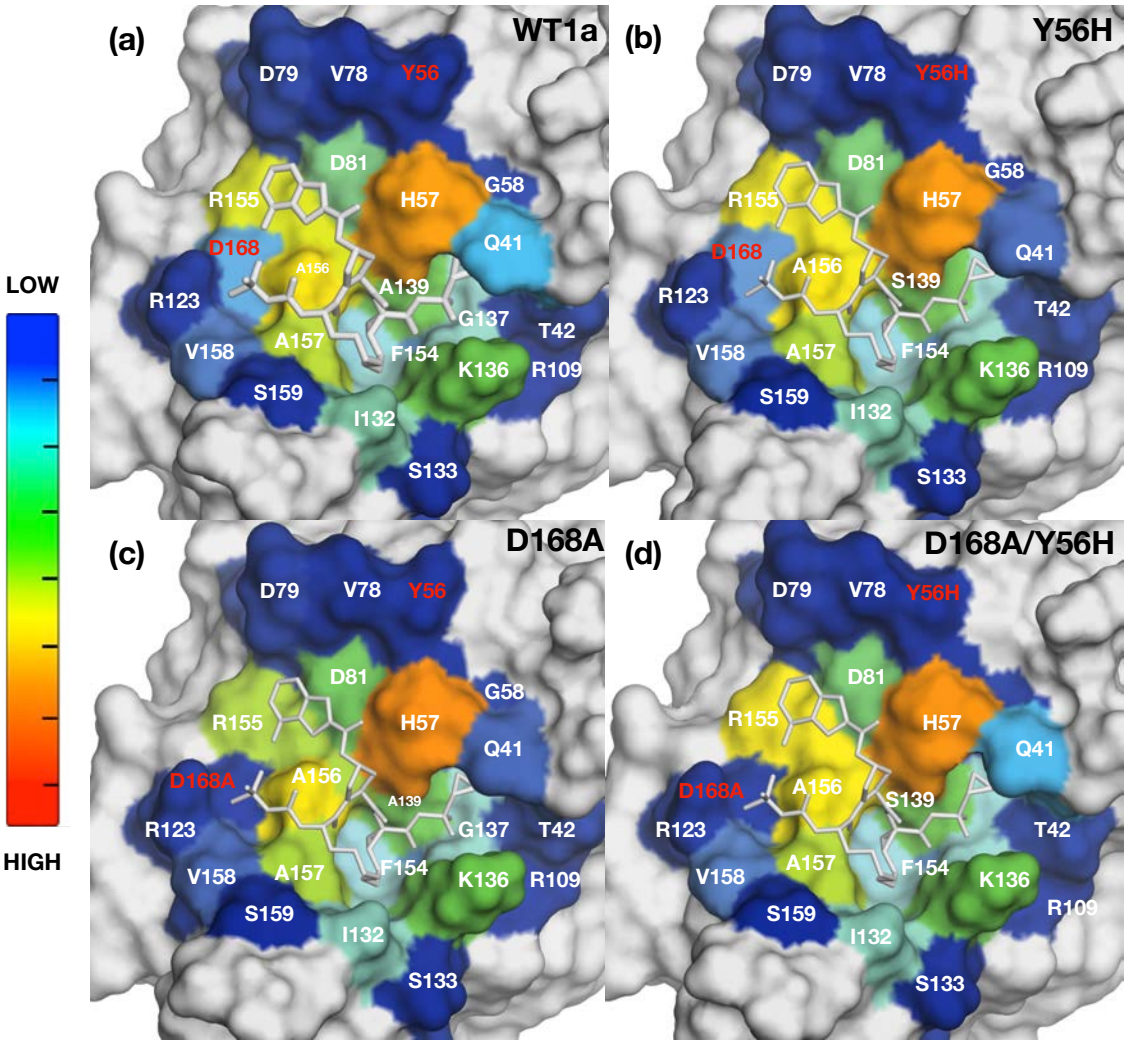

Figure 2.6: Packing of danoprevir in the active site of HCV NS3/4A protease variants.

The van der Waals (vdW) contact energies of danoprevir from crystal structures mapped onto the protease surface in (a) WT, (b) Y56H, (c) D168A and (d) Y56H/D168A proteases. The warmer (red) and cooler (blue) colors indicate more and less contacts with the inhibitor, respectively. Residues with substitutions among the variants are labeled in red.

2.3.5 Resistance mechanism of grazoprevir and analogs against single and double mutants

Grazoprevir is a P2–P4 macrocyclic inhibitor with a P2 quinoxaline moiety. Given that grazoprevir and analogs share a binding mode whereby the P2 quinoxaline moiety predominately interacts with the catalytic residues (His57 and Asp81), the mechanism of resistance against Y56H/D168A resistant protease was expected to differ from danoprevir.

The P1–P3 macrocyclic analogs of grazoprevir, JZ01-15, 5172-mcP1P3 and AM-07, exhibited resistance profiles similar to grazoprevir against the single and double substitution variants. JZ01-15 exhibited the best profile with similar activity against the D168A substitution as grazoprevir. We recently showed that P1–P3 macrocyclic inhibitors with small substitutions at the 3-position of the P2 quinoxaline, such as JZ01-15 and 5172-mcP1P2, maintain potency against single RASs.[124] In contrast, AM-07 has a larger thiophene-substituted quinoxaline that makes cation-π interactions with Arg155 and hydrophobic interactions with Tyr56. As a result of this binding mode, this inhibitor is highly susceptible to D168A, resulting in a higher loss in potency against the double substitution variant compared to grazoprevir and the other two analogs. Thus, structural features of the inhibitor, especially the identity of the P2 heterocyclic moiety, determine susceptibility to the Y56H/D168A protease variant.

To investigate the molecular basis of resistance conferred by Y56H substitution, grazoprevir crystal structures bound to WT and mutant protease were analyzed and compared. The comparative structural analysis revealed significant changes in inhibitor packing at the P2 quinoxaline and P2–P4 macrocycle region due to Y56H substitution. The P2 quinoxaline moiety moved away from the catalytic residue His57 toward the S2 subsite residues, weakening the critical π-π interactions between the quinoxaline and His57 ring (**Figure 2.4C**). His57 side chain adopted an alternate confirmation relative to WT, further affecting the stacking interactions with the P2 moiety. Moreover, Asp168 shifted closer to the Arg155 residue, exhibiting a conformation similar to other inhibitor-protease co-complexes.[89] Thus unlike danoprevir, the active site of protease and stacking of grazoprevir were perturbed by the Y56H substitution.

Compared to WT protease, the structure and binding mode of grazoprevir to D168A variant was minimally altered (**Figure 2.4D**). However, as we previously reported, grazoprevir resistance against the D168A variant is due to disruption of the ionic network between Arg155 and Asp168.[89] As indicated by the structural analysis, the individual Y56H and D168A substitutions have different mechanisms in conferring resistance, and combination of these substitutions cause a significant reduction in grazoprevir potency. However, whether Y56H and D168A substitutions together further alter inhibitor packing, or exacerbate the loss of critical interactions with the His57 ring observed in the Y56H co-complex is unclear.

2.3.6 Altered dynamics correlate with structural mechanisms of resistance

To interrogate the resistance mechanism against the double substitution variant further and complement our experimental data we turned to computational methods. Molecular dynamics simulations also augmented our structural analysis, as extensive crystallization efforts failed to result in a co-complex structure of grazoprevir bound to the Y56H/D168A protease, possibly due to the significant loss in binding affinity. Molecular dynamics simulations were performed to investigate the dynamic mechanism of resistance for both danoprevir and grazoprevir, as we have previously shown that changes in HCV protease dynamics underlie susceptibility to resistance.[111]

To assess inhibitor packing against the protease active site, inter-molecular vdW interactions were assessed over the MD trajectories for each residue at the active site (**Figures 2.7, 2.8**). Both single substitution and the double substitution variants showed an overall decrease in total vdW contact energies (5 kcal/mol and 10 kcal/mol, respectively) relative to WT protease for grazoprevir and danoprevir, consistent with the experimental loss in binding affinity. As expected, D168A substitution decreased contacts of this residue with grazoprevir in both the single and double substitution proteases (**Figures 2.7A-D, 2.8A**). Interestingly, the Y56H substitution not only decreased grazoprevir interactions at this position but also at other binding site residues, especially at the catalytic His57. This loss was compounded when D168A was combined with Y56H, with

considerable loss of contacts not only locally at the site of mutation but distributed throughout the binding site, including at residues Thr42, Gly58, and Gly137. There was a striking ~2.5 kcal/mol loss in vdW interactions of grazoprevir with His57 relative to WT protease, indicating that the addition of Y56H substitution to the D168A background causes severe loss of interactions with the neighboring catalytic His57 residue.

In contrast to grazoprevir, danoprevir binding to the active site was similar to WT when bound to each single and double substitution variant, with more localized loss of interactions due to the substitutions (**Figures 2.7E–5H, 2.8B**). While the D168A substitution caused decreased interactions with both this residue and the catalytic His57, the addition of Y56H alleviated this loss in the double substitution variant, in direct contrast to the case of grazoprevir. Overall, the binding landscape of danoprevir was relatively unaltered in the variants relative to WT protease in the dynamic analysis (**Figure 2.7**), similar to what was seen in the crystal structures (**Figure 2.6**).

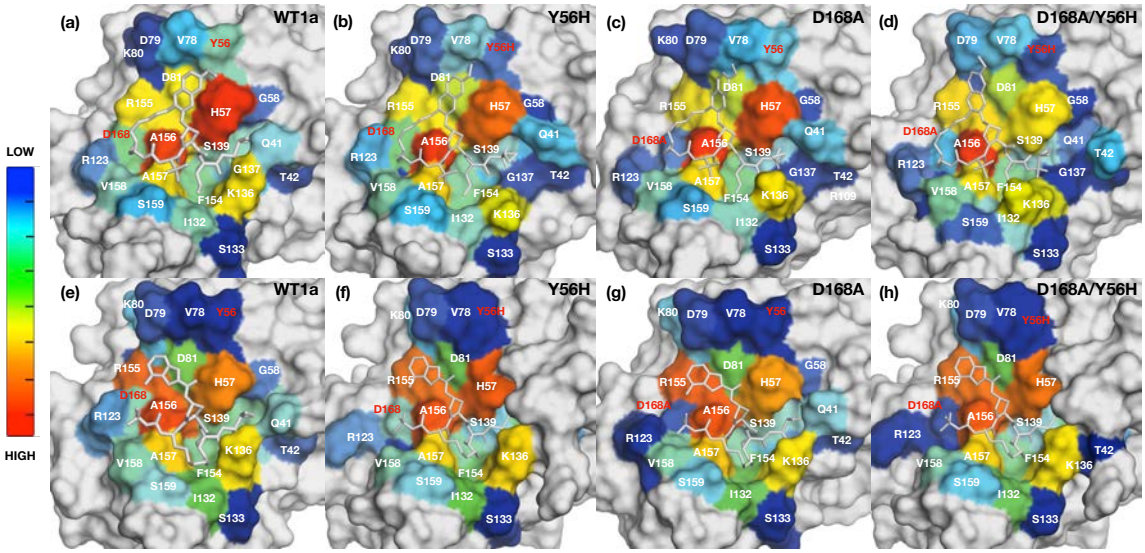

Figure 2.7: Packing of inhibitors in the NS3/4A protease active site during MD trajectories.

The van der Waals (vdW) contact potentials averaged from MD simulations of protease active site residues for grazoprevir bound to (a) WT1a, (b) Y56H, (c) D168A, (d) Y56H/D168A and danoprevir bound to (e) WT1a, (f) Y56H, (g) D168A, (h) and Y56H/D168A proteases, respectively. The warmer (red) and cooler (blue) colors indicate more and less contacts with the inhibitor, respectively. Drug resistance residues are highlighted in red.

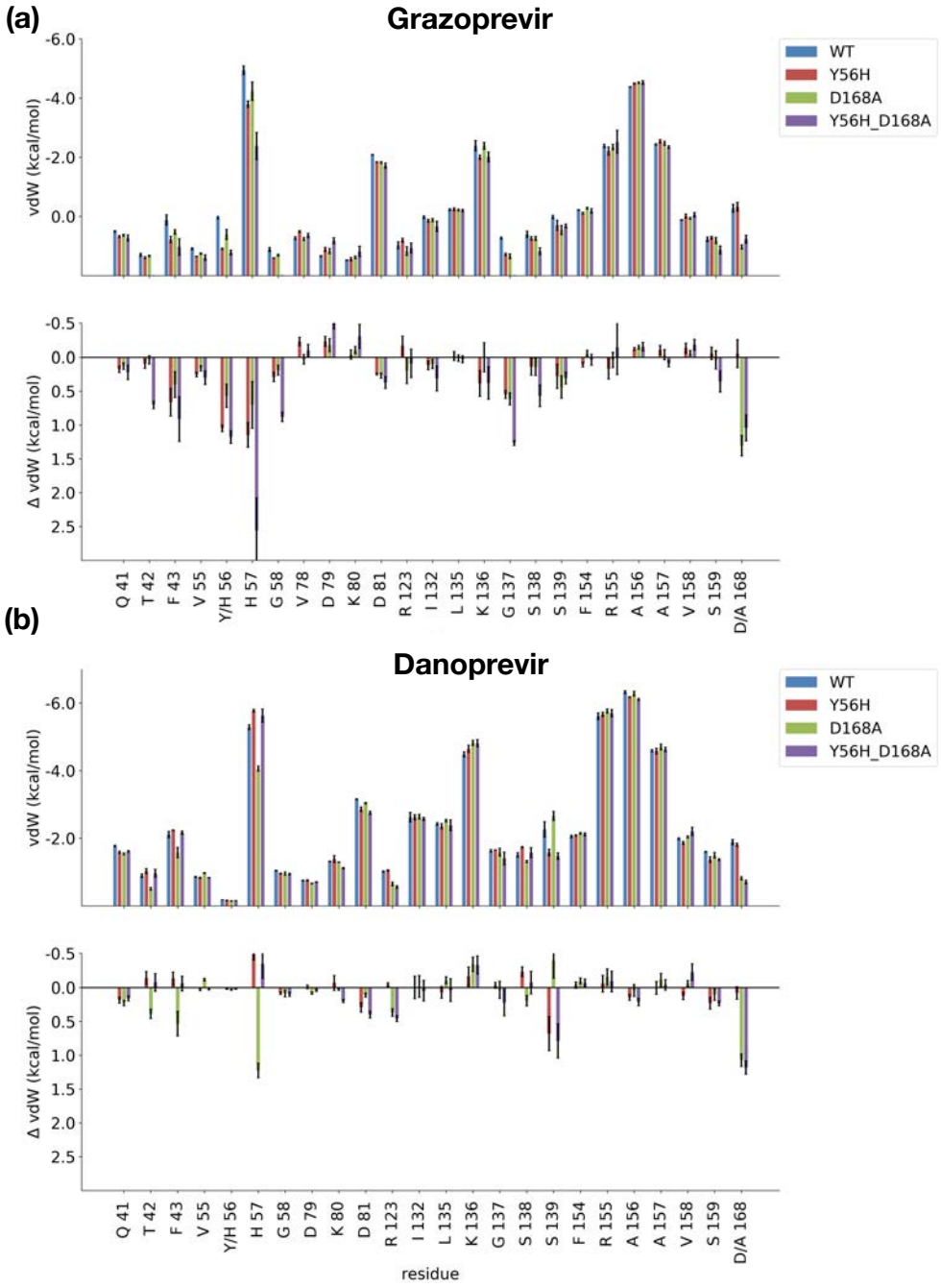

Figure 2.8: Inhibitor interactions with wildtype HCV NS3/4A protease and variants by residue.
The van der Waals (vdW) contact energies and change in vdW (ΔvdW) relative to wildtype for (a) grazoprevir, and (b) danoprevir bound to protease variants, calculated from MD trajectories. These vdW values are mapped onto the protease surface in **Figure 2.7**.

The loss of correlation of motions between the inhibitor and protease can be an indicator of resistance, as we have previously shown for GT3 HCV NS3/4A protease.[108] To examine the coupling of atomic fluctuations between the inhibitor and protease, the correlation coefficients between the inhibitor and the protease backbone were calculated (**Figure 2.9**). In the WT complex, the dynamics of grazoprevir were highly correlated with the motions of the residues in the active site (**Figure 2.9A**). This coupling was the most pronounced for active site residues 134–136 and 156–157, displaying correlations with all inhibitor moieties. The dynamics of the P1 and P1' moieties of grazoprevir were highly coupled to the dynamics of residue His57. Additionally, the dynamics of P2 quinoxaline, and P1 and P1' moieties were coupled with catalytic residue Asp81, and Leu82. Neither of these correlations was present when the Tyr56 was mutated to a histidine. Apart from this loss of correlations, Y56H substitution had only little effect on intra-molecular dynamics.

In contrast, the D168A substitution severely reduced the dynamic coupling of grazoprevir with the protease active site. In addition to the loss of P1 and P1' coupling with catalytic residues His57 and Asp81, correlation between the P2 quinoxaline and residues 132–138 were severely reduced. In the Y56H/D168A protease, the correlation of motions between grazoprevir and residues 132–138 was completely lost, in addition to severe weakening of the coupled dynamics between residue 157 and the inhibitor moieties. Thus, the loss of coupling between inhibitor and protease dynamics correlated with reduced inhibitor

potency against both the single mutant and the Y56H/D168A double substitution variant.

The dynamics of danoprevir–protease complexes were also in agreement with the structural mechanisms of resistance revealed from crystal structures (**Figure 2.9B**). In the WT complex, danoprevir dynamic coupling with active site residues were most pronounced at residues 56–58, 135–136 and 156–157. The correlations of danoprevir with the Y56H protease were essentially unaltered relative to WT complex. This similarity is in agreement with structural analysis, as the Tyr56 substitution does not impact the binding of danoprevir (**Figure 2.4**). In the D168A complex, correlations of the P1' moiety with residues 55–58 were reduced, while P2+ isoindoline moiety had increased correlations with residue K136, in agreement with increased intermolecular vdW contacts (**Figure 2.7**). In the Y56H/D168A variant, the correlations of motions were similar to those seen in the D168A variant. Thus, for inhibitors with binding modes similar to danoprevir, substitutions at Asp168 are the primary cause of resistance to the double substitution variant Y56H/D168A.

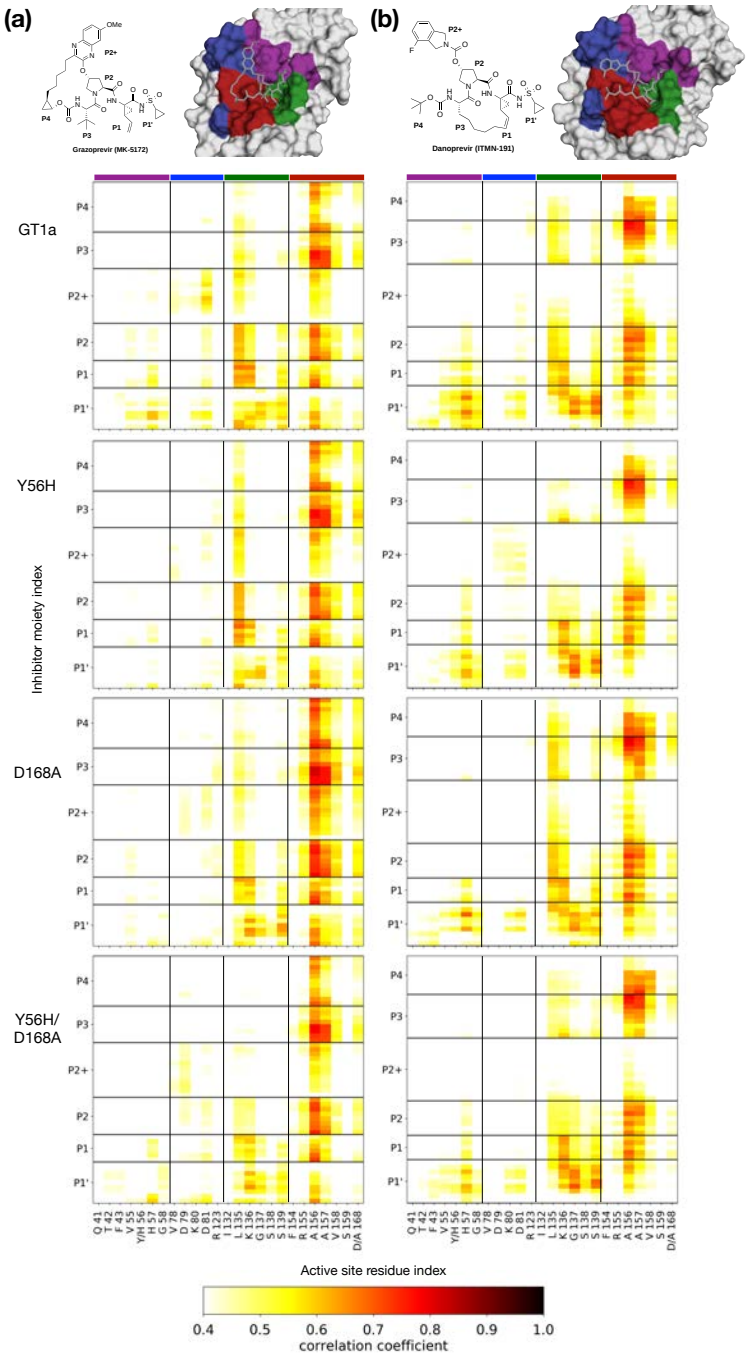

Figure 2.9: Cross-correlation coefficients of inhibitors and atomic fluctuations of active site residues mapped onto protease surface.
Protease-inhibitor dynamic coupling of (a) grazoprevir and (b) danoprevir bound to GT1a, Y56H, D168A, and Y56H/D168A proteases. Warm colors in the matrices indicate increased correlations. Residues are colored on the surface to indicate their location in the active site.

2.4 Discussion

Although drug resistance has been a major problem in the efficacy of anti-HCV therapeutics, especially for NS3/4A PIs, newer generation inhibitors are robust against single-site substitutions that were once detrimental to PI clinical viability. More importantly, there are currently two all-oral regimens that have pan-genotypic HCV activity including against the evasive GT3.[51] Though much progress has been made in anti-HCV therapeutics, a new challenge that may threaten the success of PIs is the emergence of viral variants with more than one substitution in the protease.[51,98] In this study we reveal the structural and dynamic mechanisms of drug resistance for the Y56H/D168A protease, a double-site RAS variant that has been identified in patients who failed therapy with PI-containing regimens.

The Y56H/D168A variant was resistant to all tested PIs, and the inhibitor binding mode determined the molecular mechanism of resistance. Prior to the development of grazoprevir, PIs typically contained large heterocyclic P2 moieties that strongly interacted with S2 subsite residues.[89,106] This binding mode resulted in detrimental loss of potency against single-site RASs in the protease active site, especially at residues Arg155 and Asp168.[89,106] In the inhibitor-bound state, HCV NS3/4A protease has an extensive active site electrostatic network that spans the catalytic triad residues His57 and Asp81 all the way to S2 subsite residues Arg155, Asp168 and Arg123. Residues Arg155 and Asp168, located beyond the substrate envelope, form a salt bridge that is critical to inhibitor

binding and disrupted upon substitution at either residue.[90] For inhibitors with a binding mode similar to danoprevir, disruption of this electrostatic network due to an Asp168 substitution causes rearrangement of the Arg155 side chain, resulting in the loss of favorable cation-π interactions between the P2 isoindoline and Arg155 guanidinium group.[89,109] For such inhibitors that do not stack on the catalytic residues and have no physical interactions with Tyr56, resistance to the double substitution is predominantly due to the D168A change. Thus the addition of Y56H substitution to D168A protease does not cause any further active site changes or loss in potency, and the individual Asp168 substitution is responsible for the decreased inhibitor binding affinity.

Grazoprevir and newer generation inhibitors have a P2 quinoxaline moiety that makes extensive interactions with the catalytic triad residues, reducing susceptibility to single-site RASs at the S2 subsite.[111] However, this binding mode causes vulnerability for grazoprevir and inhibitors with a similar binding mode to substitutions that result in loss of critical π-π stacking interactions with the catalytic residue His57. The crystal structure of grazoprevir bound to the Y56H protease determined here, reveals that this interaction is weakened when neighboring Tyr56 mutates to a smaller His residue. This loss is compounded in the double substitution Y56H/D168A variant, thereby destabilizing the binding of grazoprevir. The alterations due to the Y56H substitution and the double substitution Y56H/D168A are unlikely to impact the recognition and processing of the viral substrates (**Table S1**), as unlike grazoprevir the substrates do not stack

on the aromatic surface of the catalytic His57.[89,90,101] The substrates also make no direct contact with Tyr56, so substitutions at Tyr56 are unlikely to either directly or indirectly impact substrate turnover. As a general rule, the reliance of an inhibitor on interactions with the target that are not essential for biological function creates an opportunity for resistance causing substitutions.[89,111,126] When these interactions are within the substrate envelope or with catalytic residues, the chances of resistance emerging is minimized. Nevertheless, in this study we observe a new indirect mechanism of resistance to packing at the active site, that disrupts interactions with the catalytic residue through substitution in a neighboring residue not involved in substrate recognition.

Robustness of grazoprevir against single-site RASs has led to drug design efforts by pharmaceutical companies to pursue PIs with similar scaffolds to grazoprevir. Pan-genotypic PIs voxilaprevir and glecaprevir have a P2 quinoxaline and P2–P4 macrocycle as in grazoprevir. Considering the high similarity in the scaffolds of these latest-generation inhibitors, there is a danger that all PIs currently in clinic might be susceptible to the same resistant variants, including Y56H/D168A. While these inhibitors have low susceptibility to single-site substitutions at residues Arg155 and Asp168, they have selected for double substitution variants in *in vitro* studies.[51] In fact, *in vitro* resistance testing of glecaprevir selected for resistance against GT3 double substitution variant Y56H/Q168R losing almost 1400-fold in potency.[15] This suggests that double

substitution variants containing Y56H may emerge in other genotypes and reduce the clinical effectiveness of PIs.

Under increased drug pressure, more protease variants with more than one substitution will likely become clinically relevant. The accumulation of additional substitutions can allow RAS variants to emerge that alone are not viable, but in combination can rescue the viral fitness. We previously demonstrated that inhibitors with a P2–P4 macrocycle are highly susceptible to substitutions at Ala156, as a change to a larger side chain results in steric clashes with the inhibitor's macrocycle. Ala156 substitutions cause low replicative capacity, but additional changes at other positions in the NS3/4A protease can improve enzymatic activity and thus viral fitness, leading to clinically relevant variants. Voxilaprevir and glecaprevir also select for substitutions at Ala156 *in vitro*, which causes a large fold shift in inhibitor potency. Moreover, Ala156-Asp168 double substitutions have been selected *in vitro*, which improve fitness. Although not yet observed clinically, the A156T substitution if coupled with such a fitness-rescuing second substitution could cause resistance to all P2–P4 macrocyclic PIs with a P2 quinoxaline moiety. In fact, the additional substitution does not have to occur at the active site. We have shown in HIV-1 protease that active site and distal substitutions often occur in combination to confer resistance.[127] Similarly, glecaprevir selected substitutions at Ala156 in combination with Gln/Pro89 in GT 1a/b, which is located outside of the active site. This additional substitution at position 89 appears to have improved replicative efficiency to 100%.[51]

Understanding the molecular mechanisms of resistance and enzymatic fitness of these multi-substituted variants will be necessary to improve potency of PIs against emerging resistant variants.

One strategy used in rational drug design of PIs to avoid drug resistance is exploiting interactions with the catalytic triad residues. The catalytic triad residues are critical for the biological function of the protease and thus almost always invariant. However, we find that even though the catalytic residues themselves cannot mutate to confer resistance, this drug design strategy can be circumvented by selecting substitutions at other locations that disrupt critical inhibitor interactions of these residues. The Y56H substitution severely disrupts the favorable interactions of grazoprevir's P2 moiety with catalytic His57 residue. While exploiting interactions with evolutionarily constrained residues is still one of the best strategies for inhibitor design, diverse PIs need to be considered, preferably with enhanced interactions with the catalytic residues that cannot be disrupted by nearby changes in the protease active site. As new drugs and combinations are developed, drug resistance needs to be considered at the outset of inhibitor design to minimize the emergence of resistance. Additionally, the arsenal of PIs needs to be diversified, as the similarity in scaffold is likely to lead to cross-resistance and susceptibility to multi-substituted variants.

2.5 Methods

2.5.1 Inhibitor Synthesis

Grazoprevir, paritaprevir, danoprevir and grazoprevir analogs were synthesized in-house using previously reported methods. Grazoprevir was prepared following a reported synthetic method.[120] Paritaprevir, danoprevir, and grazoprevir analogs were synthesized similarly using our convergent reaction sequence as previously described, with minor modifications.[106]

2.5.2 Expression and Purification of NS3/4A Constructs

The HCV GT1a NS3/4A protease gene described in the Bristol Myers Squibb patent was synthesized by GenScript and cloned into a PET28a expression vector.[128] The D168A, Y56H and Y56H/D168A genes were engineered using the site-directed mutagenesis protocol from Stratagene. Protein expression and purification were carried out as previously described with minor modifications.[89] Briefly, transformed *Escherichia coli* BL21(DE3) cells were grown in TB media containing 30 µg/mL of kanamycin antibiotic at 37 °C. After reaching an OD_{600} of 0.8, cultures were induced with 1 mM IPTG and harvested after 3 h of expression. Cells were pelleted by centrifugation, resuspended in Resuspension buffer (RB) [50 mM phosphate buffer, 500 mM NaCl, 10% glycerol, 2 mM β-ME, pH 7.5] and frozen at −80 °C for storage.

Cell pellets were thawed and lysed via cell disruptor (Microfluidics Inc.) two times to ensure sufficient DNA shearing. Lysate was centrifuged at 19,000 rpm,

for 25 min at 4 °C. The soluble fraction was applied to a nickel column (Qiagen) pre-equilibrated with RB. The beads and soluble fraction were incubated at 4 °C for 1.5 h and the lysate was allowed to flow through. Beads were washed with RB supplemented with 20 mM imidazole and eluted with RB supplemented with 200 mM imidazole. The eluent was dialyzed overnight (MWCO 10 kD) to remove the imidazole, and the His-tag was simultaneously removed with thrombin treatment. The eluate was judged >90% pure by polyacrylamide gel electrophoresis, concentrated, flash frozen, and stored at −80 °C.

2.5.3 Determination of the Inner Filter Effect

The inner filter effect (IFE) for the NS3/4A protease substrate was determined using a previously described method.[129] Briefly, fluorescence end-point readings were taken for substrate concentrations between 0 µM and 20 µM. Afterward, free 5-FAM fluorophore was added to a final concentration of 25 µM to each substrate concentration and a second round of fluorescence end-point readings was taken. The fluorescence of free 5-FAM was determined by subtracting the first fluorescence end point reading from the second round of readings. IFE corrections were then calculated by dividing the free 5-FAM florescence at each substrate concentration by the free 5-FAM florescence at zero substrate.

2.5.4 Determination of Michaelis–Menten (K_m) Constant

K_m constants for GT1 and D168A protease were previously determined.[106] The K_m of Y56H and Y56H/D168A proteases were determined using the following method. A 20 μM concentration of substrate [Ac-DE-Dap(QXL520)- EE-Abu-γ-[COO]AS-C(5-FAMsp)-NH2] (AnaSpec) was serially diluted into assay buffer [50 mM Tris, 5% glycerol, 10 mM DTT, 0.6 mM LDAO, and 4% dimethyl sulfoxide] and proteolysis was initiated by rapid injection of 10 μL protease (final concentration 20 nM) in a reaction volume of 60 μL. The fluorescence output from the substrate cleavage product was measured kinetically using an EnVision plate reader (Perkin-Elmer) with excitation wavelength at 485 nm and emission at 530 nm. Inner filter effect corrections were applied to the initial velocities (V_o) at each substrate concentration. V_o versus substrate concentration graphs were globally fit to the Michaelis–Menten equation to obtain the K_m value.

2.5.5 Enzyme Inhibition Assays

For each assay, 2 nM of NS3/4A protease (GT1a, Y56H, D168A and Y56H/D168A) was pre-incubated at room temperature for 1 h with increasing concentration of inhibitors in assay buffer (50 mM Tris, 5% glycerol, 10 mM DTT, 0.6 mM LDAO, and 4% dimethyl sulfoxide, pH 7.5). Inhibition assays were performed in non-binding surface 96-well black half-area plates (Corning) in a reaction volume of 60 μL. The proteolytic reaction was initiated by the injection of 5 μL of HCV NS3/4A protease substrate (AnaSpec), to a final concentration of

200 nM and kinetically monitored using a Perkin Elmer EnVision plate reader (excitation at 485 nm, emission at 530 nm). Three independent data sets were collected for each inhibitor with each protease construct. Each inhibitor titration included at least 12 inhibitor concentration points, which were globally fit to the Morrison equation to obtain the K_i value. Gibbs free energy of binding was calculated using the following equation: $\Delta G = RT\ln K_i$

2.5.6 Cell-Based Drug Susceptibility Assays

Mutations (Y56H, D168A, and Y56H/D168A) were constructed by site-directed mutagenesis using a Con1 (genotype 1b) luciferase reporter replicon containing the H77 (genotype 1a) NS3 sequence.[130] Replicon RNA of each protease variant was introduced into Huh7 cells by electroporation. Replication was then assessed in the presence of increasing concentrations of protease inhibitors by measuring luciferase activity (relative light units) 96 h after electroporation. The drug concentrations required to inhibit replicon replication by 50% (EC_{50}) were calculated directly from the drug inhibition curves.

2.5.7 Crystallization and structure determination

Protein expression and purification were carried out as previously described.[89] The Ni-NTA purified WT1a protein was thawed, concentrated to 3 mg/mL, and loaded on a HiLoad Superdex75 16/60 column equilibrated with gel filtration buffer (25 mM MES, 500 mM NaCl, 10% glycerol, and 2 mM DTT, pH

6.5). The protease fractions were pooled and concentrated to 25 mg/mL with an Amicon Ultra-15 10 kDa filter unit (Millipore). The concentrated samples were incubated for 1 h with 3:1 molar excess of inhibitor. Diffraction-quality crystals were obtained overnight by mixing equal volumes of concentrated protein solution with precipitant solution (20–26% PEG-3350, 0.1 M sodium MES buffer, 4% ammonium sulfate, pH 6.5) at RT or 15 °C in 24-well VDX hanging drop trays. Crystals were harvested and data was collected at 100 K. Cryogenic conditions contained the precipitant solution supplemented with 15% glycerol or ethylene glycol.

X-ray diffraction data were collected at Advance Photon Source beamline 23-ID-B or our in-house Rigaku X-ray system with a Saturn 944 detector. All datasets were processed using HKL-3000.[131] Structures were solved by molecular replacement using PHASER.[132] Model building and refinement were performed using Coot[133] and PHENIX,[134] respectively. The final structures were evaluated with MolProbity[135] prior to deposition in the PDB. To limit the possibility of model bias throughout the refinement process, 5% of the data were reserved for the free R-value calculation.[136] Structure analysis, superposition and figure generation were done using PyMOL.[137] X-ray data collection and crystallographic refinement statistics are presented above (**Table 2.4**).

2.5.8 System Preparation for Molecular Dynamics Simulations

Crystal structures of HCV protease bound to grazoprevir were taken from the Protein Databank (PDB IDs 3SUD and 3SUF).[89] When there were multiple copies of the protease–inhibitor complex in the crystallographic unit, the complex with the lowest overall B-Factors was chosen. In the case of the double substitution variant, the complex was modeled *in silico* using the Prime structure prediction wizard.[138] Protein structures were then prepared for simulation using the Protein Preparation Wizard from the Schrodinger Suite,[139] keeping all co-crystallized water molecules. Missing atom were added using Prime.[140] The protonation state of the protein side chains at pH 7.0 was determined using PROPKA.[141,142] The hydrogen bond network was optimized by exhaustive sampling of the orientation of crystallographic waters and side chains of polar amino acids. Finally, the structure was subjected to gradient minimization with convergence criterion 0.5 Å using Impref.[143]

2.5.9 Molecular Dynamics Simulations

Molecular dynamic simulations of protein-inhibitor complexes were carried out as previously described.[127] The protein-inhibitor complex was placed in a cubic solvent box maintaining at least 1.5 nm spacing between any solute atom and the box boundaries. The system's net charge was neutralized by adding chloride ions; additionally, sodium and chloride ions were added to a total salt concentration of 0.15 M.

MD simulations were carried out using the Desmond software suite.[144] Protein and ligand were parameterized using the OPLS3 force field.[145] For the water molecules, TIP3P force field parameters were used.[146] During simulations, long-range electrostatic forces were calculated using the Particle Mesh Ewald method.[147] Short-range non-bonded forces were truncated smoothly at 1.2 nm. The RESPA integrator was used with a 2 fs time step for bonded and short-range non-bonded forces and a 6 fs time step for long-range electrostatic forces.[148]

Before running MD simulations, the solvated system was energy minimized using a stepwise protocol. In the first iteration, all solvent molecules were minimized using 10 steepest decent steps followed by up to 5000 L-BSFG minimization steps. The convergence criterion was an energy gradient of 0.5 kcal mol^{-1} $Å^{-1}$ while applying solute heavy atoms a force constant of 1000 kcal mol^{-1} $Å^{-2}$. In the second iteration only the backbone restraints were kept and the system was subjected to the same minimization procedure as in the first iteration. In the third step, the restraints on the backbone heavy atoms were lowered to 5 kcal mol^{-1} $Å^{-2}$. For the final minimization step, all restraints were removed and the system was minimized using the L-BFSG method until an energy gradient of 0.05 kcal mol^{-1} $Å^{-1}$ was reached.

Following minimization, a number of short MD simulations were performed to equilibrate the system. Initially a 12 ps simulation in the NVT ensemble using the Berendsen thermostat at 10 K was performed. The backbone position was restrained using a force constant of 50 kcal mol^{-1} $Å^{-2}$. This was followed by a 24

ps simulation in the NPT ensemble maintaining the restraints on the protein backbone. Subsequently a 50 ps unrestrained NPT simulation was run during which the temperature was increased from 10 K to the target temperature of 300 K. This was followed by a 500 ps NPT simulation at 300 K allowing the system to thermalize. The final production stage consisted of a 100 ns simulation in the NPT ensemble at 300 K and 1bar. Atomic coordinates were recorded every 5 ps. All simulations were run in triplicate using the aforementioned protocol.

2.5.10 Correlated Motions

To measure both linear and non-linear correlated protein dynamics, the Linear Mutual Information between atom pairs was calculated. This is based on the approach proposed by Lange and Grubmueller.[149] Briefly, correlated dynamics were measured by calculating their mutual information $I[x;y] = \sum_{x;y} \frac{p(x;y)}{p(x)P(y)}$ where x and y are two sets of atomic coordinates, p(x) and p(y) are there marginal probability distributions and p(x;y) is the joint probability distribution. If the two atoms x and y are fully independent the joint probability distribution p(x;y) equals the sum of its marginal probability distributions, thus I[x;y] becomes 0. If the two atoms are not completely independent I[x;y] assumes a positive value. To improve interpretability the mutual information I(x;y) is subsequently transformed into the generalized correlation coefficient $r_{MI}[x;y] = \sqrt{\{1 - \exp(-2I[x;y]/d)\}}$ with d=3 since x and y are Euclidean coordinates. $r_{MI}[x;y]$ has a value of 0 for fully independent motions and a value of 1 for fully

coupled dynamics. To calculate the generalized correlation coefficient, snapshots were taken from a trajectory at 5ps intervals. Global, translational and rotational motions were minimized by aligning all snapshots to the first frame of the trajectory. Pairwise and marginal probability distribution were estimated by a Gaussian distribution. This approach has the advantage to capture both linear and non-linear correlated motions while avoiding computationally more demanding density estimates.

2.6 Acknowledgements

This research used resources of the Advanced Photon Source, a U.S. Department of Energy (DOE) Office of Science User Facility operated for the DOE Office of Science by Argonne National Laboratory under Contract No. DE-AC02-06CH11357. We thank beam line specialist at 23-ID-B for their help in data collection. This work was supported by a grant from the National Institute of Allergy and Infectious Diseases of the NIH (R01 AI085051). ANM was also supported by the National Institute of General Medical Sciences of the NIH (F31 GM119345). We thank Profs. Brian Kelch, Daniel Bolon, Paul Thompson and William Royer for helpful discussions.

Chapter III

Hepatitis C Virus NS3/4A Protease Inhibitors Incorporating Flexible P2 Quinoxalines Target Drug Resistant Viral Variants

Preface

Chapter III is a collaborative study that has been previously published.

Reprinted with permission from:

Matthew, A. N.; Zephyr, J.; Hill, C. J.; Jahangir, M.; Newton, A.; Petropoulos, C. J.; Huang, W.; Kurt Yilmaz, N.; Schiffer, C. A.; Ali, A. Hepatitis C virus NS3/4A protease inhibitors incorporating flexible P2 quinoxalines target drug resistant viral variants. *J. Med. Chem.* **2017,** 60, 5699–5716

Contributions from Ashley N. Matthew:

I participated in the synthesis of compounds for the SAR studies. I performed protein expression, purification and solved two crystal structures for this study. I also performed all enzyme inhibition studies against GT1a, GT3a and D168A proteases. I performed the structural analysis and interpretation of both structural and biochemical data with the guidance of my thesis mentor Celia A. Schiffer and Akbar Ali. Additionally, I wrote the manuscript with Akbar Ali with input from both Celia A. Schiffer and Nese Kurt Yilmaz.

3.1 Abstract

A substrate envelope-guided design strategy is reported for improving the resistance profile of HCV NS3/4A protease inhibitors. Analogues of 5172-mcP1P3 were designed by incorporating diverse quinoxalines at the P2 position that predominantly interact with the invariant catalytic triad of the protease. Exploration of structure-activity relationships showed that inhibitors with small hydrophobic substituents at the 3-position of P2 quinoxaline maintain better potency against drug resistant variants, likely due to reduced interactions with residues in the S2 subsite. In contrast, inhibitors with larger groups at this position were highly susceptible to mutations at Arg155, Ala156 and Asp168. Excitingly, several inhibitors exhibited exceptional potency profiles with EC_{50} values ≤ 5 nM against major drug resistant HCV variants. These findings support that inhibitors designed to interact with evolutionarily constrained regions of the protease, while avoiding interactions with residues not essential for substrate recognition, are less likely to be susceptible to drug resistance.

3.2 Introduction

Hepatitis C virus (HCV) infects over 130 million people globally and is the leading cause of chronic liver disease, cirrhosis, and hepatocellular carcinoma.[1] HCV is known as a “silent killer” as a majority of affected patients remain unaware of their infection, and over time the acute infection progresses to chronic liver disease.[150] The rate of cirrhosis is estimated to increase from 16%

to 32% by the year 2020 due to the high number of untreated patients.[151] Thus, there is an urgent need to ensure that patients infected with HCV receive proper treatment. However, HCV infection is difficult to treat, as the virus is genetically diverse with six known genotypes (genotype 1–6), each of which is further sub-divided into numerous subtypes.[6] Genotype 1 (GT1) and genotype 3 (GT3) are the most prevalent accounting for 46% and 30% of global infections, respectively.[6,7] Therapeutic regimen and viral response are largely genotype dependent with most treatments being efficacious only against GT1.[22]

The recent advent of direct-acting antivirals (DAAs) targeting essential viral proteins NS3/4A, NS5A, and NS5B has remarkably improved therapeutic options and treatment outcomes for HCV infected patients.[22,23] Four new all-oral combination treatments have been approved by the US FDA: (1) sofosbuvir/ledipasvir,[152] (2) ombitasvir/paritaprevir/ritonavir/dasabuvir,[40] (3) elbasvir/grazoprevir,[41] and (4) sofosbuvir/velpatasvir.[42] The DAA-based therapies are highly effective against GT1 with sustained virological response (SVR) rates greater than 90%.[22,23] However, most of the FDA approved treatments and those in clinical development are not efficacious against other genotypes, especially GT3.[23] Moreover, except for sofosbuvir, all current DAAs are susceptible to drug resistance.[107] Therefore, more robust DAAs need to be developed with higher barriers to drug resistance and a broad spectrum of activity against different HCV genotypes.

The HCV NS3/4A protease is a major therapeutic target for the development of pan-genotypic HCV inhibitors.[153,154] The NS3/4A protease inhibitors (PIs) telaprevir[155] and boceprevir[156] were the first DAAs approved for the treatment of HCV GT1 infection in combination therapy with pegylated-interferon and ribavirin.[31,33] Three recently approved PIs, simeprevir,[85] paritaprevir[91] and grazoprevir[120] are integral components of various combination therapies currently used as the standard of care for HCV infected patients.[22,23,154] Two other NS3/4A PIs, asunaprevir[81] and vaniprevir,[88] have been approved in Japan. In addition, a number of next generation NS3/4A PIs are in clinical development including glecaprevir[45] and voxilaprevir[121] (**Figure 3.1**).

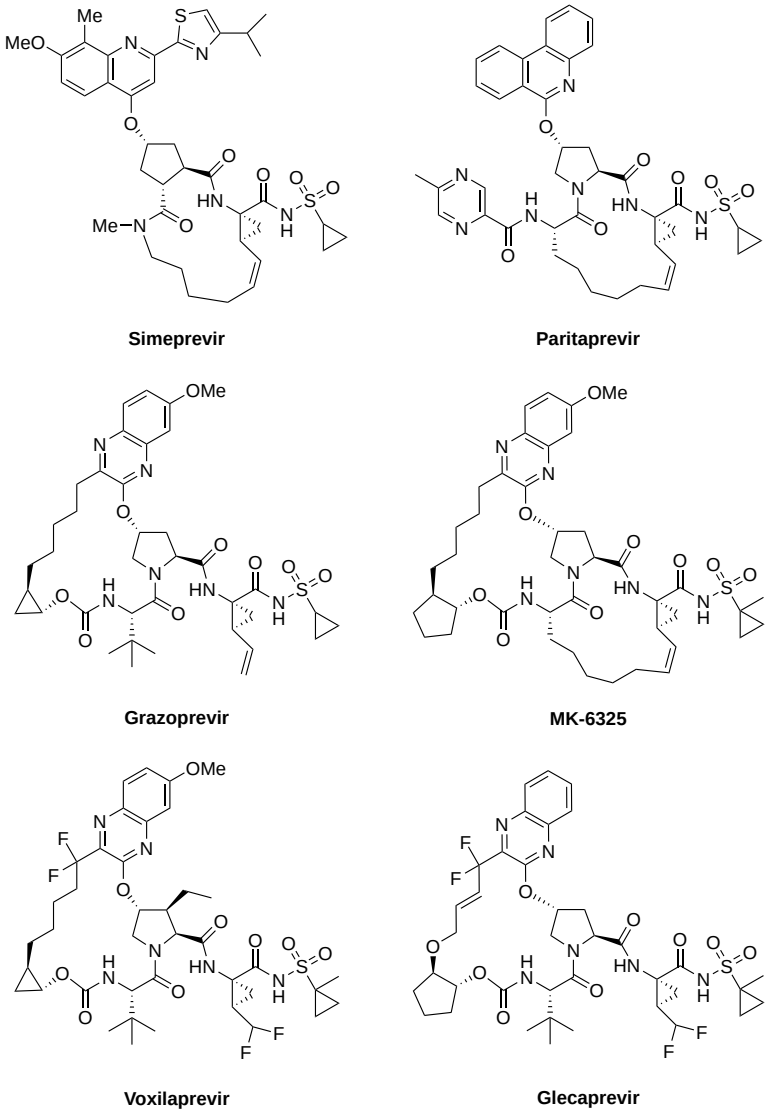

Figure 3.1: Chemical structures of HCV NS3/4A protease inhibitors.
Simeprevir, paritaprevir and grazoprevir are approved by the FDA; voxilaprevir and glecaprevir are in clinical development.

All NS3/4A PIs share a common peptidomimetic scaffold and are either linear or macrocyclic; the macrocycle is located either between P1–P3 or P2–P4 moieties.[154] In addition, these inhibitors contain a large heterocyclic moiety attached to the P2 proline, which significantly improves inhibitor potency against wild-type (WT) NS3/4A protease.[80,157] However, all NS3/4A PIs are susceptible to drug resistance, especially due to single site mutations at protease residues Arg155, Ala156 and Asp168.[92,158] Notably, D168A/V mutations are present in nearly all patients who fail treatment with PIs.[107] Moreover, natural polymorphisms at this position are responsible for significantly reduced inhibitor potency against GT3.[122] We previously determined the molecular mechanisms of drug resistance due to single site mutations by solving high-resolution crystal structures of PIs bound to WT and mutant proteases.[89,90,108,123] These crystal structures revealed that the large heterocyclic P2 moieties of PIs bind outside the substrate binding region, defined as the substrate envelope, and make extensive interactions with residues Arg155, Ala156 and Asp168.[89,123] The inhibitor P2 moiety induces an extended S2 subsite by forcing the Arg155 side chain to rotate nearly 180° relative to its conformation in substrate complexes.[90] This altered Arg155 conformation is stabilized by electrostatic interactions with Asp168, providing additional hydrophobic surface that is critical for efficient inhibitor binding. Disruption of electrostatic interactions between Arg155 and Asp168 due to mutations underlies drug resistance against NS3/4A PIs.[89,90,109,123] Moreover,

we have shown that structural differences at the P2 moiety largely determine the resistance profile of these inhibitors.[106]

Grazoprevir (MK-5172, **1**), one of the most potent HCV NS3/4A PIs, has a unique binding mode where the P2 quinoxaline moiety interacts with residues of the catalytic triad, avoiding direct interactions with Arg155 and Asp168 (**Figure 3.2**).[89] As a result, **1** has an excellent potency profile across different genotypes and relatively low susceptibility to drug resistance due to mutations at Arg155 and Asp168.[96,120] However, **1** is highly susceptible to mutations at Ala156, mainly due to steric clashes of larger side chains with the P2–P4 macrocycle. We have shown that the P1–P3 macrocyclic analogue 5172-mcP1P3 (**2**) avoids this steric clash while still maintaining the unique binding mode of **1** (**Figure 3.2**).[111] Compound **2**, though slightly less potent than **1** against WT HCV, has an excellent potency profile with EC_{50} values in the single digit nanomolar range against drug resistant variants including A156T. Similar to **1**, the P2 quinoxaline moiety in **2** stacks against the catalytic residues His57 and Asp81 and largely avoids direct interactions with residues around the S2 subsite.[111] But unlike **1**, the flexible P2 quinoxaline moiety in **2** better accommodates mutations at Ala156, resulting in an overall improved resistance profile.[106,111] Thus, the P1–P3 macrocyclic analogue **2** is a promising lead compound for structure-activity relationship (SAR) studies to further improve potency against drug resistant variants and other genotypes.

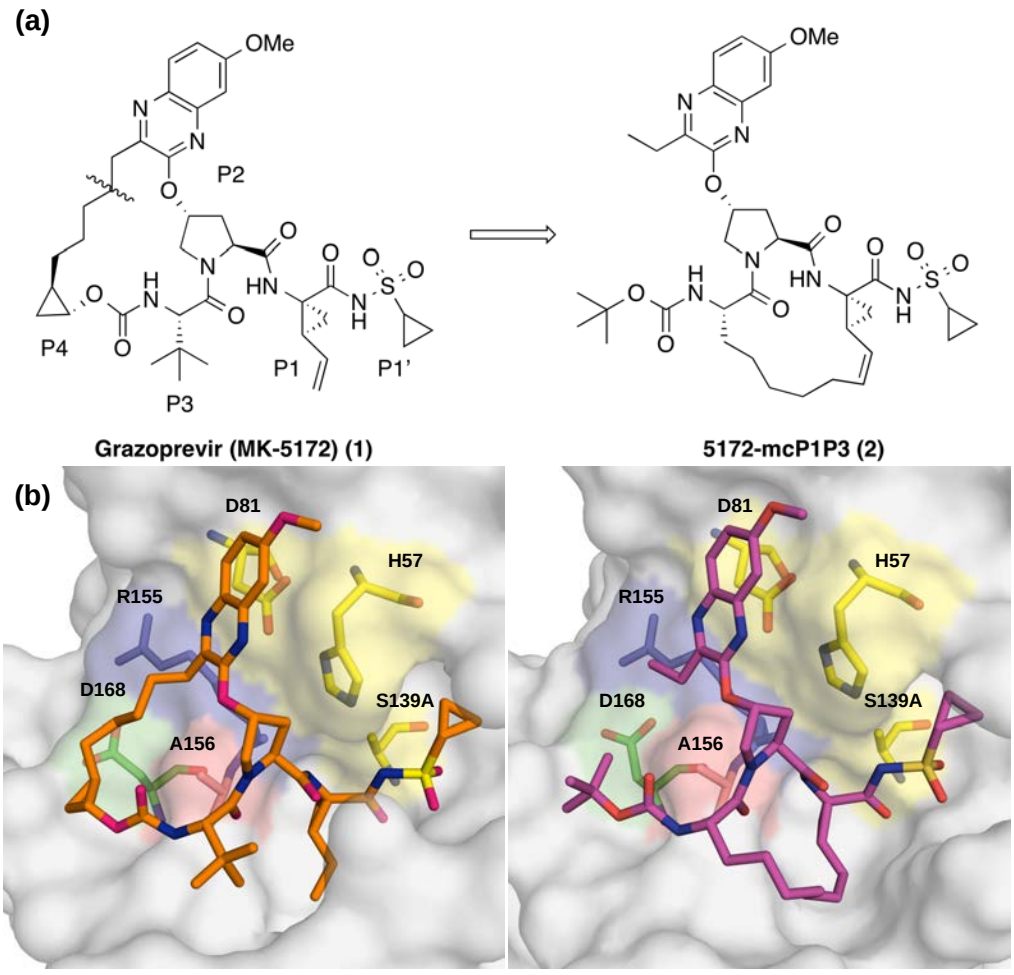

Figure 3.2: Chemical structures and binding modes of grazoprevir (1) and analogue 2.

(a) Compound **2** was designed by replacing the P2–P4 macrocycle in **1** with a P1–P3 macrocycle. (b) The binding conformation of **1** (PDB code: 3SUD) and **2** (PDB code: 5EPN) in the active site of wild-type NS3/4A protease. Compound **2** maintains the unique binding mode of **1** whereby the P2 quinoxaline makes strong interactions with the catalytic residues avoiding contacts with known drug resistance residues. The catalytic triad is highlighted in yellow and drug resistance residues Arg155, Ala156, and Asp168 are shown in blue, red and green, respectively. The canonical nomenclature for drug moiety positioning is indicated using grazoprevir.

The substrate envelope model provides a rational approach to design NS3/4A PIs with improved resistance profiles by exploiting interactions with the protease residues essential for function and avoiding direct contacts with residues that can mutate to confer drug resistance.[159-161] Another approach applied to design PIs with improved resistant profiles involves incorporation of conformational flexibility that can allow the inhibitor to adapt to structural changes in the protease active site due to mutations.[109] Here, we describe a structure-guided strategy that combines these two approaches and, together with our understanding of the mechanisms of drug resistance, led to the design of NS3/4A PIs with exceptional potency profiles against major drug resistant HCV variants. Based on the lead compound **2**, a series of analogues were designed and synthesized with diverse substituents at the 3-position of P2 quinoxaline moiety. Investigation of SARs identified P2 quinoxaline derivatives that predominantly interact with the invariant catalytic triad and avoid contacts with the S2 subsite residues. The results indicate that combining the substrate envelope model with optimal conformational flexibility provides a general strategy for the rational design of NS3/4A PIs with improved resistance profiles.

3.3 Chemistry

The NS3/4A PIs with diverse P2 quinoxaline moieties were synthesized using the reaction sequence outlined in **Scheme 3.1**. A Cs_2CO_3-mediated S_N2 reaction of 3-substituted quinoxalin-2-ones **8a-g** with the activated proline derivative **3**

provided the key P2 intermediates **9a-g** in 75–90% yield. The alternate S_NAr reaction between activated quinoxaline derivatives and Boc-protected hydroxy-proline resulted in lower yields, and purification of the resulting P2 acid products was significantly more challenging. The 3-substituted 7-methoxy-quinoxalin-2-ones **8a-b** and **8d-e** were prepared by condensation reactions of 4-methoxybenzene-1,2-diamine with the corresponding ethyl glyoxylates. The 3-chloro-7-methoxyquinoxalin-2-one **8c** was prepared according to a reported method.[120]

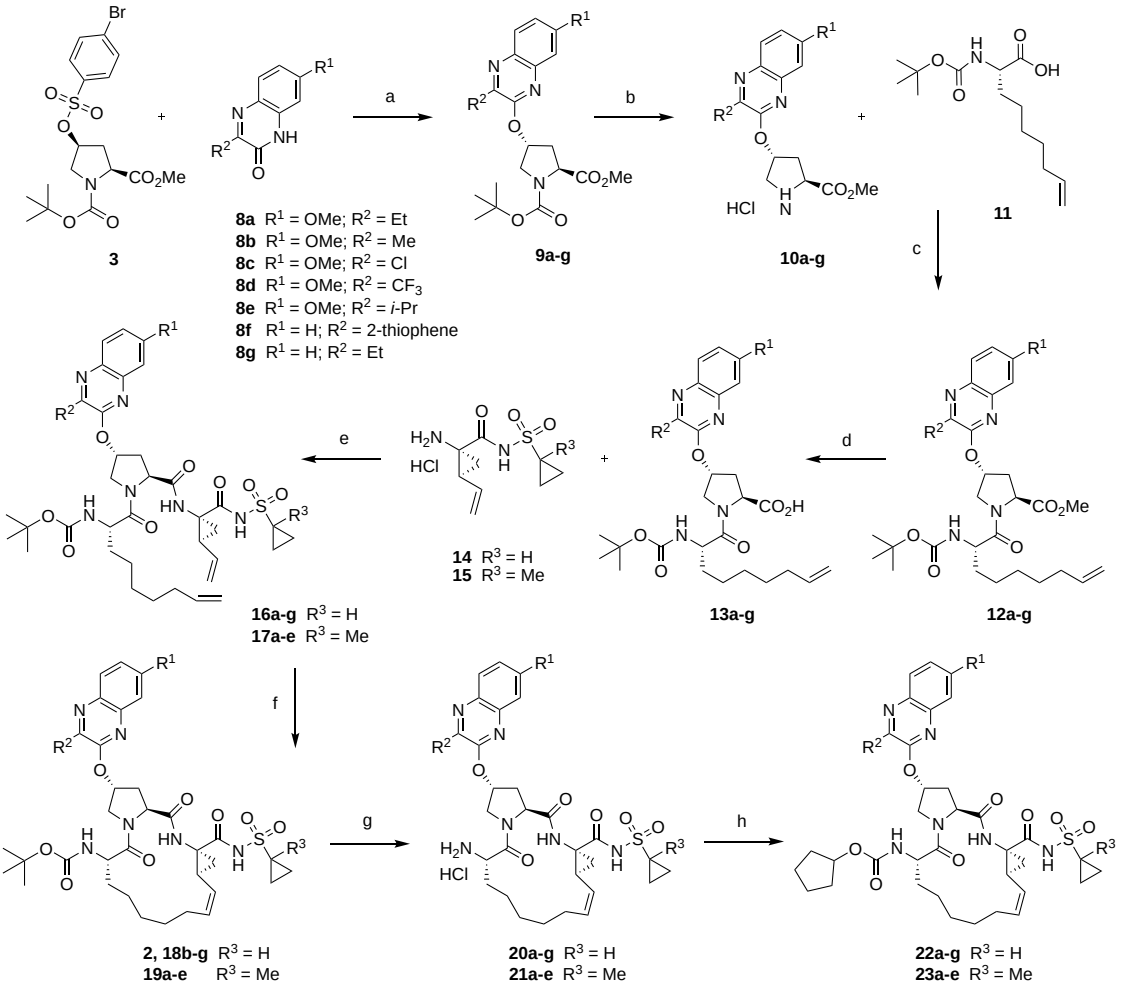

Scheme 3.1: Synthesis of HCV NS3/4A protease inhibitors. Reagents and conditions: (a) Cs_2CO_3, NMP, 55 °C, 6 h; (b) 4 N HCl in dioxane, CH_2Cl_2, RT, 3 h; (c) HATU, DIEA, DMF, RT, 4 h; (d) $LiOH.H_2O$, THF, H_2O, RT, 24 h; (e) HATU, DIEA, DMF, RT, 2 h; (f) Zhan 1B catalyst, 1,2-DCE, 70 °C, 6 h; (g) 4 N HCl, dioxane, RT, 3 h; (h) *N*-(cyclopentyloxycarbonyloxy)-succinimide, DIEA, CH_3CN, RT, 36 h.

The P1–P3 macrocyclic PIs were assembled from the P2 intermediates **9a-g** using a sequence of deprotection and peptide coupling steps followed by the ring-closing metathesis (RCM) reaction (Method A). Removal of the Boc group in **9a-g** using 4 N HCl provided the amine salts **10a-g**, which were coupled with the amino acid **11** in the presence of HATU and DIEA to yield the P2–P3 ester intermediates **12a-g**. Hydrolysis of these esters with LiOH and reaction of the resulting carboxylic acids **13a-g** with the P1–P1' fragments **14**[162] and **15**[163] under HATU/DIEA coupling conditions provided the bis-olefin intermediates **16a-g** and **17a-e**. Finally, cyclization of the bis-olefin intermediates was accomplished using a highly efficient RCM catalyst Zhan 1B, and provided the inhibitors **18b-g** and **19a-e** in 45–80% yield. Interestingly, RCM reactions of bis-olefins **17a-e** bearing the 1-methylcyclopropylsulfonamide provided higher yield than the corresponding cyclopropylsulfonamide analogues **16a-g**. Finally, removal of the Boc group and reaction of the resulting amine salts **20a-g** and **21a-e** with the *N*-(cyclopentyloxycarbonyloxy)-succinimide in the presence of DIEA afforded the inhibitors **22a-g** and **23a-e** with the N-terminal cyclopentyl P4 moiety.

A subset of inhibitors was synthesized using an alternate reaction sequence that allowed late-stage modification at both the P1' and P4 positions as illustrated in **Scheme 3.2** (Method B). The P2–P3 acid intermediates **13a-d** were reacted with the commercially available amine salt **24** under HATU/DIEA coupling conditions to afford the bis-olefin intermediates **25a-d**. RCM reaction in the presence of Zhan 1B catalyst provided the macrocyclic intermediates **26a-d** in

75–90% yield, which was better than that obtained in the presence of the P1' acylsulfonamide. The P1–P3 macrocyclic core intermediates **26a-d** can be modified in either direction after removing the C- or N-terminal protecting groups. Thus, hydrolysis of the C-terminal ethyl ester with LiOH provided the acids **27a-d**, which were then reacted with either cyclopropylsulfonamide **28** or 1-methylcyclopropylsulfonamide **29** in the presence of CDI and DBU to afford the final inhibitors **18b-d** and **19a-d**. The N-terminal *tert*-butyl capping group was replaced with the cyclopentyl moiety as described earlier to provide the target inhibitors **22a-d** and **23a-d**.

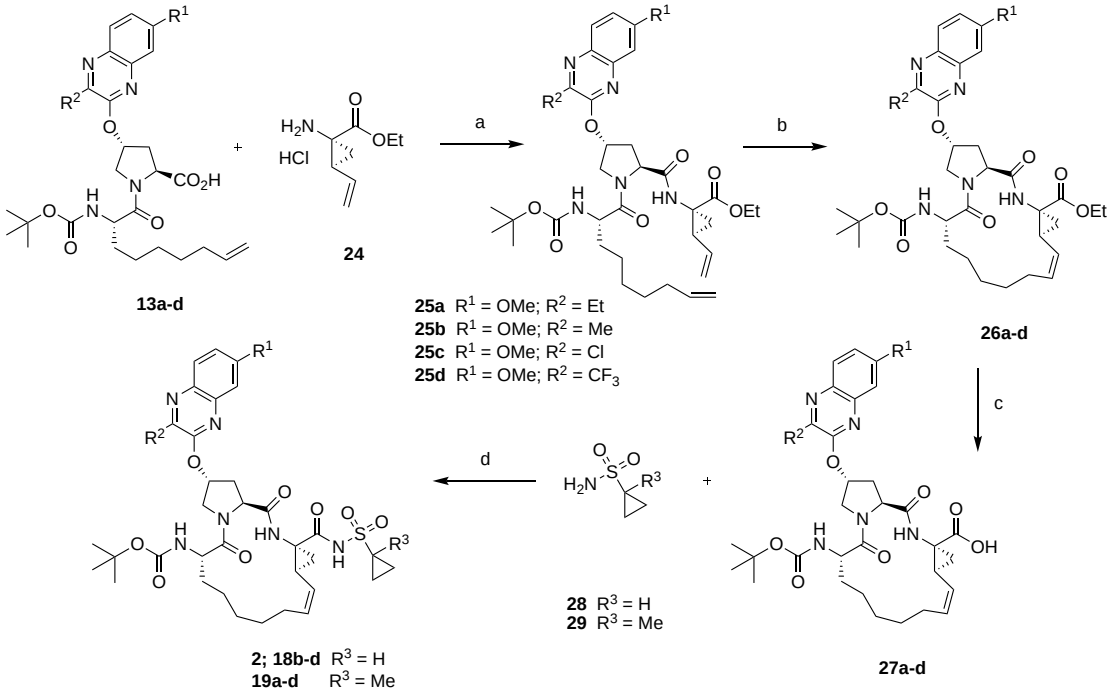

Scheme 3.2: Alternate synthesis of HCV NS3/4A protease inhibitors.
Reagents and conditions: (a) HATU, DIEA, DMF, RT, 2 h; (b) Zhan 1B catalyst, 1,2-DCE, 70 °C, 5 h; (c) $LiOH.H_2O$, THF, MeOH, H_2O, RT, 24 h; (d) CDI, THF, DBU, reflux, 1.5 h, RT, 36 h.

3.4 Results and Discussion

Our goal was to develop a structure-guided design strategy to improve the resistance profile of HCV NS3/4A PIs based on the substrate envelope model.[159,160] Compound **2** is an attractive scaffold for exploring this strategy due to the unique structural features: (1) the P2 quinoxaline moiety that predominantly interacts with the highly conserved catalytic residues Asp81 and His57 and (2) the conformational flexibility that allows the inhibitor to efficiently accommodate structural changes in the S2 subsite due to resistance mutations. Despite these promising features, optimization of substituents at the P2 quinoxaline and the N-terminal capping may be key to discovering analogues with improved potency and resistance profiles. Therefore, efforts were focused on exploration of SARs at the P2 quinoxaline moiety in **2**, specifically substituting the ethyl group at the 3-position that directly interacts with protease S2 subsite residues Arg155 and Ala156. The SAR strategy was based on insights from detailed structural analysis of **1** and **2** bound to wild-type NS3/4A protease and drug resistant variants.[89,111] Based on these insights, we hypothesized that small hydrophobic groups at the 3-position of the quinoxaline would be preferred for retaining inhibitor potency against drug resistant variants, but larger groups that make extensive interactions with Arg155, Ala156 and Asp168 would result in inhibitors highly susceptible to mutations at these positions. To test this hypothesis, a series of inhibitors with diverse substituents at the 3-position of P2 quinoxaline were designed and synthesized.

The potency and resistance profiles of NS3/4A PIs were assessed using biochemical and replicon assays. The enzyme inhibition constants (*K*i) were determined against wild-type GT1a NS3/4A protease, drug-resistant variant D168A, and GT3a NS3/4A protease (**Table 3.1**). The cellular antiviral potencies (EC_{50}) were determined using replicon-based antiviral assays against wild-type HCV and drug-resistant variants R155K, A156T, D168A, and D168V (**Table 3.2**). Grazoprevir (GZR, **1**) was used as a control in all assays. The observed antiviral potencies are generally higher than protease inhibitory potencies, likely because biochemical assays were performed using the protease domain alone rather then the full-length NS3/4A.

Table 3.1: Inhibitory activity against wild-type NS3/4A protease and drug resistant variants

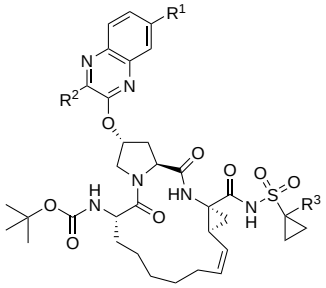

2; 18b-g; 19a-e

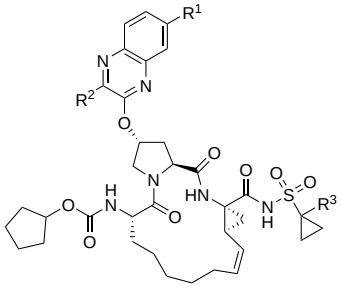

22a-g; 23a-e

Inhibitor	R^1	R^2	R^3	*K*i (nM)		
				GT1a WT Protease	GT1a D168A Protease	GT3a Protease
2	OMe	Et	H	3.29 ± 0.52	82.4 ± 4.4	204 ± 19
19a	OMe	Et	Me	1.82 ± 0.38	55.2 ± 5.3	171 ± 23
22a	OMe	Et	H	1.24 ± 0.14	52.3 ± 3.2	211 ± 18
23a	OMe	Et	Me	1.37 ± 0.34	55.2 ± 5.3	186 ± 30
18b	OMe	Me	H	3.40 ± 0.47	50.9 ± 3.7	152 ± 18
19b	OMe	Me	Me	3.60 ± 0.44	52.0 ± 2.4	119 ± 18
22b	OMe	Me	H	0.93 ± 0.15	31.9 ± 2.5	147 ± 20
23b	OMe	Me	Me	1.13 ± 0.22	36.3 ± 1.8	121 ± 16
18c	OMe	Cl	H	1.07 ± 0.17	39.8 ± 3.4	67.5 ± 8.0
19c	OMe	Cl	Me	1.11 ± 0.38	77.7 ± 6.1	53.6 ± 5.9
22c	OMe	Cl	H	0.49 ± 0.15	30.6 ± 2.6	85.6 ± 11
23c	OMe	Cl	Me	0.44 ± 0.15	25.7 ± 1.8	61.0 ± 12
18d	OMe	CF_3	H	13.3 ± 3.9	157 ± 12	344 ± 141
19d	OMe	CF_3	Me	5.77 ± 1.78	118 ± 13	231 ± 74
22d	OMe	CF_3	H	7.55 ± 2.39	115 ± 12	757 ± 334
23d	OMe	CF_3	Me	8.14 ± 2.37	110 ± 14	433 ± 206
18e	OMe	*i*-Pr	H	4.27 ± 1.34	239 ± 20	NT
19e	OMe	*i*-Pr	Me	0.58 ± 0.08	211 ± 19	NT
22e	OMe	*i*-Pr	H	1.44 ± 0.46	161 ± 11	NT
23e	OMe	*i*-Pr	Me	1.34 ± 0.48	156 ± 17	NT
18f	H	2-thiophene	H	1.03 ± 0.13	1823 ± 347	NT
22f	H	2-thiophene	H	1.59 ± 0.56	900 ± 81	NT
18g	H	Et	H	7.18 ± 1.02	190 ± 13	NT
22g	H	Et	H	1.99 ± 0.48	107 ± 7.0	NT
GZR (1)				0.21 ± 0.03	49.1 ± 1.6	30.3 ± 1.9

NT: not tested

Table 3.2: Antiviral activity against wild-type HCV and drug resistant variants.

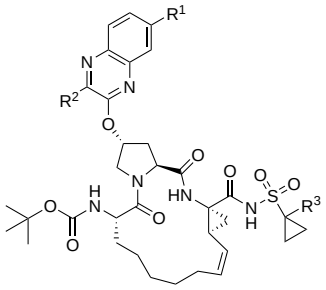

2; 18b-g; 19a-e

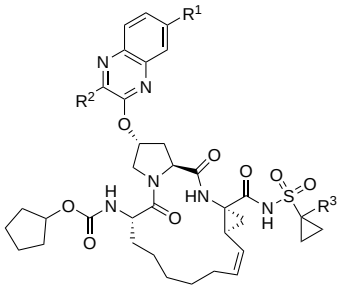

22a-g; 23a-e

Inhibitor	R^1	R^2	R^3	Replicon EC_{50} (nM)				
				WT	R155K	A156T	D168A	D168V
2	OMe	Et	H	0.33	1.75	9.65	6.31	9.10
19a	OMe	Et	Me	0.43	1.80	4.52	4.97	6.42
22a	OMe	Et	H	0.14	2.08	11.8	3.60	11.9
23a	OMe	Et	Me	0.16	2.07	10.6	3.45	7.08
18b	OMe	Me	H	0.39	1.17	5.95	4.24	3.17
19b	OMe	Me	Me	0.30	0.80	1.57	2.37	1.60
22b	OMe	Me	H	0.11	0.89	2.88	2.63	4.32
23b	OMe	Me	Me	0.13	1.09	3.99	2.16	2.85
18c	OMe	Cl	H	0.16	0.44	16.2	1.42	0.73
19c	OMe	Cl	Me	0.18	0.40	8.86	1.07	0.49
22c	OMe	Cl	H	0.15	0.59	3.55	1.32	1.55
23c	OMe	Cl	Me	0.15	0.56	4.32	0.97	1.09
18d	OMe	CF_3	H	1.98	3.45	36.2	16.8	17.1
19d	OMe	CF_3	Me	1.52	2.30	20.5	8.64	8.31
22d	OMe	CF_3	H	4.86	7.97	117	15.1	24.0
23d	OMe	CF_3	Me	4.04	6.90	75.9	8.46	11.4
18e	OMe	*i*-Pr	H	1.43	5.02	25.7	15.3	23.7
19e	OMe	*i*-Pr	Me	1.86	4.14	21.2	11.9	18.1
22e	OMe	*i*-Pr	H	0.48	7.63	32.1	7.96	30.1
23e	OMe	*i*-Pr	Me	0.59	6.83	27.6	7.91	18.2
18f	H	2-thiophene	H	0.98	21.7	256	111	193
22f	H	2-thiophene	H	0.40	19.2	183	42.2	70.0
18g	H	Et	H	0.46	1.81	10.6	8.55	14.0
22g	H	Et	H	0.24	4.28	24.6	7.50	19.3
GZR (1)				0.14	1.89	238	9.69	5.41

Compound **1** showed sub-nanomolar inhibitory potency against WT NS3/4A protease and maintained nanomolar activity against drug resistant variant D168A and GT3a protease. Similarly, in replicon assays **1** exhibited an excellent potency profile with sub-nanomolar activity against WT HCV (EC_{50} = 0.14 nM) and low nanomolar activity against drug resistant variants R155K, D168A, and D168V. However, in line with previous reports,[106] **1** was highly susceptible to the A156T mutation (EC_{50} = 238 nM), losing over 1000-fold potency against this variant. Compared to **1**, the P1–P3 macrocyclic analogue **2** exhibited lower inhibitory potency against WT protease and the D168A variant. Also, the inhibitory activity of **2** against the GT3a protease was considerably lower than that of **1**. However, as we have previously shown,[106] **2** displayed a superior potency profile in replicon assays with sub-nanomolar activity against WT HCV (EC_{50} = 0.33 nM) and maintained single digit nanomolar potency against all drug-resistant variants tested. Notably, unlike **1**, compound **2** maintained low nanomolar potency against the A156T variant (EC_{50} = 9.65 nM). Thus, with an improved resistance profile compared to **1**, the P1–P3 macrocyclic analogue **2** is an attractive lead compound for further optimization.

3.4.1 Modifications of P1’ and P4 Capping Groups

Initial SAR efforts to optimize lead compound **2** focused on exploring changes at the P1’ position and N-terminal capping group. Recent SAR studies of diverse NS3/4A PIs indicate that replacement of the cyclopropylsulfonamide moiety at

the P1’ position with a slightly more hydrophobic 1-methylcyclopropylsulfonamide improves inhibitor potency in replicon assays.[163,164] Moreover, changes at the P4 position have been shown to significantly affect inhibitor potency against drug resistant variants, as these groups bind in close proximity to the pivotal drug resistance site Asp168.[165] For carbamate-linked P4 capping groups, generally bulky hydrophobic moieties are preferred but the size of the group appears to be dependent on the heterocyclic moiety present at the P2 position.[109]

First, replacing the cyclopropylsulfonamide at the P1’ position in **2** with 1-methylcyclopropylsulfonamide provided the analogue **19a**. Compared to the parent compound **2**, **19a** showed slightly better *K*i values against WT, D168A and GT3a proteases and exhibited similar or slightly better antiviral potency against WT and drug resistant variants. Next, the *tert*-butyl P4 capping group in both **2** and **19a** was replaced with a larger cyclopentyl moiety, resulting in analogues **22a** and **23a**. Unlike the change at the P1’ position, the P4 cyclopentyl modification provided mixed results. Compound **22a** afforded a 2-fold increase in potency than **2** in biochemical assays against WT protease and a slight improvement against the D168A variant, but was equipotent to **2** against GT3a protease. Similarly, in replicon assays **22a** exhibited 2-fold enhanced potency against WT HCV and D168A variant, but showed similar potency as **2** against the R155K and D168V variants. Compound **23a**, with a 1-methylcyclopropylsulfonamide moiety at the P1’ position and a cyclopentyl group at the P4 position, exhibited potency profile largely similar to **22a**. Surprisingly, a

slight loss in potency was observed against the A156T variant for compounds with a cyclopentyl versus *tert*-butyl capping group. Overall, these minor modifications at the P1' and N-terminal capping regions of inhibitor **2** were tolerated and provided analogues with improved potency profiles.

3.4.2 SAR Exploration of P2 Quinoxaline

Next, SARs at the P2 quinoxaline in compound **2** were explored. Efforts mainly focused on replacing the 3-position ethyl group with diverse functional groups with respect to size and electronic properties. Replacement of the ethyl group in **2** with a smaller methyl group provided analogue **18b**. As expected, reducing the size of the hydrophobic group at this position resulted in improved potency profile. Compound **18b** showed slightly enhanced potency against drug resistant variants in biochemical and antiviral assays, with a notable ~2-fold improvement against the D168V variant (EC_{50} = 3.17 nM). The introduction of 1-methylcyclopropylsulfonamide moiety at the P1' position afforded inhibitor **19b** with protease inhibitory activity comparable to the parent compound **18b**. However, similar to the 3-ethylquinoxaline analogue (**19a)**, compound **19b** demonstrated significant gain in potency in replicon assays. In fact, compared to **2**, **19b** exhibited 2- to 6-fold enhancement in potency against drug resistant variants R155K (EC_{50} = 0.80 nM), A156T (EC_{50} = 1.57 nM), D168A (EC_{50} = 2.37 nM), and D168V (EC_{50} = 1.6 nM). Replacement of the *tert*-butyl P4 capping in **18b** and **19b** with a cyclopentyl group, providing **22b** and **23b**, resulted in an

increase in WT and D168A inhibitory activity as well as 2- to 3-fold increase in WT replicon potency. Unlike the corresponding 3-ethylquinoxaline analogues (**22a** and **23a**), the 3-methyquinoxaline compounds **22b** and **23b** maintained the excellent potency profile observed for the corresponding *tert*-butyl analogues. Remarkably, with the exception of **18b** (A156T EC_{50} = 5.95 nM), all compounds in the 3-methylquinoxaline series display exceptional potency profiles with EC_{50} values below 5 nM against WT and clinically relevant drug resistant variants.

To gain insights into the excellent potency profile observed for the 3-methyquinoxaline series, we determined the X-ray crystal structure of inhibitor **19b** in complex with the WT NS3/4A protease at a resolution of 1.8 Å (**Figure 3.3**, **Table 3.3**, PDB code: 5VOJ). The WT-**19b** complex structure was compared with the previously reported structures of compound **2** in complex with WT protease and the A156T variant (PDB codes: 5EPN and 5EPY).[111] The two WT structures overlap very well, with only minor differences in the S1 and S2 subsites because of modifications in the inhibitor structure. In the WT-**2** crystal structure, the 3-ethyl group at the P2 quinoxaline makes hydrophobic interactions with the hydrocarbon portion of the Arg155 side-chain, while the methylene portion of this group interacts with the side-chain of Ala156. The smaller methyl group at this position in the WT-**19b** structure maintains hydrophobic interactions with Ala156, while minimizing chances of steric clash with a larger side-chain, such as in A156T.

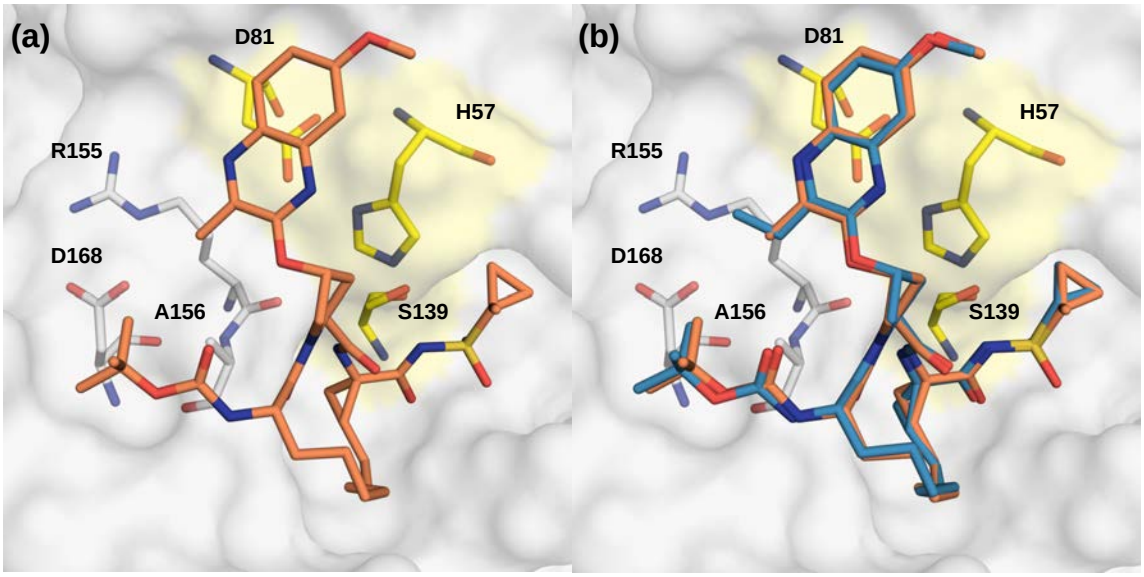

Figure 3.3: Binding mode of 19b in the HCV NS3/4A protease active site.
(a) X-ray crystal structure of WT1a HCV NS3/4A protease in complex with inhibitor **19b** (b) and superposition of WT-**2** and WT-**19a** complexes. The protease active site is shown as a surface with inhibitor **19b** shown in orange and **2** shown in blue. The catalytic triad is highlighted in yellow and drug resistance residues Arg155, Ala156, and Asp168 are shown as sticks.

Table 3.3: X-ray data collection and crystallographic refinement statistics.

	WT1a-**19b**	WT1a-**18f**
PDB code	5VOJ	5VP9
Resolution	1.80 Å	1.86 Å
Space group	$P2_12_12_1$	$P2_12_12_1$
Molecules in AU[a]	1	1
Cell dimensions		
a (Å)	55.4	54.8
b (Å)	58.6	58.4
c (Å)	59.9	60.4
β (°)	90	90
Completeness (%)	94.1	99.9
Total reflections	120670	111301
Unique reflections	17608	16852
Average I/σ	7.8	15.7
Redundancy	6.9	6.6
R_{sym} (%)[b]	5.0 (15.9)	6.0 (31.7)
RMSD[c] in		
Bond lengths (Å)	0.005	0.005
Bond angles (°)	1.1	0.9
R_{factor} (%)[d]	16.0	16.8
R_{free} (%)[e]	19.3	20.8

[a]AU, asymmetric unit.
[b]$R_{sym} = \Sigma \mid I - \langle I \rangle \mid / \Sigma I$, where I = observed intensity, $\langle I \rangle$ = average intensity over symmetry equivalent; values in parentheses are for the highest resolution shell.
[c]RMSD, root mean square deviation.
[d]$R_{factor} = \Sigma \mid\mid F_o \mid - \mid F_c \mid\mid / \Sigma \mid F_o \mid$.
[e]R_{free} was calculated from 5% of reflections, chosen randomly, which were omitted from the refinement process.

Unlike inhibitor **1**, the P1–P3 macrocyclic analogues retain potency against the A156T variant. Comparison of the WT-**2** and A156T-**2** (PDB code: 5EPY) structures shows subtle changes in inhibitor interactions with the mutant protease.[111] In the A156T-**2** structure the P2 quinoxaline largely maintains interactions with the catalytic residues, but the ethyl group is shifted away from Arg155 side chain toward A156T. Moreover, to accommodate a larger Thr side-chain, the Asp168 side chain adopts another conformation, moving away from Arg155. These changes underlie reduced inhibitor potency against the A156T variant, but unlike **1**, inhibitor **2** is able to better accommodate these changes due to a flexible P2 moiety. The 3-methylquinoxaline analogues are more potent against the A156T variant than the corresponding 3-ethylquinoxaline compounds likely due the reduced interactions of the smaller methyl group with the Thr side-chain. Replacing the methyl group with hydrogen at the 3-position of quinoxaline would further reduce interactions with the S2 subsite residues, but could result in a highly flexible P2 moiety, likely destabilizing interactions with the catalytic residues. Thus, a small hydrophobic group at the 3-position of P2 quinoxaline is preferred to maintain favorable interactions with Ala156 and avoid steric clashes with the Thr side-chain in the A156T variant.

The improved potency profile of 3-methyquinoxaline compounds led to exploration of bioisosteric replacements of the 3-methyl group with varied size and electronic properties. To that end, analogues **18c** and **19c** bearing the 3-chloro-7-methoxyquinoxaline at the P2 position were prepared. The protease

inhibitory potency profiles of these compounds were excellent and showed improvement against WT, D168A and GT3a over **2**. These potency gains were not only maintained in replicon assays but were more significant, with the only exception of A156T variant. Both compounds **18c** and **19c** were more active than the corresponding 3-methylquinoxaline analogues (**18b** and **19b**) with EC_{50} values less than 1 nM against WT, R155K and D168V and less than 2 nM against the D168A variant, but experienced about 3- to 6-fold reduction in potency against the A156T variant. However, potency losses against the A156T variant were largely reversed when the P4 *tert*-butyl group in **18c** and **19c** was replaced with a larger cyclopentyl moiety to afford **22c** and **23c**. Similar to the 3-methylquinoxaline compounds, the 3-chloroquinoxaline analogues displayed exceptional potency profiles with EC_{50} values of less than 5 nM against all drug resistant variants including A156T. These results clearly demonstrate that small hydrophobic groups with weak electron-donating properties at the 3-position of P2 quinoxaline can be replaced with weak electron-withdrawing groups without affecting the overall potency profile.

Next, a larger and strongly electron-withdrawing trifluoromethyl moiety was explored at the 3-position of P2 quinoxaline, leading to inhibitors **18d** and **19d**. This modification, however, resulted in significant potency losses in both biochemical and replicon assays. Compound **18d** was about 2- to 4-fold less active than **2** against WT protease and variants. Analogue **19d** with the 1-methylcyclopropylsulfonamide moiety at the P1’ position showed similar trends

when compared to the corresponding **19a**. In line with biochemical data, both **18d** and **19d** suffered 2- to 6-fold decrease in replicon potency against WT and drug resistant variants, though **19d** maintained relatively good potency profile. In contrast to the results in previous series, the introduction of the larger cyclopentyl P4 capping group, as in **22d** and **23d**, was detrimental to replicon potency, particularly against the A156T variant. Moreover, compounds in the 3-(trifluoromethyl)quinoxaline series were among the least active against the GT3a protease in biochemical assays. These results indicate that strong electron-withdrawing groups at the 3-position of the P2 quinoxaline may be detrimental to potency. However, a recent SAR study indicates that PIs incorporating the 3-(trifluoromethyl)quinoxaline can be optimized with modifications at the 7-position of quinoxaline in combination with changes at the P1–P3 macrocycle and P4 capping group.[166]

In the absence of a co-crystal structure, the lower inhibitory potencies of compounds in the 3-(trifluoromethyl)quinoxaline series against WT protease could not be explained by molecular modeling, which suggested a similar binding conformation of the P2 quinoxaline in **18d** as observed for **2** (**Figure 3.4A**). Perhaps there are repulsive interactions between trifluoromethyl moiety and the side chain of Asp168, and/or the strong electron-withdrawing effect may weaken the overall interactions of the P2 quinoxaline with the catalytic residues. Potency losses against resistant variants may also result from the larger size of the

trifluoromethyl moiety, which is comparable to that of an ethyl group, though both have different topographical shapes.[167]

To isolate the effects of larger size versus electronic properties on potency, inhibitors **18e** and **19e** with the larger isopropyl group at the 3-position of the P2 quinoxaline were designed and evaluated. These compounds showed WT protease inhibitory activity similar to the corresponding 3-ethylquinoxaline analogues (**2** and **19a**), but experienced 2- to 4-fold reduced activity against the D168A variant. A broader reduction in potency was observed for both **18e** and **19e** in replicon assays against WT and drug resistant variants. The cyclopentyl P4 group in analogues **22e** and **23e** slightly improved biochemical and replicon potency against WT and D168A variants, but was largely unfavorable to replicon potency against R155K and A156T variants. This trend is broadly similar to the results observed with the 3-(trifluoromethyl)quinoxaline series, indicating that both electronic properties and size of the group at the 3-position of P2 quinoxaline are important for maintaining potency against drug resistant variants. Modeling indicated that compared to **2** the P2 quinoxaline moiety in **18e** has to shift away from the catalytic triad in order to accommodate the larger isopropyl group thereby weakening critical stacking interactions with His57 (**Figure 3.4B**). Overall, SAR data from the 3-isopropyl- and 3-(trifluoromethyl)-quinoxaline series supports the hypothesis that large substituents at the 3-position of P2 quinoxaline have detrimental effect on inhibitor potency against drug resistant variants.

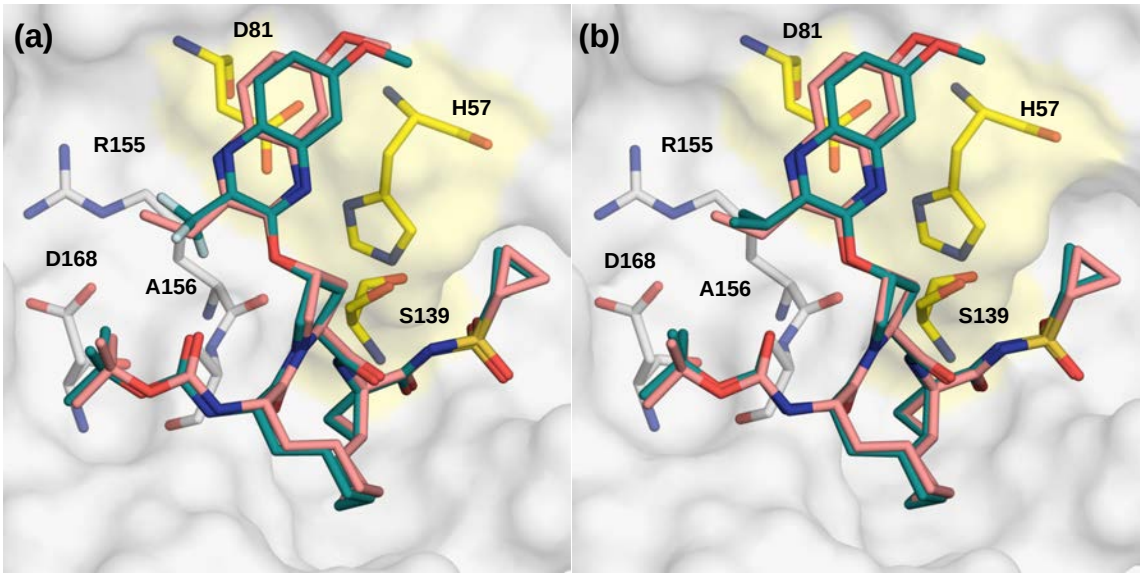

Figure 3.4: Comparison of lead compound 2 with analogues (a) 18d, and (b) 18e, modeled in the active site of WT HCV NS3/4A protease.
Compound **2** is shown in salmon and modified inhibitors are in green. The catalytic triad is highlighted in yellow and drug resistance residues Arg155, Ala156, and Asp168 are in sticks.

These findings were further reinforced by the results obtained for the 3-(thiophen-2-yl)quinoxaline analogues **18f** and **22f**. Based on molecular modeling, the large thiophene moiety in these compounds was expected to make extensive interactions with the residues Arg155 and Ala156, resulting in improved potency against WT protease. However, mutations at these positions as well as at Asp168 would cause significant potency losses, as these residues are crucial for efficient inhibitor binding. As expected, compound **18f** (a previously reported NS3/4A PI incorrectly labeled as ABT-450)[85,168] showed a 3-fold enhancement in WT biochemical potency but was dramatically less active against the D168A variant, losing over 1800-fold potency. Similarly, in replicon assays analogue **18f** showed considerably reduced potency against all drug resistant variants with losses ranging from 20- to 250-fold compared to WT (**Tables 3.4** and **3.5**). The cyclopentyl P4 analogue **22f** also experienced large potency losses against the variants, albeit to a lesser extent than **18f**. Thus inhibitors with large groups at the 3-position of P2 quinoxaline are highly susceptible to mutations at residues Arg155, Ala156 and Asp168, leading to poor resistance profiles.

Table 3.4: Fold change in inhibitory activity against wild-type GT3 NS3/4A protease and drug resistant variants relative to WT

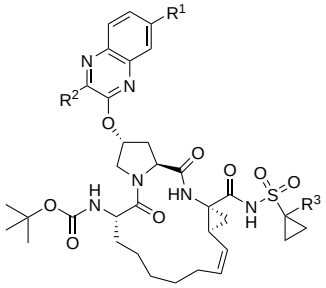

2; 18b-g; 19a-e

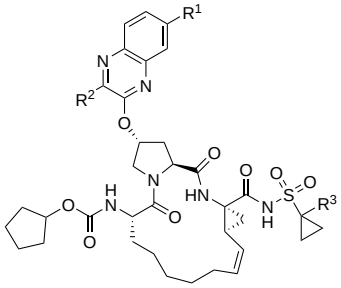

22a-g; 23a-e

Inhibitor	R^1	R^2	R^3	Fold change relative to WT	
				GT1a D168A Protease	GT3a Protease
2	OMe	Et	H	25	62
19a	OMe	Et	Me	30	94
22a	OMe	Et	H	42	170
23a	OMe	Et	Me	40	136
18b	OMe	Me	H	15	45
19b	OMe	Me	Me	14	33
22b	OMe	Me	H	34	158
23b	OMe	Me	Me	32	107
18c	OMe	Cl	H	37	63
19c	OMe	Cl	Me	70	48
22c	OMe	Cl	H	62	175
23c	OMe	Cl	Me	58	139
18d	OMe	CF_3	H	12	26
19d	OMe	CF_3	Me	20	40
22d	OMe	CF_3	H	15	100
23d	OMe	CF_3	Me	14	53
18e	OMe	*i*-Pr	H	56	NT
19e	OMe	*i*-Pr	Me	364	NT
22e	OMe	*i*-Pr	H	112	NT
23e	OMe	*i*-Pr	Me	116	NT
18f	H	2-thiophene	H	1770	NT
22f	H	2-thiophene	H	566	NT
18g	H	Et	H	26	NT
22g	H	Et	H	54	NT
GZR (1)				234	144

Table 3.5: Fold change in antiviral activity against drug resistant variants relative to WT

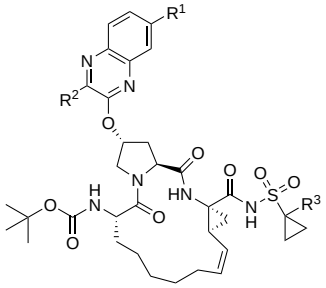

2; 18b-g; 19a-e

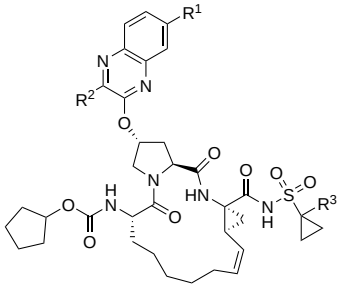

22a-g; 23a-e

Inhibitor	R^1	R^2	R^3	Replicon EC_{50} (nM) (Fold change)			
				R155K	A156T	D168A	D168V
2	OMe	Et	H	(5)	(29)	(19)	(28)
19a	OMe	Et	Me	(4)	(11)	(12)	(15)
22a	OMe	Et	H	(15)	(84)	(26)	(85)
23a	OMe	Et	Me	(13)	(66)	(22)	(44)
18b	OMe	Me	H	(3)	(15)	(11)	(8)
19b	OMe	Me	Me	(3)	(5)	(8)	(5)
22b	OMe	Me	H	(8)	(26)	(24)	(39)
23b	OMe	Me	Me	(8)	(31)	(17)	(22)
18c	OMe	Cl	H	(3)	(101)	(9)	(5)
19c	OMe	Cl	Me	(2)	(49)	(6)	(3)
22c	OMe	Cl	H	(4)	(24)	(9)	(10)
23c	OMe	Cl	Me	(4)	(29)	(6)	(7)
18d	OMe	CF_3	H	(2)	(18)	(8)	(9)
19d	OMe	CF_3	Me	(2)	(13)	(6)	(5)
22d	OMe	CF_3	H	(2)	(24)	(3)	(5)
23d	OMe	CF_3	Me	(2)	(19)	(2)	(3)
18e	OMe	*i*-Pr	H	(4)	(18)	(11)	(17)
19e	OMe	*i*-Pr	Me	(2)	(11)	(6)	(10)
22e	OMe	*i*-Pr	H	(16)	(67)	(17)	(63)
23e	OMe	*i*-Pr	Me	(12)	(47)	(13)	(31)
18f	H	2-thiophene	H	(22)	(261)	(113)	(197)
22f	H	2-thiophene	H	(48)	(458)	(106)	(175)
18g	H	Et	H	(4)	(23)	(19)	(30)
22g	H	Et	H	(18)	(103)	(31)	(80)
GZR (1)				(14)	(1700)	(69)	(39)

The X-ray crystal structure of inhibitor **18f** in complex with WT NS3/4A protease was determined at a resolution of 1.9 Å, providing insights into the binding modes of P2 quinoxaline with a larger thiophene substituent at the 3-position (**Figure 3.5**, **Table 3.3**, PDB code: 5VP9). Comparison of the WT-**18f** and WT-**2** crystal structures showed significant differences in the interactions of quinoxaline moieties with the catalytic triad and S2 subsite residues. As predicted, the quinoxaline moiety in WT-**18f** structure is shifted toward the active site to accommodate the larger thiophene substituent. The thiophene ring makes extensive interactions with residues in the S2 subsite, including cation-π interactions with Arg155, likely contributing to the improved potency against the WT protease. As this Arg155 conformation is stabilized by electrostatic interactions with Asp168, mutations at either residue would disrupt inhibitor binding by loss of direct interactions as well as indirect structural effects. In addition, the A156T mutation would result in a steric clash with the thiophene ring, as reflected in the antiviral data for this variant. These biochemical and structural findings are in line with previous studies that show inhibitors that are dependent on extensive interactions with the S2 subsite residues for potency are highly susceptible to mutations at residues Arg155, Ala156 and Asp168.

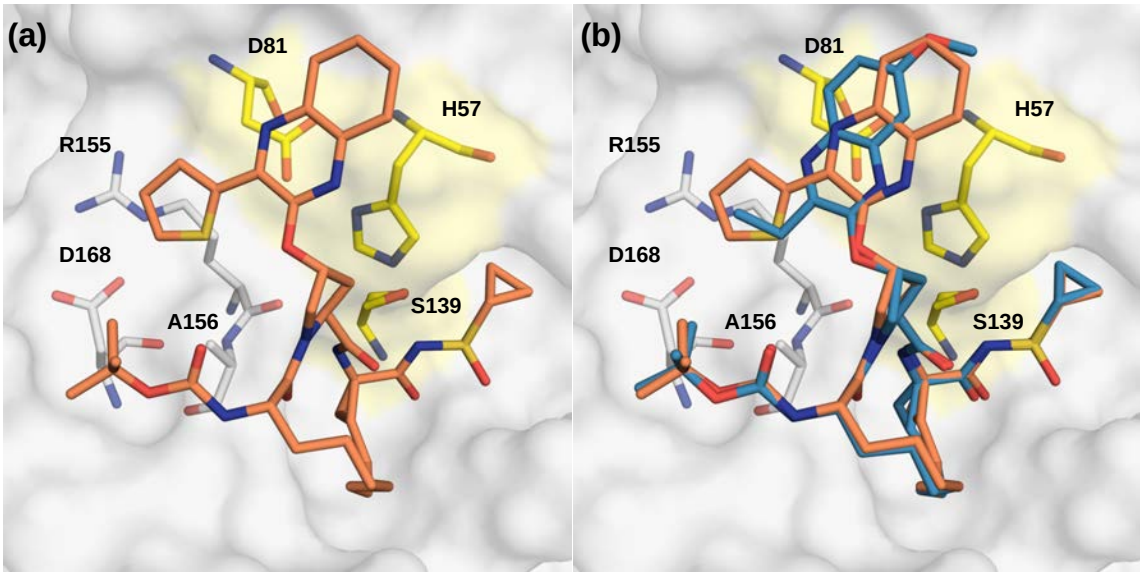

Figure 3.5: X-ray crystal structure of WT1a HCV NS3/4A protease in complex with inhibitor 18f (a) and superposition of WT-2 and WT-18f complexes (b).
The protease active site is shown as a surface with inhibitor **18f** shown in orange and **2** shown in blue. The catalytic triad is highlighted in yellow and drug resistance residues Arg155, Ala156, and Asp168 are shown as sticks.

As compounds **18f** and **22f** lacked the C-7 substituent at the P2 quinoxaline, analogues **18g** and **22g** were prepared to investigate the effect of this group on inhibitor potency. Compared to **2**, analogue **18g** experienced about 2-fold decrease in biochemical potency and only minor loss in replicon potency against WT and drug resistant variants. The P4 cyclopentyl analogue **22g** resulted in about 2-fold reduced potency compared to the corresponding compound **22a**. Thus removal of the C-7 methoxy group has minimal effect on inhibitor potency. The slightly reduced potency of **18g** and **22g** is likely due to the reduced hydrophobic interactions with the aromatic ring of Tyr56 and the methylene portion of His57 of the catalytic triad. In contrast, the observed potency losses against resistant variants for the 3-(thiophen-2-yl)quinoxaline compounds most likely result from loss of interactions of the 2-thiophene moiety with the S2 subsite residues of the protease.

3.4.3 Effects of P2 Substituent Size and Flexibility

Taken together, our SAR results indicate that resistance profiles of compound **2** and analogues are strongly influenced by the substituent at the 3-position of P2 quinoxaline and *N*-terminal capping group. While all PIs showed reduced potency against drug resistance variants in both enzyme inhibition and replicon assays, fold potency losses varied significantly depending on the substituents at the 3-position of P2 quinoxaline. To evaluate susceptibility to the clinically important D168A variant, to which all current NS3/4A PIs are susceptible, potencies were

normalized to WT for PIs with the same P4 capping groups (**Figure 3.6**). Fold changes in *K*i against the D168A protease variant for PIs with the same P1' and P4 capping groups largely trended with the size of the substituent at the 3-position of P2 quinoxaline, with the exception of trifluoromethyl compounds. Losses in potency were significantly higher for compounds with the larger 2-thiophene substituent at the P2 quinoxaline. These results strongly support using the substrate envelope model to reduce direct inhibitor interactions in the S2 subsite, thereby reducing inhibitor susceptibility to drug resistance.

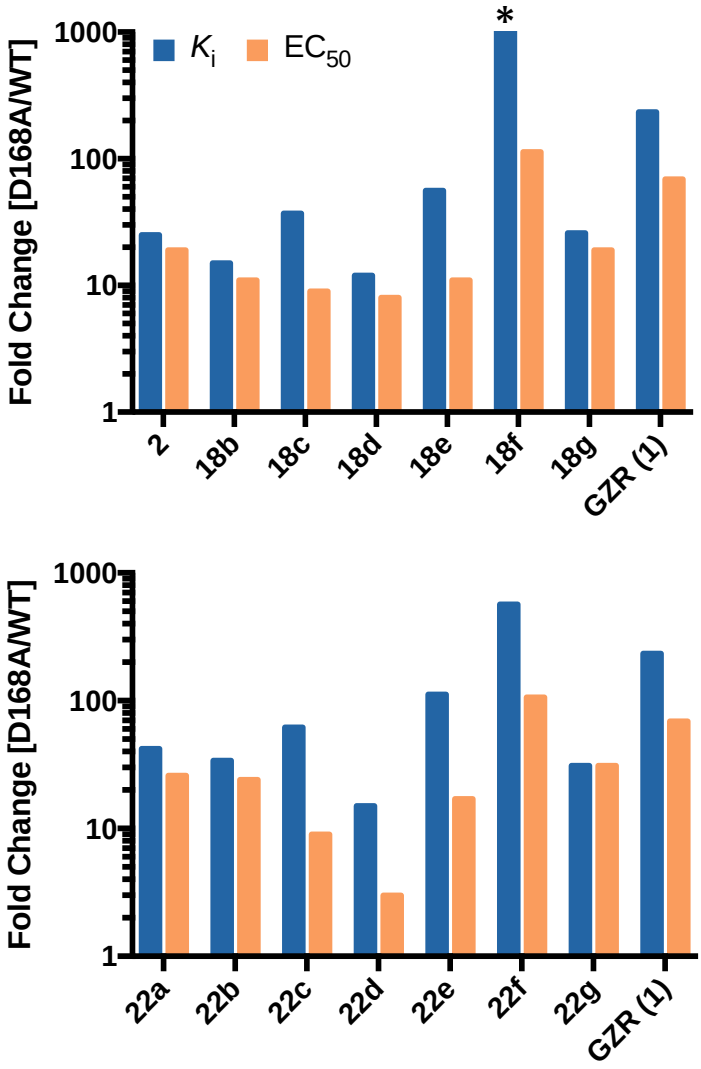

Figure 3.6: Resistance profiles of protease inhibitors in enzyme inhibition and antiviral assays for PIs with (a) *tert*-butyl and (b) cyclopentyl P4 capping groups.

Enzyme inhibitory (blue bars) and antiviral (orange bars) activities against the D168A variant were normalized with respect to the wild-type NS3/4A protease domain or wild-type HCV replicon. *Indicates value higher than 1000.

As we and others have shown,[89,90,109,123] the reduced potencies of NS3/4A PIs against drug resistant variants R155K, A156T, and D168A/V mainly result from disruption of the electrostatic interactions between Arg155 and Asp168. Compared to **1**, compound **2** and most analogues incorporating flexible P2 quinoxaline showed lower fold-changes in potency against these variants (**Tables 3.4** and **3.5**). In these P1–P3 macrocyclic PIs the conformational flexibility of the P2 allows this moiety to adapt to the structural changes caused by mutations at Arg155, Ala156 and Asp168, resulting in better resistance profiles. Potency losses were higher for compound **1** because constraint imposed by the macrocycle does not allow the P2 moiety to adapt to the structural changes resulting from these mutations. Compound **1** and similar P2–P4 macrocyclic PIs, such as voxilaprevir and glecaprevir, are likely to be more susceptible to mutations that cause significant structural changes in the protease active site. However, the P1–P3 macrocyclic compounds reported here, as well as those reported in patent literature that incorporate similar flexible P2 quinoxaline moieties,[169] are likely to be more effective against clinically relevant drug resistant variants. More broadly, combining the substrate envelope model with optimal conformational flexibility provides a rational approach to design NS3/4A PIs with improved resistance profiles.

3.5 Conclusions

Drug resistance is a major problem across all DAA classes targeting HCV. As new therapies are developed the potential for drug resistance must be minimized at the outset of inhibitor design. The substrate envelope model provides a rational approach to design robust NS3/4A PIs with improved resistance profiles. Our SAR findings support the hypothesis that reducing PI interactions with residues in the S2 subsite leads to inhibitors with exceptional potency and resistance profiles. Specifically, the P1–P3 macrocyclic inhibitors incorporating flexible P2 quinoxaline moieties bearing small hydrophobic groups at the 3-position maintain excellent potency in both enzymatic and antiviral assays against drug resistant variants. While these inhibitors protrude from the substrate envelope, they leverage interactions with the essential catalytic triad residues and avoid direct contacts with residues that can mutate to confer resistance. Moreover, conformational flexibility at the P2 moiety is essential to efficiently accommodate structural changes due to mutations in the S2 pocket in order to avoid resistance. These insights provide strategies for iterative rounds of inhibitor design with the paradigm that designing inhibitors with flexible P2 quinoxalines, leveraging evolutionarily constrained areas in the protease active site and expanding into the substrate envelope may provide inhibitors that are robust against drug resistant variants.

3.6 Methods

3.6.1 General

All reactions were performed in oven-dried round bottomed or modified Schlenk flasks fitted with rubber septa under argon atmosphere, unless otherwise noted. All reagents and solvents, including anhydrous solvents, were purchased from commercial sources and used as received. Flash column chromatography was performed using silica gel (230–400 mesh, EMD Millipore). Thin-layer chromatography (TLC) was performed using silica gel (60 F-254) coated aluminum plates (EMD Millipore), and spots were visualized by exposure to ultraviolet light (UV), exposure to iodine adsorbed on silica gel, and/ or exposure to an acidic solution of *p*-anisaldehyde (anisaldehyde) followed by brief heating. ^{1}H NMR and ^{13}C NMR spectra were acquired on Varian Mercury 400 MHz and Bruker Avance III HD 500 MHz NMR instruments. Chemical shifts are reported in ppm (δ scale) with the residual solvent signal used as reference and coupling constant (J) values are reported in hertz (Hz). Data are presented as follows: chemical shift, multiplicity (s = singlet, d = doublet, dd = doublet of doublet, t = triplet, q = quartet, m = multiplet, br s = broad singlet), coupling constant in Hz, and integration. High-resolution mass spectra (HRMS) were recorded on a Thermo Scientific Orbitrap Velos Pro mass spectrometer coupled with a Thermo Scientific Accela 1250 UPLC and an autosampler using electrospray ionization (ESI) in the positive mode. The purity of final compounds was determined by analytical HPLC and was found to be ≥95% pure. HPLC was

performed on a Waters Alliance 2690 system equipped with a Waters 2996 photodiode array detector and an autosampler under the following conditions: column, Phenomenex Luna-2 RP-C18 (5 µm, 4.6 × 250 mm, 120 Å, Torrance, CA); solvent A, H_2O containing 0.1% formic acid (FA), solvent B, CH_3CN containing 0.1% FA; gradient, 50% B to 100% B over 15 min followed by 100% B over 5 min; injection volume, 10 µL; flow rate, 1 mL/ min. Retention times and purity data for each target compound are provided in the experimental section. (For additional synthesis of macrocyclic final compounds and intermediates please see **Appendix C**).

3.6.2 Typical procedures for the synthesis of protease inhibitors using Method A:

1-(*tert*-Butyl) 2-methyl (2*S*,4*R*)-4-((3-ethyl-7-methoxyquinoxalin-2-yl)oxy)pyrrolidine-1,2-dicarboxylate (9a). A solution of 3-ethyl-7-methoxyquinoxalin-2-one **8a** (3.0 g, 14.7 mmol) in anhydrous NMP (45 mL) was treated with Cs_2CO_3 (7.40 g, 22.7 mmol). After stirring the reaction mixture at room temperature for 15 min, proline derivative **3** (6.20 g, 13.3 mmol) was added in one portion. The reaction mixture was heated to 55 °C, stirred for 4 h, and then another portion of proline derivative **3** (0.48 g, 1.0 mmol) was added. The resulting reaction mixture was stirred at 55 °C for an additional 2 h, cooled to room temperature, quenched with aqueous 1 N HCl solution (150 mL), and extracted with EtOAc (300 mL). The organic fraction was washed successively

with saturated aqueous $NaHCO_3$ and NaCl (150 mL each), dried (Na_2SO_4), filtered, and evaporated under reduced pressure. The residue was purified by flash column chromatography using 15–30% EtOAc/hexanes as the eluent to provide **9a** (5.50 g, 87%) as a white foamy solid. ^{1}H NMR (400 MHz, $CDCl_3$) (mixture of rotamers, major rotamer) δ 7.85 (d, J = 9.0 Hz, 1 H), 7.18 (m, 1H), 7.11 (d, J = 2.8 Hz, 1 H), 5.73 (br s, 1 H), 4.47 (t, J = 8.0 Hz, 1 H), 3.98–3.86 (m, 5 H), 3.78 (s, 3 H), 2.92 (q, J = 7.2 Hz, 2 H), 2.68–2.60 (m, 1 H), 2.43–2.36 (m, 1 H), 1.43 (s, 9 H), 1.31 (t, J = 7.2 Hz, 3 H) ppm; ^{13}C NMR (100 MHz, $CDCl_3$) δ 173.56, 160.59, 155.38, 154.02, 148.95, 141.26, 134.12, 129.07, 119.02, 106.11, 80.76, 73.81, 58.43, 55.93, 52.73, 52.40, 36.88, 28.47, 26.68, 11.97 ppm; HRMS (ESI) *m/z*: $[M + H]^+$ calcd for $C_{22}H_{30}N_3O_6$, 432.2129; found 432.2135.

1-(*tert*-Butyl) 2-methyl (2*S*,4*R*)-4-((7-methoxy-3-(trifluoromethyl)quinoxalin-2-yl)oxy)pyrrolidine-1,2-dicarboxylate (9d). The same procedure was used as described above for compound **9a**. 7-methoxy-3-(trifluoromethyl)quinoxalin-2(1*H*)-one **8d** (4.76 g, 19.5 mmol) in NMP (65 mL) was treated with Cs_2CO_3 (9.80 g, 30.0 mmol) and proline derivative **3** (9.0 g, 19.3 mmol) to provide **9d** (6.50 g, 71%) as a pale yellow foamy solid. ^{1}H NMR (500 MHz, $CDCl_3$) (mixture of rotamers, major rotamer) δ 7.77 (d, J = 9.0 Hz, 1 H), 7.48–7.43 (m, 2 H), 5.76 (br s, 1 H), 4.50 (t, J = 8.0 Hz, 1 H), 3.97–3.91 (m, 5 H), 3.78 (s, 3 H), 2.69–2.64 (m, 1 H), 2.41–2.34 (m, 1 H), 1.42 (s, 9 H) ppm; ^{13}C NMR (125 MHz, $CDCl_3$) δ 173.43, 159.58, 153.98, 152.11, 138.39, 137.22, 127.99, 125.73, 120.70 (q, J = 273.4 Hz), 107.64, 80.69, 74.62, 58.27, 56.02,

52.32, 52.11, 36.70, 28.34 ppm; ^{19}F NMR (470 MHz, $CDCl_3$); −67.73 ppm; HRMS (ESI) *m/z*: $[M + H]^+$ calcd for $C_{21}H_{25}F_3N_3O_6$, 472.1690; found 472.1689.

Methyl (2*S*,4*R*)-1-((*S*)-2-((*tert*-butoxycarbonyl)amino)non-8-enoyl)-4-((3-ethyl-7-methoxyquinoxalin-2-yl)oxy)pyrrolidine-2-carboxylate (12a). A solution of ester **9a** (4.80 g, 11.1 mmol) in anhydrous CH_2Cl_2 (30 mL) was treated with a solution of 4 N HCl in 1,4-dioxane (30 mL). After stirring the reaction mixture at room temperature for 3 h, solvents were evaporated under reduced pressure, and the residue was dried under high vacuum. The pale yellow solid was triturated with diethyl ether (3 × 30 mL) and dried under high vacuum to yield the amine salt **10a** (4.0 g, 98%) as an off-white powder.

A mixture of amine salt **10a** (4.0 g, 10.9 mmol) and (*S*)-2-((*tert*-butoxycarbonyl)amino)non-8-enoic acid **11** (3.0 g, 11.1 mmol) in anhydrous DMF (60 mL) was treated with DIEA (7.30 mL, 44.2 mmol) and HATU (6.35 g, 16.7 mmol). The resulting reaction mixture was stirred at room temperature for 4 h, then diluted with EtOAc (400 mL), and washed successively with aqueous 0.5 N HCl, saturated aqueous $NaHCO_3$, and saturated aqueous NaCl (250 mL each). The organic portion was dried (Na_2SO_4), filtered, and evaporated under reduced pressure. The residue was purified by flash chromatography using 20–30% EtOAc/hexanes as the eluent to provide **12a** (5.50 g, 86%) as a white foamy solid. ^{1}H NMR (400 MHz, $CDCl_3$) (mixture of rotamers, major rotamer) *δ* 7.86 (d, *J* = 8.8 Hz, 1 H), 7.20 (dd, *J* = 9.2, 2.8 Hz, 1 H), 7.12 (d, *J* = 2.8 Hz, 1 H), 5.87–5.75 (m, 2 H), 5.20 (d, *J* = 8.4 Hz, 1 H), 5.02–4.92 (m, 2 H), 4.73 (t, *J* = 8.4 Hz, 1

H), 4.38 (q, *J* = 7.2 Hz, 1 H), 4.17 (d, *J* = 12.0 Hz, 1 H), 4.06 (dd, *J* = 11.6, 4.4 Hz, 1 H), 3.94 (s, 3 H), 3.78 (s, 3 H), 2.90 (q, *J* = 7.6 Hz, 2 H), 2.69–2.64 (m, 1 H), 2.41–2.34 (m, 1 H), 2.05 (app q, *J* = 6.8 Hz, 2 H), 1.82–1.74 (m, 1 H), 1.63–1.56 (m, 1 H), 1.45–1.25 (m, 18 H) ppm; ^{13}C NMR (100 MHz, $CDCl_3$) *δ* 172.34, 171.96, 160.61, 155.61, 155.13, 148.95, 141.08, 139.18, 129.22, 119.08, 114.58, 106.14, 79.84, 74.48, 58.19, 55.91, 52.88, 52.67, 52.05, 35.16, 33.88, 32.88, 29.14, 28.96, 28.46, 26.52, 24.92, 11.86 ppm; HRMS (ESI) *m/z*: $[M + H]^+$ calcd for $C_{31}H_{45}N_4O_7$ 585.3283; found 585.3286.

Methyl (2*S*,4*R*)-1-((*S*)-2-((*tert*-butoxycarbonyl)amino)non-8-enoyl)-4-((7-methoxy-3-(trifluoromethyl)quinoxalin-2-yl)oxy)pyrrolidine-2-carboxylate (12d). The same procedure was used as described above for compound **12a**. Compound **9d** (6.0 g, 12.7 mmol) was treated with 4 N HCl (40 mL) to afford amine salt **10d** (5.10 g, 12.5 mmol), which was coupled with acid **11** (3.80 g, 14.0 mmol) using DIEA (9.25 mL, 56.0 mmol) and HATU (7.60 g, 20.0 mmol) to provide **12d** (6.40 g, 81%) as a pale yellow foamy solid. ^{1}H NMR (500 MHz, $CDCl_3$) (mixture of rotamers, major rotamer) *δ* 7.78 (d, *J* = 9.0 Hz, 1 H), 7.48 (dd, *J* = 9.0, 2.5 Hz, 1 H), 7.44 (d, *J* = 2.5 Hz, 1 H), 5.86 (br s, 1 H), 5.84–5.78 (m, 1 H), 5.18 (d, *J* = 9.0 Hz, 1 H), 5.01–4.92 (m, 2 H), 4.75 (t, *J* = 8.0 Hz, 1 H), 4.35 (q, *J* = 7.5 Hz, 1 H), 4.19 (d, *J* = 12.0 Hz, 1 H), 4.08 (dd, *J* = 11.5, 4.5 Hz, 1 H), 3.95 (s, 3 H), 3.78 (s, 3 H), 2.70–2.65 (m, 1 H), 2.41–2.35 (m, 1 H), 2.04 (app q, *J* = 7.0 Hz, 2 H), 1.80–1.75 (m, 1 H), 1.60–1.54 (m, 1 H), 1.45–1.28 (m, 15 H) ppm; ^{13}C NMR (125 MHz, $CDCl_3$) *δ* 172.10, 171.60, 159.99, 155.37, 151.78,

138.98, 138.41, 136.93, 134.40 (q, *J* = 36.3 Hz), 127.85, 125.66, 120.53 (q, *J* = 273.4 Hz), 114.33, 107.54, 79.58, 75.05, 57.83, 55.91, 52.44, 52.33, 51.75, 34.77, 33.65, 32.70, 28.91, 28.73, 28.18, 24.70 ppm; ^{19}F NMR (470 MHz, $CDCl_3$); −67.73 ppm; HRMS (ESI) *m/z*: $[M + H]^+$ calcd for $C_{30}H_{40}F_3N_4O_7$, 625.2844; found 625.2844.

***tert*-Butyl ((*S*)-1-((2*S*,4*R*)-2-(((1*R*,2*S*)-1-((cyclopropylsulfonyl)carbamoyl)-2-vinylcyclopropyl)carbamoyl)-4-((3-ethyl-7-methoxyquinoxalin-2-yl)oxy)pyrrolidin-1-yl)-1-oxonon-8-en-2-yl)carbamate (16a).** A solution of ester **12a** (5.86 g, 10.0 mmol) in THF-H_2O mixture (1:1, 140 mL) was treated with $LiOH.H_2O$ (1.40 g, 33.4 mmol). The resulting reaction mixture was stirred at room temperature for 24 h. The reaction mixture was cooled to ~5 °C, acidified to a pH of 2.0 by slow addition of aqueous 0.25 N HCl (~ 200 mL), and extracted with EtOAc (2 × 400 mL). The organic portions were washed separately with saturated aqueous NaCl (200 ml), dried (Na_2SO_4), filtered, and evaporated under reduced pressure. The gummy residue was dissolved in $CHCl_3$ (50 mL), concentrated under reduced pressure, and the residue was dried under high vacuum overnight to yield the acid **13a** (5.70 g, 100%) as a white foamy solid.

A mixture of acid **13a** (2.10 g, 3.7 mmol) and amine salt **14**[162] (1.20 g, 4.5 mmol) in anhydrous DMF (35 mL) was treated with DIEA (2.43 mL, 14.7 mmol) and HATU (2.1 g, 5.5 mmol). The resulting reaction mixture was stirred at room temperature for 2.5 h, then diluted with EtOAc (300 mL) and washed successively with aqueous 0.5 N HCl, saturated aqueous $NaHCO_3$, and

saturated aqueous NaCl (200 mL each). The organic portion was dried (Na_2SO_4), filtered, and evaporated under reduced pressure. The residue was purified by flash chromatography using 50–70% EtOAc/hexanes as the eluent to provide the bis-olefin compound **16a** (2.50 g, 86%) as a white solid. ^{1}H NMR (400 MHz, $CDCl_3$) δ 10.24 (s, 1 H), 7.84 (d, *J* = 8.8 Hz, 1 H), 7.18 (dd, *J* = 8.8, 2.4 Hz, 1 H), 7.13 (d, *J* = 2.8 Hz, 1 H), 7.04 (s, 1 H), 5.91 (br s, 1 H), 5.85–5.73 (m, 2 H), 5.32 (d, *J* = 8.4 Hz, 1 H), 5.27 (d, *J* = 17.2 Hz, 1 H), 5.14 (d, *J* = 11.2 Hz, 1 H), 5.01–4.90 (m, 2 H), 4.47 (t, *J* = 7.6 Hz, 1 H), 4.38–4.33 (m, 1 H), 4.20 (d, *J* = 11.6 Hz, 1 H), 4.02 (dd, *J* = 11.2, 4.0 Hz, 1 H), 3.94 (s, 3 H), 2.96–2.84 (m, 3 H), 2.56–2.51 (m, 2 H), 2.11 (q, *J* = 8.8 Hz, 1 H), 2.05–1.99 (m, 3 H), 1.74–1.54 (m, 2 H), 1.47–1.10 (m, 21 H), 1.08–1.03 (m, 2 H) ppm; ^{13}C NMR (100 MHz, $CDCl_3$) δ 174.09, 172.58, 168.69, 160.54, 155.89, 154.99, 148.88, 140.95, 139.07, 134.69, 132.71, 129.45, 119.02, 118.77, 114.67, 106.13, 80.0, 74.66, 60.61, 55.91, 53.42, 52.62, 41.83, 35.46, 34.47, 33.89, 32.40, 31.39, 28.98, 28.89, 28.47, 26.68, 25.47, 23.83, 11.85, 6.68, 6.26 ppm; HRMS (ESI) *m/z*: $[M + H]^+$ calcd for $C_{39}H_{55}N_6O_9S$, 783.3746; found 783.3734.

***tert*-Butyl ((*S*)-1-((2*S*,4*R*)-4-((3-ethyl-7-methoxyquinoxalin-2-yl)oxy)-2-(((1*R*,2*S*)-1-(((1-methylcyclopropyl)sulfonyl)carbamoyl)-2-vinylcyclopropyl)carbamoyl)pyrrolidin-1-yl)-1-oxonon-8-en-2-yl)carbamate (17a).** The same procedure was used as described above for compound **16a**. Acid **13a** (1.50 g, 2.6 mmol) was coupled with amine salt **15**[163] (0.90 g, 3.2 mmol) using DIEA (1.75 mL, 10.6 mmol) and HATU (1.50 g, 3.9 mmol) to provide the

bis-olefin compound **17a** (1.75 g, 84%) as a white solid. ^{1}H NMR (400 MHz, $CDCl_3$) δ 10.02 (s, 1 H), 7.84 (d, *J* = 9.2 Hz, 1 H), 7.19 (dd, *J* = 8.8, 2.8 Hz, 1 H), 7.13 (d, *J* = 2.8 Hz, 1 H), 7.06 (s, 1 H), 5.90 (br s, 1 H), 5.83–5.73 (m, 2 H), 5.37 (d, *J* = 9.2 Hz, 1 H), 5.27 (d, *J* = 17.2 Hz, 1 H), 5.14 (d, *J* = 10.8 Hz, 1 H), 5.98 (dd, *J* = 17.2, 1.6 Hz, 1 H), 4.92 (dd, *J* = 10.4, 1.2 Hz, 1 H), 4.48 (t, *J* = 8.0 Hz, 1 H), 4.39–4.33 (m, 1 H), 4.16 (d, *J* = 12.0 Hz, 1 H), 4.02 (dd, *J* = 11.6, 4.0 Hz, 1 H), 3.94 (s, 3 H), 2.89 (q, *J* = 7.6 Hz, 2 H), 2.57–2.50 (m, 2 H), 2.12 (q, *J* = 8.8 Hz, 1 H), 2.05–1.99 (m, 3 H), 1.75–1.58 (m, 4 H), 1.49 (s, 3 H), 1.45–1.18 (m, 19 H), 0.93–0.79 (m, 2 H) ppm; ^{13}C NMR (100 MHz, $CDCl_3$) δ 173.79, 172.41, 167.51, 160.31, 155.71, 154.76, 148.63, 140.73, 138.85, 134.41, 132.60, 129.18, 118.80, 118.54, 114.41, 105.89, 79.74, 74.42, 60.36, 55.68, 53.17, 52.43, 41.71, 36.56, 35.23, 34.22, 33.64, 32.19, 28.70, 28.67, 28.25, 26.43, 25.35, 23.49, 18.37, 14.27, 13.29, 11.64 ppm; HRMS (ESI) *m/z*: $[M + H]^+$ calcd for $C_{40}H_{57}N_6O_9S$, 797.3902; found 797.3887.

***tert*-Butyl ((2*R*,6*S*,13a*S*,14a*R*,16a*S*,*Z*)-14a-((cyclopropylsulfonyl)carbamoyl)-2-((3-ethyl-7-methoxyquinoxalin-2-yl)oxy)-5,16-dioxo-1,2,3,5,6,7,8,9,10,11,13a,14,14a,15,16,16a-hexadecahydrocyclopropa[*e*]pyrrolo[1,2-*a*][1,4]diazacyclopentadecin-6-yl)carbamate (2).** A degassed solution of bis-olefin **16a** (1.40 g, 1.8 mmol) in 1,2-DCE (300 mL) was heated to 50 °C under argon, then Zhan 1b catalyst (0.150 g, 0.20 mmol) was added in two portions over 10 min. The resulting reaction mixture was heated to 70 °C and stirred for 6 h. The reaction mixture

was cooled to room temperature and concentrated under reduced pressure. The residue was purified by flash chromatography using 50–80% EtOAc/hexanes as the eluent to yield the P1–P3 macrocyclic product **2** (0.72 g, 53%) as an off-white solid. ^{1}H NMR (400 MHz, $CDCl_3$) δ 10.28 (s, 1 H), 7.84 (d, J = 9.6 Hz, 1 H), 7.20–7.15 (m, 2 H), 6.91 (s, 1 H), 5.90 (br s, 1 H), 5.69 (q, J = 8.8 Hz, 1 H), 5.14 (d, J = 7.6 Hz, 1 H), 4.96 (t, J = 9.2 Hz, 1 H), 4.59 (t, J = 7.6 Hz, 1 H), 4.49 (d, J = 11.6 Hz, 1 H), 4.30–4.24 (m, 1 H), 4.02 (dd, J = 10.8, 4.0 Hz, 1 H), 3.94 (s, 3 H), 2.94–2.85 (m, 3 H), 2.70–2.51 (m, 3 H), 2.31 (q, J = 8.8 Hz, 1 H), 1.93–1.64 (m, 2 H), 1.60–1.05 (m, 24 H), 0.95–0.89 (m, 1 H) ppm; ^{13}C NMR (100 MHz, $CDCl_3$) δ 177.15, 173.28, 168.02, 160.29, 155.00, 154.90, 148.66, 140.88, 136.31, 134.28, 128.90, 124.47, 118.82, 105.91, 79.84, 74.68, 59.45, 55.72, 53.08, 51.92, 44.57, 34.65, 32.81, 31.01, 29.70, 28.14, 27.11, 27.16, 26.31, 26.06, 22.16, 20.92, 11.56, 6.67, 6.12 ppm; HRMS (ESI) *m/z*: $[M + H]^+$ calcd for $C_{37}H_{51}N_6O_9S$, 755.3433; found 755.3410. Anal. HPLC: t_R 14.23 min, purity 97%.

***tert*-Butyl ((2*R*,6*S*,13a*S*,14a*R*,16a*S*,*Z*)-2-((3-ethyl-7-methoxyquinoxalin-2-yl)oxy)-14a-(((1-methylcyclopropyl)sulfonyl)carbamoyl)-5,16-dioxo-1,2,3,5,6,7,8,9,10,11,13a,14,14a,15,16,16a-hexadecahydrocyclopropa[*e*]pyrrolo[1,2-*a*][1,4]diazacyclopentadecin-6-yl)carbamate (19a).** The same procedure was used as described above for compound **2**. Bis-olefin **17a** (1.45 g, 1.8 mmol) was treated with Zhan 1b catalyst (0.150 g, 0.20 mmol) in 1,2-DCE (300 mL) to afford the P1–P3 macrocyclic product **19a** (1.0 g, 71%) as an off-white solid. ^{1}H NMR (400 MHz, $CDCl_3$) δ

10.16 (s, 1 H), 7.82 (d, *J* = 10.0 Hz, 1 H), 7.18–7.15 (m, 2 H), 6.94 (s, 1 H), 5.90 (br s, 1 H), 5.69 (q, *J* = 9.2 Hz, 1 H), 5.16 (d, *J* = 8.0 Hz, 1 H), 4.99 (t, *J* = 9.2 Hz, 1 H), 4.59 (t, *J* = 8.0 Hz, 1 H), 4.49 (d, *J* = 11.6 Hz, 1 H), 4.30–4.25 (m, 1 H), 4.04 (dd, *J* = 11.6, 4.0 Hz, 1 H), 3.94 (s, 3 H), 2.87 (q, *J* = 7.6 Hz, 2 H), 2.70–2.51 (m, 3 H), 2.33 (q, *J* = 8.0 Hz, 1 H), 1.92–1.68 (m, 4 H), 1.60–1.15 (m, 24 H), 0.85–0.78 (m, 2 H) ppm; ^{13}C NMR (100 MHz, $CDCl_3$) *δ* 177.19, 173.24, 167.0, 160.23, 154.99, 154.88, 148.73, 140.84, 136.26, 134.25, 129.03, 124.89, 118.72, 105.92, 79.84, 74.67, 59.48, 55.72, 53.11, 51.92, 44.71, 36.43, 34.68, 32.80, 29.62, 28.14, 27.09, 26.38, 26.12, 22.19, 20.93, 18.17, 14.51, 12.50, 11.54 ppm; HRMS (ESI) *m/z*: $[M + H]^+$ calcd for $C_{38}H_{53}N_6O_9S$, 769.3589; found 769.3561. Anal. HPLC: t_R 15.01 min, purity 99%.

Cyclopentyl ((2*R*,6*S*,13a*S*,14a*R*,16a*S*,*Z*)-14a-((cyclopropylsulfonyl)carbamoyl)-2-((3-ethyl-7-methoxyquinoxalin-2-yl)oxy)-5,16-dioxo-1,2,3,5,6,7,8,9,10,11,13a,14,14a,15,16,16a-hexadecahydrocyclopropa[*e*]pyrrolo[1,2-*a*][1,4]diazacyclopentadecin-6-yl)carbamate (22a). Compound **2** (0.40 g, 0.53 mmol) was treated with a solution of 4 N HCl in 1,4-dioxane (10 mL). The reaction mixture was stirred at room temperature for 3 h, then concentrated under reduced pressure, and the residue was dried under high vacuum. The off-white solid was triturated with diethyl ether (3 × 10 mL) and dried under high vacuum to yield the amine salt **20a** (0.37 g, 100%) as a white powder.

A solution of the above amine salt **20a** (0.37 g, 0.53 mmol) in anhydrous CH_3CN (15 mL) was treated with DIEA (0.35 mL, 2.1 mmol) and *N*-(cyclopentyloxycarbonyloxy)-succinimide (0.15 g, 0.66 mmol). The reaction mixture was stirred at room temperature for 36 h, then concentrated under reduced pressure and dried under high vacuum. The residue was purified by flash chromatography using 50–90% EtOAc/hexanes as the eluent to provide the target compound **22a** (0.32 g, 79%) as a white solid. ^{1}H NMR (400 MHz, $CDCl_3$) δ 10.29 (s, 1 H), 7.83 (d, *J* = 9.6 Hz, 1 H), 7.21–7.16 (m, 2 H), 6.94 (s, 1 H), 5.93 (br s, 1 H), 5.70 (q, *J* = 8.8 Hz, 1 H), 5.26 (d, *J* = 8.0 Hz, 1 H), 4.96 (t, *J* = 8.4 Hz, 1 H), 4.86–4.82 (m, 1 H), 4.60 (t, *J* = 7.6 Hz, 1 H), 4.45 (d, *J* = 11.2 Hz, 1 H), 4.34–4.28 (m, 1 H), 4.03 (dd, *J* = 11.2, 4.0 Hz, 1 H), 3.94 (s, 3 H), 2.93–2.85 (m, 3 H), 2.70–2.48 (m, 3 H), 2.30 (q, *J* = 8.8 Hz, 1 H), 1.93–1.23 (m, 23 H), 1.15–1.06 (m, 2 H), 0.96–0.88 (m, 1 H) ppm; ^{13}C NMR (100 MHz, $CDCl_3$) δ 177.18, 173.03, 168.04, 160.28, 155.65, 154.93, 148.78, 140.90, 136.27, 134.20, 128.92, 124.46, 118.80, 105.92, 77.87, 74.55, 59.47, 55.72, 53.01, 52.17, 44.54, 34.58, 32.72, 32.63, 32.59, 31.01, 29.70, 27.14, 27.05, 26.40, 26.05, 23.56, 22.16, 20.90, 11.61, 6.67, 6.12 ppm; HRMS (ESI) *m/z*: $[M + H]^+$ calcd for $C_{38}H_{51}N_6O_9S$, 767.3433; found 767.3408. Anal. HPLC: t_R 14.50 min, purity 98%.

Cyclopentyl ((2*R*,6*S*,13a*S*,14a*R*,16a*S*,*Z*)-2-((3-ethyl-7-methoxyquinoxalin-2-yl)oxy)-14a-(((1-methylcyclopropyl)sulfonyl)carbamoyl)-5,16-dioxo-1,2,3,5,6,7,8,9,10,11,13a,14,14a,15,16,16a-hexadecahydrocyclopropa[*e*]pyrrolo[1,2-*a*][1,4]diazacyclopentadecin-6-

yl)carbamate (23a). The same procedure was used as described above for compound **22a**. Compound **19a** (0.40 g, 0.52 mmol) was treated with 4 N HCl in 1,4-dioxane (10 mL) to yield the amine salt **21a**, which was treated with DIEA (0.35 mL, 2.1 mmol) and *N*-(cyclopentyloxycarbonyloxy)-succinimide (0.15 g, 0.66 mmol) to provide the target compound **23a** (0.30 g, 74%) as a white solid. ^{1}H NMR (400 MHz, $CDCl_3$) δ 10.17 (s, 1 H), 7.81 (d, J = 9.6 Hz, 1 H), 7.21–7.16 (m, 2 H), 6.93 (s, 1 H), 5.92 (br s, 1 H), 5.70 (q, J = 9.2 Hz, 1 H), 5.26 (d, J = 7.6 Hz, 1 H), 4.99 (t, J = 9.6 Hz, 1 H), 4.86–4.81 (m, 1 H), 4.59 (t, J = 7.6 Hz, 1 H), 4.45 (d, J = 11.2 Hz, 1 H), 4.34–4.28 (m, 1 H), 4.04 (dd, J = 11.6, 4.0 Hz, 1 H), 3.94 (s, 3 H), 2.87 (q, J = 7.2 Hz, 2 H), 2.70–2.48 (m, 3 H), 2.32 (q, J = 8.8 Hz, 1 H), 1.92–1.23 (m, 27 H), 0.85–0.78 (m, 2 H) ppm; ^{13}C NMR (100 MHz, $CDCl_3$) δ 177.21, 172.99, 166.98, 160.22, 155.63, 154.90, 148.84, 140.85, 136.22, 134.36, 129.05, 124.88, 118.70, 105.93, 77.86, 74.54, 59.51, 55.71, 53.05, 52.16, 44.70, 36.43, 34.61, 32.72, 32.64, 32.58, 29.63, 27.13, 27.06, 26.47, 26.12, 23.56, 22.18, 20.94, 18.17, 14.49, 12.50, 11.59 ppm; HRMS (ESI) *m/z*: $[M + H]^+$ calcd for $C_{39}H_{53}N_6O_9S$, 781.3589; found 781.3561. Anal. HPLC: t_R 15.25 min, purity 99%.

3.6.3 Typical procedures for the synthesis of protease inhibitors using Method B:

Ethyl (1*R*,2*S*)-1-((2*S*,4*R*)-1-((*S*)-2-((*tert*-butoxycarbonyl)amino)non-8-enoyl)-4-((7-methoxy-3-(trifluoromethyl)quinoxalin-2-yl)oxy)pyrrolidine-2-

carboxamido)-2-vinylcyclopropane-1-carboxylate (25d). A solution of ester **12d** (6.40 g, 10.25 mmol) in THF-H_2O (1:1 mixture, 140 mL) was treated with LiOH.H_2O (1.38 g, 32.0 mmol). The resulting reaction mixture was stirred at room temperature for 24 h, then cooled to ~5 °C, acidified to a pH of 2.0 by slow addition of aqueous 0.25 N HCl (~ 200 mL), and extracted with EtOAc (2 × 500 mL). The organic portions were washed separately with saturated aqueous NaCl (250 ml), dried (Na_2SO_4), filtered, and evaporated under reduced pressure. The gummy residue was dissolved in $CHCl_3$ (50 mL), concentrated under reduced pressure, and the residue was dried under high vacuum to yield the acid **13d** (6.12 g, 98%) as a pale yellow foamy solid.

A solution of acid **13d** (6.12 g, 10.0 mmol) and amine salt **24** (2.50 g, 13.0 mmol) in anhydrous CH_2Cl_2 (100 mL) was treated with DIEA (9.10 mL, 55.0 mmol), HATU (5.30 g, 14.0 mmol) and DMAP (0.60 g, 4.9 mmol). The resulting reaction mixture was stirred at room temperature for 14 h, then diluted with EtOAc (500 mL), and washed successively with aqueous 1.0 N HCl, saturated aqueous $NaHCO_3$, and saturated aqueous NaCl (250 mL each). The organic portion was dried (Na_2SO_4), filtered, and evaporated under reduced pressure. The residue was purified by flash chromatography using 25–35% EtOAc/hexanes as the eluent to provide the bis-olefin compound **25d** (6.54 g, 87%) as a pale yellow foamy solid. ^{1}H NMR (500 MHz, $CDCl_3$) (mixture of rotamers, major rotamer) δ 7.78 (d, J = 9.2 Hz, 1 H), 7.53 (br s, 1 H), 7.47 (dd, J = 9.2, 2.8 Hz, 1 H), 7.43 (d, J = 2.4 Hz, 1 H), 5.88 (br s, 1 H), 5.81–5.70 (m, 2 H), 5.30 (dd, J =

16.8, 0.8 Hz, 1 H), 5.14–5.10 (m, 2 H), 5.01–4.89 (m, 2 H), 4.79 (dd, *J* = 14.0, 5.6 Hz, 1 H), 4.35–4.29 (m, 1 H), 4.21–4.08 (m, 3 H), 3.94 (s, 3 H), 2.90–2.82 (m, 1 H), 2.48–2.38 (m, 1 H), 2.16 (q, *J* = 9.0 Hz, 1 H), 2.04–1.98 (m, 2 H), 1.86 (dd, *J* = 8.0, 5.2 Hz, 1 H), 1.66–1.52 (m, 2 H), 1.46 (dd, *J* = 9.6, 5.6 Hz, 1 H), 1.43–1.21 (m, 19 H) ppm; ^{13}C NMR (125 MHz, $CDCl_3$) *δ* 173.02, 171.00, 169.87, 159.62, 155.52, 152.03, 138.92, 138.48, 137.16, 133.66, 128.02, 125.73, 120.72 (q, *J* = 273.6 Hz), 118.08, 114.52, 107.66, 79.98, 75.26, 61.40, 58.41, 56.02, 52.58, 52.43, 40.14, 33.89, 33.77, 32.76, 32.62, 28.97, 28.78, 28.31, 25.18, 23.11, 14.48 ppm; ^{19}F NMR (470 MHz, $CDCl_3$); −67.77 ppm; HRMS (ESI) *m/z*: $[M + H]^+$ calcd for $C_{37}H_{49}F_3N_5O_8$, 748.3528; found 748.3514.

Ethyl (2*R*,6*S*,13a*S*,14a*R*,16a*S*,*Z*)-6-((*tert*-butoxycarbonyl)amino)-2-((7-methoxy-3-(trifluoromethyl)quinoxalin-2-yl)oxy)-5,16-dioxo-1,2,3,6,7,8,9,10,11,13a,14,15,16,16a-tetradecahydrocyclopropa[*e*]pyrrolo[1,2-*a*][1,4]diazacyclopentadecine-14a(5*H*)-carboxylate (26d). A degassed solution of bis-olefin **25d** (1.50 g, 2.0 mmol) in 1,2-DCE (300 mL) was heated to 50 °C under argon, then Zhan 1b catalyst (0.150 g, 0.20 mmol) was added in two portions over 10 min. The resulting mixture was heated to 70 °C and stirred for 5 h. The reaction mixture was cooled to room temperature and concentrated under reduced pressure. The residue was purified by flash chromatography using 25–35% EtOAc/hexanes as the eluent to yield the P1–P3 macrocyclic product **26d** (1.0 g, 70%) as an off-white foamy solid. ^{1}H NMR (400 MHz, $CDCl_3$) *δ* 7.77 (d, *J* = 8.8 Hz, 1 H), 7.47

(dd, *J* = 8.8, 2.8 Hz, 1 H), 7.44 (d, *J* = 2.4 Hz, 1 H), 7.03 (br s, 1 H), 5.84–5.80 (m, 1 H), 5.56–5.49 (m, 1 H), 5.32–5.22 (m, 2 H), 4.92 (q, *J* = 4.4 Hz, 1 H), 4.49 (t, *J* = 7.6 Hz, 1 H), 4.24–4.05 (m, 4 H), 3.95 (s, 3 H), 3.05–2.99 (m, 1 H), 2.41–2.35 (m, 1 H), 2.24–2.14 (m, 3 H), 1.93–1.86 (m, 2 H), 1.66–1.60 (m, 1 H), 1.55 (dd, *J* = 96, 5.2 Hz, 1 H), 1.46–1.20 (m, 18 H) ppm; ^{13}C NMR (100 MHz, $CDCl_3$) *δ* 172.81, 171.95, 169.74, 159.69, 155.21, 152.20, 138.56, 137.25, 134.50, 128.08, 125.91, 125.84, 120.80 (q, *J* = 276 Hz), 107.73, 80.04, 75.42, 61.50, 58.08, 56.13, 52.21, 51.39, 41.36, 32.16, 31.77, 28.45, 28.10, 28.02, 26.37, 25.74, 23.70, 22.57, 14.72 ppm; HRMS (ESI) *m/z*: $[M + H]^+$ calcd for $C_{35}H_{45}F_3N_5O_8$, 720.3215; found 720.3203.

***tert*-Butyl ((2*R*,6*S*,13a*S*,14a*R*,16a*S*,*Z*)-14a-((cyclopropylsulfonyl)carbamoyl)-2-((7-methoxy-3-(trifluoromethyl)quinoxalin-2-yl)oxy)-5,16-dioxo-1,2,3,5,6,7,8,9,10,11,13a,14,14a,15,16,16a-hexadecahydrocyclopropa[*e*]pyrrolo[1,2-*a*][1,4]diazacyclopentadecin-6-yl)carbamate (18d).** A solution of ester **26d** (1.0 g, 1.4 mmol) in THF-MeOH-H_2O (1:1:1 mixture, 20 mL) was treated with $LiOH.H_2O$ (0.18 g, 4.2 mmol). The resulting reaction mixture was stirred at room temperature for 24 h, then cooled to ~5 °C, acidified to a pH of 2.0 by slow addition of aqueous 0.25 N HCl, and extracted with EtOAc (2 × 150 mL). The organic portions were washed separately with saturated aqueous NaCl (100 ml), dried (Na_2SO_4), filtered, and evaporated under reduced pressure. The gummy residue was dissolved in $CHCl_3$

(10 mL), concentrated under reduced pressure, and the residue was dried under high vacuum to yield the acid **27d** (0.95 g, 98%) as a pale yellow foamy solid.

A mixture of acid **27d** (0.40 g, 0.58 mmol) and CDI (0.131 g, 0.81 mmol) in anhydrous THF (8 mL) was heated at reflux for 1.5 h. The solution was cooled to room temperature and slowly added to a solution of cyclopropanesulfonamide **28** (0.10 g, 0.82 mmol) in anhydrous THF (4 mL) followed by DBU (0.12 mL, 0.81 mmol). The resulting reaction mixture was stirred at room temperature for 24 h, then quenched with aqueous 0.5 N HCl to pH ~2. Solvents were partially evaporated under reduced pressure, and the residue was extracted with EtOAc (2 × 100 mL). The combined organic portions were washed with saturated aqueous NaCl (100 mL), dried (Na_2SO_4), filtered, and evaporated under reduced pressure. The residue was purified by flash chromatography using 40–70% EtOAc/hexanes as the eluent to afford the title compound **18d** (0.28 g, 60%) as a white solid. ^{1}H NMR (400 MHz, $CDCl_3$) δ 10.28 (s, 1 H), 7.83 (d, J = 9.2 Hz, 1 H), 7.49 (dd, J = 8.8, 2.8 Hz, 1 H), 7.42 (d, J = 2.8 Hz, 1 H), 6.87 (s, 1 H), 5.92 (br s, 1 H), 5.70 (q, J = 8.8 Hz, 1 H), 5.13 (d, J = 7.6 Hz, 1 H), 4.97 (t, J = 8.4 Hz, 1 H), 4.62–4.56 (m, 2 H), 4.23–4.17 (m, 1 H), 4.01 (dd, J = 11.6, 3.2 Hz, 1 H), 3.94 (s, 3 H), 2.93–2.87 (m, 1 H), 2.68–2.50 (m, 3 H), 2.31 (q, J = 8.8 Hz, 1 H), 1.95–1.54 (m, 2 H), 1.53–1.02 (m, 21 H), 0.96–0.88 (m, 1 H) ppm; ^{13}C NMR (100 MHz, $CDCl_3$) δ 176.99, 173.31, 167.91, 159.45, 154.93, 151.76, 138.27, 136.99, 136.32, 134.56 (q, J = 36.2 Hz), 127.99, 125.57, 124.53, 120.8 (q, J = 274.0 Hz), 107.40, 79.76, 75.54, 59.44, 55.89, 52.72, 51.86, 44.65, 34.61, 32.82, 31.02,

29.61, 28.02, 27.04, 25.99, 22.21, 20.93, 6.67, 6.12 ppm; HRMS (ESI) *m/z*: $[M + H]^+$ calcd for $C_{36}H_{46}F_3N_6O_9S$, 795.2994; found 795.2974. Anal. HPLC: t_R 14.59 min, purity 100%.

***tert*-Butyl ((2*R*,6*S*,13a*S*,14a*R*,16a*S*,*Z*)-2-((7-methoxy-3-(trifluoromethyl)quinoxalin-2-yl)oxy)-14a-(((1-methylcyclopropyl)sulfonyl)carbamoyl)-5,16-dioxo-1,2,3,5,6,7,8,9,10,11,13a,14,14a,15,16,16a-hexadecahydrocyclopropa[*e*]pyrrolo[1,2-*a*][1,4]diazacyclopentadecin-6-yl)carbamate (19d).** The same procedure was used as described above for compound **18d**. Acid **27d** (0.43 g, 0.62 mmol) was treated with CDI (0.141 g, 0.87 mmol), 1-methylcyclopropanesulfonamide **29** (0.118 g, 0.87 mmol) and DBU (0.13 mL, 0.87 mmol) to afford the title compound **19d** (0.34 g, 68%) as a white solid. ^{1}H NMR (400 MHz, $CDCl_3$) δ 10.15 (s, 1 H), 7.83 (d, J = 9.2 Hz, 1 H), 7.48 (dd, J = 9.2, 2.8 Hz, 1 H), 7.42 (d, J = 2.8 Hz, 1 H), 6.90 (s, 1 H), 5.91 (s, 1 H), 5.70 (q, J = 9.2 Hz, 1 H), 5.14 (d, J = 7.6 Hz, 1 H), 5.00 (t, J = 9.2 Hz, 1 H), 4.62–4.55 (m, 2 H), 4.24–4.18 (m, 1 H), 4.02 (dd, J = 11.6, 3.6 Hz, 1 H), 3.94 (s, 3 H), 2.71–2.51 (m, 3 H), 2.33 (q, J = 8.4 Hz, 1 H), 1.93–1.75 (m, 4 H), 1.56–1.18 (m, 21 H), 0.85–0.78 (m, 2 H) ppm; ^{13}C NMR (100 MHz, $CDCl_3$) δ 177.30, 173.46, 167.15, 159.68, 155.16, 152.01, 138.50, 137.23, 136.50, 134.60 (q, J = 36.0 Hz), 128.23, 125.79, 125.19, 120.83 (d, J = 274.0 Hz), 107.65, 80.01, 75.79, 59.70, 56.12, 52.97, 52.08, 45.03, 36.65, 34.86, 33.06, 29.81, 28.26, 27.31, 27.24, 26.32, 22.47, 21.21, 18.42, 14.73, 12.77 ppm; HRMS (ESI) *m/z*: $[M + H]^+$ calcd

for $C_{37}H_{48}F_3N_6O_9S$, 809.3150; found 809.3129. Anal. HPLC: t_R 15.23 min, purity 99%.

Cyclopentyl ((2*R*,6*S*,13a*S*,14a*R*,16a*S*,*Z*)-14a-((cyclopropylsulfonyl)carbamoyl)-2-((7-methoxy-3-(trifluoromethyl)quinoxalin-2-yl)oxy)-5,16-dioxo-1,2,3,5,6,7,8,9,10,11,13a,14,14a,15,16,16a-hexadecahydrocyclopropa[*e*]pyrrolo[1,2-*a*][1,4]diazacyclopentadecin-6-yl)carbamate (22d). Compound **18d** (0.40 g, 0.52 mmol) was treated with a solution of 4 N HCl in 1,4-dioxane (10 mL). The reaction mixture was stirred at room temperature for 3 h, concentrated under reduced pressure, and the residue was dried under high vacuum. The pale yellow solid was triturated with diethyl ether (3 × 10 mL) and dried under high vacuum to yield the amine salt **20d** (0.37 g, 100%) as a white powder.

A solution of the above amine salt **20d** (0.37 g, 0.52 mmol) in anhydrous CH_3CN (15 mL) was treated with DIEA (0.35 mL, 2.1 mmol) and *N*-(cyclopentyloxycarbonyloxy)-succinimide (0.15 g, 0.66 mmol). The reaction mixture was stirred at room temperature for 24 h, then concentrated under reduced pressure and dried under high vacuum. The residue was purified by flash chromatography using 50–90% EtOAc/hexanes as the eluent to provide the target compound **22d** (0.30 g, 74%) as a white solid. ^{1}H NMR (400 MHz, $CDCl_3$) δ 10.27 (s, 1 H), 7.82 (d, J = 9.2 Hz, 1 H), 7.48 (dd, J = 9.2, 2.8 Hz, 1 H), 7.42 (d, J = 2.8 Hz, 1 H), 6.78 (s, 1 H), 5.95 (s, 1 H), 5.70 (q, J = 9.6 Hz, 1 H), 5.23 (d, J =

8.0 Hz, 1 H), 4.98 (t, *J* = 8.8 Hz, 1 H), 4.74–4.69 (m, 1 H), 4.60 (t, *J* = 7.6, 1 H), 4.54 (d, *J* = 11.6, 1 H), 4.25–4.19 (m, 1 H), 3.99 (dd, *J* = 11.6, 4.0 Hz, 1 H), 3.94 (s, 3 H), 2.94–2.88 (m, 1 H), 2.68–2.50 (m, 3 H), 2.31 (q, *J* = 8.8 Hz, 1 H), 1.94–1.24 (m, 21 H), 1.20–1.07 (m, 2 H), 0.96–0.89 (m, 1 H) ppm; ^{13}C NMR (100 MHz, $CDCl_3$) *δ* 177.33, 173.29, 168.27, 159.68, 155.87, 152.08, 138.56, 137.24, 136.47, 134.74 (q, *J* = 36.0 Hz), 128.24, 125.75, 124.79, 120.87 (d, *J* = 273.2 Hz), 107.62, 78.02, 75.70, 59.68, 56.11, 52.90, 52.35, 44.83, 34.71, 32.92, 32.81, 32.64, 31.26, 29.87, 27.27, 26.24, 23.81, 23.75, 22.49, 21.11, 6.89, 6.34 ppm; HRMS (ESI) *m/z*: [M + H]+ calcd for $C_{37}H_{46}F_3N_6O_9S$, 807.2994; found 807.2976. Anal. HPLC: t_R 14.98 min, purity 99%.

Cyclopentyl ((2*R*,6*S*,13a*S*,14a*R*,16a*S*,*Z*)-2-((7-methoxy-3-(trifluoromethyl)quinoxalin-2-yl)oxy)-14a-(((1-methylcyclopropyl)sulfonyl)carbamoyl)-5,16-dioxo-1,2,3,5,6,7,8,9,10,11,13a,14,14a,15,16,16a-hexadecahydrocyclopropa[*e*]pyrrolo[1,2-*a*][1,4]diazacyclopentadecin-6-yl)carbamate (23d). The same procedure was used as described above for compound **22d**. Compound **19d** (0.40 g, 0.52 mmol) was treated with 4 N HCl in 1,4-dioxane (10 mL) to yield the amine salt **21d**, which was treated with DIEA (0.35 mL, 2.1 mmol) and *N*-(cyclopentyloxycarbonyloxy)-succinimide (0.15 g, 0.66 mmol) to provide the target compound **23d** (0.30 g, 74%) as a white solid. ^{1}H NMR (400 MHz, CDCl3) *δ* 10.18 (s, 1 H), 7.83 (d, *J* = 9.6 Hz, 1 H), 7.48 (dd, *J* = 8.8, 2.8 Hz, 1 H), 7.41 (d, *J* = 2.8 Hz, 1 H), 6.94 (s, 1 H), 5.94 (s, 1 H), 5.70 (q,

J = 8.8 Hz, 1 H), 5.28 (d, *J* = 7.6 Hz, 1 H), 5.00 (t, *J* = 8.8 Hz, 1 H), 4.74–4.69 (m, 1 H), 4.60 (t, *J* = 7.6, 1 H), 4.54 (d, *J* = 12.0, 1 H), 4.25–4.19 (m, 1 H), 4.00 (dd, *J* = 11.6, 3.6 Hz, 1 H), 3.94 (s, 3 H), 2.68–2.50 (m, 3 H), 2.31 (q, *J* = 8.4 Hz, 1 H), 1.92–1.20 (m, 24 H), 0.85–0.78 (m, 2 H) ppm; ^{13}C NMR (100 MHz, $CDCl_3$) *δ* 177.33, 173.25, 167.13, 159.68, 155.84, 152.08, 138.56, 137.24, 136.44, 134.75 (q, *J* = 35.2 Hz), 128.25, 125.74, 125.21, 120.86 (d, *J* = 274.0 Hz), 107.62, 78.02, 75.71, 59.73, 56.12, 52.89, 52.34, 45.03, 36.65, 34.73, 32.93, 32.82, 32.64, 29.83, 27.26, 27.21, 26.29, 23.81, 23.75, 22.52, 21.23, 18.42, 14.73, 12.76 ppm. HRMS (ESI) *m/z*: $[M + H]^+$ calcd for $C_{38}H_{48}F_3N_6O_9S$, 821.3150; found 821.3133. Anal. HPLC: t_R 15.65 min, purity 97%.

3.6.4 Expression and Purification of NS3/4A Constructs

The HCV GT1a NS3/4A protease gene described in the Bristol Myers Squibb patent[128] was synthesized by GenScript and cloned into a PET28a expression vector. The D168A gene was engineered using the site-directed mutagenesis protocol from Stratagene. Protein expression and purification were carried out as previously described.[89] Briefly, transformed *Escherichia coli* BL21(DE3) cells were grown in LB media containing 30 µg/mL of kanamycin antibiotic at 37 °C. After reaching an OD_{600} of 0.8, cultures were induced with 1 mM IPTG and harvested after 4 h of expression. Cells were pelleted by centrifugation, resuspended in Resuspension buffer [50 mM phosphate buffer, 500 mM NaCl, 10% glycerol, 2 mM β-ME, pH 7.5] and frozen at −80 °C for storage.

Cell pellets were thawed and lysed via cell disruptor (Microfluidics Inc.) two times to ensure sufficient DNA shearing. Lysate was centrifuged at 19,000 rpm, for 25 min at 4 °C. The soluble fraction was applied to a nickel column (Qiagen) pre-equilibrated with Resuspension buffer. The beads and soluble fraction were incubated at 4 °C for 1.5 h and the lysate was allowed to flow through. Beads were washed with Resuspension buffer supplemented with 20 mM imidazole and eluted with Resuspension buffer supplemented with 200 mM imidazole. The eluent was dialyzed overnight (MWCO 10 kD) to remove the imidazole, and the His-tag was simultaneously removed with thrombin treatment. The eluate was judged >90% pure by polyacrylamide gel electrophoresis, concentrated, flash frozen, and stored at −80 °C.

The HCV GT3a NS3/4A protease gene was synthesized by GenScript. Transformed *Escherichia coli* BL21(DE3) cells were grown in LB media containing 30 µg/mL of kanamycin antibiotic at 37 °C. After reaching an OD_{600} 0.7, cultures were incubated at 4 °C for 20 min before being induced with 1 mM IPTG and placed at 18 °C for overnight expression. Cells were pelleted by centrifugation, resuspended in Resuspension buffer and frozen at –80 °C for storage.

Cell pellets were thawed and lysed via cell disruptor (Microfluidics Inc.) two times to ensure sufficient DNA shearing and treated with DNaseI. The lysate was treated and purified using a nickel column as above, with an additional wash with 1 M NaCl prior to elution. The protein was further purified using a HiLoad

Superdex75 16/60 column equilibrated with Resuspension buffer. The eluate was judged >90% pure by polyacrylamide gel electrophoresis, concentrated, flash frozen, and stored at −80 °C .

3.6.5 Determination of the Inner Filter Effect

The inner filter effect (IFE) for the NS3/4A protease substrate was determined using a previously described method.[129] Briefly, fluorescence end-point readings were taken for substrate concentrations between 0 µM and 20 µM. Afterward, free 5-FAM fluorophore was added to a final concentration of 25 µM to each substrate concentration and a second round of fluorescence end-point readings was taken. The fluorescence of free 5-FAM was determined by subtracting the first fluorescence end point reading from the second round of readings. IFE corrections were then calculated by dividing the free 5-FAM florescence at each substrate concentration by the free 5-FAM florescence at zero substrate.

3.6.6 Determination of Michaelis–Menten (K_m) Constant

K_m constants for GT1 and D168A protease were previously determined.[106] The K_m of GT3 protease was determined using the following method. A 20 µM concentration of substrate [Ac-DE-Dap(QXL520)- EE-Abu-γ-[COO]AS-C(5-FAMsp)-NH2] (AnaSpec) was serially diluted into assay buffer [50 mM Tris, 5% glycerol, 10 mM DTT, 0.6 mM LDAO, and 4% dimethyl sulfoxide] and proteolysis was initiated by rapid injection of 10 µL GT3 protease (final concentration 20 nM)

in a reaction volume of 60 µL. The fluorescence output from the substrate cleavage product was measured kinetically using an EnVision plate reader (Perkin-Elmer) with excitation wavelength at 485 nm and emission at 530 nm. Inner filter effect corrections were applied to the initial velocities (V_o) at each substrate concentration. V_o versus substrate concentration graphs were globally fit to the Michaelis–Menten equation to obtain the K_m value.

3.6.7 Enzyme Inhibition Assays

For each assay, 2 nM of NS3/4A protease (GT1a, D168A and GT3a) was pre-incubated at room temperature for 1 h with increasing concentration of inhibitors in assay buffer [50 mM Tris, 5% glycerol, 10 mM DTT, 0.6 mM LDAO, and 4% dimethyl sulfoxide]. Inhibition assays were performed in nonbinding surface 96-well black half-area plates (Corning) in a reaction volume of 60 µL. The proteolytic reaction was initiated by the injection of 5 µL of HCV NS3/4A protease substrate (AnaSpec), to a final concentration of 200 nM and kinetically monitored using a Perkin Elmer EnVision plate reader (excitation at 485 nm, emission at 530 nm). Three independent data sets were collected for each inhibitor with each protease construct. Each inhibitor titration included at least 12 inhibitor concentration points, which were globally fit to the Morrison equation to obtain the K_i value.

3.6.8 Cell-Based Drug Susceptibility Assays

Mutations (R155K, A516T, D168A and D168V) were constructed by site-directed mutagenesis using a Con1 (genotype 1b) luciferase reporter replicon containing the H77 (genotype 1a) NS3 sequence.[130] Replicon RNA of each protease variant was introduced into Huh7 cells by electroporation. Replication was then assessed in the presence of increasing concentrations of protease inhibitors by measuring luciferase activity (relative light units) 96 h after electroporation. The drug concentrations required to inhibit replicon replication by 50% (EC_{50}) were calculated directly from the drug inhibition curves.

3.6.9 Crystallization and Structure Determination

Protein expression and purification were carried out as previously described.[89] The Ni-NTA purified WT1a protein was thawed, concentrated to 3 mg/mL, and loaded on a HiLoad Superdex75 16/ 60 column equilibrated with gel filtration buffer (25 mM MES, 500 mM NaCl, 10% glycerol, and 2 mM DTT, pH 6.5). The protease fractions were pooled and concentrated to 25 mg/mL with an Amicon Ultra-15 10 kDa filter unit (Millipore). The concentrated samples were incubated for 1 h with 3:1 molar excess of inhibitor. Diffraction-quality crystals were obtained overnight by mixing equal volumes of concentrated protein solution with precipitant solution (20–26% PEG-3350, 0.1 M sodium MES buffer, 4% ammonium sulfate, pH 6.5) at RT or 15 °C in 24-well VDX hanging drop trays. Crystals were harvested and data was collected at 100 K. Cryogenic

conditions contained the precipitant solution supplemented with 15% glycerol or ethylene glycol.

Diffraction data were collected using an in-house Rigaku X-ray system with a Saturn 944 detector. All datasets were processed using HKL-3000.[131] Structures were solved by molecular replacement using PHASER.[132] The WT-**2** complex structure (PDB code: 5EPN)[111] was used as the starting structure for all structure solutions. Model building and refinement were performed using Coot[133] and PHENIX,[134] respectively. The final structures were evaluated with MolProbity[135] prior to deposition in the PDB. To limit the possibility of model bias throughout the refinement process, 5% of the data were reserved for the free R-value calculation.[136] Structure analysis, superposition and figure generation were done using PyMOL.[137] X-ray data collection and crystallographic refinement statistics are presented above (**Table 3.3**).

3.6.10 Molecular Modeling

Molecular modeling was carried out using MacroModel (Schrödinger, LLC, New York, NY).[170] Briefly, inhibitors were modeled into the active site of WT1a and A156T proteases using the WT-**2** and A156T-**2** co-complex structures (PDB code: 5EPN and 5EPY).[111] Structures were prepared using the Protein Preparation tool in Maestro 11. 2D chemical structures were modified with the appropriate changes using the Build tool in Maestro. Once modeled, molecular energy minimizations were performed for each inhibitor–protease complex using

the PRCG method with 2500 maximum iterations and 0.05 gradient convergence threshold. PDB files of modeled complexes were generated in Maestro for structural analysis.

3.7 Acknowledgement

This work was supported by a grant from the National Institute of Allergy and Infectious Diseases of the NIH (R01 AI085051). ANM was also supported by the National Institute of General Medical Sciences of the NIH (F31 GM119345). MJ was supported by a Postdoctoral Fellowship from the Higher Education Commission of Pakistan (HEC). We thank Dr. Kiran K. Reddy and members of the Schiffer and Miller laboratories for helpful discussions.

Chapter IV

Design of HCV NS3/4A PIs leveraging untapped regions of the substrate envelope

Preface

Chapter IV is a collaborative study that is in preparation.

Matthew, A. N.; Lockbaum, G. L.; Kamran, W.; Timm, J.; Henes, M.; Kosovrasti, K.; Carbone, C.; Loring, H.; Ali, A.; Kurt Yilmaz, N.; Schiffer, C. Design of HCV NS3/4A PIs leveraging untapped regions of the substrate envelope.

Contributions from Ashley N. Matthew:

I performed the protein expression and purification of GT1a, D168A proteases for this study. I solved seven structures for this study with help from Jennifer Timm, Heather Loring, and Christine Carbone. I created all of the figures and tables for this study. I performed the biochemical and structural analyses and wrote the manuscript with guidance from Nese Kurt Yilmaz and Celia A. Schiffer.

4.1 Abstract

In HCV, rapid selection of resistance-associated variants often leads to reduced efficacy of NS3/4A protease inhibitors (PIs). One strategy to combat resistance is to constrain inhibitors within evolutionarily conserved regions in the protease active site. The substrate envelope provides a rational drug design strategy to exploit evolutionary constraints that mimic substrate interactions to limit susceptibility to resistance. We designed HCV NS3/4A PIs with modified P4 capping groups or modified P4 amino acids with P5 capping groups that extend in the P4 direction, leveraging unexploited areas in the substrate envelope. Inhibition assays revealed that inhibitors have flatter resistant profiles and higher affinity over FDA-approved NS3/4A PI grazoprevir and parent compound JZ01-15 against resistant variants. Crystal structures confirmed that inhibitors fit within the substrate envelope and that extending into the S4 pocket of the substrate envelope improve both resistance profile and inhibitor potency. Thus, the HCV substrate envelope is a powerful tool for the design of robust PIs and further modification of the P4 position on the inhibitor scaffold may lead to more efficacious PIs toward the eradication of HCV infection.

4.2 Introduction

Drug resistance is a major threat to the treatment of patients infected with Hepatitis C virus (HCV). The clinical sequelae of HCV infection include chronic liver disease, cirrhosis from prolonged inflammation and hepatocellular

carcinoma.[1] The severe liver damage caused by the insidious progression of HCV infection has made this virus the leading cause of liver transplantation in most countries.[171] Despite advancements in treatment options and outcomes with the development of direct-acting antivirals (DAAs) against essential viral proteins encoded by the HCV genome, drug resistance remains a problem with the rapid emergence of resistance–associated substitutions (RASs) affecting all viral targets.[22,23,51,107,112,119] This rapid selection of RASs is in part due to the high replication rate of HCV and the low fidelity of the RNA-dependent RNA polymerase (RdRp).[116,117] At baseline, patients can be infected with a diverse viral population known as quasispecies.[172] At the start of antiviral therapy, the selective drug pressure often leads to the rise of additional resistant viral species that are not effectively inhibited by the administered drug.[173] Thus, drugs with increased efficacy and minimized susceptibility to resistance are needed to effectively eradicate HCV infection.

The NS3/4A protease is an excellent target for the development of novel and robust DAAs. This essential protease proteolytically cleaves the HCV polyprotein precursor into functional components necessary for viral replication and maturation.[174] The NS3/4A viral substrates share little sequence homology except a cysteine at P1 and an acid at P6 positions.[101] The diversity of the NS3/4A cleavage sites implies that a specific sequence motif is not the basis of substrate specificity. However, when the substrates are bound to the protease active site, they occupy a similar consensus volume termed the *substrate*

envelope (SE).[90] This consensus volume is the basis of molecular recognition for the NS3/4A protease substrates. Drug resistance is loss of inhibitor binding affinity while maintaining substrate processing. In the NS3/4A protease, resistance substitutions occur where inhibitors protrude outside the substrate envelope and contact residues of the enzyme that are unessential in substrate recognition.[89]

The FDA has approved five protease inhibitors (PIs) for the treatment of HCV: simeprevir,[85] paritaprevir,[91] grazoprevir,[120] glecaprevir[51] and voxilaprevir.[121] All protease inhibitors (PIs) have large heterocyclic P2 moieties that significantly improve potency.[80] However, the identity of the P2 moiety strongly influences the inhibitor resistance profile. The P2 moiety of older generation PIs protrudes beyond the substrate envelope and contacts the S2 subsite residues Arg155, Ala156 and Asp168.[89] These residues are where the most common drug resistance substitutions occur. Notably, Asp168 RASs are present in nearly all patients who fail therapy with a PI-containing regimen.[107] Arg155 and Asp168 are critical residues that contribute to an electrostatic network necessary for efficient inhibitor binding. High-resolution crystal structures of PIs bound to wildtype and resistant proteases revealed that disruption of this electrostatic network due to substitutions at Arg155 or Asp168 underlie the mechanism of resistance for older NS3/4A PIs.[89,109]

While protrusion beyond the substrate envelope at the P2 position on the inhibitor scaffold is inevitable without compromising potency, utilization of

evolutionarily constrained residues in the protease active site may still enable circumvention of resistance. In the case of grazoprevir, although the P2 quinoxaline protrudes outside of the substrate envelope, this moiety stacks against the invariant catalytic triad and minimizes contact with the S2 subsite residues.[89,111] Grazoprevir is a P2–P4 macrocyclic inhibitor with a P2 quinoxaline moiety that predominantly binds on catalytic triad residues His57 and Asp81. Substitution of any of the catalytic triad residues would disrupt enzymatic activity, preventing the likelihood of viable resistance. However, grazoprevir is still highly susceptible to the A156T substitution as the larger threonine side chain clashes with the inhibitor macrocycle, and is moderately susceptible to Asp168 substitutions.[111] Nevertheless, given the relatively improved resistance profile of grazoprevir, drug companies have exploited this inhibitor scaffold leading to the development of newer generation P2–P4 macrocyclic inhibitors glecaprevir and voxilaprevir.

Macrocyclization status also plays a critical role in inhibitor susceptibility to resistance substitutions. Design of 5172-mcP1P3, a P1–P3 macrocyclic analog of grazoprevir, led to an inhibitor with an improved resistance profile that was less susceptible to single site substitutions in the protease active site, particularly A156T.[106] Moreover, change of the macrocycle from the P2–P4 to the P1–P3 position maintained the binding mode of the parent compound grazoprevir.[111] Further modifications of the P2 quinoxaline moiety of the 5172-mcP1P3 scaffold revealed that small substituents at the 3-position such as the methyl group in

JZ01-15, are better at maintaining activity against drug resistant variants due to limited contact with S2 subsite residues.[124]

An additional strategy that can be employed to thwart resistance is to design inhibitors to fit within the substrate envelope. Previous studies with HIV-1 protease demonstrate that the substrate envelope can successfully be used as a drug design constraint. Ten inhibitors based on the FDA-approved drug darunavir were designed to better fit in the substrate envelope and exhibited robust activity against multi-drug resistant HIV-1 variants.[175] The scaffold of all current HCV PIs only spans the P4–P1' positions with a small P4 capping group. In fact, the volume remaining in the substrate envelope is almost equal to the volume of the inhibitor that protrudes outside the envelope.[160] Thus, current protease inhibitors can be extended into the P4–P5 pockets of the HCV substrate envelope. Analysis of the dynamic substrate envelope revealed that the P1–P5 positions are quite conserved with the P6 position being the most dynamic.[160] Therefore, further elaboration to the inhibitor scaffold may benefit by modifications at the P4 and P5 positions. To design more robust inhibitors, our design incorporated the following strategies: fit within the substrate envelope, leverage interactions unexploited by current inhibitors, and incorporate moieties that interact with the invariant catalytic triad minimizing contacts with unessential residues. Thus, leveraging our knowledge of the binding modes of current inhibitors and substrates, and the mechanisms of drug resistance, the aim was to design inhibitors that are less susceptible to resistance.

We used the substrate envelope strategy to optimize HCV PIs based on the JZ01-15 scaffold by incorporating modifications at the P4–P5 positions that fit within the substrate envelope. The modifications extend toward the region of the HCV NS3/4A substrate envelope that is not utilized by current inhibitors. A panel of 9 inhibitors was designed, synthesized, and assayed, and a select subset was co-crystallized bound to wildtype and D168A protease. Biochemical analysis revealed that all inhibitors designed to fit within the substrate envelope exhibited flatter resistance profiles than FDA-approved drug grazoprevir. Crystal structures of 5 of the PIs bound to wildtype and D168A protease have been determined, and confirmed that these inhibitors fit within the substrate envelope as designed. Structural analysis of the carbamate-linked P4 compounds revealed that the improved activity observed against the D168A variant is due to enhanced filling of the S4 pocket, utilization of additional space in the substrate envelope, and optimization of interactions in the substrate binding site. Thus use of the substrate envelope in NS3/4A PI design can be successfully incorporated at the outset of inhibitor design providing inhibitors with improved potency and resistance profiles against drug resistant variants.

4.3 Results

Substitutions in the protease active site can result in detrimental loss of potency for many PIs. Specifically, Asp168 is a pivotal residue as substitutions at this position often weaken the ability of inhibitors to bind efficiently.[89,106] Though

newer generation inhibitors glecaprevir and voxilaprevir are not susceptible to Asp168 substitutions, they are still highly susceptible to Ala156 substitutions due their P2–P4 macrocycle.[51] Thus the P1–P3 macrocyclic JZ01-15 scaffold (**Figure 4.1**) was targeted to elaborate as this is an inhibitor not susceptible to the A156T substitution; this strategy may lead to inhibitors that fit within the substrate envelope and that are less susceptible to resistance. Moreover, polymorphisms at the Asp168 position, which is Gln168 in genotype 3, underlie reduced efficacy of most PIs.[108] Thus, designing novel inhibitors using the substrate envelope approach to have better activity against Asp168 substitutions in genotype 1 may give rise to improved activity against other genotypes.

Modifications to the JZ01-15 scaffold were made at the P4–P5 positions to utilize unexploited space in the substrate envelope. Hydrophobic moieties at the P4 position were used to mimic substrate interactions, as HCV substrates across genotypes have hydrophobic residues at this position.[11] Our goal was to extend toward the S4 substrate-binding pocket and leverage specific interactions common to substrates including backbone hydrogen bonds to residues in this binding groove. We used two general approaches to sample the chemical space in the substrate envelope by synthesizing a set of 9 inhibitors with either a modified carbamate linked P4-cap (P4–cap inhibitors) or a modified P4 amino acid with a small P5 capping group (P4–P5-cap inhibitors) (**Figure 4.1**).

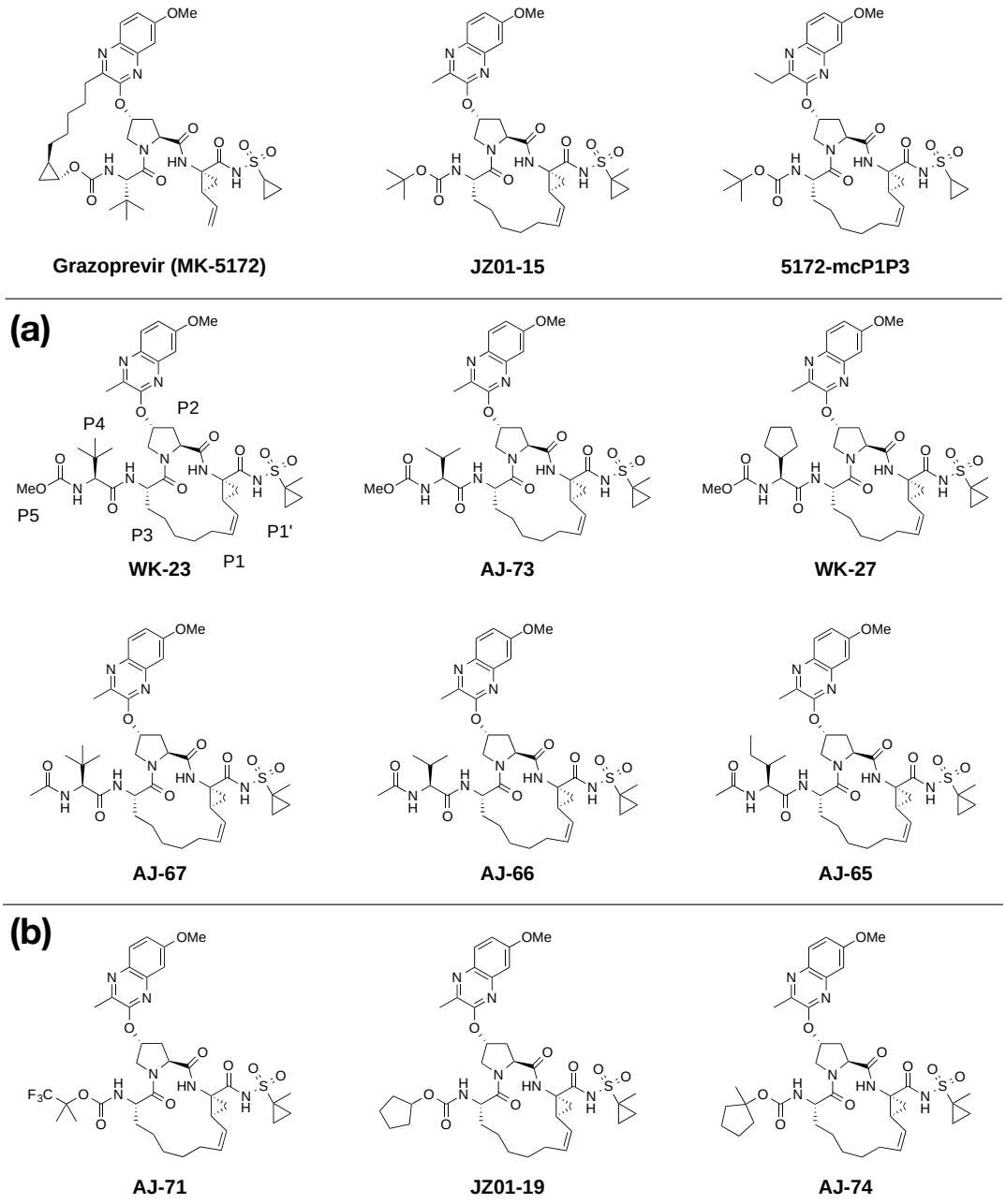

Figure 4.1: Chemical structures of designed HCV NS3/4A protease inhibitors.

Grazoprevir is an FDA-approved PI. Change of the macrocycle location and modification of the P2 quinoxaline moiety of 5172-mcP1P3 led to the development of JZ01-15. The designed inhibitors (a) P4–P5-cap and (b) P4–cap were based on the JZ01-15 scaffold with modifications at the P4 and P4–P5 regions. The canonical nomenclature for drug moiety positioning is indicated for WK-23.

4.3.1 Designed compounds inhibit wildtype protease

The enzyme inhibition constants (K_i values) of the designed inhibitors were determined against wildtype protease and the D168A drug resistant variant. All 9 inhibitors were potent against wildtype protease with K_i values ranging from 1.13 – 29.5 nM (**Figure 4.2A**). Overall inhibitors with a modified P4 capping group were more potent than inhibitors with a modified P4 amino acid and small P5 capping group. WK-23, a P4–P5-cap inhibitor with a t-butyl P4 moiety and small carbamate-linked P5 methoxy capping group, exhibited reduced potency against wildtype protease (K_i = 29.5 nM) relative to parent compound JZ01-15 (K_i = 3.6 nM). To test the effect of the capping group, we designed AJ-67, which is identical to WK-23 except for the N-acetyl capping group. Both AJ-67 and WK-23 showed similar activity against wildtype protease. This trend was also observed with AJ-66 and AJ-73, two P4 isopropyl inhibitors that differ only at the P5 position, suggesting that the capping change tested here does not affect inhibitor potency.

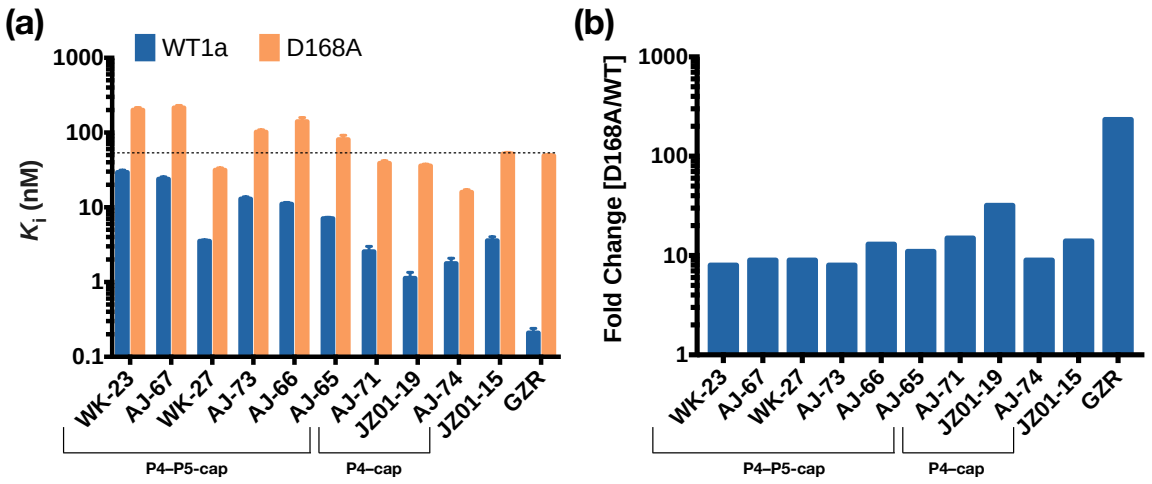

Figure 4.2: Resistance profile of NS3/4A protease inhibitors.
a) Enzyme inhibition constants against wildtype (blue) and D168A (orange) protease and b) fold change of enzyme inhibitory activity against the D168A variant normalized with respect to the wild-type NS3/4A protease.

The P4–cap inhibitors (AJ-71, JZ01-19 and AJ-74) overall had improved potency against wildtype protease relative to both P4–P5-cap inhibitors and parent compound JZ01-15. The K_i values of these compounds ranged from 1.13–2.56 nM. JZ01-19 was 3-fold more potent than parent compound JZ01-15 and only 5 fold less potent than grazoprevir. While no inhibitor exhibited sub-nanomolar activity against wildtype protease as the FDA-approved P2–P4 macrocyclic grazoprevir (K_i = 0.21 nM), we were able to modify the P4–cap of inhibitors and gain potency. Thus modification at the P4 position using a substrate envelope guided approach yielded inhibitors with improved potency relative to the parent compound.

4.3.2 Designed inhibitors have improved resistance profile against the D168A variant

To understand if the substrate envelope as a constraint in inhibitor design results in compounds that are less susceptible to resistance, we tested the pivotal D168A variant. All PIs tested lost considerable activity against the D168A variant including grazoprevir, as has previously been reported.[106,124] P4–P5-cap inhibitors were less potent against the D168A variant than the P4–cap inhibitors, similar to wildtype protease. All P4–cap inhibitors had improved activity against the D168A variant (K_i range: 16 – 39 nM) relative to parent compound JZ01-15 (K_i = 52 nM). Remarkably, AJ-74, a P4–cap inhibitor with a methylcyclopentyl capping group exhibited 3-fold improved potency against the D168A variant compared to grazoprevir (Ki = 16 and 49 nM, respectively).

While all PIs showed reduced potency against the D168A variant relative to WT protease in the enzyme inhibition assay, the fold change losses were much smaller for all 9 designed inhibitors (**Figure 4.2B**). Grazoprevir is highly susceptible to the D168A variant exhibiting over a 230-fold reduction in potency. All inhibitors designed to fit within the substrate envelope exhibited between 9- to 32-fold reductions in potency, much smaller than observed for grazoprevir. Thus inhibitors designed using the substrate envelope have flatter resistance profiles and suggest that substrate envelope guided design can produce compounds with low nanomolar potency and reduced susceptibility to drug resistance.

4.3.3 Structure determination of protease-inhibitor complexes

To understand the molecular basis for the observed resistance profiles of the inhibitors as well as to determine if the inhibitors fit within the substrate envelope as designed, crystal structures of select inhibitors bound to wildtype and D168A proteases were determined (**Table 4.1**). A total of seven new crystal structures with resolutions ranging from 1.6 – 1.9 Å were determined for this study. Five crystal structures of WK-23, AJ-67, AJ-71, JZ01-19, and AJ-74 were determined in complex with wildtype protease. Crystallization efforts with drug resistant variant D168A were successful with inhibitors AJ-67 and AJ-71. All structures were analyzed in comparison with previously determined crystal structures of parent compound JZ01-15 (PDB ID: 5VOJ for wildtype) and grazoprevir (PDB IDs: 3SUD for wildtype and 3SUF for D168A, respectively).[89,124]

Table 4.1: X-ray data collection and crystallographic refinement statistics.

	WT-WK-23	**WT-AJ-67**	**WT-AJ-71**	**WT-JZ01-19**	**WT-AJ-74**	**D168A-AJ-67**	**D168A-AJ-71**
Resolution	1.58 Å	1.75 Å	1.92 Å	1.79 Å	1.87 Å	1.83Å	1.80Å
Space group	$P2_12_12_1$	$P2_12_12_1$	$P2_12_12_1$	$P2_12_12_1$	$P2_12_12_1$	$P2_12_12_1$	$P2_12_12_1$
Molecules in AU[a]	1	1	1	1	1	1	1
Cell dimensions:							
a (Å)	55.5	55.1	55.6	55.3	55.1	55.5	55.7
b (Å)	58.5	59.8	58.6	58.6	59.6	58.7	58.6
c (Å)	59.9	58.5	60.0	59.8	58.5	60.0	60.1
β (°)	90	90	90	90	90	90	90
Completeness (%)	91.3	97.0	96.7	98.1	97.4	98.1	92.6
Total reflections	250177	119548	106822	118729	110776	115996	120162
Unique reflections	25037	19508	14999	18610	16126	17556	17476
Average I/σ	7.9	8.8	19.8	14.5	12.7	12.8	6.3
Redundancy	10	6.1	7.1	6.4	6.9	6.6	6.9
R_{sym} (%)[b]	5.7 (15.2)	4.3 (18.3)	10.6 (45.8)	7.1 (28.4)	6.3 (19.6)	7.0 (21.6)	3.9 (11.7)
RMSD[c] in:							
Bond lengths (Å)	0.007	0.009	0.01	0.004	0.02	0.006	0.01
Bond angles (°)	1.0	1.3	1.0	0.8	0.6	1.1	1.5
R_{factor} (%)[d]	15.1	14.6	18.7	18.2	18.3	16.1	13.8
R_{free} (%)[e]	18.3	19.3	22.7	22.9	23.3	19.4	18.0

[a]AU, asymmetric unit.
[b]$R_{sym} = \Sigma \mid I - \langle I \rangle \mid / \Sigma I$, where I = observed intensity, $\langle I \rangle$ = average intensity over symmetry equivalent; values in parentheses are for the highest resolution shell.
[c]RMSD, root mean square deviation.
[d]$R_{factor} = \Sigma \mid\mid F_o \mid - \mid F_c \mid\mid / \Sigma \mid F_o \mid$.
[e]R_{free} was calculated from 5% of reflections, chosen randomly, which were omitted from the refinement process.

The binding mode of all of the designed inhibitors was very similar to parent compound JZ01-15 and grazoprevir. The P2 quinoxaline maintained the π-π stacking interaction with catalytic His57 residue irrespective of modifications at the P4 and P5 positions as expected (**Figure 4.3**). In fact, changes in the binding mode occurred only at the positions that were modified, with the P3–P1' positions of the ligand relatively unchanged. In all structures, inhibitors formed conserved hydrogen bonds with backbone atoms in the protease including: 1) P1 amide nitrogen with the backbone carbonyl of Arg155, 2) P3 amide nitrogen with the backbone carbonyl of Ala157, 3) P3 cabonyl with the backbone nitrogen of Ala157 and 4) the P1' acylsulfonamide moiety with backbone atoms of residues 137–139 in the oxyanion hole. Additionally, the Nε nitrogen of His57 made a hydrogen bond with the sulfonamide nitrogen in all inhibitor complexes. Differences in hydrogen bonding were observed in the S4 pocket where modifications to the inhibitor were made.

4.3.4 Inhibitors with the P4–P5 modifications fit within the substrate envelope and gain substrate-like interactions

Grazoprevir, although potent, protrudes from the substrate envelope making this inhibitor highly susceptible to drug resistance mutations especially at Ala156 and Asp168 due to the positioning of the P2–P4 macrocycle and P4 moiety (**Figure 4.3A**). Modification of the macrocycle location and the P2 position led to JZ01-15, which fits better in the substrate envelope (**Figure 4.3B**). The crystal structures of parent compound JZ01-15 bound to wildtype protease and the

additional 5 inhibitor-wildtype protease structures superimpose extremely well. Moreover, the designed inhibitors fit within the substrate envelope, utilizing unexplored space and leveraging substrate-like contacts (**Figure 4.3C**). Thus, crystal structures confirm that inhibitors fit within the substrate envelope as they were designed.

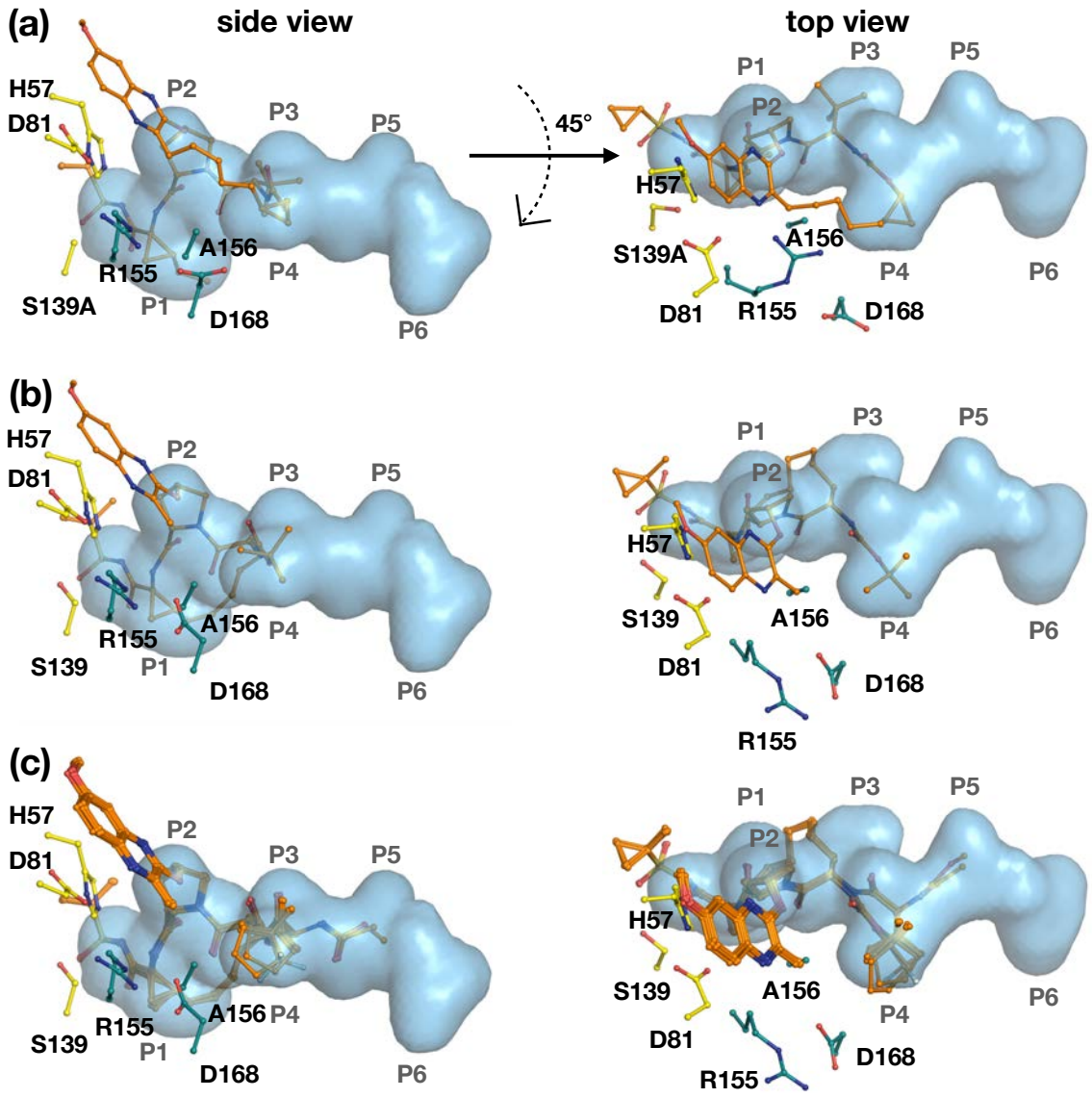

Figure 4.3: Fit of NS3/4A protease inhibitors within the substrate envelope. Inhibitors a) grazoprevir, b) JZ01-15 and c) designed inhibitors WK-23, AJ-67, AJ-71, JZ01-19 and AJ-74 shown as sticks (orange) in the substrate envelope (blue). The side chains of the catalytic triad and common drug resistance residues are shown as yellow and green sticks, respectively. A side view and top view of the inhibitors in the substrate envelope are shown with the P1–P6 positions of the envelope labeled.

4.3.5 Active site hydrogen bond network is conserved for inhibitors

WK-23 is a P4–P5-cap inhibitor with a t-butyl moiety at the P4 position and a carbamate-linked P5 methoxy capping group. Crystal structures of this inhibitor bound to wildtype protease revealed that the carbonyl group of the P5 cap gains hydrogen bonds with the backbone nitrogen and side chain of Ser159 (**Figure 4.4A**). This interaction is reminiscent of the protease-substrate complexes as this backbone hydrogen bond to Ser159 is conserved in all structures of bound substrates. Alteration of the P5 capping group to an N-acetyl cap did not change the binding mode of this inhibitor relative to WK-23 (**Figure 4.4B**). In fact, the hydrogen bonds to the backbone and side chain of Ser159 are maintained in the presence of a different capping group (**Figure 4.5**). This is in agreement with our biochemical data as both inhibitors had similar potency against wildtype protease. Interestingly, WK-23 and AJ-67 bind very similarly to viral substrates (**Figure 4.4C, D**). Although these inhibitors are not as potent as parent compound JZ01-15, they demonstrate that the substrate envelope can be utilized to design inhibitors that mimic substrate binding.

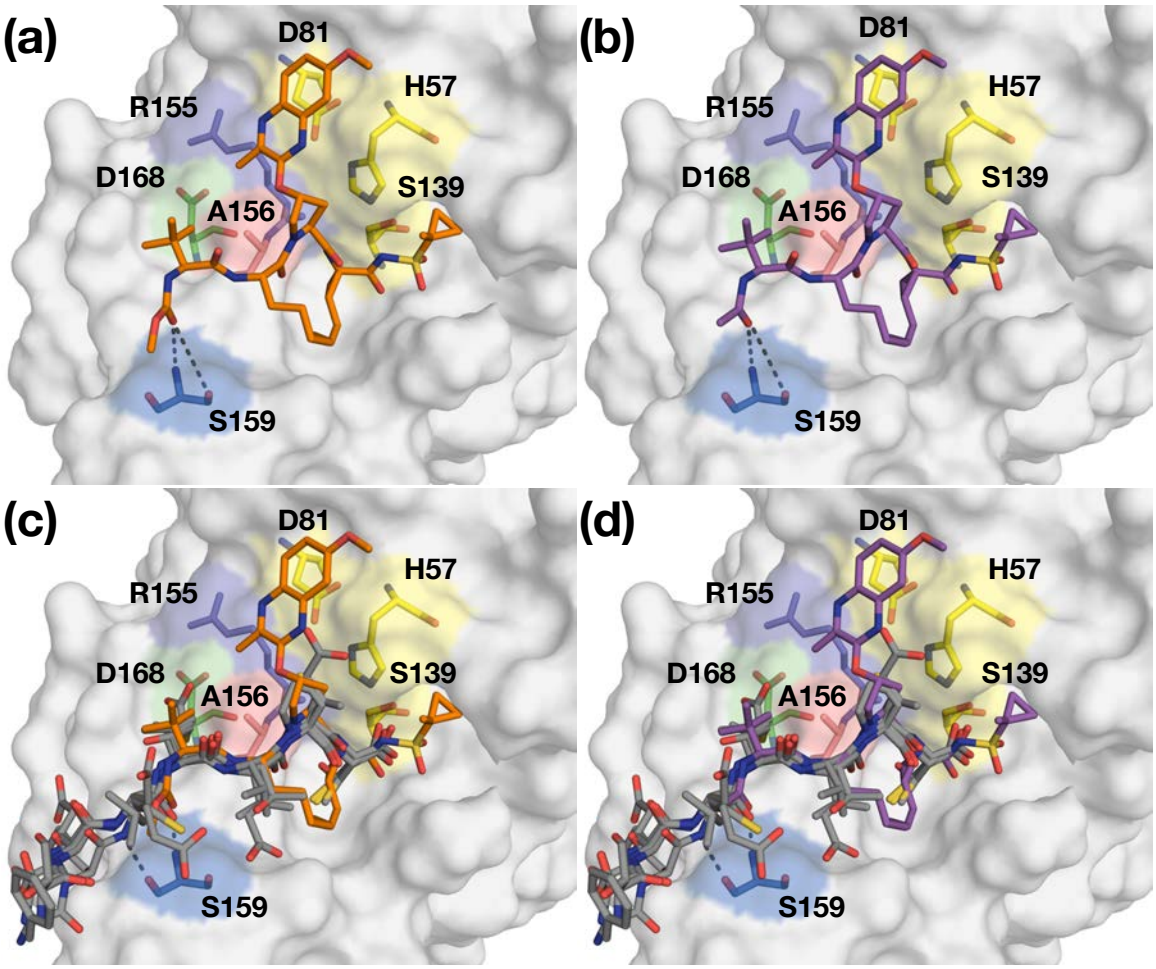

Figure 4.4: Binding modes of P4–P5-cap inhibitors.
(a) Surface representation of (a) WK-23 (orange) and (b) AJ-67 (purple) bound to the active site of wildtype NS3/4A protease. Superposition of viral substrates (gray) and (c) WK-23 and (d) AJ-67. Substrate hydrogen bonds to Ser159 are shown in panel (c) and (d). Catalytic triad residues are highlighted in yellow and drug resistance residues Arg155, Ala156, Asp168 and Ser159 are shown as purple, red, green and blue sticks, respectively.

4.3.6 Loss of hydrogen bond with Ser159 side chain underlies reduced efficacy of P4–P5-cap inhibitors to the D168A variant

To investigate the molecular basis of reduced potency for the P4–P5-cap modified inhibitors against the D168A resistant variant, crystal structures of AJ-67 bound to wildtype protease and the mutant protease were comparatively analyzed. Similar to grazoprevir, loss in potency is likely due to loss of the electrostatic network as a result the D168A substitution (**Figure 4.5A**).[89] The overall structure of AJ-67 bound to the D168A is very similar to this inhibitor bound to wildtype protease. However, the major change occurs at residue Ser159. This residue adopts an altered confirmation of the side chain where the hydroxyl group is pointed away from the inhibitor (**Figure 4.5B, 4.6**). As a result, the hydrogen bond of AJ-67 with the Ser159 side chain that is present in the wildtype structure is lost. Additionally, the P5 capping group of AJ-67 shifts by 0.5 Å (**Figure 4.6**). This results in reduced interactions with the S4 subsite. It is likely that this mechanism for reduced potency against D168A variant is the same for all inhibitors that bind similar to AJ-67 including WK-23 and other P4–P5-cap inhibitors.

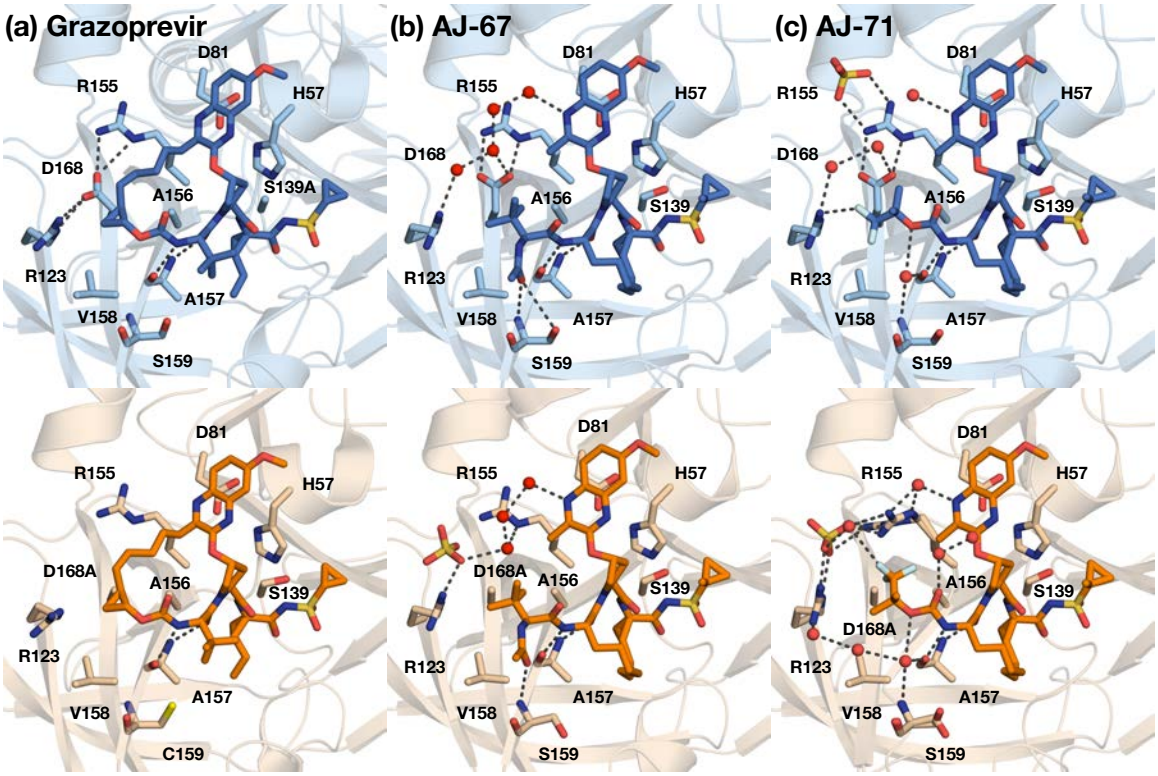

Figure 4.5: Hydrogen bond network in the protease active site of grazoprevir and designed PIs.
Cartoon representation of (a) grazoprevir, (b) AJ-67 and (c) AJ-71 bound to wildtype (blue) and D168A (orange) proteases. The catalytic triad and S4 subsite residues are shown as sticks. Water molecules are shown as non-bonded spheres (red) and dash lines represent hydrogen bonds (black).

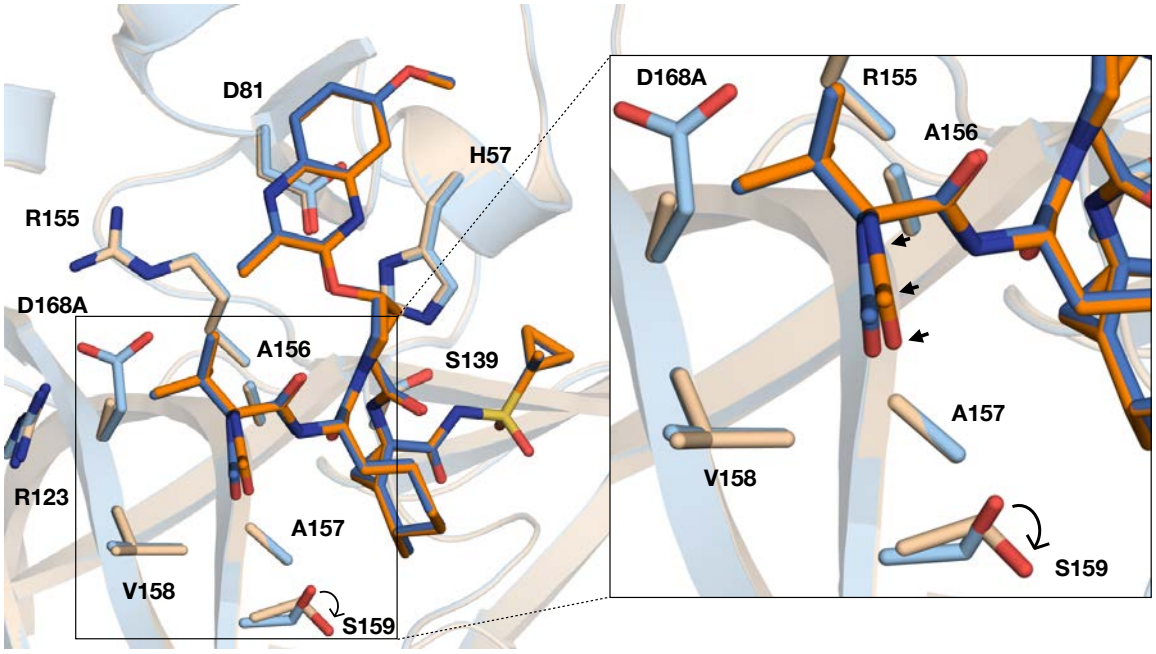

Figure 4.6: Crystal structure of AJ-67 bound to wildtype and mutant proteases.
Superposition of AJ-67 bound to (a) wildtype (blue) and (b) D168A (orange) proteases. S4 subsite residues and catalytic triad residues His57, Asp81 and S139 are shown as sticks. Inset shows a zoomed-in view of the P4–P5 moieties. Atoms that differ by .2 Å are displayed with a black arrow. The greatest deviation occurs at the P5 capping group.

4.3.7 Electronegative moieties at the P4 position allow for additional hydrogen bonds to S4 pocket residues

The P4–cap inhibitors had an improved potency profile than the P4–P5-cap inhibitors. The crystal structure of AJ-71 showed that this inhibitor when bound to wildtype protease has an extensive hydrogen bond network including the conserved hydrogen bond between Arg155 and Asp168 (**Figure 4.5C**). Additionally there is water-bridge between the ether oxygen of the carbamate group and backbone nitrogen of Ser159 mimicking the substrate-protease interaction also observed in the P4–P5-cap inhibitors. The trifluoro-2,2-dimethylpropane moiety can make a hydrogen bond with the NH2 group Arg123, an additional interaction that is not present in parent compound JZ01-15 or grazoprevir. Thus, the addition of this electronegative P4 group allows for enhanced interaction with the S4 pocket of the protease.

4.3.8 Hydrogen bond network of P4–cap inhibitor is conserved when bound to D168A protease

The P4–cap inhibitors were more potent than the P4–P5 extended inhibitors against D168A protease. Unlike the P4–P5-cap inhibitors, the hydrogen bond network is unaltered in D168A relative to wildtype protease. AJ-71 adopts two different conformations in the protease active site when bound to the D168A protease. One conformation (**Figure 4.5C**) is stabilized by a water-bridge hydrogen bond between the fluoro group and NH1 hydrogen of Arg155. Interestingly, Arg155 adopts two unique conformations that are stabilized by the

presence of a sulfate ion. A phosphate ion, which is present in the buffer in which our biochemical assays were performed, could also stabilize the Arg155 residue in these conformations for AJ-71 to bind. The alternate conformation of AJ-71 in complex with D168A protease retains the flouro-mediated hydrogen bond with Arg123 present when bound to wildtype protease. Although the potency of this inhibitor is reduced against the D168A variant, this inhibitor likely maintains potency better than the JZ01-15 or grazoprevir due to the conserved hydrogen bond network.

4.3.9 Packing of the designed inhibitors differs at the S4 pocket of the wildtype NS3/4A protease

To assess the molecular details of inhibitor packing at the S4 pocket, van der Waals (vdW) contact energies were calculated for each protease-inhibitor structure. Total vdW energies ranged from -90 to -87 kcal/mol. Most designed inhibitors had increased vdW contacts with the protease relative to parent compound JZ01-15 and grazoprevir (total vdW = -85 and -88 respectively). While the overall vdW profiles of each inhibitor class (P4 vs P4–P5-cap) were relatively the same in the areas of the inhibitor scaffold that are common (P1'–P3), most changes occurred at the S4 subsite (**Figure 4.7).** The P4–P5 inhibitors WK-23 and AJ-67, which are larger in size than the P4–cap inhibitors, had between a 1-3 kcal/mol increase in vdW contact energy relative to JZ01-15 with S4 subsite residues Ala157, Val158 and Ser159 when bound to wildtype protease (**Figure 4.7A**). Residues Ala157 and Val158 form the base of the S4 pocket whereas

Ser159 is located right outside of the S4 pocket. Relative to JZ01-15 and grazoprevir, WK-23 and AJ-67 had fewer interactions with Asp168, a residue that forms one wall of the S4 pocket. This suggests that P4–P5-cap inhibitors bind more outside of the pocket rather than extending into the pocket.

This is not the case for the P4–cap inhibitors. Relative to JZ01-15, all 3 P4–cap inhibitors had increased hydrophobic contacts with Arg123, Val158 and Asp168 especially JZ01-19 and AJ-74 with the cyclopentyl and methycyclopentyl capping group, respectively (**Figure 4.7B**). The P4–cap inhibitors actually fit better in the S4 pocket than the P4–P5-cap inhibitors that override the pocket similar to grazoprevir (**Figure 4.8**). The P4 cyclopropyl capping group of grazoprevir and the t-butyl P4 moiety of AJ-67 are positioned over the S4 pocket unlike AJ-71. Moreover, P4–cap inhibitors JZ01-19 and AJ-74 with hydrophobic cyclic rings pack well against the aliphatic portion of the Arg155 and Asp168 side chains and also interact with the nonpolar residue Ala156 (**Figure 4.9**). AJ-71 with the electronegative CF3 group also utilizes the space in the S4 pocket similarly to JZ01-19 and AJ-74 (**Figure 4.8**). Thus, the enhanced potency of these inhibitors against wildtype protease compared to the P4–P5-capping inhibitors likely stems from more efficient filling of the S4 pocket.

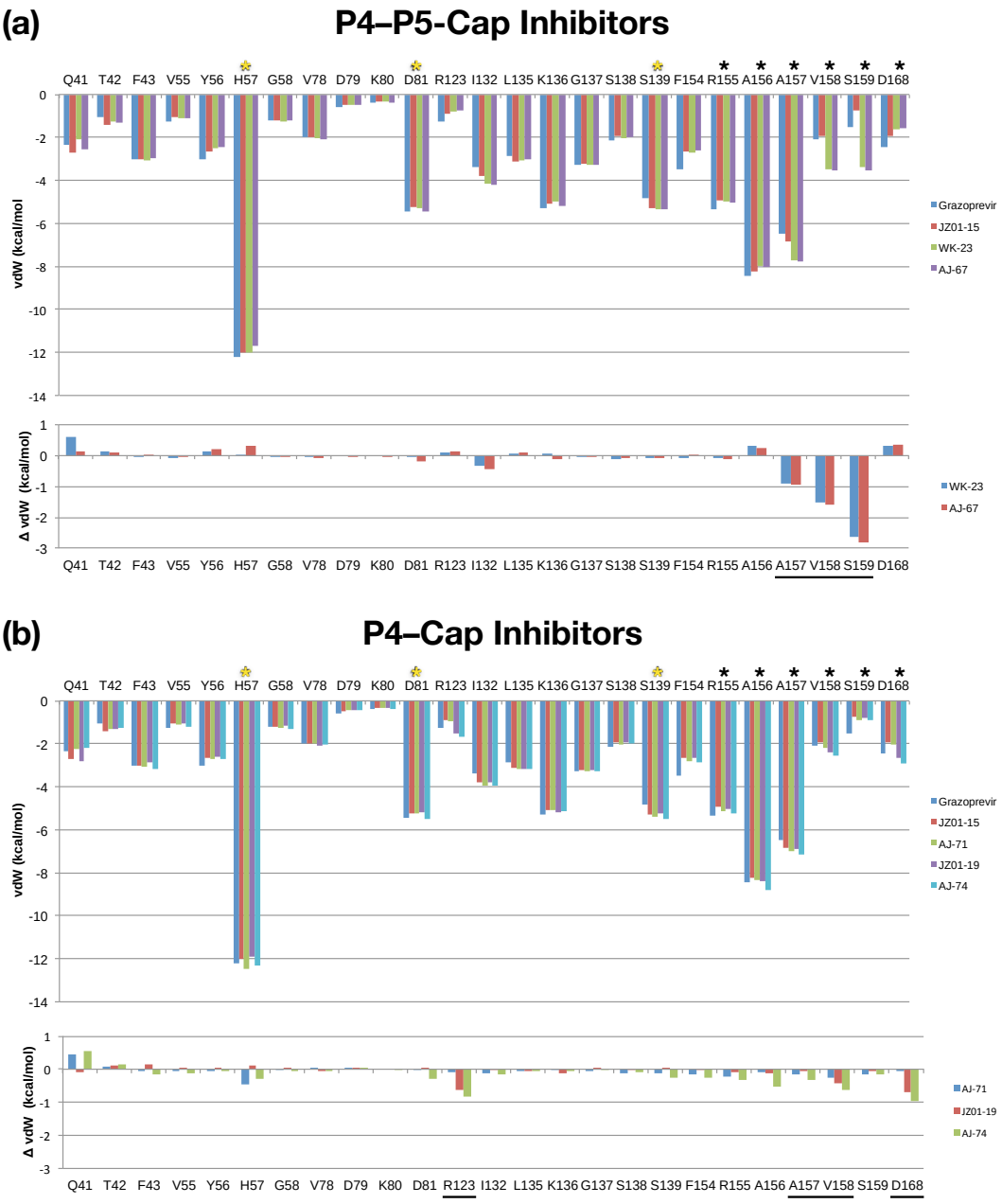

Figure 4.7: Inhibitor vdW interactions with wildtype HCV NS3/4A protease. (a) The van der Waals (vdW) contact energies for P4–P5-cap inhibitors and (b) change in vdW (Δ vdW) relative to parent compound JZ01-15. (c) vdW contact energies for P4–cap inhibitors AJ-71, JZ01-19 and AJ-74 and (d) Δ vdW relative to JZ01-15. These vdW values were calculated from the wildtype crystal structures of each inhibitor complex. Catalytic residues and S4 subsite residues are highlighted with a yellow and black star, respectively. Residues with the largest changes in vdW contact energies for both inhibitors classes are underlined.

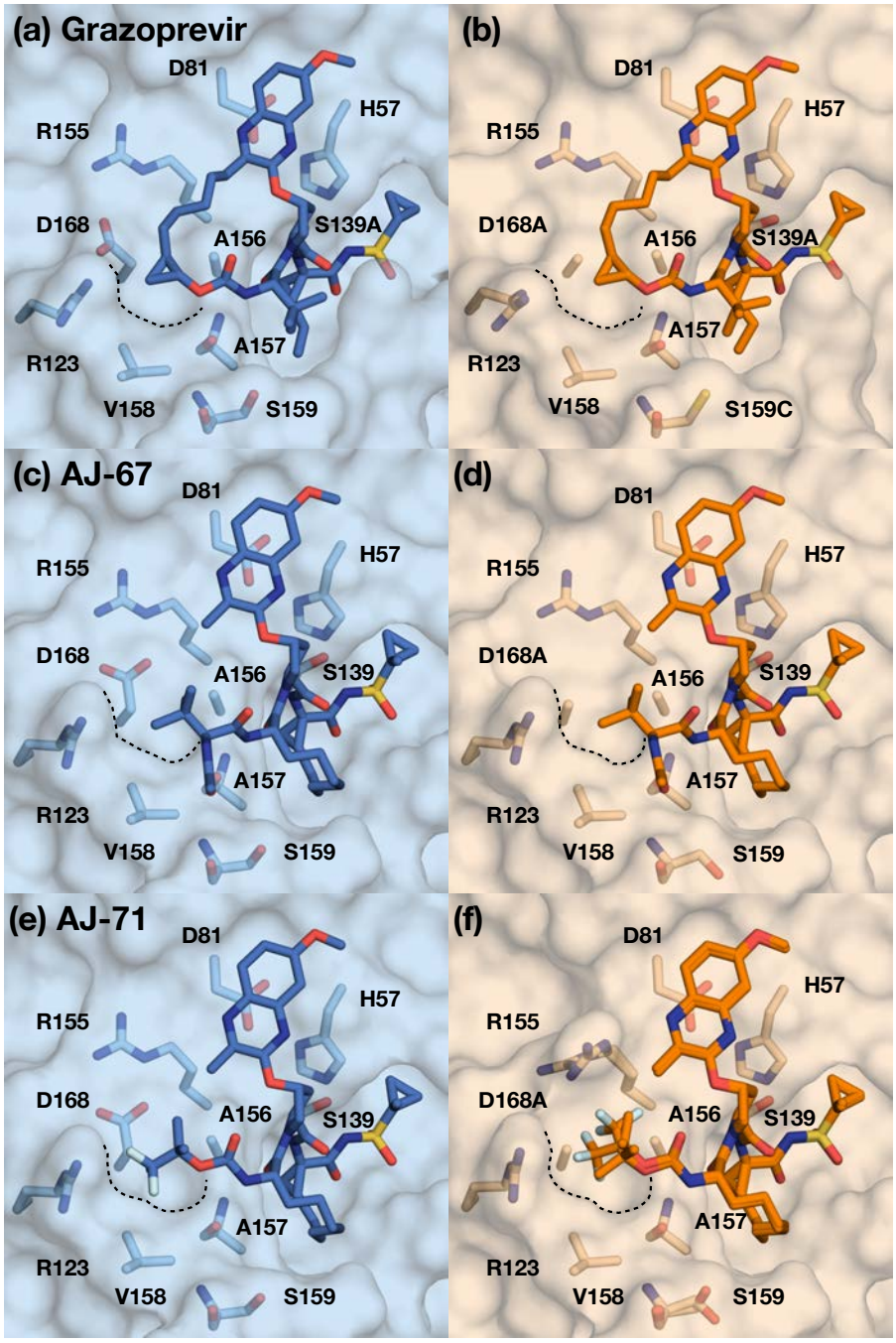

Figure 4.8: Packing of inhibitors at S4 pocket of wildtype and D168A protease.
Surface view of grazoprevir, AJ-67 and AJ71 bound to wildtype (blue) and D168A (orange) proteases. AJ-71 occupies two conformations in the protease active site when bound to D168A protease. The S4 pocket is outlined using a dashed line. Catalytic triad residues and S4 subsite residues are shown as sticks.

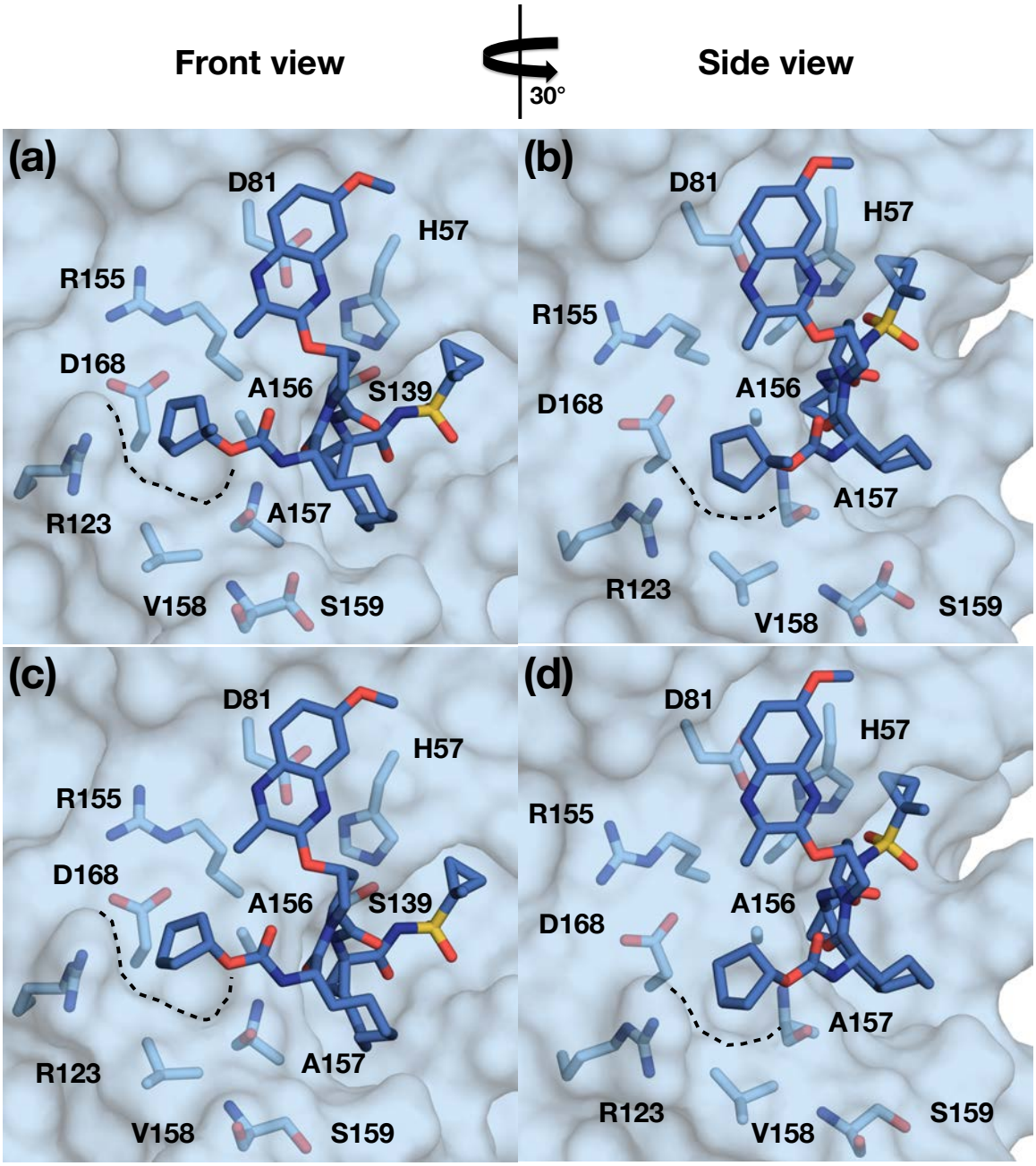

Figure 4.9: Packing of P4–cap inhibitors at the S4 pocket of wildtype protease.
(a) Front view and (b) side view of AJ-74 bound to wildtype protease. (c) Front view and (d) side view of JZ01-19 bound to wildtype protease. The protease is shown in surface representation. Inhibitors, S4 subsite residues and catalytic triad residues are shown as sticks.

4.3.10 D168A substitution alters the packing of P4–P5-cap inhibitors at the S4 pocket

The substitution of Asp168 to a nonpolar alanine residue results in an approximately 2 kcal/mol reduction of vdW contact energies for P4–P5-cap inhibitor AJ-67 (total vdW -90 and -89 kcal/mol wildtype and D168A protease, respectively). The largest reductions in contacts occur at residues 168 and 159 (**Figure 4.10**). This inhibitor relies on interactions with Ser159 as observed in hydrogen bond analysis. The P4–cap inhibitor AJ-71, which is more potent against D168A protease compared to AJ-67, has a more conserved vdW profile against the D168A variant losing about 1 kcal/mol in contacts (total vdW -87 and -86 kcal/mol wildtype and D168A respectively). AJ-71 loses the most contact with Asp168. However, the crystal structure shows that AJ-71 can adopt multiple conformations that gain other interactions including hydrogen bonds in the protease active site to accommodate the D168A substitution.

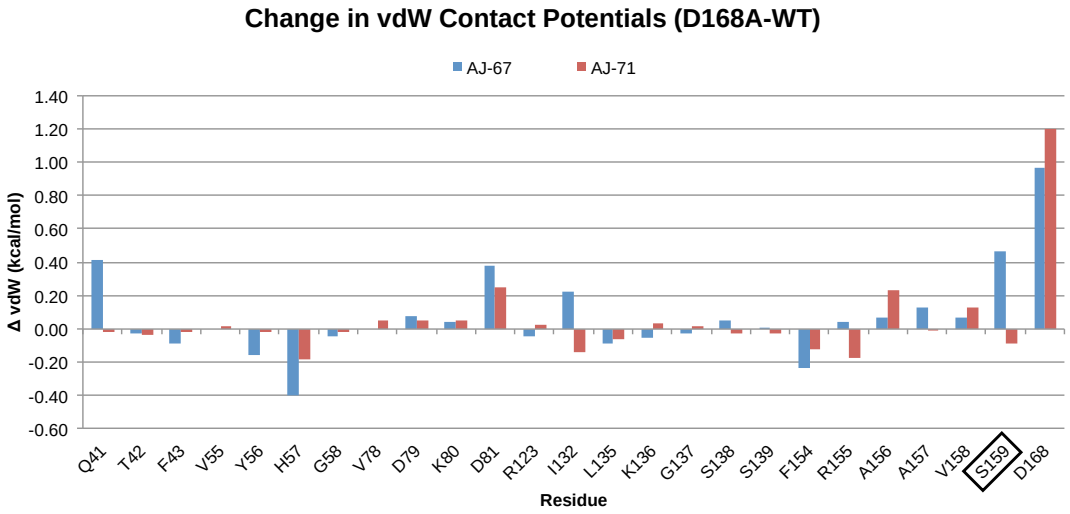

Figure 4.10: Changes in vdW interactions in D168A variant relative to wildtype protease.
Changes for inhibitors AJ-67 and AJ-71 are shown in blue and red, respectively. vdW interactions were calculated from crystal structures of inhibitors bound to wildtype and D168A proteases.

4.4 Discussion

A major obstacle in the design of inhibitors that remain active against rapidly evolving disease targets is drug resistance. As is the case with HCV, the emergence of resistance due to low fidelity of the NS5B RdRp leads to a heterogeneous population of viral species in the infected patient. Thus, to combat resistance, exploiting evolutionarily conserved regions in the protease active site is one strategy that may provide more “resistance-proof” inhibitors. The substrate envelope offers an added constraint in structure-based drug design allowing inhibitors to mimic substrates and avoid interactions with residues that are unessential in substrate processing. In this study, we demonstrate that the substrate envelope can successfully guide the design of inhibitors with improved resistance profiles against the pivotal D168A drug resistant variant in HCV protease.

While in this study we focused on the D168A variant, other common single-site substitutions to older generation inhibitors include R155K and A156T.[101] Grazoprevir, a drug with a P2 quinoxaline that binds on the catalytic residues His57 and Asp81, provides an inhibitor scaffold that is not susceptible to R155K substitutions due to limited interactions with this residue.[89,106] However, grazoprevir is highly susceptible to A156T due to steric clash with the inhibitor’s P2–P4 macrocycle.[111] The most recent FDA-approved HCV PIs voxilaprevir and glecaprevir share a very similar scaffold to grazoprevir including the P2–P4 macrocycle, and both are susceptible to the A156T resistance substitution.[51]

Modification of grazoprevir's P2–P4 macrocycle to the P1–P3 position led to the development of analogs with the P2 quinoxaline moieties such as JZ01-15 that have reduced susceptibility to R155K and A156T substitutions.[124] It is necessary to identify such new inhibitor scaffolds to diversity our arsenal of PIs to limit cross-resistance. Further alteration of the P1–P3 macrocyclic inhibitor scaffold in conserved regions of the substrate envelope, especially the P4 region, proved to be a viable strategy to improve resistance profiles by use of substrate mimicry.

Toward that end, two approaches were used to design novel PIs with either a P4–cap or a P4 modified amino acid and P5 capping group to explore unleveraged space in the substrate envelope. The P4–P5-cap inhibitors were less potent against both wildtype and D168A compared to parent compound JZ01-15 and FDA-approved inhibitor grazoprevir. However, these inhibitors exhibited flatter resistance profiles against the D168A substitution with an overall fold change in potency relative to wildtype less than 15 compared to 234 for grazoprevir. Although this scaffold allowed for additional backbone hydrogen bonds similar to those observed in viral substrates and side chain interactions with residues in the S4 subsite, these additional interactions were lost upon substitution at Asp168.

In contrast to the P4–P5-cap inhibitors, the P4–cap inhibitors adequately utilize space in the substrate envelope gaining hydrogen bonds and vdW interactions that enhance the potency of these inhibitors, while maintaining improved resistance profiles. The P4–P5-cap inhibitors have flatter resistance

profiles but the P4 moiety does not adequately fill the S4 pocket. Like grazoprevir, these inhibitors have P4 groups that simply override the pocket instead of targeting the S4 space directly. The t-butyl P4 group of parent compound JZ01-15, somewhat extends into the S4 pocket but additional modifications to this scaffold here significantly improved filling of the S4 pocket and the potency. Our results demonstrate that the fit of the inhibitor in the substrate envelope and optimal filling of the S4 pocket is necessary to improve potency.

Our findings suggest that additional alterations of the P4 moiety that fit within the substrate envelope may lead to inhibitors with improved potency against wildtype and mutant proteases. Structure activity relationship of P4 capping groups on other scaffolds have led to the development of more potent NS3/4A PIs with improved pharmacokinetic profiles.[176,177] However, these inhibitors were not designed in the context of the substrate envelope and were only tested for activity against wildtype protease. Inhibitors designed without evolutionary constraints may be susceptible to resistance due to interactions with residues that are functionally unimportant in substrate processing. The exploration of other hydrophobic moieties that pack well in the S4 pocket may further improve vdW interactions. In addition, as in AJ-71, other hydrogen bond acceptors at the P4 position of the inhibitors scaffold could improve interactions with Arg123 as the conformation of this residue is highly conserved in substrate and inhibitor complexes. Therefore, the combination of the substrate envelope constraint, P1–

P3 macrocycle and exploration of additional of diverse P4 groups may identify PIs with further improved resistance profiles.

In a quickly evolving disease target having an inhibitor that binds with high potency against the wildtype enzyme of interest is not sufficient. Instead, leveraging evolutionarily conserved regions of the target is critical, especially the substrate-binding pocket when designing competitive inhibitors. Substrate mimicry should be utilized at the outset of drug design to avoid resistance, as substitutions that disrupt inhibitor binding will then likely affect substrate processing as well. The substrate envelope provides a rational design strategy toward this goal, for the identification of inhibitors that are more robust against drug resistant variants. Use of the substrate envelope in conjunction with design of novel inhibitors with diverse P4 moieties may give rise to next-generation P1–P3 macrocyclic inhibitors that have broad activity against multi-substituted protease variants and low susceptibility to cross-resistance.

4.5 Methods

4.5.1 Inhibitor Synthesis

Grazoprevir, JZ01-15 and substrate envelope designed analogs were synthesized in-house using previously reported methods. Grazoprevir was prepared following a reported synthetic method.[120] JZ01-15 and analogs were synthesized using our convergent reaction sequence as previously described, with minor modifications.[106]

4.5.2 Expression and Purification of NS3/4A Constructs

The HCV GT1a NS3/4A protease gene described in the Bristol Myers Squibb patent was synthesized by GenScript and cloned into a PET28a expression vector.[128] Cys159 was mutated to a serine residue to prevent disulfide bond formation and facilitate crystallization. The D168A gene were engineered using the site-directed mutagenesis protocol from Stratagene. Protein expression and purification were carried out as previously described.[89] Briefly, transformed *Escherichia coli* BL21(DE3) cells were grown in TB media containing 30 µg/mL of kanamycin antibiotic at 37 °C. After reaching an OD_{600} of 0.7, cultures were induced with 1 mM IPTG and harvested after 3 h of expression. Cells were pelleted by centrifugation, resuspended in Resuspension buffer (RB) [50 mM phosphate buffer, 500 mM NaCl, 10% glycerol, 2 mM β-ME, pH 7.5] and frozen at −80 °C for storage.

Cell pellets were thawed and lysed via cell disruptor (Microfluidics Inc.) two times to ensure sufficient DNA shearing. Lysate was centrifuged at 19,000 rpm, for 25 min at 4 °C. The soluble fraction was applied to a nickel column (Qiagen) pre-equilibrated with RB. The beads and soluble fraction were incubated at 4 °C for 1.5 h and the lysate was allowed to flow through. Beads were washed with RB supplemented with 20 mM imidazole and eluted with RB supplemented with 200 mM imidazole. The eluent was dialyzed overnight (MWCO 10 kD) to remove the imidazole, and the His-tag was simultaneously removed with thrombin

treatment. The eluate was judged >90% pure by polyacrylamide gel electrophoresis, concentrated, flash frozen, and stored at −80 °C.

4.5.3 Correction for the Inner Filter Effect

The inner filter effect (IFE) for the NS3/4A protease substrate was determined using a previously described method.[129] Briefly, fluorescence end-point readings were taken for substrate concentrations between 0 µM and 20 µM. Afterward, free 5-FAM fluorophore was added to a final concentration of 25 µM to each substrate concentration and a second round of fluorescence end-point readings was taken. The fluorescence of free 5-FAM was determined by subtracting the first fluorescence end point reading from the second round of readings. IFE corrections were then calculated by dividing the free 5-FAM florescence at each substrate concentration by the free 5-FAM florescence at zero substrate.

4.5.4 Determination of Michaelis–Menten (K_m) Constant

K_m constants for GT1 and D168A protease were previously determined.[106] Briefly, a 20 µM concentration of substrate [Ac-DE-Dap(QXL520)- EE-Abu-γ-[COO]AS-C(5-FAMsp)-NH2] (AnaSpec) was serially diluted into assay buffer [50 mM Tris, 5% glycerol, 10 mM DTT, 0.6 mM LDAO, and 4% dimethyl sulfoxide] and proteolysis was initiated by rapid injection of 10 µL protease (final concentration 20 nM) in a reaction volume of 60 µL. The fluorescence output from the substrate cleavage product was measured kinetically using an EnVision

plate reader (Perkin-Elmer) with excitation wavelength at 485 nm and emission at 530 nm. Inner filter effect corrections were applied to the initial velocities (V_o) at each substrate concentration. V_o versus substrate concentration graphs were globally fit to the Michaelis–Menten equation to obtain the K_m value.

4.5.5 Enzyme Inhibition Assays

For each assay, 2 nM of NS3/4A protease (GT1a and D168A) was pre-incubated at room temperature for 1 h with increasing concentration of inhibitors in assay buffer (50 mM Tris, 5% glycerol, 10 mM DTT, 0.6 mM LDAO, and 4% dimethyl sulfoxide, pH 7.5). Inhibition assays were performed in non-binding surface 96-well black half-area plates (Corning) in a reaction volume of 60 µL. The proteolytic reaction was initiated by the injection of 5 µL of HCV NS3/4A protease substrate (AnaSpec), to a final concentration of 200 nM and kinetically monitored using a Perkin Elmer EnVision plate reader (excitation at 485 nm, emission at 530 nm). Three independent data sets were collected for each inhibitor with each protease construct. Each inhibitor titration included at least 12 inhibitor concentration points, which were globally fit to the Morrison equation to obtain the K_i value.

4.5.6 Crystallization and Structure Determination

Protein expression and purification were carried out as previously described.[89] Briefly, the Ni-NTA purified WT1a protein was thawed, concentrated

to 3 mg/mL, and loaded on a HiLoad Superdex75 16/60 column equilibrated with gel filtration buffer (25 mM MES, 500 mM NaCl, 10% glycerol, and 2 mM DTT, pH 6.5). The protease fractions were pooled and concentrated to 25 mg/mL with an Amicon Ultra-15 10 kDa filter unit (Millipore). The concentrated samples were incubated for 1 h with 3:1 molar excess of inhibitor. Diffraction-quality crystals were obtained overnight by mixing equal volumes of concentrated protein solution with precipitant solution (20–26% PEG-3350, 0.1 M sodium MES buffer, 4% ammonium sulfate, pH 6.5) at RT or 15 °C in 24-well VDX hanging drop trays. Crystals were harvested and data was collected at 100 K. Cryogenic conditions contained the precipitant solution supplemented with 15% glycerol or ethylene glycol.

X-ray diffraction data were collected in-house using our Rigaku X-ray system with a Saturn 944 detector. All datasets were processed using HKL-3000.[131] Structures were solved by molecular replacement using PHASER.[132] Model building and refinement were performed using Coot[133] and PHENIX,[134] respectively. The final structures were evaluated with MolProbity[135] prior to deposition in the PDB. To limit the possibility of model bias throughout the refinement process, 5% of the data were reserved for the free R-value calculation.[136] Structure analysis, superposition and figure generation were done using PyMOL.[137] X-ray data collection and crystallographic refinement statistics are presented above (**Table 4.1**).

4.5.7 Construction of HCV Substrate Envelope

The HCV substrate envelope was computed using a method previously described.[89] The HCV viral substrates representing the product complex 3-4A (residues 626–631 of full-length HCV PDB ID: 1CU1), 4A/4B (chain B, PDB ID: 3M5M), 4B/5A (chain D, PDB ID: 3M5N) and 5A/5B (chain A, PDB ID: 3M5O) were used to construct the envelope. All structure were aligned in PyMOL using the Cα atoms of protease residues 137–139 and 154–160. Following superposition of all structures, Gaussian object maps at a contour of 0.5 were generated for each cleavage product in PyMOL.[53,89] Four consensus maps were generated representing the minimum volume occupied by any 3 viral substrates. The four consensus maps were summed together to generate the final substrate envelope representing the shared van der Waals volume of the viral substrates.

Chapter V
Discussion

5.1 Elucidation of mechanisms of resistance is paramount to the design of novel antivirals

In rapidly evolving disease targets, the acquisition of drug resistance is almost inevitable. Though many argue that use of combination therapies to treat HCV including drugs against multiple viral proteins essential in the viral life cycle can potentially prevent resistance, there are other factors that need to be considered. Patient compliance, adherence to the drug regimen and taking the medicine correctly, is an important factor that is preventable. Differences in host genes from patient to patient can lead to variations of drug absorption, distribution, metabolism, and excretion (ADME) properties which can affect the effective dosing. Moreover, cost of the drugs can be a huge barrier to patients completing a course of treatment. All of these factors can lead to sub-optimal dosing, which is a nidus for the rise of resistant viral species.

Resistance is a change in the molecular recognition of the target for the drug, usually due to mutation, with minimal effect on substrate processing. The most optimal drug design approach is one that incorporates strategies to evade resistance at the outset of inhibitor design. However, evidence that a drug may become resistant is not always available a priori. Thus, when resistance does occur, it is paramount to understand the particular mechanisms of resistance at play and use those insights toward iterative rounds of drug design. In Chapter II of this thesis, I elucidated the mechanisms of resistance for highly potent inhibitors including grazoprevir against the Y56H/D168A protease variant. This

chapter demonstrated that even with the most potent inhibitors against the NS3/4A protease, HCV can incorporate multiple substitutions that disrupt inhibitor binding while still maintaining substrate processing. Chapters III and IV demonstrated that the use of insights from mechanisms of resistance determined prior to the start of this thesis research can be used to successfully design novel inhibitors that are more robust against resistance associated substitutions. Therefore, it is my hope that the mechanisms I have discovered will be used to design a diverse arsenal of HCV PIs with improved resistance profiles and effectiveness against highly mutated viral species.

5.2 Implications for other multi-substituted protease variants

Throughout this thesis, I have highlighted the importance of elucidating the mechanisms of drug resistance to inform drug design and development. Though I elucidated the resistance mechanisms of PIs against the Y56H/D168A variant, other double and even triple substitution variants consisting of Y56H, A156T, and D168A/N have been observed in patients who fail therapy with grazoprevir.[98] In fact, resistance selection assays with glecaprevir selected double substitutions including A156T.[51] This substitution has never been a threat as Ala156 substitutions cause low replicative capacity. However, an additional substitution may improve enzymatic fitness by restoring substrate turnover, and allow viral variants to emerge that are detrimental to inhibitor potency. The aforementioned primary substitutions are located in the protease active site where the inhibitor

binds. However, additional substitutions do not have to occur at the active site. In HIV-1 protease, active site and distal substitutions often occur in combination to confer resistance.[127] A recent study with glecaprevir selected substitutions at Ala156 in combination with Gln/Pro89 in GT 1a/b, which is located outside of the active site. This additional substitution at position 89 appears to have improved replicative efficiency to 100%.[51] It is necessary to understand the molecular underpinning of resistance to these multi-substituted proteases, as there is a high likelihood of cross-resistance to glecaprevir and voxilaprevir given the structural similarity of these drugs. Understanding the molecular mechanisms of resistance and enzymatic fitness of these multi-substituted proteases will be necessary to improve potency of PIs against emerging resistant viral variants.

In Chapter II, double mutant cycle analysis provided insights into how mutations may work together or independently to confer resistance. This analysis is a powerful tool to study the coupling of amino acids substitutions in double-substitution variants. However, to fully understand the scope of resistance, we must also study the single substitution proteins individually. This may not always be feasible structurally, so I cannot overstate the value of computational techniques, especially molecular dynamics simulations, to understand how mutations change protein flexibility and dynamics on the atomistic scale. To further elucidate why two or three particular substitutions occur together, experimental techniques should be used to investigate changes protein stability, substrate turnover, and replicative capacity in single and multi-substituted

variants. These experiments may shed light on viral evolution and why particular substitutions occur together to confer resistance.

5.3 Exploiting evolutionarily constrained regions in the protease active site to avoid resistance

Evolutionarily constrained regions in the protease active site are comprised of residues that are critical to substrate turnover. The NS3/4A protease is a serine protease with the canonical catalytic triad consisting of residues His57, Asp81, and Ser139.[53] Substitution of any one of these residues would be detrimental to the protease function. Thus, designing inhibitors that strongly interact with conserved residues such as the catalytic triad in the target protein is one strategy that can reduce the susceptibility to resistance, as substitutions will affect both inhibitor and substrate binding.

The P2 quinoxaline moiety of grazoprevir utilizes interactions with catalytic triad residues His57 and Asp81.[89,111] Crystal structures solved in Chapter III–IV as well as **Appendix A** of inhibitors with modified P2 quinoxaline moieties demonstrate that regardless of location of the inhibitor macrocycle and substituents on the P2 quinoxaline, this binding mode is conserved for all inhibitors. Moreover, newer generation inhibitors voxilaprevir and glecaprevir designed based on the grazoprevir scaffold have a P2 quinoxaline. Although there are no crystal structures of these inhibitors bound to wildtype protease, in my opinion, they likely have a binding mode similar to grazoprevir. This binding mode was once thought to be “resistance proof.” However, Chapter II

demonstrates that substitution of neighboring residue Tyr56 to a smaller histidine residue actually impacts the binding of the quinoxaline moiety, weakening the critical π–π interactions with the heterocyclic ring of His57.

To maintain strong interactions with the catalytic triad even in the presence of such mutations, rational design of other P2 candidate moieties that have the propensity to bind similarly to the P2 quinoxaline should be considered. Additionally, other strategies to strengthen the stacking interactions of the pyrazine ring of the quinoxaline with His57 may provide new inhibitors that are less susceptible to the Y56H/D168A double mutant. Some studies suggest that replacement of a CH group with a nitrogen atom may improve inhibitor binding and pharmacokinetic properties.[178] Thus, the addition of a pyridopyrazine moiety at the P2 position of the inhibitor scaffold may yield antivirals with enhanced interactions with the His57 ring.

In addition to optimizing inhibitor interactions with the catalytic triad residues, the substrate envelope can be used as an added constraint in novel PI design. Drugs designed to stay within the volume of the substrate envelope should be less susceptible to resistance. This has been demonstrated in HIV-1 protease where inhibitor pairs were synthesized that either intentionally extended beyond or were contained within the substrate envelope.[179] Inhibitors that respected the substrate envelope constraint were more robust against drug resistant variants. In Chapter IV, crystal structure analysis and biochemical data showed that HCV PIs that fit within the substrate envelope have flatter resistance profiles.

Moreover, inhibitors that exploit the S4 pocket of the substrate envelope are not only less resistant, but also gain potency against the D168A variant.

Our lab has an extensive history in exploring structure-activity relationships of different PI scaffolds for both HIV-1 and HCV protease.[124,180-184] The substrate envelopes in HIV-1 protease and now HCV protease have successfully provided inhibitors that have improved resistance profiles against some of the most resistant variants.[175,183] Thus, future SAR studies at the P4 position of the NS3/4A PI scaffold should incorporate the substrate envelope at the outset of novel inhibitor design. Diverse P4 moieties can be incorporated to interact with residues of the S4 pocket that are important in substrate recognition. Inhibitors should be biochemically characterized against wildtype GT1, other genotypes and resistant variants. Crystal structures should confirm fit with the envelope as well as evaluate new interactions that are gained or potentially lost with alterations at the P4 position. Hopefully, future SAR studies will generate a new arsenal of PIs that are more robust against common and emerging resistant variants.

5.4 Role of macrocycle location in resistance

The location of the inhibitor macrocycle greatly impacts the potency and resistance profile of HCV PIs. Our lab has demonstrated that the addition of a macrocycle to the inhibitor scaffold often improves the potency by 1 to 4 orders of magnitude.[106] Inhibitors with a P2–P4 macrocycle, which connects the P2 moiety

to the P4 moiety, are often times more potent than the P1–P3 inhibitors. However, where P1–P3 macrocyclic inhibitor lack in potency, they make up the difference in their resistance profile. P1–P3 macrocyclic inhibitors have flatter resistance profiles likely due to their inherent flexibility. P2–P4 macrocyclic inhibitors are more susceptible to drug resistance substitutions because their P2 and P4 groups are more constrained, restricting the ability to adapt to substitutions that change the binding site.[106,124] Chapter III confirms this finding as well, as our P1–P3 macrocyclic analogs of grazoprevir although some were less potent had flatter resistance profiles.

Voxilaprevir and glecaprevir, as aforementioned, are pan-genotypic P2–P4 macrocyclic inhibitors with little susceptibility to most single substitutions in the NS3/4A protease. All P2–P4 macrocyclic inhibitors are highly susceptible to the A156T substitution, as the macrocycle will sterically clash with the larger threonine residue.[106,111] These drugs, like grazoprevir, the FDA-approved inhibitor they are most similar to, select for substitutions at Ala156 *in vitro*, which causes a large fold shift in inhibitor potency. Moreover, Ala156-Asp168 double substitutions have been selected *in vitro*, which improve fitness. Although not yet observed clinically, the A156T substitution if coupled with such a fitness-rescuing second substitution could cause resistance to all P2–P4 macrocyclic PIs with a P2 quinoxaline moiety.

Therefore, it is necessary to structurally analyze glecaprevir and voxilaprevir and design P1–P3 macrocyclic inhibitors that can obtain the same potency with

little susceptibility to RASs. Crystal structures of these inhibitors bound to wildtype, D168A, and other double substitution proteases could be determined and comparatively analyzed with grazoprevir, and P1–P3 macrocyclic analogs bound to the same variants. Structural analysis would provide mechanistic information about how subtle modifications to an inhibitor scaffold result in little change in activity against the most elusive resistant variants that were once detrimental to inhibitor potency. These insights can then be incorporated into the design of better P1–P3 macrocyclic inhibitors. This would lessen the threat of multi-mutant variants with the A156T substitution as P1–P3 macrocyclic inhibitors are not susceptible to this substitution. Moreover, incorporating inhibitor features of glecaprevir and voxilaprevir into P1–P3 macrocyclic inhibitor design may give rise to the first P1–P3 macrocyclic inhibitors with excellent potency and pan-genotypic activity.

5.5 Exploration of other genotypes

At the conception of this thesis, one of my goals was to explore other GTs of HCV. Although I did assay compounds against GT3a protease in Chapter III, my thesis work primarily focused on GT1a. Rational drug design approaches for HCV PIs use GT1 as a surrogate for efficacy across genotypes. There is an abundance of structural data for GT1 protease, but limited structural data for other GTs has hampered drug design efforts. Although pan-genotypic PIs have

received FDA-approval, their mechanism for potency against other genotypes or mutations they may select in other genotypes remains unknown.

Globally, HCV genotypes differ at the nucleotide level by greater than 30% and subtypes differ by 20-25%.[9] Interestingly, the active site of GT1 and GTs 4–6 are 100% identical. GT2 and GT3 differ by 1 and 2 polymorphisms compared to GT1, respectively. In GT2, Thr160 is replaced by a smaller nonpolar residue alanine. GT3 has the polymorphisms D168Q and R123T.[108] Protein engineering studies performed in our lab led to the design of a GT3 chimera consisting of a construct with a GT1 background and the active site polymorphism found in GT3 as well as the additional mutation I132T. Crystal structures and MD simulations revealed that the differential efficacy of PIs observed against GT3 is due to changes in the protease hydrogen bond network and dynamic fluctuations as a result of the D168Q substitution.[108] Crystal structures of glecaprevir and voxilaprevir bound to GT3 chimera may allow us to obtain mechanistic insights into the improved potency of these inhibitors against GT3.

Although this chimera is amenable to crystallization and has led to valuable knowledge about GT3 protease, the differential efficacy of PIs against other non-GT1 proteases where the active site is unchanged remains to be explained. Potentially, global changes outside of the active site might play a role in inhibitor efficacy against various GTs. As others and myself have performed extensive crystallization efforts with other non-GT1 proteases without any hits, novel techniques and approaches may be necessary to glean structural differences of

non-GT1-PI complexes. Even apo structures might afford structural information that can be used to investigate the mechanism of differential efficacy of PIs against non-GT1 protease variants. These findings can then be used in the design of optimal P1–P3 macrocyclic inhibitors that have pan-genotypic activity.

Recent advances in single-particle cryoelectron microscopy (cryo-EM), another structural technique, may facilitate structure determination of non-GT1 proteases.[185-187] Full-length HCV NS3/4A protease is approximately 70 kDa. One limitation of this approach is that cryo-EM is more amenable to structure determination of large complexes (>150 kDa).[187] However, a structure of isocitrate dehydrogenase (93 kDa) was solved to near-atomic resolution, demonstrating that with recent developments, cryo-EM may be applicable to smaller proteins.[187] The difficulty with smaller proteins is that the alignment error of individual projections becomes higher as the size of the protein decreases due to decreased signal to noise ratio. Nevertheless, advance in microscopes, cameras and contrast via volta phase plates have led to improvement that may enable structure determination of smaller proteins.[188,189] Additionally, the use of 1-2 fragment antibodies (Fabs), which are about 50 kDa, allows one to increase the size of the molecule. Fabs also have the added benefit of helping with orientation determination.[190]

A major focus in our lab is elucidating how small molecule inhibitors bind to wildtype and mutant proteins of different genotypes and exhibit differential efficacy. Studies have shown that cryo-EM can resolve density for small

molecule inhibitors bound to proteins.[187,191] Thus, this technique may allow us to understand how inhibitors differentially bind to non-GT1 or mutant proteases in the context of full-length protease, which is currently not known in the field. Although cryo-EM can now reach resolutions similar to that of crystallography, a common opinion that others and I share, is that these two techniques should be used to complement one another. Both techniques have their own set of advantages in disadvantages. However the extensive crystal structure database of GT1a protease in our lab should be used in the analysis of future structures determined by cryo-EM as each could potentially represent different biological states that may be important in iterative rounds of inhibitor design.

5.6 Design of PIs that target the helicase domain

In the full-length NS3/4A protein, the C-terminus consists of the helicase domain. Although this thesis focused on the protease domain, there are many reasons why the full-length protein should be considered in future drug design strategies. The helicase domain enhances the proteolytic activity of the protease domain.[192] Additionally, drug resistance mutations to protease inhibitors can occur in the helicase domain.[193] Hence, substrate and inhibitor recognition may be influenced by the presence of the helicase domain. Structures of full-length NS3/4A bound to substrate and PIs will be necessary to interrogate the interactions of the helicase domain in substrate and inhibitor complexes.

Helicase-protease inhibitors (HPIs) have the ability to block both helicase

unwinding and protease substrate processing via binding to an allosteric site located between the interfaces of the domains.[194,195] These inhibitors have demonstrated activity against multiple genotypes and PI resistant variants. One group showed that HPIs and PIs actually work synergistically and that potentially HPIs stabilize the full-length protein in a conformation that facilitates PI binding.[195] Thus, one strategy for future drug design would be to elaborate our P1–P3 PI scaffold to design inhibitors that can also disrupt helicase activity. The quinoxaline moiety, which interacts with conserved residues of the catalytic triad, binds close to the helicase-protease interface. Elaboration of the methoxy group at the 7-position of the P2 quinoxaline may provide inhibitors that can destabilize helicase activity while simultaneously blocking protease activity. This approach may reduce the susceptibility of HPIs to resistance, as inhibitors that bind in allosteric sites are likely to evolve resistance more rapidly because the allosteric site may be less conserved and not necessary for substrate recognition.

5.7 Viral proteases of other rapidly evolving disease targets

HCV is a member of the Flavividae family of positive stranded RNA viruses. Other closely related members of this family include Yellow Fever, Dengue, West Nile Virus (WNV) and Zika viruses to name a few.[18,196-198] All of these viruses like HCV encode a protease that cleaves the viral polyprotein into functional and structural elements, which is a crucial step in the life cycle. HCV PIs are a success story in the treatment of HCV and in absence of treatment options for

other flaviviruses, a lot of effort in the field has been the development of DAAs against the viral protease in these viruses.[199-202] To date, there are no FDA-approved PIs against any of these viral proteases.

Dengue and Zika NS2B-NS3 protease are closely related to HCV NS3/4A protease.[203] Each virus like HCV encodes an RdRp with low fidelity, which implies that these viruses must recognize diverse substrates. Therefore, it is feasible that these viruses have their own unique substrate envelope that may be used in inhibitor design. In the absence of the selective pressure of a drug, it is difficult to predict residues that are likely to evolve resistance. However, one study provides strong evidence that resistance to a Dengue PIs can develop readily.[204] The substrate envelope model has demonstrated benefit in improving or reducing susceptibility to resistance in two independent systems (HCV and HIV-1).[183] Throughout this thesis, I have demonstrated that exploiting evolutionarily conserved regions in the protease and substrate mimicry are viable strategies to circumvent resistance. Substrate-protease structures of these and other viral proteases will be needed to construct the substrate envelope, which can then be very beneficial at the outset of inhibitor design.

Zika and Dengue NS2B-NS3 proteases are serine proteases that share the canonical catalytic triad.[203] In Chapter II and throughout this thesis, I have shown that a critical interaction of grazoprevir and HCV PIs that have been developed in the Schiffer laboratory is the stacking interactions between the P2 quinoxaline

and the His57 ring. Is it possible to develop Dengue or Zika PIs that leverage this same interaction? Could other heterocyclic rings be employed in inhibitor design and evaluated using the substrate envelope, with computational and biophysical techniques? One recent study demonstrated that repurposing HCV PIs that were discovered in high-throughput screens could yield promising Zika PIs.[201] Incorporation of HCV PI pharmacophores that predominantly interact with catalytic residues at the outset of DAA design may limit evolution of resistance and result in robust inhibitors against other viral proteases.

5.8 Concluding Remarks

In the duration of this thesis research, the treatment options and outcomes for HCV infection have truly transformed. However, even with these improvements, drug resistance still remains a problem with many people failing therapy. This thesis elucidates the mechanisms of drug resistance for PIs against a highly resistant variant and uses previously determined mechanistic resistance knowledge in iterative rounds of drug design with the goal of improving resistance profiles. My studies have shed light on a novel mechanism of drug resistance that may affect all newly FDA-approved PIs due to cross-resistance. In addition, I demonstrated that minimized contact with known residues that mutate to confer resistance and use of evolutionarily constrained regions in the protease active site are strategies that can successfully be employed to design inhibitors with better or maintained activity against resistance associated

variants. Future studies for following up on this work would be to determine the mechanisms of resistance for other relevant multi-substituted protease variants, and interrogate why particular substitutions occur together. Moreover, elucidating the differential potency of PIs against other genotypes, possibly using cryo-EM, may help design diverse inhibitors that are pan-genotypic, less susceptible to cross-resistance and more robust against resistance associated variants. My hope is that this work will guide future drug design efforts that will one day lead to the eradication of HCV infection. Although there are other public health factors including access to treatment, IV drug use, patient non-adherence that must also be addressed, my hope is that this thesis contributes to solving the drug resistance problem and providing cure for each and every HCV-infected patient.

Appendix A

Quinoxaline-Based Linear HCV NS3/4A Protease Inhibitors Exhibit Potent Activity and Reduced Susceptibility to Drug Resistant Variants

Preface

Appendix A is a collaborative study that is in preparation.

Rusere, L. N.; **Matthew, A. N.**; Lockbuam, G. J.; Jahangir, M.; Newton, A.; Petropoulos, C. J.; Huang, W.; Kurt Yilmaz, N.; Schiffer, C. A.; Ali, A. Quinoxaline-Based Linear HCV NS3/4A Protease Inhibitors Exhibit Potent Activity and Reduced Susceptibility to Drug Resistant Variants.

Contributions from Ashley N. Matthew:

I expressed and purified all wildtype and mutant proteins used in this study. I performed a subset of the enzyme inhibition assays. I solved all the protease-inhibitor crystal structures and interpreted the data. I also wrote part of the manuscript and made all the figures of solved crystal structures.

A.1 Abstract

A series of linear HCV NS3/4A protease inhibitors was designed by eliminating the P2–P4 macrocyclic linker in grazoprevir, which in addition to conferring conformational flexibility allowed SAR exploration of diverse quinoxalines at the P2 position. Biochemical and replicon data indicated preference for small hydrophobic groups at the 3-position of P2 quinoxaline for maintaining potency against drug resistant variants R155K, A156T and D168A/V. The linear inhibitors, though generally less potent than the corresponding macrocyclic analogues, were relatively easier to synthesize and less susceptible to drug resistance. X-ray crystal structures of three inhibitors bound to wild-type NS3/4A protease revealed slightly different binding conformation of the P2 quinoxaline depending on the substituent at the 3-position, which significantly impacted inhibitor potency and resistance profile. The SAR and structural analysis highlight inhibitor features that strengthen interactions of the P2 moiety with the catalytic triad residues, providing valuable insights to improve potency and resistance profile.

A.2 Introduction

Hepatitis C virus (HCV) is a serious global health problem. The most recent estimates indicate that at least 70 million people worldwide have chronic HCV infection, and about 1.75 million new cases are recorded each year.[1] HCV is the leading cause of liver diseases such as cirrhosis, fibrosis and liver cancer, and more than 50% of liver transplant cases result from chronic HCV infection. The treatment of HCV infection has been challenging due to high genetic diversity of the virus and a lack of antiviral drugs that effectively target all HCV genotypes.[2] Fortunately, recent advances in direct-acting antivirals (DAAs) targeting the HCV NS3/4A, NS5A and NS5B proteins have significantly improved sustained virological response (SVR) in patients across HCV genotypes.[3] However, the high genetic diversity of HCV and the rapid emergence of drug resistance necessitate the use of combination therapies with two or three drugs from different classes to effectively treat infected patients.

The HCV NS3/4A protease inhibitors (PIs) are a key component of new all-oral combination therapies.[3] The five FDA approved PIs are all macrocyclic acylsulfonamides with different heterocyclic moieties at the P2 position.[4] Of these, paritaprevir and grazoprevir are active against most HCV genotypes,[5,6] while recently approved drugs glecaprevir and voxilaprevir exhibit pan-genotypic activity.[7,8] These new PIs are also significantly more active against most polymorphic and drug resistant HCV variants.[9] The development of NS3/4A PIs

with pan-genotypic activity and improved resistance profiles marks a major milestone in anti-HCV drug discovery.

Despite remarkable improvements in potency and resistance profiles, the current NS3/4A PIs are still susceptible to drug resistance due to substitutions at one or more amino acid positions in the target protein.[10,11] The most common resistance-associated substitutions (RASs) in the NS3/4A protease occur at residues Arg155, Ala156, and Asp168. Inhibitors show varying susceptibility to RASs at these and other positions depending on the heterocyclic moiety at the P2 position and the location of the macrocycle.[12,13] Grazoprevir (**1**) (**Figure A.1**) was the first NS3/4A PI to show activity against most HCV genotypes and RASs due to its unique binding conformation.[12,14] The P2 quinoxaline moiety in **1** largely avoids direct interactions with residues Arg155 and Asp168, but instead interacts with the catalytic His57 and Asp81.[12] As a result, **1** maintains potency against substitutions at Arg155 and is only moderately susceptible to substitutions at Asp168. However, the P2–P4 macrocycle in **1** causes steric clashes with larger substitutions at Ala156, resulting in drastically reduced potency.[12] Both glecaprevir and voxilaprevir are also P2–P4 macrocyclic compounds structurally similar to grazoprevir and are expected to bind in similar conformations, as indicated by their particularly high susceptibility to substitutions at Ala156.[9,15] These three PIs currently in clinical use indeed exhibit similar resistance profiles and thus are prone to cross-resistance. Therefore, more

robust NS3/4A PIs need to be developed, preferably incorporating diverse structural features.

We have shown that the unique binding conformation of **1** does not depend on the P2–P4 macrocycle, as the P1−P3 macrocyclic and linear analogues, 5172-mcP1P3 (**2**) and 5172-linear (**3**) (**Figure A.1**), still bind in a similar conformation as the parent compound.[16] In the absence of the P2–P4 macrocyclic constraint, the conformationally flexible P2 quinoxaline moiety can help the inhibitor better adapt to structural changes in the protease active site due to RASs, particularly at Ala156. Accordingly, compared to **1**, the P1–P3 macrocyclic analogue **2** exhibits similar potency against RASs at Arg155 and Asp168 but is significantly less susceptible to substitutions at Ala156, resulting in an overall improved resistance profile.[13]

In addition to conferring conformational flexibility, elimination of the P2–P4 macrocycle in **1** provides opportunities to further improve potency and resistance profiles by exploring structure-activity relationship (SAR) at the 3-position of P2 quinoxaline in both the P1–P3 macrocyclic (**2**) and linear (**3**) analogues. Toward this end, we recently developed a substrate envelope guided design strategy that aims to exploit interactions with the invariant catalytic triad, minimize interactions with the S2 subsite residues and incorporate conformational flexibility at the P2 moiety, which led to the identification of P1–P3 macrocyclic analogues of **2** with exceptional potency and resistance profiles.[17] These exciting findings encouraged us to explore SAR of linear compound **3** to identify analogues with

improved potency against drug resistance HCV variants. In this letter, we report the structure-guided design, synthesis, and SAR studies of a series of quinoxaline-based linear NS3/4A PIs. In addition, we report co-crystal structures of three linear inhibitors with different P2 quinoxaline moieties bound to NS3/4A protease, providing valuable structural insights to further optimize potency and resistance profiles.

A.3 Chemistry

The synthesis of linear NS3/4A PI with diverse P2 quinoxaline moieties is outlined in **Scheme A.1**. The key Boc-protected P2 intermediates **4a-e** were prepared from the corresponding 3-substituted 7-methoxy-quinoxalin-2-ones by an S_N2 displacement reaction with the activated *cis*-hydroxyproline derivative as described previously.[17] The P2 intermediates **4a-e** were treated with 4N HCl to provide the proline derivatives **5a-e**, which were subsequently reacted with N-Boc-*L*-*tert*-leucine using HATU and DIEA to afford the P2–P3 intermediates **6a-e**. The proline methyl ester intermediates were then hydrolyzed with LiOH to afford the acid intermediates **7a-e**. Finally, the P2–P3 acids **7a-e** were coupled with the P1–P1' acylsulfonamide intermediates **8** and **9**, which were prepared following reported methods,[18,19] to afford the target inhibitors **3**, **10b-e** and **11a-e**. The *tert*-butyl-capped compounds were converted to the corresponding cyclopentyl-capped derivatives by removal of the Boc protecting group followed by reaction of the resulting amine salts with the *N*-(cyclopentyloxycarbonyloxy)-succinimide

carbonate using DIEA as a base to furnish the desired compounds **14a-e** and **15a-e**. (For synthesis of linear final compounds and intermediates please see **Appendix C**).

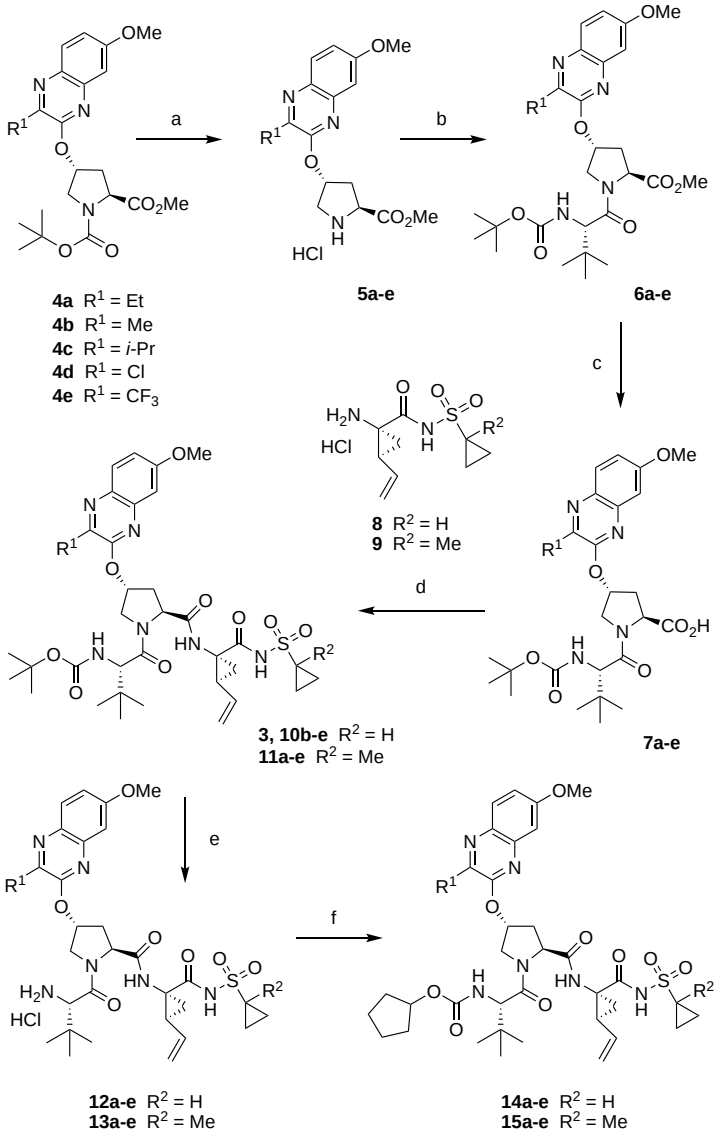

Scheme A.1: Synthesis of HCV NS3/4A protease inhibitors.
Reagents and conditions: (a) 4 N HCl in dioxane, CH_2Cl_2, RT, 3 h; (b) Boc-Tle-OH, HATU, DIEA, DMF, RT, 4 h; (c) $LiOH.H_2O$, THF, H_2O, RT, 24 h; (d) HATU, DIEA, DMF, RT, 2 h; (e) 4 N HCl in dioxane, RT, 3 h; (f) *N*-(cyclopentyloxycarbonyloxy)-succinimide, DIEA, CH_3CN, RT, 36 h.

A.4 Results and Discussion

Although linear NS3/4A PIs are generally less potent compared to the corresponding macrocyclic analogues, they offer noteworthy advantages over the latter, including conformational flexibility that permits adaptability to RASs. Moreover, facile synthesis enables rapid sampling of inhibitor chemical space to optimize potency and pharmacokinetic properties. While all the current FDA approved NS3/4A PIs are macrocyclic, a number of linear inhibitors have been successfully developed including asunaprevir,[20] which has been approved in Japan. Thus, despite reduced potency, linear inhibitors can serve as potential lead compounds to develop cheaper alternatives to complex, synthetically challenging macrocyclic drugs.

We employed a structure-guided design strategy to identify analogues of the linear inhibitor **3** with improved potency and reduced susceptibility to clinically relevant HCV variants. The SAR exploration was focused on optimizing interactions of the P2 quinoxaline moiety and minimizing direct interactions with S2 subsite residues. In addition to exploring SAR at the 3-position of the P2 quinoxaline, modifications at the P1′ and the *N*-terminal capping groups were also investigated (**Figure A.1**). The potency and resistance profiles of the resulting linear PIs were evaluated using biochemical and replicon assays. The enzyme inhibition constants (*K*i) were determined against WT GT1a NS3/4A protease and drug-resistant variants R155K and D168A (**Table A.1**). For a subset of compounds, cellular antiviral potencies (EC_{50}) were determined using

replicon-based antiviral assays against WT HCV and drug-resistant variants R155K, A156T, D168A, and D168V (**Table A.2**). Grazoprevir (**1**) was used as a control in all assays.

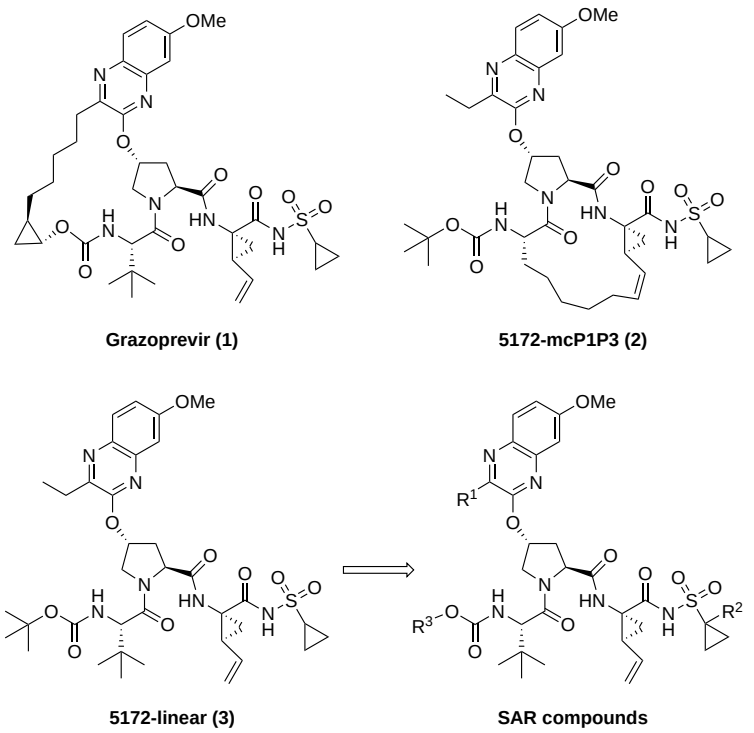

Figure A.1: Structures of the HCV NS3/4A protease inhibitors.
Grazoprevir (1), P1–P3 macrocyclic analogue 5172-mcP1P3 (2), linear analogue 5172-linear (3), and SAR compounds.

Table A.1: Inhibitory activity against wild-type NS3/4A protease and drug resistant variants

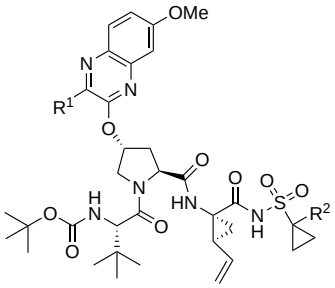

3, 10b-e; **11a-e**

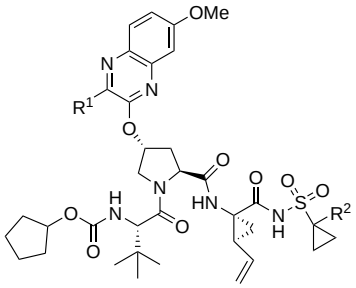

14a-e; **15a-e**

Inhibitor	R^1	R^2	GT1a NS3/4A Protease *K*i (nM) (fold change)		
			WT	R155K	D168A
3	Et	H	19 ± 2.7	17 ± 2.3 (0.9)	642 ± 101 (34)
11a	Et	Me	16 ± 1.3	14 ± 1.1 (0.9)	385 ± 31 (24)
14a	Et	H	9.8 ± 2.0	15 ± 2.2 (1.5)	350 ± 30 (36)
15a	Et	Me	6.9 ± 0.5	13 ± 2.7 (1.9)	145 ± 14 (21)
10b	Me	H	18 ± 1.6	8.5 ± 2.1 (0.5)	290 ± 24 (16)
11b	Me	Me	14 ± 2.1	14 ± 1.7 (1.0)	265 ± 26 (19)
14b	Me	H	9.2 ± 0.9	9.6 ± 0.9 (1.0)	144 ± 23 (16)
15b	Me	Me	7.1 ± 1.1	10 ± 1.3 (1.4)	140 ± 13 (20)
10c	*i*-Pr	H	32 ± 5.1	49 ± 11 (1.5)	1086 ± 137 (34)
11c	*i*-Pr	Me	29 ± 9.4	27 ± 5.6 (0.9)	1179 ± 170 (41)
14c	*i*-Pr	H	17 ± 3.2	55 ± 11 (3)	985 ± 106 (58)
15c	*i*-Pr	Me	21 ± 2.6	43 ± 11 (2.0)	1000 ± 80 (48)
10d	Cl	H	7.8 ± 1.1	2.2 ± 0.4 (0.3)	128 ± 16 (16)
11d	Cl	Me	6.1 ± 1.1	3.8 ± 0.6 (0.7)	119 ± 16 (31)
14d	Cl	H	3.8 ± 0.6	4.1 ± 0.5 (1.1)	99 ± 10 (26)
15d	Cl	Me	3.9 ± 0.7	5.2 ± 0.8 (1.3)	51 ± 6.0 (13)
10e	CF_3	H	87 ± 18	24 ± 3.3 (0.3)	723 ± 80 (8)
11e	CF_3	Me	46 ± 9.6	12 ± 1.7 (0.3)	513 ± 50 (11)
14e	CF_3	H	34 ± 8.3	26 ± 7.7 (0.8)	703 ± 63 (21)
15e	CF_3	Me	22 ± 3.4	22 ± 6.9 (1.0)	516 ± 61 (24)
5172-mcP1P3			2.0 ± 0.1	3.1 ± 0.34 (1.6)	91 ± 10 (46)
Grazoprevir			0.20 ± 0.1	0.80 ± 0.3 (4)	40 ± 5.0 (200)

Table A.2: Antiviral activity against wild-type HCV and drug resistant variants

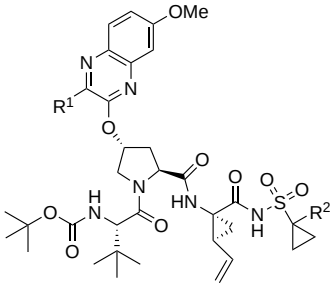

3, 10b-e; **11a-e**

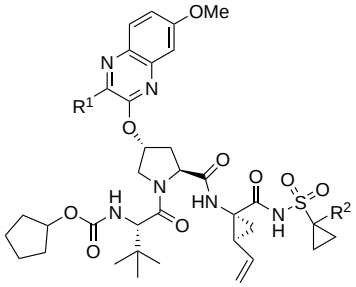

14a-e; **15a-e**

Inhibitor	R^1	R^2	Replicon EC_{50} (nM) (fold change)				
			WT	R155K	A156T	D168A	D168V
3	Et	H	24	50 (2.1)	73 (3.0)	>500 (>21)	>500 (>21)
11a	Et	Me					
14a	Et	H					
15a	Et	Me					
10b	Me	H					
11b	Me	Me					
14b	Me	H	10	48 (4.8)	164 (16)	101 (10)	150 (15)
15b	Me	Me	4.5	28 (6.2)	87 (19)	45 (10)	59 (13)
10c	*i*-Pr	H					
11c	*i*-Pr	Me					
14c	*i*-Pr	H					
15c	*i*-Pr	Me					
10d	Cl	H	6.6	10 (1.5)	107 (16)	38 (5.8)	12 (1.8)
11d	Cl	Me	6.3	10 (1.6)	100 (16)	30 (4.8)	12 (1.9)
14d	Cl	H	7.4	40 (5.4)	292 (40)	50 (6.8)	54 (7.3)
15d	Cl	Me	3.1	27 (8.7)	163 (53)	25 (8.1)	23 (7.4)
10e	CF_3	H					
11e	CF_3	Me					
14e	CF_3	H					
15e	CF_3	Me					
5172-mcP1P3			0.33	1.8 (5.5)	9.7 (29)	6.3 (19)	9.1 (28)
Grazoprevir			0.12	1.9 (16)	200 (1667)	11 (92)	5.3 (44)

Compared to the macrocyclic PIs **1** and **2**, the linear analogue **3** exhibited significantly lower potency against WT protease (K_i = 19 nM) and experienced an even larger reduction in antiviral potency (EC_{50} = 24 nM), which is in line with our previous reports.[13] Compound **3** was also less potent than **1** and **2** against drug-resistant variants R155K, D168A and D168V in both enzyme inhibition and replicon assays. The significant potency losses for the linear compound **3** are likely due to the increase in conformational flexibility and associated entropic penalty of binding to the protease. However, close examination of the overall resistance profile revealed that fold losses in potency were generally lower for compound **3** than **1** in both enzyme inhibition and replicon assays. Moreover, while **1** was highly susceptible to the A156T variant (EC_{50} = 200 nM), with >1600-fold loss in potency compared to WT, compound **3** showed better antiviral potency against this variant (EC_{50} = 73 nM). The reduced susceptibility to RAS variants, particularly at residue Ala156, observed for **3** demonstrates that removal of the macrocyclic linker and the resulting conformational flexibility allows the inhibitor to adapt to substitutions in the S2 subsite.

To improve the potency profile of inhibitor **3**, analogues with modifications at the P1' and P4 capping regions were prepared and tested. Replacement of the P1' cyclopropylsulfonamide with a more hydrophobic 1-methylcyclopropylsulfonamide moiety generally improved potency of the resulting analogues. Thus, compared to **3**, analogue **11a** afforded a slight increase in enzyme potency against WT protease and RAS variants R155K and D168A.

Similarly, replacing the *tert*-butyl P4 capping group with a bulkier cyclopentyl moiety in **14a** provided compounds with improved potency. Analogue **15a** with the 1-methyl-cyclopropylsulfonamide moiety at P1' and cyclopentyl P4 capping group was 2- and 4-fold more potent than **3** against WT (*K*i = 6.9 nM) and D168A (*K*i = 145 nM) but showed similar potency against the R155K protease. Thus, minor modifications at the P1' and P4 moieties of inhibitor **3** provided analogues with improved potency against WT protease and the D168A variant.

We have shown that minimizing inhibitor interactions in the S2 subsite resulted in an overall improvement in potency and resistance profiles.[17] Although the P2 quinoxaline in **3** largely avoids direct interactions with residues in the S2 subsite, the ethyl group at the 3-position of this moiety makes hydrophobic interactions with the hydrocarbon portion of the Arg155 side chain as well as with Ala156. Thus, in an effort to optimize interactions with these residues, we explored changes at the 3-position of P2 quinoxaline moiety. Based on the co-crystal structures and SAR results from the P1–P3 macrocyclic series,[17] we expected that replacing the ethyl group with a smaller methyl group at this position, while reducing overall inhibitor interactions in the S2 subsite, would maintain important hydrophobic interactions with side chains of Arg155 and Ala156. As expected, compound **10b** incorporating the 3-methylquinoxaline was 2-fold more potent than **3** against the R155K and D168A protease variants in enzyme inhibition assays. However, analogue **11b** with the 1-methylcyclopropylsulfonamide moiety at P1' position did not show much

improvement in enzyme potency compared to **10b**. Compounds **14b** and **15b** with the cyclopentyl P4 capping group were slightly more potent than the corresponding *tert*-butyl analogues **10b** and **11b** against WT and D168A. Furthermore, compounds **14b** and **15b** showed nanomolar potency in replicon assays against WT HCV, and despite losing about 5–20-fold potency, **15b** maintained significant potency against all variants tested. Although both the 3-ethyl and 3-methyl-quinoxaline compounds showed similar potencies against WT and R155K protease variants, PIs with the smaller methyl substituent were generally more potent against the D168A variant. Together, the enzyme inhibition and replicon data indicate a preference for smaller substituents at the 3-position of the P2 quinoxaline to maintain potency against RAS variants.

Next, a larger isopropyl group was incorporated in compounds **10c** and **11c** to further explore the optimal size of the substituent at the 3-position of P2 quinoxaline that can be accommodated in the S2 subsite without causing unfavorable interactions. These compounds displayed considerably lower potency compared to the 3-methyl- and 3-ethyl-quinoxaline compounds across all variants in enzyme inhibition assays. Moreover, compounds with a larger isopropyl group at this position were highly susceptible to RAS variants at residues Arg155 and Asp168 with K_i values in the millimolar range against the D168A protease. Analogues **14c** and **15c**, with a cyclopentyl P4 capping group, showed similar trends to the corresponding *tert*-butyl analogues across all protease variants tested. These findings further support our hypothesis that large

substituents at the 3-position of the P2 quinoxaline are detrimental to potency against the RAS variants.

After determining optimal size of the substituent at the 3-position of the P2 quinoxaline, we next focused our efforts on identifying isosteric replacements with variant electronic properties. Thus, a set of compounds bearing a 3-chloroquinoxaline P2 moiety, with comparable spatial size to the 3-methylquinoxaline, was analyzed by enzyme inhibition and antiviral assays. In general, compounds with the 3-chloroquinoxaline were significantly more potent than the corresponding 3-ethyl- and 3-methyl-quinoxaline analogues. Compounds **10d** and **11d**, with a *tert*-butyl P4 capping group, showed about 2-fold better potency than the corresponding 3-methylquinoxaline analogues **10b** and **11b** against WT, R155K and D168A proteases. Similarly, the cyclopentyl-capped compounds **14d** and **15d** (WT *K*i = 3.8 and 3.9 nM, respectively) were more potent than the corresponding **14b** and **15b**, showing excellent potency against WT protease and RAS variants. In fact, both **14d** and **15d** exhibited *K*i values against WT and RAS protease variants in the same range as the macrocyclic inhibitor **2** (WT *K*i = 2.0 nM), indicating that potency of the quinoxaline-based linear PIs could be improved significantly by SAR exploration. In replicon assays, the 3-chloroquinoxaline compounds exhibited the best overall potency profile among the linear compounds, with PIs **10d**, **11d** and **15d** showing significant improvement in replicon potency against the multidrug resistant HCV variants D168A/V (EC_{50} = 12–38 nM). However, these compounds were more

susceptible to the A156T substitution than the corresponding macrocyclic analogues.[17] The improved potency profiles of the 3-chloroquinoxaline compounds compared to the corresponding 3-methylquinoxaline analogues indicate that the chloro group likely renders more favorable electronic properties to the P2 quinoxaline moiety, which improves the critical π-π stacking interactions with the catalytic residue His57.

To further investigate the effect of electron-withdrawing groups on the activity of the inhibitors, derivatives with a more electronegative, although relatively larger, 3-trifluoromethylquinoxaline were examined. In contrast to the 3-chloroquinoxaline inhibitors, compounds **10e** and **11e** showed considerable loss in potency against WT protease. However, despite relatively lower potency against WT, the 3-trifluoromethylquinoxaline analogues were slightly more potent than the corresponding 3-isopropylquinoxaline PIs against RAS variants R155K and D168A. Similar trends were observed for inhibitors **14e** and **15e** with the cyclopentyl P4 capping groups. While it is difficult to separate the effects of electronic properties of the chloro- and trifluoromethyl-quinoxaline moieties, it is likely that size played a more important role in determining the overall potency profile of these inhibitors.

We determined crystal structures of three linear HCV NS3/4A PIs in complex with WT NS3/4A protease (**Table A.3**) in an effort to explain the observed potency and resistance profiles. The x-ray crystal structures of WT-**15b**, -**15c** and -**15d** co-complexes with PIs incorporating different P2 quinoxaline moieties were

compared with our previously determined structures of **1** and **3** (PDB IDs 3SUD and 5EQQ, respectively).[12,16] These high-resolution structures provided details of protein-inhibitor interactions to elucidate the structural differences that underlie varied potency and susceptibility to RAS variants.

Table A.3: X-ray data collection and crystallographic refinement statistics.

	WT1a-**15b**	WT1a-**15c**	WT1a-**15d**
PDB code	6CVW	6CVX	6CVY
Resolution	1.78 Å	1.78 Å	1.80 Å
Space group	$P2_12_12_1$	$P2_12_12_1$	$P2_12_12_1$
Molecules in AU[a]	1	1	1
Cell dimensions			
a (Å)	55.2	55.3	55.5
b (Å)	58.5	58.5	58.5
c (Å)	59.9	59.8	59.7
β (°)	90	90	90
Completeness (%)	98.3	99.1	96.4
Total reflections	70790	119454	116526
Unique reflections	18870	19054	17991
Average I/σ	18.5	15.1	15.2
Redundancy	3.8	6.3	6.5
R_{sym} (%)[b]	7.8 (25.6)	7.1 (27.3)	8.5 (30.7)
RMSD[c] in			
Bond lengths (Å)	0.014	0.019	0.009
Bond angles (°)	1.4	1.5	1.1
R_{factor} (%)[d]	14.9	15.6	14.7
R_{free} (%)[e]	18.5	19.4	18.4

[a]AU, asymmetric unit.
[b]$R_{sym} = \Sigma \mid I - \langle I \rangle \mid / \Sigma I$, where I = observed intensity, $\langle I \rangle$ = average intensity over symmetry equivalent; values in parentheses are for the highest resolution shell.
[c]RMSD, root mean square deviation.
[d]$R_{factor} = \Sigma \mid\mid F_o \mid - \mid F_c \mid\mid / \Sigma \mid F_o \mid$.
[e]R_{free} was calculated from 5% of reflections, chosen randomly, which were omitted from the refinement process.

The overall binding mode of linear inhibitors **15b-d** is similar to that of macrocyclic inhibitors **1–2** and the parent compound **3**, where the P2 quinoxaline predominately interacts with the catalytic triad residues (**Figure A.2**). These structures confirm that the quinoxaline moiety maintains this unique binding conformation irrespective of macrocyclization and the substituent at the 3-position. The inhibitors **15b-d** span the S1'–S4 pockets in the active site with a conserved hydrogen bond network present in all WT NS3/4A protease structures. Specifically, hydrogen bonds with the backbone carbonyl of Arg155 and nitrogen of Ala157 are maintained, and the P1' acylsulfonamide moiety is positioned in the oxyanion hole, stabilized by hydrogen bonds with residues His57, Gly137, Ser138 and Ser139. Although the overall binding mode of linear analogues is similar to that of compound **1**, there are subtle changes in the binding of P2 quinoxaline that appear to impact inhibitor potency considerably.

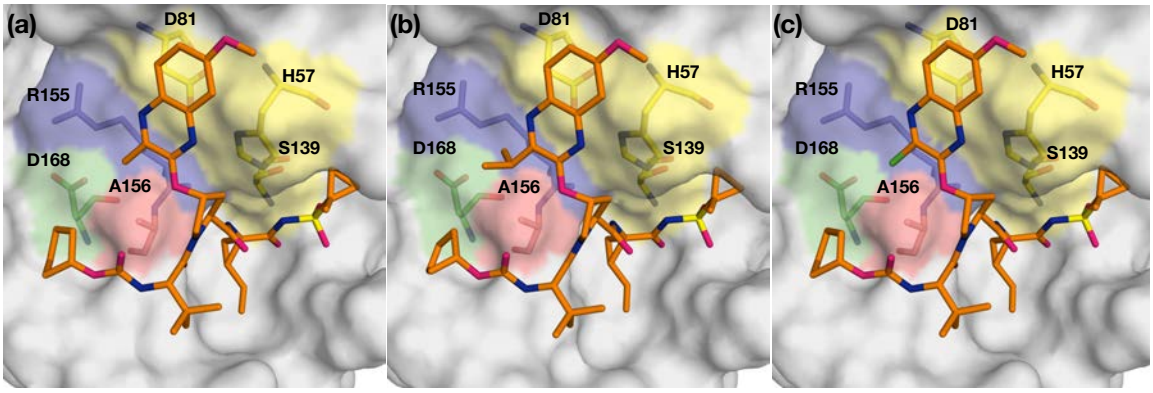

Figure A.2: X-ray crystal structures of WT1a HCV NS3/4A protease in complex with linear inhibitors (a) 15b, (b) 15c, and (c) 15d.
The protease active site is presented as a light grey surface with bound inhibitors depicted as orange sticks. The catalytic triad is highlighted in yellow, and drug resistance residues Arg155, Ala156, and Asp168 are shown as sticks.

The differences between the WT-**1** and the 3-methylquinoxaline inhibitor **15b** structures occur predominantly in the S2 subsite (**Figure A.3A**). Relative to WT-**1**, the Asp168 side chain in the WT-**15b** structure is shifted to allow additional hydrogen bonding with the side chain of Arg155. This confirmation of Asp168, which allows the P4 cyclopentyl capping group to occupy the S4 pocket, is observed in all of the linear inhibitor structures and other WT protease-inhibitor complexes.[12,17] The 3-methylquinoxaline moiety is shifted away from the catalytic residues toward the S2 subsite relative to the conformation of P2 quinoxaline in WT-**1** structure. This shift was also observed in the parent compound **3**, though to a lesser extent, likely to accommodate the larger ethyl group at the 3-position of quinoxaline (**Figure A.4**). However, despite larger shift of the 3-methylquinoxaline moiety, inhibitor **15b** has an improved potency profile against RAS variants compared to **3**, likely due to weaker contacts of the smaller methyl group with residues in the S2 subsite that mutate to confer resistance. Thus, while a slight shift of the P2 quinoxaline toward the S2 subsite does not appear to affect the overall potency profile, the substituent at the 3-position of this moiety significantly impacts inhibitor potency against RAS variants.

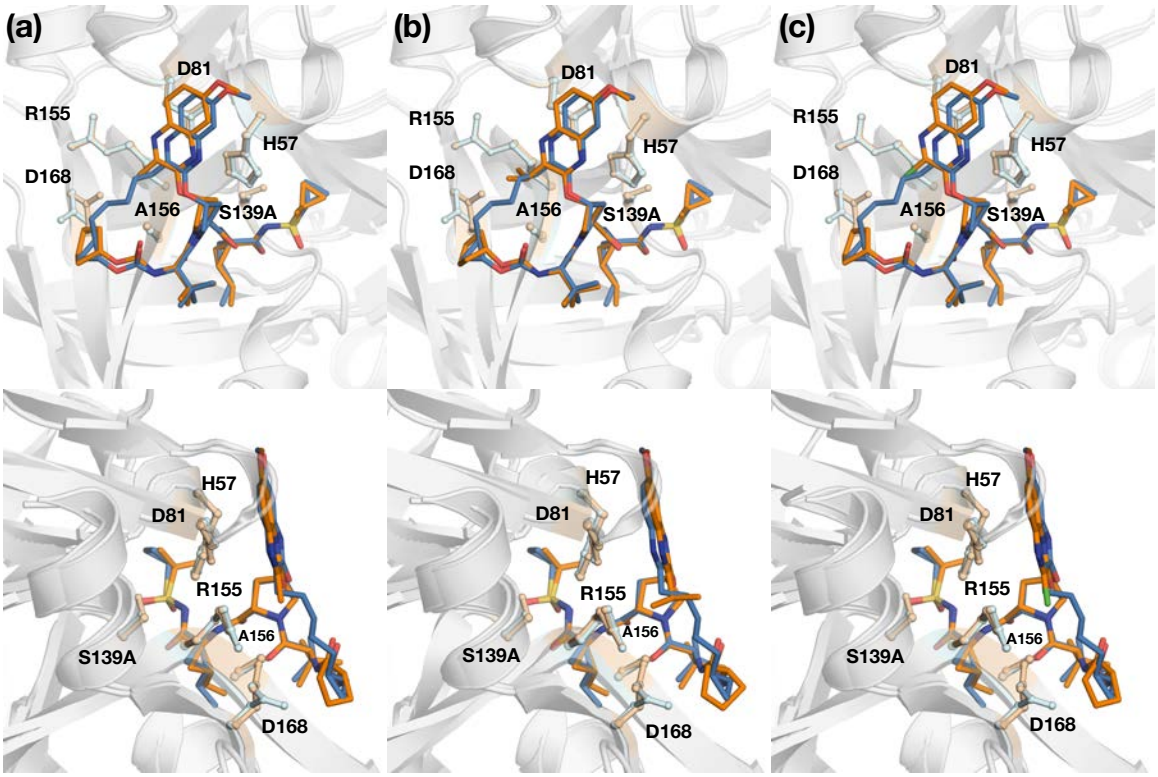

Figure A.3: Superposition of WT-1 and (a) WT-15b, (b) WT-15c, and (c) WT-15d complexes, focusing on the differences at the P2 quinoxaline.
The protease is in ribbon representation (light grey), with bound inhibitors **1** (blue) and **15b-d** (orange) depicted as sticks. The side chains of catalytic triad and drug resistance residues Arg155, Ala156, and Asp168 are shown as sticks.

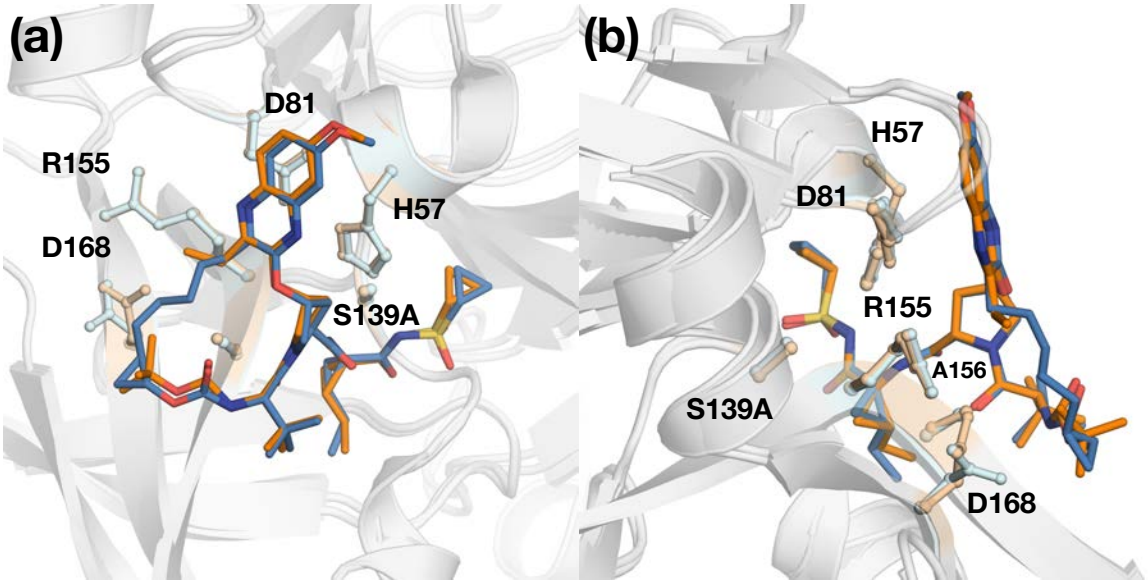

Figure A.4: Superposition of WT-1 and WT-3 complexes, focusing on the differences at the P2 quinoxaline.
The protease is in ribbon representation (light grey), with bound inhibitors **1** (blue) and **3** (orange) depicted as sticks. The side chains of catalytic triad and drug resistance residues Arg155, Ala156, and Asp168 are shown as sticks.

The shift of the quinoxaline moiety toward the S2 subsite residues was also observed in the WT-**15c** and WT-**15d** complexes (**Figure A.3B–C**), as well as in **2** and other structures of the P1–P3 macrocyclic analogues.[17] However, the crystal structure of inhibitor **15c** with the 3-isopropyl substituted quinoxaline revealed an additional rearrangement of the P2 moiety. Compared to **1**, the P2 quinoxaline in **15c**, with a larger isopropyl substituent, packs less against the catalytic His57 residue and instead moves toward the solvent exposed surface of the binding pocket (**Figure A.3B**). This movement of the quinoxaline away from the catalytic His57 is not observed in the inhibitor complexes with smaller substituents at the 3-position (**Figure A.3A** and **3C**). Interestingly, this binding conformation is reminiscent of the conformation of **1** when bound to the A156T protease variant (PDB ID 3SUG) (**Figure A.5**), where the larger threonine residue causes steric clash with the P2–P4 macrocycle (cite).[12,16] To accommodate the larger side chain in the A156T protease inhibitor **1** undergoes a rearrangement resulting in the shift of the P2 quinoxaline moiety toward the solvent exposed binding surface, weakening the critical π–π interactions with the catalytic His57 (**Figure A.5A**). This altered binding conformation of **1** results in dramatic potency losses against the RAS variants at Ala156.[12]

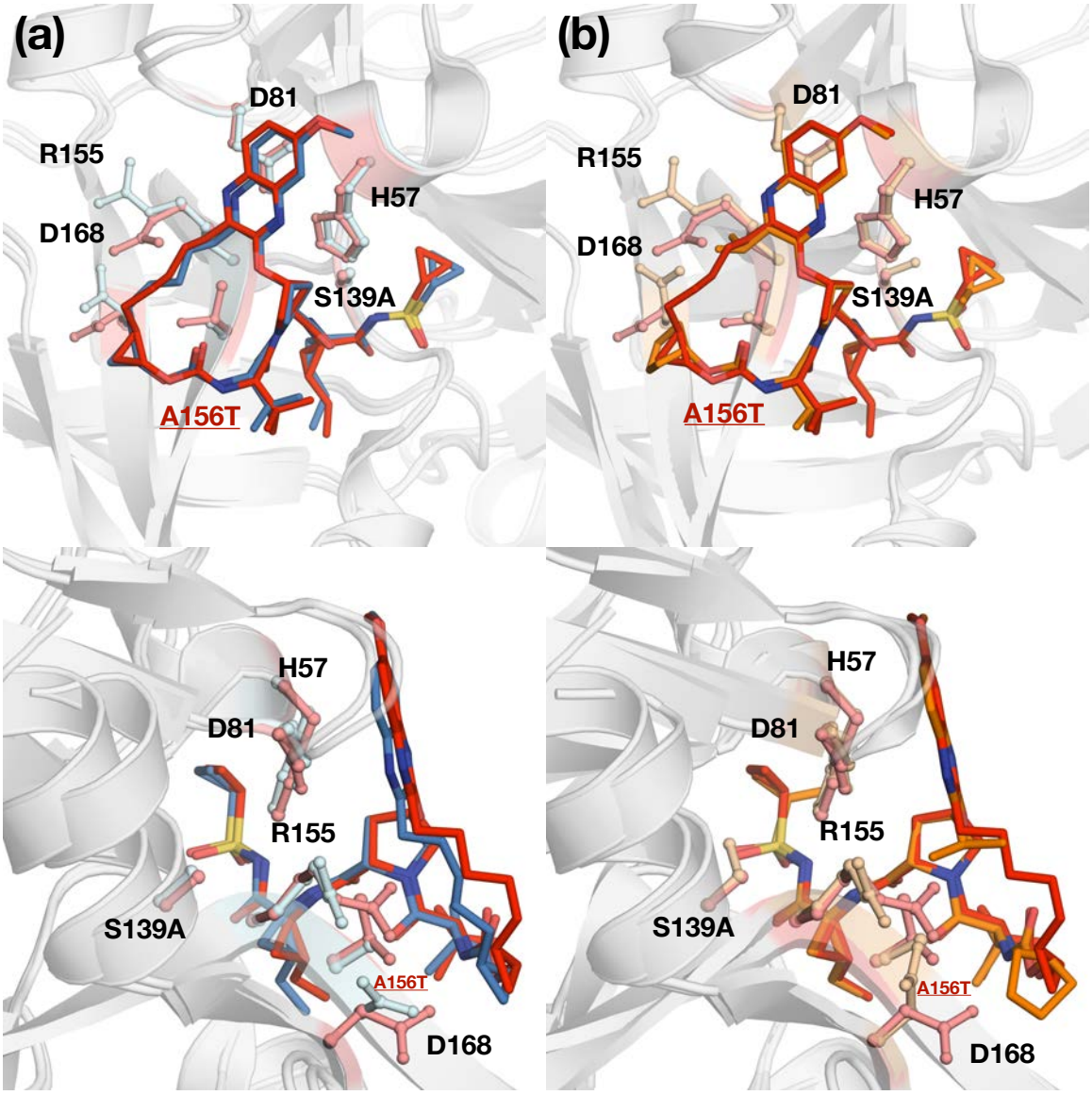

Figure A.5: (a) Superposition of WT-1 and A156T-1 and (b) A156T-1 and WT-15d complexes, focusing on the differences at the P2 quinoxaline.
The protease is in ribbon representation (light grey) with bound inhibitor **1** depicted as sticks in blue (WT) and red (A156T), and inhibitor **15d** (WT) in orange. The side chains of catalytic triad and drug resistance residues Arg155, Ala156, and Asp168 are shown as sticks.

Comparison of the A156T-**1** and the WT-**15c** structures shows complete superposition of the inhibitors' P2 quinoxaline moieties (**Figure A.5B**). The binding conformation of inhibitor **15c** is altered relative to other linear compounds with smaller groups at the P2 quinoxaline to accommodate the bulky isopropyl substituent in the S2 subsite. This altered conformation of the 3-isopropylquinoxaline results in significantly reduced interactions with the catalytic His57 residue. Any perturbation to the protease active site via substitution of the S2 subsite residues may further reduce interactions with the catalytic His57 residue. These results reinforce the inhibition data, which shows that the 3-isopropylquinoxaline compounds exhibit reduced potency against WT relative to the parent compound **3** and are the most susceptible to RAS variants. Moreover, these crystal structures highlight an important feature of inhibitor binding, suggesting that modifications of the inhibitor scaffold that cause movement of the quinoxaline away from the His57 toward the solvent exposed binding pocket are highly detrimental to potency. Whereas, movement of the quinoxaline away from His57 toward the S2 subsite residues has less of an effect on inhibitor potency when a smaller substituent is present at the 3-position of P2 quinoxaline.

The 3-chloroquinoxaline series exhibited an excellent potency profile against WT and RAS variants even with a shift of the P2 quinoxaline moiety toward the S2 subsite. Interestingly, comparison of the WT-**15b** and WT-**15d** structures (**Figure A.3C**) did not reveal any noticeable difference in binding poses for the 3-methyl- and 3-chloro-quinoxaline analogues that could explain the disparity in

inhibitory activity. The electronic effects of the chloro group appear to improve stacking interactions of the quinoxaline moiety with the catalytic residue His57, which are crucial for the binding of inhibitors with a P2 quinoxaline moiety. Thus, enhancing interactions with the catalytic triad residues by modifying the inhibitor P2 quinoxaline moiety is likely to improve overall binding energy and potency profiles.

Interestingly, most of the linear PIs did not show any notable differences between potencies against the WT and R155K proteases. In fact, elevation in potency was observed for inhibitors with the 3-chloro- and 3-trifluoromethyl-quinoxaline P2 moieties. Molecular modeling studies revealed that lysine side chain in R155K protease forms a salt bridge with Asp168 and another water mediated hydrogen bond with the backbone carbonyl of Lys80, while Asp168 carboxylate forms two hydrogen bonds with the guanidinium group of Arg123 (**Figure A.6**). This extensive network of interactions provides the hydrophobic surface that adequately accommodates the substituents at the 3-position of P2 quinoxaline and hydrophobic groups at the P4 capping. This binding surface mimics the hydrophobic surface maintained by electrostatic interactions between Arg155 guanidinium and Asp168 carboxylate groups in WT protease and is likely responsible for the retention of potency by most of the linear analogues against the R155K variant. The additional water mediated hydrogen bonds between the quinoxaline ring nitrogen and Asp79 backbone carbonyl and Lys155 might be responsible for the enhancement in potency observed for some of the inhibitors.

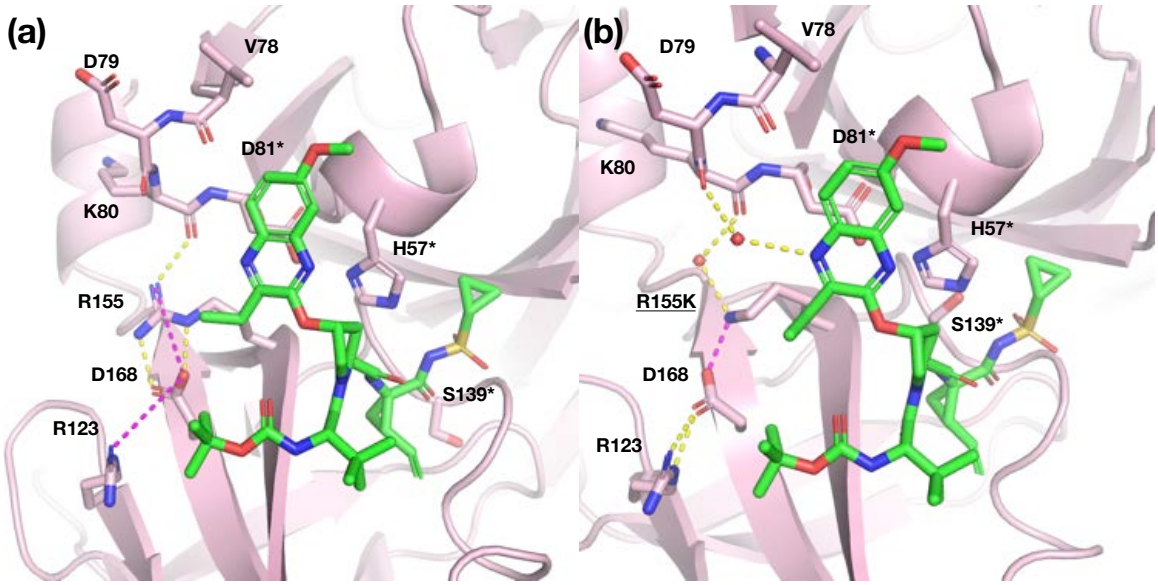

Figure A.6: Energy minimized models of inhibitor 3 in the active site of (a) WT NS3/4A protease (5EQQ) and (b) drug resistant variant R155K (3SUE). The R155K mutation is shown underlined. Yellow and magenta dashed lines indicate hydrogen bonds or salt bridges, respectively. Catalytic triad residues are highlighted with an *.

A.5 Conclusion

In summary, we have investigated the SAR of quinoxaline-based linear HCV NS3/4A PIs using a structure-guided design strategy to improve potency against drug resistant variants. X-ray crystal structures of three inhibitors with different P2 moieties bound to WT protease revealed the structural basis for the observed potency and resistance profiles. Inhibitors with small substituents at the 3-position of the P2 quinoxaline were preferred for maintaining potency against drug resistant protease variants due to decreased interactions with the S2 subsite residues. Compounds with larger groups at this position cause the P2 quinoxaline moiety to shift out of the active site, weakening critical stacking interactions with the catalytic His57. These findings further support our hypothesis that optimizing inhibitor interactions with the S2 subsite residues in the protease active site results in improved potency and resistance profiles. Moreover, in the absence of a macrocycle, the quinoxaline-based linear PIs could be optimized by SAR exploration to provide compounds with high potency and improved resistance profiles.

A.6 Methods

A.6.1 Expression and Purification of NS3/4A Protease Constructs

The HCV GT1a NS3/4A protease gene described in the Bristol Myers Squibb patent[21] was synthesized by GenScript and cloned into a PET28a expression

vector. The D168A and R155K genes were engineered using the site-directed mutagenesis protocol from Stratagene. Protein expression and purification were carried out as previously described. Briefly, transformed *Escherichia coli* BL21(DE3) cells were grown in LB media containing 30 µg/mL of kanamycin antibiotic at 37 °C. After reaching an OD_{600} of 0.8, cultures were induced with 1 mM IPTG and harvested after 4 h of expression. Cells were pelleted by centrifugation, resuspended in Resuspension buffer [50 mM phosphate buffer, 500 mM NaCl, 10% glycerol, 2 mM β-ME, pH 7.5] and frozen at −80 °C for storage.

Cell pellets were thawed and lysed via cell disruptor (Microfluidics Inc.) two times to ensure sufficient DNA shearing. Lysate was centrifuged at 19,000 rpm, for 25 min at 4 °C. The soluble fraction was applied to a nickel column (Qiagen) pre-equilibrated with Resuspension buffer. The beads and soluble fraction were incubated at 4 °C for 1.5 h and the lysate was allowed to flow through. Beads were washed with Resuspension buffer supplemented with 20 mM imidazole and eluted with Resuspension buffer supplemented with 200 mM imidazole. The eluent was dialyzed overnight (MWCO 10 kD) to remove the imidazole, and the His-tag was simultaneously removed with thrombin treatment. The eluate was judged >90% pure by polyacrylamide gel electrophoresis, concentrated, flash and stored at −80 °C.

A.6.2 Enzyme Inhibition Assays

For each assay, 2 nM of NS3/4A protease (GT1a, R155K and D168A) was pre-incubated at room temperature for 1 h with increasing concentration of inhibitors in assay buffer (50 mM Tris, 5% glycerol, 10 mM DTT, 0.6 mM LDAO, and 4% dimethyl sulfoxide, pH 7.5). Inhibition assays were performed in non-binding surface 96-well black half-area plates (Corning) in a reaction volume of 60 µL. The proteolytic reaction was initiated by the injection of 5 µL of HCV NS3/4A protease substrate (AnaSpec), to a final concentration of 200 nM and kinetically monitored using a Perkin Elmer EnVision plate reader (excitation at 485 nm, emission at 530 nm). Three independent data sets were collected for each inhibitor with each protease construct. Each inhibitor titration included at least 12 inhibitor concentration points, which were globally fit to the Morrison equation to obtain the K_i value.

A.6.3 Cell-Based Drug Susceptibility Assays

Mutations (R155K, D168A and A156T) were constructed by site-directed mutagenesis using a Con1 (genotype 1b) luciferase reporter replicon containing the H77 (genotype 1a) NS3 sequence.[22] Replicon RNA of each protease variant was introduced into Huh7 cells by electroporation. Replication was then assessed in the presence of increasing concentrations of protease inhibitors by measuring luciferase activity (relative light units) 96 h after electroporation. The

drug concentrations required to inhibit replicon replication by 50% (EC_{50}) were calculated directly from the drug inhibition curves.

A.6.4 Crystallization and Structure Determination

Protein expression and purification were carried out as previously described. The Ni-NTA purified WT1a protein was thawed, concentrated to 3 mg/mL, and loaded on a HiLoad Superdex75 16/60 column equilibrated with gel filtration buffer (25 mM MES, 500 mM NaCl, 10% glycerol, and 2 mM DTT, pH 6.5). The protease fractions were pooled and concentrated to 25 mg/mL with an Amicon Ultra-15 10 kDa filter unit (Millipore). The concentrated samples were incubated for 1 h with 3:1 molar excess of inhibitor. Diffraction-quality crystals were obtained overnight by mixing equal volumes of concentrated protein solution with precipitant solution (20–26% PEG-3350, 0.1 M sodium MES buffer, 4% ammonium sulfate, pH 6.5) at RT in 24-well VDX hanging drop trays. Crystals were harvested and data was collected at 100 K. Cryogenic conditions contained the precipitant solution supplemented with 15% glycerol or ethylene glycol.

X-ray diffraction data were collected in-house using our Rigaku X-ray system with a Saturn 944 detector. All datasets were processed using HKL-3000.[23] Structures were solved by molecular replacement using PHASER.[24] Model building and refinement were performed using Coot[25] and PHENIX,[26] respectively. The final structures were evaluated with MolProbity[27] prior to deposition in the PDB. To limit the possibility of model bias throughout the

refinement process, 5% of the data were reserved for the free R-value calculation.[28] Structure analysis, superposition and figure generation were done using PyMOL.[29] X-ray data collection and crystallographic refinement statistics are presented in **Table A.3**.

Appendix A – References

1. World Health Organization (WHO). Hepatitis C, Fact Sheet (Updated October 2017): http://www.who.int/mediacentre/factsheets/fs164/en/. (Accessed January 24, 2018).
2. Fried, M. W.; Shiffman, M. L.; Reddy, K. R.; Smith, C.; Marinos, G.; Goncales, F. L., Jr.; Haussinger, D.; Diago, M.; Carosi, G.; Dhumeaux, D.; Craxi, A.; Lin, A.; Hoffman, J.; Yu, J. Peginterferon alfa-2a plus ribavirin for chronic hepatitis C virus infection. *N. Engl. J. Med.* **2002,** 347, 975–982.
3. Falade-Nwulia, O.; Suarez-Cuervo, C.; Nelson, D. R.; Fried, M. W.; Segal, J. B.; Sulkowski, M. S. Oral Direct-Acting Agent Therapy for Hepatitis C Virus Infection: A Systematic Review. *Ann. Intern. Med.* **2017,** 166, 637–648.
4. McCauley, J. A.; Rudd, M. T. Hepatitis C virus NS3/4a protease inhibitors. *Curr. Opin. Pharmacol.* **2016,** 30, 84–92.
5. Pilot-Matias, T.; Tripathi, R.; Cohen, D.; Gaultier, I.; Dekhtyar, T.; Lu, L.; Reisch, T.; Irvin, M.; Hopkins, T.; Pithawalla, R.; Middleton, T.; Ng, T.; McDaniel, K.; Or, Y. S.; Menon, R.; Kempf, D.; Molla, A.; Collins, C. In vitro and in vivo antiviral activity and resistance profile of the hepatitis C virus NS3/4A protease inhibitor ABT-450. *Antimicrob. Agents Chemother.* **2015,** 59, 988–997.
6. Summa, V.; Ludmerer, S. W.; McCauley, J. A.; Fandozzi, C.; Burlein, C.; Claudio, G.; Coleman, P. J.; DiMuzio, J. M.; Ferrara, M.; Di Filippo, M.; Gates, A. T.; Graham, D. J.; Harper, S.; Hazuda, D. J.; McHale, C.; Monteagudo, E.; Pucci, V.; Rowley, M.; Rudd, M. T.; Soriano, A.; Stahlhut, M. W.; Vacca, J. P.; Olsen, D. B.; Liverton, N. J.; Carroll, S. S. MK-5172, a selective inhibitor of hepatitis C virus NS3/4a protease with broad activity across genotypes and resistant variants. *Antimicrob. Agents Chemother.* **2012,** 56, 4161–4167.
7. Kwo, P. Y.; Poordad, F.; Asatryan, A.; Wang, S.; Wyles, D. L.; Hassanein, T.; Felizarta, F.; Sulkowski, M. S.; Gane, E.; Maliakkal, B.; Overcash, J. S.; Gordon, S. C.; Muir, A. J.; Aguilar, H.; Agarwal, K.; Dore, G. J.; Lin, C. W.; Liu, R.; Lovell, S. S.; Ng, T. I.; Kort, J.; Mensa, F. J. Glecaprevir and pibrentasvir yield high response rates in patients with HCV genotype 1-6 without cirrhosis. *J. Hepatol.* **2017,** 67, 263–271.
8. Bourliere, M.; Gordon, S. C.; Flamm, S. L.; Cooper, C. L.; Ramji, A.; Tong, M.; Ravendhran, N.; Vierling, J. M.; Tran, T. T.; Pianko, S.; Bansal, M. B.; de Ledinghen, V.; Hyland, R. H.; Stamm, L. M.; Dvory-Sobol, H.; Svarovskaia, E.; Zhang, J.; Huang, K. C.; Subramanian, G. M.; Brainard, D. M.; McHutchison, J. G.; Verna, E. C.; Buggisch, P.; Landis, C. S.; Younes, Z. H.; Curry, M. P.; Strasser, S. I.; Schiff, E. R.; Reddy, K. R.; Manns, M. P.; Kowdley, K. V.; Zeuzem, S.; Polaris; Investigators, P.-. Sofosbuvir, Velpatasvir, and Voxilaprevir for Previously Treated HCV Infection. *N. Engl. J. Med.* **2017,** 376, 2134–2146.
9. Ng, T. I.; Tripathi, R.; Reisch, T.; Lu, L.; Middleton, T.; Hopkins, T. A.; Pithawalla, R.; Irvin, M.; Dekhtyar, T.; Krishnan, P.; Schnell, G.; Beyer, J.; McDaniel, K. F.; Ma, J.; Wang, G.; Jiang, L. J.; Or, Y. S.; Kempf, D.; Pilot-Matias, T.; Collins, C. In Vitro Antiviral Activity and Resistance Profile of the Next-

Generation Hepatitis C Virus NS3/4A Protease Inhibitor Glecaprevir. *Antimicrob. Agents Chemother.* **2017**.
10. Pawlotsky, J. M. Hepatitis C virus resistance to direct-acting antiviral drugs in interferon-free regimens. *Gastroenterology* **2016,** 151, 70–86.
11. Sarrazin, C. The importance of resistance to direct antiviral drugs in HCV infection in clinical practice. *J. Hepatol.* **2016,** 64, 486–504.
12. Romano, K. P.; Ali, A.; Aydin, C.; Soumana, D.; Özen, A.; Deveau, L. M.; Silver, C.; Cao, H.; Newton, A.; Petropoulos, C. J.; Huang, W.; Schiffer, C. A. The molecular basis of drug resistance against hepatitis C virus NS3/4A protease inhibitors. *PLoS Pathog.* **2012,** 8, e1002832.
13. Ali, A.; Aydin, C.; Gildemeister, R.; Romano, K. P.; Cao, H.; Özen, A.; Soumana, D.; Newton, A.; Petropoulos, C. J.; Huang, W.; Schiffer, C. A. Evaluating the role of macrocycles in the susceptibility of hepatitis C virus NS3/4A protease inhibitors to drug resistance. *ACS Chem. Biol.* **2013,** 8, 1469–1478.
14. Harper, S.; McCauley, J. A.; Rudd, M. T.; Ferrara, M.; DiFilippo, M.; Crescenzi, B.; Koch, U.; Petrocchi, A.; Holloway, M. K.; Butcher, J. W.; Romano, J. J.; Bush, K. J.; Gilbert, K. F.; McIntyre, C. J.; Nguyen, K. T.; Nizi, E.; Carroll, S. S.; Ludmerer, S. W.; Burlein, C.; DiMuzio, J. M.; Graham, D. J.; McHale, C. M.; Stahlhut, M. W.; Olsen, D. B.; Monteagudo, E.; Cianetti, S.; Giuliano, C.; Pucci, V.; Trainor, N.; Fandozzi, C. M.; Rowley, M.; Coleman, P. J.; Vacca, J. P.; Summa, V.; Liverton, N. J. Discovery of MK-5172, a macrocyclic hepatitis C virus NS3/4a protease inhibitor. *ACS Med. Chem. Lett.* **2012,** 3, 332–336.
15. Lawitz, E.; Yang, J. C.; Stamm, L. M.; Taylor, J. G.; Cheng, G.; Brainard, D. M.; Miller, M. D.; Mo, H.; Dvory-Sobol, H. Characterization of HCV resistance from a 3-day monotherapy study of voxilaprevir, a novel pangenotypic NS3/4A protease inhibitor. *Antivir. Ther.* **2017**.
16. Soumana, D. I.; Kurt Yilmaz, N.; Prachanronarong, K. L.; Aydin, C.; Ali, A.; Schiffer, C. A. Structural and thermodynamic effects of macrocyclization in HCV NS3/4A inhibitor MK-5172. *ACS Chem. Biol.* **2016,** 11, 900–909.
17. Matthew, A. N.; Zephyr, J.; Hill, C. J.; Jahangir, M.; Newton, A.; Petropoulos, C. J.; Huang, W.; Kurt-Yilmaz, N.; Schiffer, C. A.; Ali, A. Hepatitis C Virus NS3/4A Protease Inhibitors Incorporating Flexible P2 Quinoxalines Target Drug Resistant Viral Variants. *J. Med. Chem.* **2017,** 60, 5699–5716.
18. Wang, X. A.; Sun, L.-Q.; Sit, S.-Y.; Sin, N.; Scola, P. M.; Hewawasam, P.; Good, A., C.; Chen, Y.; Campbell, A. Hepatitis C Virus Inhibitors. US Patent 6995174, 2006.
19. Rudd, M. T.; Butcher, J. W.; Nguyen, K. T.; McIntyre, C. J.; Romano, J. J.; Gilbert, K. F.; Bush, K. J.; Liverton, N. J.; Holloway, M. K.; Harper, S.; Ferrara, M.; DiFilippo, M.; Summa, V.; Swestock, J.; Fritzen, J.; Carroll, S. S.; Burlein, C.; DiMuzio, J. M.; Gates, A.; Graham, D. J.; Huang, Q.; McClain, S.; McHale, C.; Stahlhut, M. W.; Black, S.; Chase, R.; Soriano, A.; Fandozzi, C. M.; Taylor, A.; Trainor, N.; Olsen, D. B.; Coleman, P. J.; Ludmerer, S. W.; McCauley, J. A. P2-quinazolinones and bis-macrocycles as new templates for next-generation

hepatitis C virus NS3/4a protease inhibitors: discovery of MK-2748 and MK-6325. *ChemMedChem* **2015,** 10, 727–735.
20. Scola, P. M.; Sun, L.-Q.; Wang, A. X.; Chen, J.; Sin, N.; Venables, B. L.; Sit, S.-Y.; Chen, Y.; Cocuzza, A.; Bilder, D. M.; D'Andrea, S. V.; Zheng, B.; Hewawasam, P.; Tu, Y.; Friborg, J.; Falk, P.; Hernandez, D.; Levine, S.; Chen, C.; Yu, F.; Sheaffer, A. K.; Zhai, G.; Barry, D.; Knipe, J. O.; Han, Y.-H.; Schartman, R.; Donoso, M.; Mosure, K.; Sinz, M. W.; Zvyaga, T.; Good, A. C.; Rajamani, R.; Kish, K.; Tredup, J.; Klei, H. E.; Gao, Q.; Mueller, L.; Colonno, R. J.; Grasela, D. M.; Adams, S. P.; Loy, J.; Levesque, P. C.; Sun, H.; Shi, H.; Sun, L.; Warner, W.; Li, D.; Zhu, J.; Meanwell, N. A.; McPhee, F. The discovery of asunaprevir (BMS-650032), an orally efficacious NS3 protease inhibitor for the treatment of hepatitis C virus infection. *J. Med. Chem.* **2014,** 57, 1730–1752.
21. Wittekind, M.; Weinheirner, S.; Zhang, Y.; Goldfarb, V. Modified forms of hepatitis C NS3 protease for facilitating inhibitor screening and structural studies of protease-inhibitor complexes. US Patent 6333186, August 8, 2002.
22. Sarkar, G.; Sommer, S. S. The "megaprimer" method of site-directed mutagenesis. *Biotechniques* **1990,** 8, 404–407.
23. Otwinowski, Z.; Minor, W. Processing of X-ray diffraction data collected in oscillation mode. *Methods Enzymol.* **1997,** 276, 307–326.
24. McCoy, A. J.; Grosse-Kunstleve, R. W.; Adams, P. D.; Winn, M. D.; Storoni, L. C.; Read, R. J. Phaser crystallographic software. *J. Appl. Crystallogr.* **2007,** 40, 658–674.
25. Emsley, P.; Cowtan, K. Coot: model-building tools for molecular graphics. *Acta Crystallogr. D Biol. Crystallogr.* **2004,** 60, 2126–2132.
26. Adams, P. D.; Afonine, P. V.; Bunkoczi, G.; Chen, V. B.; Davis, I. W.; Echols, N.; Headd, J. J.; Hung, L.-W.; Kapral, G. J.; Grosse-Kunstleve, R. W.; McCoy, A. J.; Moriarty, N. W.; Oeffner, R.; Read, R. J.; Richardson, D. C.; Richardson, J. S.; Terwilliger, T. C.; Zwart, P. H. PHENIX: a comprehensive Python-based system for macromolecular structure solution. *Acta Crystallogr. D Biol. Crystallogr.* **2010,** 66, 213–221.
27. Davis, I. W.; Leaver-Fay, A.; Chen, V. B.; Block, J. N.; Kapral, G. J.; Wang, X.; Murray, L. W.; Arendall, W. B.; Snoeyink, J.; Richardson, J. S.; Richardson, D. C. MolProbity: all-atom contacts and structure validation for proteins and nucleic acids. *Nucl. Acids Res.* **2007,** 35, W375–W383.
28. Brunger, A. T. Free R value: a novel statistical quantity for assessing the accuracy of crystal structures. *Nature* **1992,** 355, 472–475.
29. *PyMOL: The PyMOL Molecular Graphics System, Version 1.8, Schrödinger, LLC.*

Appendix B

Mavyret: A Pan-Genotypic Combination Therapy for the Treatment of Hepatitis C Infection

Preface

Appendix B is a commentary/viewpoint article that has been previously published.

Reprinted with permission from:

Matthew, A. N.; Kurt Yilmaz, N.; Schiffer, C. A. Mavyret: A Pan-Genotypic Combination Therapy for the Treatment of Hepatitis C Infection. *Biochemistry.* **2017**, A–B.

Contributions from Ashley N. Matthew:

I wrote the commentary and created the figures with input from Celia A. Schiffer and Nese Kurt Yilmaz.

Hepatitis C virus (HCV), a virus that infects more than 180 million people worldwide, is the causative agent of chronic liver disease, which often progresses to fibrosis, liver cirrhosis, and hepatocellular carcinoma (HCC). According to the World Health Organization, almost half a million patients infected with HCV die each year from cirrhosis and HCC alone. In the last several years, treatment of HCV infections has been revolutionized by the development of small molecular inhibitors that target essential proteins encoded by the viral genome. These inhibitors, known as direct-acting antivirals (DAAs), have improved treatment option and outcomes and eliminated the need for interferon injections. However, the emergence of resistance-associated variants (RAVs) and high genetic variation among the six distinct genotypes of the virus have been presenting challenges, even leading to treatment failure.

Newer all-oral DAA combination regimens for HCV infection consist of inhibitors that target the NS3/4A, NS5A, and NS5B viral proteins. Of note, NS3/4A protease inhibitors have become a mainstay of treatment as most new therapies contain an inhibitor from this class. While highly effective against other genotypes, treatment of genotype 3 infections has been the most challenging, especially in patients who failed previous therapy or have cirrhosis. Recently, AbbVie received Food and Drug Administration (FDA) approval for one of the first pan-genotypic combination therapies, Mavyret, consisting of glecaprevir and pibrentasvir, an NS3/4A protease and an NS5A inhibitor, respectively (**Figure B.1**). Given the excellent pan-genotypic response and safety profile in patients,

Mavyret was approved for the treatment of genotypes 1−6 in patients without cirrhosis, or with compensated cirrhosis. In patients with noncirrhotic chronic HCV who were treatment-naiïve or had previously been treated with pegylated interferon or ribavirin, the sustained virological response (SVR) rate was 83−100%across all genotypes.[1] In treatment-naiïve patients with compensated liver disease, 99% of patients achieved SVR with a 12-week course.[2] Mavyret was approved as an 8-week course for treatment-naiïve patients without cirrhosis, shortening the previous standard of care by an additional 4 weeks.

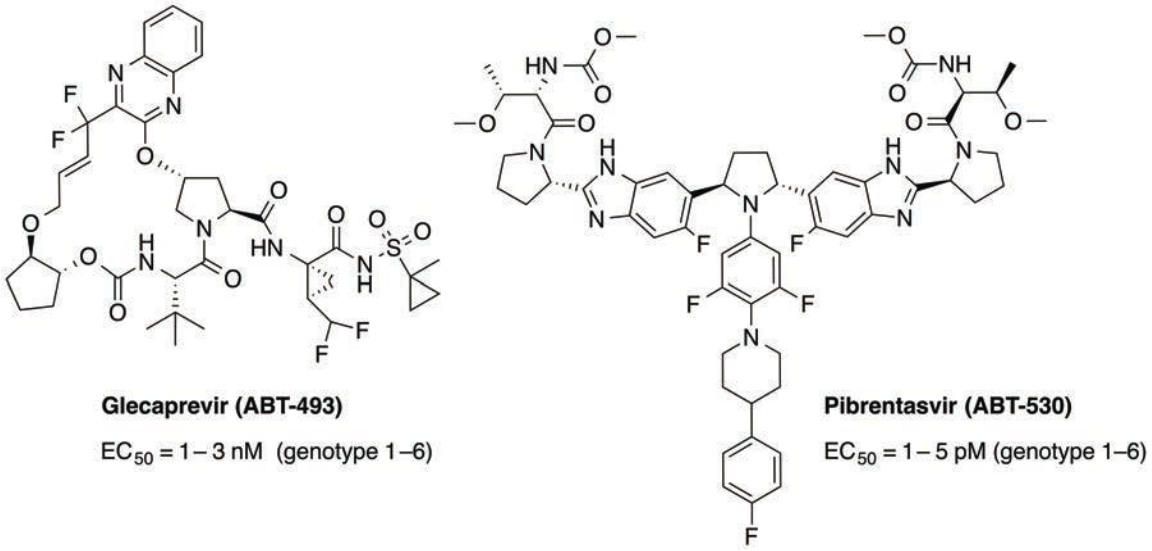

Figure B.1: 2D chemical structure of Mavyret™ combination inhibitors, Glecaprevir (ABT-493) and Pibrentasvir (ABT-530).
Glecaprevir and pibrentasvir are an NS3/4A protease and an NS5A inhibitor, respectively with pan-genotypic activity. This combination therapy has resulted in a sustained virological response of 83%-100% across genotypes and was approved by the FDA as an 8-week course shortening the standard of care by 16 weeks.

One component of the Mavyret combination, pibrentasvir (ABT-530), has excellent potency across all HCV genotypes and retains potency against common RAVs. Pibrentasvir had EC_{50} values across genotypes ranging from 1.4 to 5 pM against the HCV replicon in antiviral assays.[3] Under the selective pressure of inhibitors, RAVs emerge at positions 28, 30, 31, and 93 in the NS5A protein. In fact, all current NS5A inhibitors are susceptible to mutations at Tyr93. In vitro studies indicate pibrentasvir also selects these mutations, including Y93H, that confer resistance to other NS5A inhibitors.[3] However, pibrentasvir maintained good potency against many single-site NS5A mutations, suggesting double or triple mutants need to emerge to confer high levels of resistance against this inhibitor.

The other component of Mavyret, glecaprevir (ABT-493), is a P2−P4 macrocyclic NS3/4A protease inhibitor with subnanomolar to low nanomolar activity against all genotypes, including genotype 3.[4] NS3/4A protease inhibitors are often susceptible to single-site mutations at residues Arg155, Ala156, and Asp168. Most if not all protease inhibitors are susceptible to mutations at Asp168, which are often present in patients who fail therapy with a protease inhibitor. Notably, this active site residue is not conserved in genotype 3 and is Gln168 instead, contributing to the natural resistance of genotype 3 to most treatments. While potent against 168 variations, including genotype 3, glecaprevir is highly susceptible to A156T and A156V mutations. We have shown

that inhibitors containing P2−P4 macrocycles, as in glecaprevir, are susceptible to changes at Ala156, as substitutions with a larger side chain result in steric clash with the inhibitor's macrocycle.[5] Luckily, mutations at Ala156 do not occur alone because of reduced replicative capacity; however, additional mutations could restore the enzymatic fitness, which can lead to clinically viable multi-mutant resistant variants.

Thus, both components of Mavyret have good resistance profiles against wild type genotypes and single-mutant variants of HCV. What needs to be considered is the emergence of double, triple, or other multi-mutant variants that may have high levels of resistance to one or both components of this combination. Such multi-mutant variants potentially pose a threat to the longevity and success of HCV treatment. There are already double- and triple-mutant variants that have been isolated from patients who failed therapy with previously FDA- approved combination therapies. Considering the similarity in the inhibitor scaffolds and modes of action, there is a danger that these variants may be cross-drug resistant and not respond to any current treatment option, including Mavyret. As new drugs and combinations are developed, it will be important to understand the mechanisms of resistance for these multi- mutant variants and incorporate those insights into drug design. Rather than concentrating all effort into inhibitors from the same class with highly similar scaffolds, diversifying the arsenal of DAAs and considering triple-combination therapy may be required to avoid cases of incurable HCV infection.

The approval of Mavyret dual-combination therapy marks another milestone in the treatment of HCV infections. There had been a major effort to develop an all-oral combination therapy with activity against all genotypes. With the approval of Mavyret, this goal has been met. The newer-generation inhibitors and various combinations provide treatment options for patients and improve SVR rates across all genotypes. For many cases, Mavyret has decreased the standard of care from 24 to 8 weeks. More importantly, treatment options for patients with compensated liver disease are now available. One major remaining concern is the possible emergence of drug resistance. The newer inhibitors have better activity against single-site RAVs, but highly resistant multi-mutant strains may become clinically relevant. Preventing the emergence and spread of cross-resistant variants and developing inhibitors with improved potency against such variants may be the next challenge.

Funding

Our work is supported by a grant from the National Institutes of Health (R01-AI085051) and F31 GM119345.

Acknowledgement

We thank Dr. Akbar Ali for informative discussions.

Appendix B – References

1. Kwo, P. Y.; Poordad, F.; Asatryan, A.; Wang, S.; Wyles, D. L.; Hassanein, T.; Felizarta, F.; Sulkowski, M. S.; Gane, E.; Maliakkal, B.; Overcash, J. S.; Gordon, S. C.; Muir, A. J.; Aguilar, H.; Agarwal, K.; Dore, G. J.; Lin, C. W.; Liu, R.; Lovell, S. S.; Ng, T. I.; Kort, J.; Mensa, F. J. Glecaprevir and pibrentasvir yield high response rates in patients with HCV genotype 1-6 without cirrhosis. *J. Hepatol.* **2017,** 67, 263–271.

2. Forns, X.; Lee, S. S.; Valdes, J.; Lens, S.; Ghalib, R.; Aguilar, H.; Felizarta, F.; Hassanein, T.; Hinrichsen, H.; Rincon, D.; Morillas, R.; Zeuzem, S.; Horsmans, Y.; Nelson, D. R.; Yu, Y.; Krishnan, P.; Lin, C. W.; Kort, J. J.; Mensa, F. J. Glecaprevir plus pibrentasvir for chronic hepatitis C virus genotype 1, 2, 4, 5, or 6 infection in adults with compensated cirrhosis (EXPEDITION-1): a single-arm, open-label, multicentre phase 3 trial. *Lancet Infect Dis* **2017,** 17, 1062-1068.

3. Ng, T. I.; Krishnan, P.; Pilot-Matias, T.; Kati, W.; Schnell, G.; Beyer, J.; Reisch, T.; Lu, L.; Dekhtyar, T.; Irvin, M. In vitro antiviral activity and resistance profile of the next-generation hepatitis C virus NS5A inhibitor pibrentasvir. *Antimicrob. Agents Chemother.* **2017,** 61, e02558-16.

4. Ng, T. I.; Tripathi, R.; Reisch, T.; Lu, L.; Middleton, T.; Hopkins, T. A.; Pithawalla, R.; Irvin, M.; Dekhtyar, T.; Krishnan, P.; Schnell, G.; Beyer, J.; McDaniel, K. F.; Ma, J.; Wang, G.; Jiang, L. J.; Or, Y. S.; Kempf, D.; Pilot-Matias, T.; Collins, C. In vitro antiviral activity and resistance profile of the next-generation hepatitis c virus NS3/4A protease inhibitor glecaprevir. *Antimicrob. Agents Chemother.* **2017**.

5. Soumana, D. I.; Kurt Yilmaz, N.; Prachanronarong, K. L.; Aydin, C.; Ali, A.; Schiffer, C. A. Structural and thermodynamic effects of macrocyclization in HCV NS3/4A inhibitor MK-5172. *ACS Chem. Biol.* **2016,** 11, 900–909.

Appendix C
Synthesis of macrocyclic and linear final compounds and intermediates

Preface

The following appendix contains additional information on the synthesis of macrocyclic and linear final compounds as well as intermediates from **Chapter III** and **Appendix A**.

Synthesis of Intermediates and Macrocyclic Final Compounds

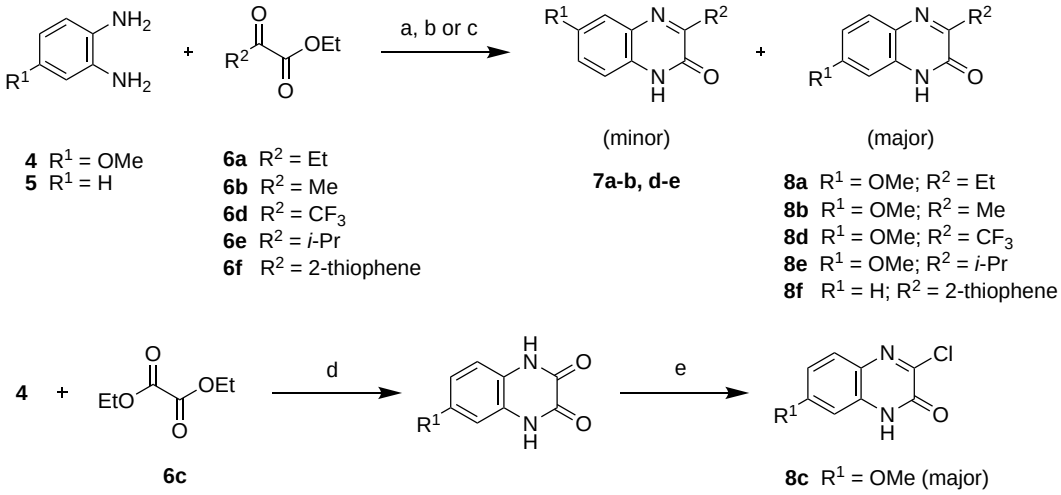

4 R^1 = OMe
5 R^1 = H

6a R^2 = Et
6b R^2 = Me
6d R^2 = CF_3
6e R^2 = *i*-Pr
6f R^2 = 2-thiophene

7a-b, d-e

8a R^1 = OMe; R^2 = Et
8b R^1 = OMe; R^2 = Me
8d R^1 = OMe; R^2 = CF_3
8e R^1 = OMe; R^2 = *i*-Pr
8f R^1 = H; R^2 = 2-thiophene

6c

8c R^1 = OMe (major)

Scheme C.1: Synthesis of quinoxalines.
Reagents and conditions: (a) AcOH, rt, overnight, 50 °C, 2 h; (b) aq. H_2SO_4 (1.8 M), rt, 24 h; (c) MeOH, rt, 24 h; (d) Et_3N, 150 °C, 2 h; (e) $SOCl_2$, DMF, 110 °C, 1.5 h.

3-Ethyl-7-methoxyquinoxalin-2(1*H*)-one (8a).

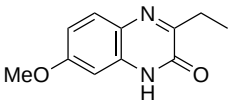

A mixture of 4-methoxy-1,2-diaminobenzene **4** (5.0 g, 36.2 mmol) and ethyl 2-oxobutanoate **6a** (5.70 g, 43.8 mmol) in AcOH (25 mL) was stirred at room temperature overnight and then heated at 50 °C for 2 h. AcOH was removed under reduced pressure, and the reside was extracted with CH_2Cl_2 (2 × 150 mL). The combined organic portions were washed with H_2O and 10% aqueous Na_2CO_3 solution, dried (Na_2SO_4), and evaporated under reduced pressure. The residue was triturated with hexanes and filtered. The solid was mixed with EtOAc (25 mL), stirred at room temperature for 30 min, filtered, and dried under high vacuum to provide the 3-ethyl-7-methoxyquinoxaline **8a** (6.0 g, 81%) as a light purple solid. ^{1}H NMR (500 MHz, DMSO-d_6) δ 12.17 (s, 1 H), 7.61 (d, J = 8.5 Hz, 1 H), 6.85 (dd, J = 9.0, 2.5 Hz, 1 H), 6.73 (d, J = 2.5 Hz, 1 H), 3.80 (s, 3 H), 2.74 (q, J = 7.5 Hz, 3 H), 1.19 (t, J = 7.5 Hz, 3 H) ppm; ^{13}C NMR (125 MHz, DMSO-d_6) δ 160.30, 159.35, 155.26, 133.63, 129.78, 127.01, 111.78, 98.26, 55.97, 26.17, 10.08 ppm; MS (ESI) *m/z*: $[M + H]^+$ calcd for $C_{11}H_{13}N_2O_2$, 205.24; found 205.90.

7-Methoxy-3-methylquinoxalin-2(1*H*)-one (8b).

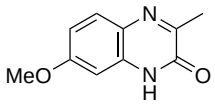

4-Methoxy-1,2-diaminobenzene **4** (130 g, 0.94 mol) was added to an aqueous solution of sulfuric acid (1.8 M, 1300 mL) and the mixture was treated with ethyl pyruvate **6b** (132 g, 1.14 mol). The resulting reaction mixture was stirred at room temperature for 24 h, then treated with an aqueous solution of 3 N NaOH till pH 7. After stirring the mixture for 30 min, the solid precipitate was filtered, washed with water and dried. The solid product was mixed with EtOAc (1000 mL), heated to 60 °C, and vigorously stirred for 1 h. The solid was filtered, washed with EtOAc and dried under high vacuum to provide the 3-methyl-7-methoxyquinoxaline **8b** (135 g, 75%) as a light purple solid.[1]H NMR (500 MHz, DMSO-d_6) δ 12.18 (s, 1 H), 7.59 (d, J = 9.0 Hz, 1 H), 6.86 (dd, J = 9.0, 3.0 Hz, 1 H), 6.73 (d, J = 2.5 Hz, 1 H), 3.81 (s, 3H), 2.34 (s, 3H) ppm; ^{13}C NMR (125 MHz, DMSO-d_6) δ 160.30, 155.85, 155.62, 133.82, 129.58, 127.02, 111.82, 98.29, 55.97, 20.63 ppm; MS (ESI) *m/z*: $[M + H]^+$ calcd for $C_{10}H_{11}N_2O_2$, 191.21; found 191.30.

3-Chloro-7-methoxyquinoxalin-2(1*H*)-one (8c)

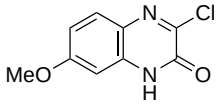

The title compound was prepared according to the method described by Harper *et al*.[1] [1]H NMR (500 MHz, DMSO-d_6) δ 7.35 (d, J = 8.5 Hz, 1 H), 6.65 (d, J = 2.5 Hz, 1 H), 6.62 (dd, J = 8.5, 2.5 Hz, 1 H), 3.77 (s, 3 H), 3.71 (br s, 1 H) ppm; ^{13}C NMR (125 MHz, DMSO-d_6) δ 159.79, 159.30, 145.76, 145.62, 128.88, 128.02, 110.57, 103.48, 55.56 ppm; MS (ESI) *m/z*: $[M + H]^+$ calcd for $C_9H_8ClN_2O_2$, 211.62; found 211.60.

7-Methoxy-3-(trifluoromethyl)quinoxalin-2(1*H*)-one (8d).

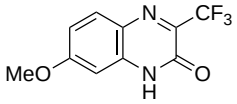

A solution of ethyl trifluoropyruvate **6d** (20.4 g, 120 mmol) in MeOH (50 mL) was slowly added to 4-methoxy-1,2-diaminobenzene **4** (15.0 g, 108 mmol). The resulting reaction mixture was stirred at room temperature for 24 h. The solid precipitate was filtered, washed with cold MeOH and dried. The solid residue was mixed with MeOH (60 mL), stirred at 50 °C for 30 min, cooled to 5 °C, filtered, and dried under high vacuum to provide the 7-methoxy-3-(trifluoromethyl)quinoxalin-2(1*H*)-one **8d** (12 g, 47%) as a mustard solid.[1]H NMR (500 MHz, DMSO-d_6) δ 13.01 (s, 1 H), 7.41 (d, J = 2.5 Hz, 1 H), 7.37 (dd, J = 9.0, 2.5 Hz, 1 H), 7.32 (d, J = 9.0 Hz, 1 H), 3.84 (s, 3H) ppm; ^{13}C NMR (125 MHz, DMSO-d_6) δ 156.33, 151.77, 144.50 (q, J = 36.4 Hz), 131.04, 128.59, 124.08, 120.66 (d, J = 274.4 Hz), 117.23, 110.88, 56.26 ppm;[19]F NMR (470 MHz, DMSO-

d_6); −68.45 ppm; MS (ESI) *m/z*: $[M + Na]^+$ calcd for $C_{10}H_7F_3N_2O_2Na$, 267.16; found 267.40.

3-Isopropyl-7-methoxyquinoxalin-2(1*H*)-one (8e).

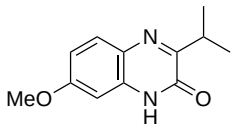

A mixture of 4-methoxy-1,2-diaminobenzene **4** (130 g, 0.94 mol) and ethyl 3-methyl-2-oxobutanoate **6e** (162 g, 1.12 mol) in AcOH (650 mL) was stirred at room temperature overnight, and then heated at 50 °C for 2 h. AcOH was removed under reduced pressure. The residue was diluted with H_2O (650 mL) and CH_2Cl_2 (800 mL) and the pH of the mixture was adjusted to pH ~ 10 by slow addition of 10% aqueous NaOH solution. The resulting precipitate was filtered, washed with CH_2Cl_2 (100 mL) and dried under vacuum to provide the 3-isopropyl-7-methoxyquinoxaline **8e** (91 g, 45%) as a light brown solid. ^{1}H NMR (500 MHz, DMSO-d_6) δ 12.22 (s, 1 H), 7.62 (d, J = 9.0 Hz, 1 H), 6.86 (dd, J = 9.0, 3.0 Hz, 1 H), 6.75 (d, J = 2.5 Hz, 1 H), 3.81 (s, 3H), 3.43–3.37 (m, 1H), 1.19 (d, J = 7.0 Hz, 6 H) ppm; ^{13}C NMR (125 MHz, DMSO-d_6) δ 162.35, 160.36, 154.91, 133.64, 129.90, 126.91, 111.80, 98.24, 55.97, 30.08, 20.57 ppm; MS (ESI) *m/z*: $[M + H]^+$ calcd for $C_{12}H_{15}N_2O_2$, 219.26; found 219.50.

3-(Thiophen-2-yl)quinoxalin-2(1*H*)-one (8f).

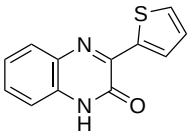

A mixture of 1,2-diaminobenzene **5** (5.41 g, 50 mmol) and ethyl 2-oxo-2-(thiophen-2-yl)acetate **6f** (9.2 g, 50 mmol) was stirred in ethanol (100 ml) at reflux for 18 h. The reaction mixture was cooled to 10 °C and stirred for 1 h. The solid precipitate was filtered, washed with ethanol (20 mL) and dried under high vacuum to give the title compound **8f** (6.0 g, 53%) as a yellow solid. ^{1}H NMR (500 MHz, DMSO-d_6) δ 12.69 (s, 1 H), 8.41 (dd, J = 4.0, 1.5 Hz, 1 H), 7.83 (dd, J = 5.0, 1.0 Hz, 1 H), 7.77 (d, J = 8.0 Hz, 1 H), 7.51 (dt, J = 8.0, 1.5 Hz, 1 H), 7.35–7.30 (m, 2 H), 7.23 (dd, J = 5.0, 3.5 Hz, 1 H) ppm; ^{13}C NMR (125 MHz, DMSO-d_6) δ 153.42, 148.88, 138.92, 132.07, 131.89, 131.41, 131.36, 129.78, 128.11, 128.0, 123.65, 115.28 ppm; MS (ESI) *m/z*: $[M + H]^+$ calcd for $C_{12}H_9N_2OS$, 229.28; found 229.50.

1-(*tert*-Butyl) 2-methyl (2*S*,4*R*)-4-((7-methoxy-3-methylquinoxalin-2-yl)oxy)pyrrolidine-1,2-dicarboxylate (9b).

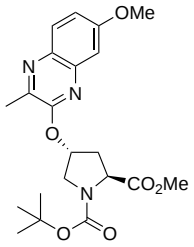

A solution of 3-ethyl-7-methoxyquinoxalin-2-one **8b** (4.0 g, 21 mmol) in anhydrous NMP (65 mL) was treated with Cs_2CO_3 (10.30 g, 31.6 mmol). After stirring the reaction mixture at room temperature for 15 min, proline derivative **3** (8.82 g, 19.0 mmol) was added in one portion. The reaction mixture was heated to 55 °C, stirred for 4 h, and then another portion of proline derivative **3** (0.68 g, 1.5 mmol) was added. The resulting reaction mixture was stirred at 55 °C for additional 2 h, cooled to room temperature, quenched with aqueous 1 N HCl solution (250 mL), and extracted with EtOAc (400 mL). The organic fraction was washed successively with saturated aqueous $NaHCO_3$ and NaCl (250 mL each), dried (Na_2SO_4), filtered, and evaporated under reduced pressure. The residue was purified by flash column chromatography using 15–30% EtOAc/hexanes as the eluent to provide **9b** (6.60 g, 75%) as a colorless gummy solid. ^{1}H NMR (500 MHz, $CDCl_3$) (mixture of rotamers, major rotamer) δ 7.80 (d, J = 9.0 Hz, 1 H), 7.17 (dd, J = 9.0, 3.0 Hz, 1 H), 7.11 (d, J = 2.5 Hz, 1 H), 5.71 (br s, 1 H), 4.48 (t, J = 8.0 Hz, 1 H), 3.99–3.91 (m, 4 H), 3.87 (d, J = 12.5 Hz, 1H), 3.78 (s, 3 H), 2.67–2.58 (m, 1 H), 2.56 (s, 3 H), 2.43–2.37 (m, 1 H), 1.43 (s, 9 H) ppm; ^{13}C NMR (125 MHz, $CDCl_3$) δ 173.36, 160.24, 155.51, 153.81, 144.60, 141.04, 134.22, 128.95, 118.63, 105.95, 80.54, 73.59, 58.20, 55.68, 52.48, 52.20, 36.70, 28.26, 19.93 ppm; HRMS (ESI) *m/z*: $[M + H]^+$ calcd for $C_{21}H_{28}N_3O_6$, 418.1973; found 418.1976.

1-(*tert*-butyl) 2-methyl (2*S*,4*R*)-4-((3-chloro-7-methoxyquinoxalin-2-yl)oxy)pyrrolidine-1,2-dicarboxylate (9c).

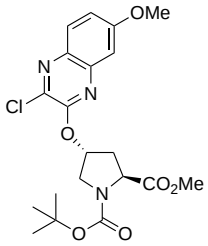

The same procedure was used as described above for compound **9b**. 3-Chloro-7-methoxyquinoxalin-2(1*H*)-one **8c** (4.0 g, 19.0 mmol) in NMP (60 mL) was treated with Cs_2CO_3 (9.30 g, 28.6 mmol) and proline derivative **3** (8.40 g, 18.1

mmol) to provide **9c** (6.30 g, 76%) as an off-white foamy solid. ^{1}H NMR (400 MHz, $CDCl_3$) (mixture of rotamers, major rotamer) *δ* 7.80 (d, *J* = 8.8 Hz, 1 H), 7.21 (dd, *J* = 8.8, 2.8 Hz, 1 H), 7.12 (d, *J* = 2.8 Hz, 1 H), 5.69 (br s, 1 H), 4.52 (t, *J* = 7.6 Hz, 1 H), 4.0–3.94 (s, 4 H), 3.88 (d, *J* = 12.8 Hz, 1 H), 3.78 (s, 3 H), 2.72–2.62 (m, 1 H), 2.45–2.37 (m, 1 H), 1.43 (s, 9 H) ppm; ^{13}C NMR (400 MHz, $CDCl_3$) *δ* 173.32, 162.35, 153.84, 152.48, 141.03, 136.11, 134.06, 129.97, 119.95, 105.83, 80.60, 75.02, 58.10, 55.81, 52.36 , 52.10, 36.64, 28.27 ppm; HRMS (ESI) *m/z*: $[M + H]^+$ calcd for $C_{20}H_{25}ClN_3O_6$, 438.1426; found 438.1438.

1-(*tert*-Butyl) 2-methyl (2*S*,4*R*)-4-((3-isopropyl-7-methoxyquinoxalin-2-yl)oxy)pyrrolidine-1,2-dicarboxylate (9e).

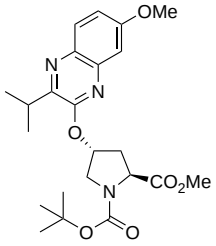

The same procedure was used as described above for compound **9b**. 3-Isopropyl-7-methoxyquinoxalin-2(1*H*)-one **8e** (4.0 g, 18.3 mmol) in NMP (65 mL) was treated with Cs_2CO_3 (9.0 g, 27.6 mmol) and proline derivative **3** (8.30 g, 17.9 mmol) to provide **9e** (7.30 g, 90%) as a colorless gummy solid. ^{1}H NMR (500 MHz, $CDCl_3$) (mixture of rotamers, major rotamer) *δ* 7.83 (d, *J* = 8.0 Hz, 1 H), 7.16 (d, *J* = 8.4 Hz, 1 H), 7.10 (s, 1 H) 5.74 (br s, 1 H), 4.48 (t, *J* = 7.5 Hz, 1 H), 3.92–3.87 (m, 5 H), 3.78 (s, 3 H), 3.41–3.36 (m, 1 H), 2.68–2.59 (m, 1 H), 2.42–2.35 (m, 1 H), 1.43 (s, 9 H), 1.31 (t, *J* = 7.0 Hz, 6 H) ppm; ^{13}C NMR (125 MHz, $CDCl_3$) *δ* 173.37, 160.19, 154.62, 153.82, 152.00, 140.68, 134.31, 129.39, 118.41, 105.80, 80.49, 73.36, 58.28, 55.67, 52.58, 52.19, 36.68, 30.81, 28.25, 20.43, 20.38 ppm; HRMS (ESI) *m/z*: $[M + H]^+$ calcd for $C_{23}H_{32}N_3O_6$, 446.2286; found 446.2287.

1-(*tert*-Butyl) 2-methyl (2*S*,4*R*)-4-((3-(thiophen-2-yl)quinoxalin-2-yl)oxy)pyrrolidine-1,2-dicarboxylate (9f).

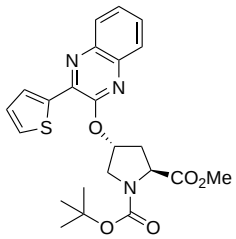

The same procedure was used as described above for compound **9b**. 3-(Thiophen-2-yl)quinoxalin-2(1*H*)-one **8f** (3.0 g, 13.1 mmol) in NMP (40 mL) was treated with Cs_2CO_3 (6.62 g, 20.3 mmol) and proline derivative **3** (6.0 g, 12.9 mmol) to provide **9f** (4.90 g, 82%) as an off-white foamy solid. ^{1}H NMR (400

MHz, $CDCl_3$) (mixture of rotamers, major rotamer) δ 8.13 (t, J = 4.0 Hz, 1 H), 8.01 (d, J = 7.6 Hz, 1H), 7.79 (t, J = 8.0 Hz, 1 H), 7.66–7.55 (m, 2 H), 7.53 (dd, J = 5.2, 1.2 Hz, 1 H), 7.20–7.14 (m, 1 H), 5.91 (br s, 1 H), 4.56 (t, J = 8.0 Hz, 1 H), 4.08 (d, J = 12.8 Hz, 1 H), 4.0–3.95 (m, 1 H), 3.79 (s, 3 H), 2.81–2.72 (m, 1 H), 2.49–2.41 (m, 1 H), 1.44 (s, 9 H) ppm; ^{13}C NMR (100 MHz, $CDCl_3$) δ 173.30, 153.80, 152.45, 140.48, 139.83, 138.93, 138.81, 130.35, 130.20, 129.45, 128.56, 128.09, 127.33, 126.72, 80.56, 74.51, 58.27, 52.66, 52.26, 36.69, 28.27 ppm; HRMS (ESI) *m/z*: $[M + H]^+$ calcd for $C_{23}H_{26}N_3O_5S$, 456.1588; found 456.1589.

1-(*tert*-Butyl) 2-methyl (2*S*,4*R*)-4-((3-ethylquinoxalin-2-yl)oxy)pyrrolidine-1,2-dicarboxylate (9g).

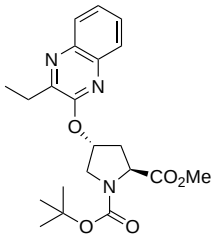

The same procedure was used as described above for compound **9b**. Commercially available 3-ethyl-quinoxalin-2(1*H*)-one **8g** (3.0 g, 17.2 mmol) in NMP (40 mL) was treated with Cs_2CO_3 (8.42 g, 25.8 mmol) and proline derivative **3** (7.80 g, 16.8 mmol) to provide **9g** (4.50 g, 65%) as a colorless gummy solid. ^{1}H NMR (400 MHz, $CDCl_3$) (mixture of rotamers, major rotamer) δ 7.95 (d, J = 7.5 Hz, 1 H), 7.76 (d, J = 8.0 Hz, 1 H), 7.62–7.52 (m, 2 H), 5.76 (br s, 1 H), 4.47 (t, J = 8.0 Hz, 1 H), 3.95–3.88 (m, 2 H), 3.78 (s, 3 H), 2.95 (q, J = 7.6 Hz, 2 H), 2.67–2.60 (m, 1 H), 2.42–2.37 (m, 1 H), 1.43 (m, 9 H), 1.33 (t, J = 7.6 Hz, 3 H) ppm; ^{13}C NMR (100 MHz, $CDCl_3$) δ 173.31, 154.69, 153.80, 152.08, 139.40, 138.79, 128.97, 128.28, 126.87, 126.69, 80.51, 73.63, 58.25, 52.52, 52.19, 36.69, 28.25, 26.91, 11.50 ppm; HRMS (ESI) *m/z*: $[M + H]^+$ calcd for $C_{21}H_{28}N_3O_5$, 402.2023; found 402.2026.

Methyl (2*S*,4*R*)-1-((*S*)-2-((*tert*-butoxycarbonyl)amino)non-8-enoyl)-4-((7-methoxy-3-methylquinoxalin-2-yl)oxy)pyrrolidine-2-carboxylate (12b).

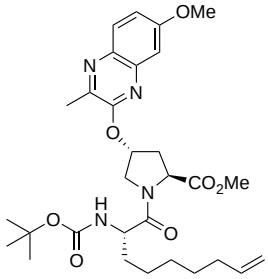

A solution of ester **9b** (3.50 g, 8.4 mmol) in anhydrous CH_2Cl_2 (25 mL) was treated with a solution of 4 N HCl in 1,4-dioxane (25 mL). After stirring the reaction mixture at room temperature for 3 h, solvents were evaporated under

reduced pressure, and the residue was dried under high vacuum. The pale yellow solid was triturated with diethyl ether (3 × 25 mL) and dried under high vacuum to yield the amine salt **10b** (3.0 g, 100%) as an off-white powder.

A mixture of amine salt **10b** (3.0 g, 8.4 mmol) and (*S*)-2-((*tert*-butoxycarbonyl)amino)non-8-enoic acid **11** (2.50 g, 9.2 mmol) in anhydrous DMF (45 mL) was treated with DIEA (6.10 mL, 36.8 mmol) and HATU (5.25 g, 13.8 mmol). The resulting reaction mixture was stirred at room temperature for 4 h, then diluted with EtOAc (400 mL), and washed successively with aqueous 0.5 N HCl, saturated aqueous $NaHCO_3$, and saturated aqueous NaCl (250 mL each). The organic portion was dried (Na_2SO_4), filtered, and evaporated under reduced pressure. The residue was purified by flash chromatography using 20–30% EtOAc/hexanes as the eluent to provide **12b** (4.0 g, 83%) as a white foamy solid. ^{1}H NMR (500 MHz, $CDCl_3$) (mixture of rotamers, major rotamer) δ 7.81 (d, J = 9.0 Hz, 1 H), 7.18 (dd, J = 9.0, 2.5 Hz, 1 H), 7.12 (d, J = 2.5 Hz, 1 H), 5.84–5.75 (m, 2 H), 5.21 (d, J = 8.5 Hz, 1 H), 5.01–4.92 (m, 2 H), 4.75 (t, J = 8.0 Hz, 1 H), 4.38 (q, J = 7.5 Hz, 1 H), 4.18 (d, J = 11.5 Hz, 1 H), 4.06 (dd, J = 12.0, 4.5 Hz, 1 H), 3.94 (s, 3 H), 3.77 (s, 3 H), 2.69–2.64 (m, 1 H), 2.54 (s, 3 H), 2.41–2.35 (m, 1 H), 2.04 (app q, J = 7.0 Hz, 2 H), 1.80–1.75 (m, 1 H), 1.63–1.55 (m, 1 H), 1.46–1.24 (m, 15 H) ppm; ^{13}C NMR (125 MHz, $CDCl_3$) δ 172.13, 171.78, 160.27, 155.40, 155.27, 144.62, 140.89, 138.96, 134.39, 129.03, 118.73, 114.35, 105.99, 79.61, 74.30, 57.97, 55.66, 52.67, 52.43, 51.83, 34.94, 33.65, 32.66, 28.91, 28.74, 28.25, 24.68, 19.87 ppm; HRMS (ESI) *m/z*: $[M + H]^+$ calcd for $C_{30}H_{43}N_4O_7$, 571.3126; found 571.3128.

Methyl (2*S*,4*R*)-1-((*S*)-2-((*tert*-butoxycarbonyl)amino)non-8-enoyl)-4-((3-chloro-7-methoxyquinoxalin-2-yl)oxy)pyrrolidine-2-carboxylate (12c).

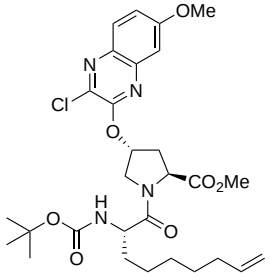

The same procedure was used as described above for compound **12b**. Compound **9c** (3.25 g, 7.4 mmol) was treated with 4 N HCl (20 mL) to afford amine salt **10c** (2.77 g, 7.4 mmol), which was coupled with acid **11** (2.0 g, 7.4 mmol) using DIEA (4.90 mL, 29.6 mmol) and HATU (4.20 g, 11.0 mmol) to provide **12c** (3.30 g, 75%) as a white foamy solid. ^{1}H NMR (400 MHz, $CDCl_3$) (mixture of rotamers, major rotamer) δ 7.82 (d, J = 9.2 Hz, 1 H), 7.23 (dd, J = 9.2, 2.8 Hz, 1 H), 7.15 (d, J = 2.8 Hz, 1 H), 5.85–5.75 (m, 2 H), 5.21 (d, J = 8.4 Hz, 1 H), 5.02–4.91 (m, 2 H), 4.79 (t, J = 8.4 Hz, 1 H), 4.37 (q, J = 8.0 Hz, 1 H), 4.24 (d, J = 11.6 Hz, 1 H), 4.07 (dd, J = 11.6, 4.4 Hz, 1 H), 3.95 (s, 3 H), 3.78 (s, 3 H),

2.74–2.68 (m, 1 H), 2.42–2.36 (m, 1 H), 2.04 (app q, *J* = 6.8 Hz, 2 H), 1.82–1.76 (m, 1 H), 1.63–1.55 (m, 1 H), 1.43–1.27 (m, 15 H) ppm; ^{13}C NMR (400 MHz, $CDCl_3$) *δ* 172.33, 171.87, 161.52, 155.59, 152.46, 141.06, 139.19, 136.28, 134.36, 129.17, 120.25, 114.58, 106.03, 79.88, 75.92, 58.16, 56.02, 52.70, 52.58, 52.00, 34.99, 33.88, 32.90, 29.14, 28.96, 28.46, 24.89 ppm; HRMS (ESI) *m/z*: $[M + H]^+$ calcd for $C_{29}H_{40}ClN_4O_7$, 591.2580; found 591.2582.

Methyl (2*S*,4*R*)-1-((*S*)-2-((*tert*-butoxycarbonyl)amino)non-8-enoyl)-4-((3-isopropyl-7-methoxyquinoxalin-2-yl)oxy)pyrrolidine-2-carboxylate (12e).

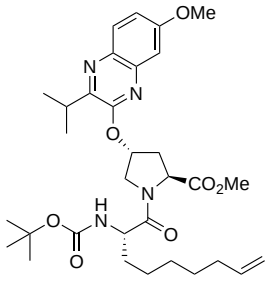

The same procedure was used as described above for compound **12b**. Compound **9e** (3.25 g, 7.3 mmol) was treated with 4 N HCl (25 mL) to afford amine salt **10e** (2.80 g, 7.3 mmol), which was coupled with acid **11** (2.20 g, 8.1 mmol) using DIEA (5.36 mL, 32.4 mmol) and HATU (4.64 g, 12.2 mmol) to provide **12e** (4.10 g, 93%) as a white foamy solid. ^{1}H NMR (500 MHz, $CDCl_3$) (mixture of rotamers, major rotamer) *δ* 7.84 (d, *J* = 8.5 Hz, 1 H), 7.18 (d, *J* = 9.0 Hz, 1 H), 7.11 (s, 1 H), 5.87 (br s, 1 H), 5.84–5.76 (m, 1 H), 5.20 (d, *J* = 8.5 Hz, 1 H), 4.99 (d, *J* = 17.5 Hz, 1 H), 4.93 (d, *J* = 10.0 Hz, 1 H), 4.72 (t, *J* = 8.0 Hz, 1 H), 4.39 (q, *J* = 7.0 Hz, 1 H), 4.15 (d, *J* = 12.0 Hz, 1 H), 4.06 (dd, *J* = 12.0, 4.0 Hz, 1 H) 3.94 (s, 3 H), 3.78 (s, 3 H), 3.40–3.34 (m, 1 H), 2.69–2.64 (m, 1 H), 2.40–2.34 (m, 1 H), 2.04 (app q, *J* = 6.5 Hz, 2 H), 1.82–1.75 (m, 1 H), 1.63–1.56 (m, 1 H), 1.45–1.20 (m, 21 H) ppm; ^{13}C NMR (125 MHz, $CDCl_3$) *δ* 172.13, 171.69, 160.24, 155.38, 154.36, 152.00, 140.52, 138.96, 134.50, 129.46, 118.53, 114.35, 105.82, 79.59, 74.03, 58.01, 55.66, 52.71, 52.43, 51.85, 34.95, 33.66, 32.68, 30.59, 28.92, 28.75, 28.23, 24.69, 20.55, 20.43 ppm; HRMS (ESI) *m/z*: $[M + H]^+$ calcd for $C_{32}H_{47}N_4O_7$, 599.3439; found 599.3440.

Methyl (2*S*,4*R*)-1-((*S*)-2-((*tert*-butoxycarbonyl)amino)non-8-enoyl)-4-((3-(thiophen-2-yl)quinoxalin-2-yl)oxy)pyrrolidine-2-carboxylate (12f).

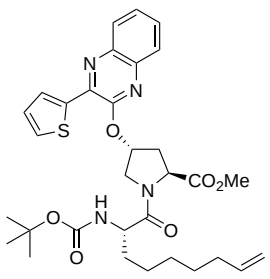

The same procedure was used as described above for compound **12b**. Compound **9f** (3.0 g, 6.6 mmol) was treated with 4 N HCl (20 mL) to afford amine salt **10f** (2.60 g, 6.6 mmol), which was coupled with acid **11** (1.80 g, 6.6 mmol) using DIEA (4.35 mL, 26.3 mmol) and HATU (3.75 g, 9.9 mmol) to provide **12f** (3.0 g, 75%) as an off-white foamy solid. ^{1}H NMR (500 MHz, $CDCl_3$) (mixture of rotamers, major rotamer) δ 8.09 (dd, J = 4.0, 1.2 Hz, 1 H), 8.02 (dd, J = 8.0, 1.6 Hz, 1 H), 7.79 (dd, J = 8.8, 1.6 Hz, 1 H), 7.65–7.56 (m, 2 H), 7.53 (dd, J = 4.8, 0.8 Hz, 1 H), 7.17 (dd, J = 5.2, 4.0 Hz, 1 H), 6.03 (br s, 1 H), 5.85–5.77 (m, 1 H), 5.19 (d, J = 8.4 Hz, 1 H), 5.03–4.92 (m, 2 H), 4.83 (t, J = 8.0 Hz, 1 H), 4.43 (q, J = 7.2 Hz, 1 H), 4.32 (d, J = 12.0 Hz, 1 H), 4.12 (dd, J = 12.0, 4.4 Hz, 1 H), 3.79 (s, 3 H), 2.83–2.77 (m, 1 H), 2.48–2.41 (m, 1 H), 2.05 (app q, J = 6.8, 2 H), 1.83–1.77 (m, 1 H), 1.65–1.57 (m, 1 H), 1.46–1.20 (m, 15 H) ppm; ^{13}C NMR (125 MHz, $CDCl_3$) δ 172.11, 171.64, 155.38, 152.25, 140.51, 139.45, 138.97, 138.76, 130.46, 130.34, 129.46, 128.60, 128.19, 127.45, 126.71, 114.36, 79.59, 75.08, 58.01, 52.72, 52.46, 51.92, 34.91, 33.66, 32.62, 28.92, 28.75, 28.22, 24.76 ppm; HRMS (ESI) *m/z*: $[M + H]^+$ calcd for $C_{32}H_{41}N_4O_6S$, 609.2741; found 609.2739.

Methyl (2*S*,4*R*)-1-((*S*)-2-((*tert*-butoxycarbonyl)amino)non-8-enoyl)-4-((3-ethylquinoxalin-2-yl)oxy)pyrrolidine-2-carboxylate (12g).

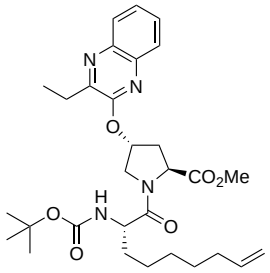

The same procedure was used as described above for compound **12b**. Compound **9g** (3.50 g, 8.4 mmol) was treated with 4 N HCl (25 mL) to afford amine salt **10g** (3.0 g, 17.2 mmol), which was coupled with acid **11** (2.50 g, 9.2 mmol) using DIEA (6.10 mL, 36.8 mmol) and HATU (5.25 g, 13.8 mmol) to provide **12g** (4.0 g, 83%) as a white foamy solid. ^{1}H NMR (400 MHz, $CDCl_3$) (mixture of rotamers, major rotamer) δ 7.97 (dd, J = 8.0, 1.6 Hz, 1 H), 7.77 (d, J = 8.0, 1.6 Hz, 1 H), 7.63–7.53 (m, 2 H), 5.88 (br s, 1H), 8.84–5.75 (m, 1 H), 5.21 (d, J = 9.2 Hz, 1 H), 5.02–4.91 (m, 2 H), 4.74 (t, J = 8.4 Hz, 1 H), 4.37 (q, J = 8.0 Hz, 1 H), 4.18 (d, J = 11.6 Hz, 1 H), 4.07 (dd, J = 11.6, 4.4 Hz, 1 H), 3.78 (s, 3 H), 2.93 (q, J = 7.6 Hz, 2 H), 2.71–2.63 (m, 1 H), 2.42–2.35 (m, 1 H), 2.05 (app q, J = 6.8 Hz, 2 H), 1.82–1.74 (m, 1 H), 1.62–1.55 (m, 1 H), 1.45–1.29 (m, 18 H) ppm; ^{13}C NMR (100 MHz, $CDCl_3$) δ 172.05, 171.85, 155.39, 154.42, 152.0, 139.20, 138.94, 138.84, 129.02, 128.27, 126.81, 114.34, 79.55, 74.23, 57.93, 52.62, 52.44, 51.81, 34.85, 33.64, 32.57, 28.87, 28.70, 28.20, 26.69, 24.70, 11.40 ppm; HRMS (ESI) *m/z*: $[M + H]^+$ calcd for $C_{30}H_{43}N_4O_6$, 555.3177; found 555.3177.

***tert*-Butyl ((*S*)-1-((2*S*,4*R*)-2-(((1*R*,2*S*)-1-((cyclopropylsulfonyl)carbamoyl)-2-vinylcyclopropyl)carbamoyl)-4-((7-methoxy-3-methylquinoxalin-2-yl)oxy)pyrrolidin-1-yl)-1-oxonon-8-en-2-yl)carbamate (16b).**

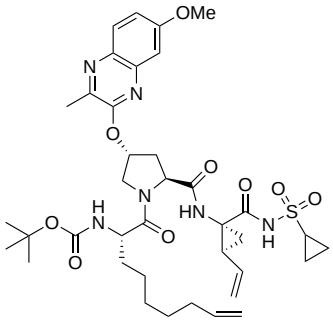

A solution of ester **12b** (3.25 g, 5.7 mmol) in THF-H_2O mixture (1:1, 100 mL) was treated with LiOH.H_2O (0.72 g, 17.2 mmol). The resulting reaction mixture was stirred at room temperature for 24 h. The reaction mixture was cooled to ~5 °C, acidified to a pH of 2.0 by slow addition of aqueous 0.25 N HCl (~ 200 mL), and extracted with EtOAc (2 × 400 mL). The organic portions were washed separately with saturated aqueous NaCl (200 ml), dried (Na_2SO_4), filtered, and evaporated under reduced pressure. The gummy residue was dissolved in $CHCl_3$ (50 mL), concentrated under reduced pressure, and the residue was dried under high vacuum overnight to yield the acid **13b** (3.17 g, 100%) as a white foamy solid.

A mixture of acid **13b** (1.60 g, 2.9 mmol) and amine salt **14** (0.93 g, 3.5 mmol) in anhydrous DMF (35 mL) was treated with DIEA (2.0 mL, 11.5 mmol) and HATU (1.75 g, 4.6 mmol). The resulting reaction mixture was stirred at room temperature for 2.5 h, then diluted with EtOAc (250 mL) and washed successively with aqueous 0.5 N HCl, saturated aqueous $NaHCO_3$, and saturated aqueous NaCl (150 mL each). The organic portion was dried (Na_2SO_4), filtered, and evaporated under reduced pressure. The residue was purified by flash chromatography using 50–70% EtOAc/hexanes as the eluent to provide the bis-olefin compound **16b** (1.57 g, 70%) as a white solid. ^{1}H NMR (400 MHz, $CDCl_3$) δ 10.24 (s, 1 H), 7.81 (d, J = 8.8 Hz, 1 H), 7.20 (dd, J = 8.8, 2.8 Hz, 1 H), 7.13 (d, J = 2.8 Hz, 1 H), 7.07 (s, 1 H), 5.89 (br s, 1 H), 5.85–5.72 (m, 2 H), 5.39 (d, J = 8.4 Hz, 1 H), 5.26 (d, J = 17.2 Hz, 1 H), 5.14 (d, J = 11.6 Hz, 1 H), 5.01–4.90 (m, 2 H), 4.45 (t, J = 8.4 Hz, 1 H), 4.38–4.32 (m, 1 H), 4.21 (d, J = 12.0 Hz, 1 H), 4.02 (dd, J = 11.6, 4.0 Hz, 1 H), 3.93 (s, 3 H), 2.95–2.89 (m, 1 H), 2.56–2.48 (m, 5 H), 2.13 (q, J = 8.4 Hz, 1 H), 2.05–1.99 (m, 3 H), 1.74–1.66 (m, 1 H), 1.62–1.54 (m, 1 H), 1.46–1.22 (m, 18 H), 1.07–1.02 (m, 2 H); ^{13}C NMR (100 MHz, $CDCl_3$) δ 173.70, 172.41, 168.53, 160.32, 155.63, 155.17, 144.38, 140.88, 138.83, 134.23, 132.47, 128.89, 118.92, 118.57, 114.44, 105.94, 79.76, 74.63, 60.33, 55.69, 53.16, 52.29, 41.56, 35.18, 34.26, 33.66, 32.20, 31.13, 28.76, 28.66, 28.25, 25.19, 23.59, 19.84, 6.48, 6.00 ppm; HRMS (ESI) *m/z*: $[M + H]^+$ calcd for $C_{38}H_{53}N_6O_9S$, 769.3589; found 769.3579.

***tert*-Butyl ((*S*)-1-((2*S*,4*R*)-4-((7-methoxy-3-methylquinoxalin-2-yl)oxy)-2-(((1*R*,2*S*)-1-(((1-methylcyclopropyl)sulfonyl)carbamoyl)-2-vinylcyclopropyl)carbamoyl)pyrrolidin-1-yl)-1-oxonon-8-en-2-yl)carbamate (17b).**

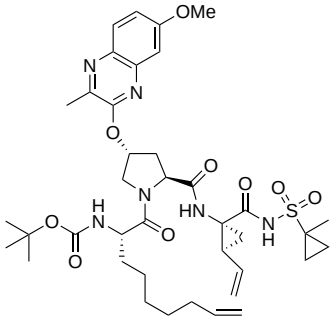

The same procedure was used as described above for compound **16b**. Acid **13b** (1.60 g, 2.9 mmol) was coupled with amine salt **15** (0.98 g, 3.5 mmol) using DIEA (2.0 mL, 11.5 mmol) and HATU (1.75 g, 4.6 mmol) to provide the bis-olefin compound **17b** (1.50 g, 66%) as a white solid. ^{1}H NMR (400 MHz, $CDCl_3$) δ 10.02 (s, 1 H), 7.81 (d, J = 8.8 Hz, 1 H), 7.18 (dd, J = 8.8, 2.8 Hz, 1 H), 7.13 (d, J = 2.8 Hz, 1 H), 7.11 (s, 1 H), 5.88 (br s, 1 H), 5.82–5.72 (m, 2 H), 5.42 (d, J = 9.2 Hz, 1 H), 5.26 (d, J = 17.2 Hz, 1 H), 5.14 (d, J = 11.6 Hz, 1 H), 5.00–4.90 (m, 2 H), 4.50 (t, J = 8.4 Hz, 1 H), 4.39–4.33 (m, 1 H), 4.18 (d, J = 11.6 Hz, 1 H), 4.02 (dd, J = 11.6, 4.0 Hz, 1 H), 3.93 (s, 3 H), 2.58–2.50 (m, 5 H), 2.10 (q, J = 8.4 Hz, 1 H), 2.05–1.98 (m, 3 H), 1.73–1.58 (m, 4 H), 1.49 (s, 3 H), 1.44–1.24 (m, 16 H), 0.92–0.86 (m, 1 H), 0.84–0.78 (m, 1 H); ^{13}C NMR (100 MHz, $CDCl_3$) δ 173.65, 172.52, 167.55, 160.31, 155.70, 155.16, 144.41, 140.87, 138.83, 134.33, 132.61, 128.96, 118.87, 118.54, 114.41, 105.96, 79.73, 74.59, 60.30, 55.67, 53.15, 52.37, 41.73, 36.56, 35.16, 34.25, 33.62, 32.24, 28.71, 28.67, 28.26, 25.31, 23.42, 19.84, 18.37, 14.27, 13.26 ppm; HRMS (ESI) *m/z*: $[M + H]^+$ calcd for $C_{39}H_{55}N_6O_9S$, 783.3746; found 783.3734.

***tert*-Butyl ((*S*)-1-((2*S*,4*R*)-4-((3-chloro-7-methoxyquinoxalin-2-yl)oxy)-2-(((1*R*,2*S*)-1-((cyclopropylsulfonyl)carbamoyl)-2-vinylcyclopropyl)carbamoyl)pyrrolidin-1-yl)-1-oxonon-8-en-2-yl)carbamate (16c).**

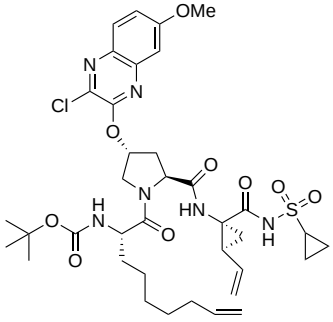

The same procedure was used as described above for compound **16b**. Ester **12c** (1.80 g, 3.0 mmol) was treated with $LiOH.H_2O$ to afford acid **13c**, which was coupled with amine salt **14** (0.96 g, 3.6 mmol) using DIEA (2.0 mL, 12.1 mmol) and HATU (1.70 g, 4.5 mmol) to provide the bis-olefin compound **16c** (1.75 g, 74%) as a white solid. ^{1}H NMR (400 MHz, $CDCl_3$) δ 10.25 (s, 1 H), 7.82 (d, J = 8.8 Hz, 1 H), 7.26–7.23 (m, 1 H), 7.17 (d, J = 2.8 Hz, 1 H), 6.99 (s, 1 H), 5.88–5.74 (m, 3 H), 5.33 (d, J = 8.8 Hz, 1 H), 5.28 (d, J = 17.2 Hz, 1 H), 5.16 (d, J = 10.4 Hz, 1 H), 5.01–4.90 (m, 2 H), 4.53 (t, J = 8.4 Hz, 1 H), 4.37–4.32 (m, 1 H), 4.28 (d, J = 11.6 Hz, 1 H), 4.03 (dd, J = 12, 4.0 Hz, 1 H), 3.96 (s, 3 H), 2.96–2.90 (m, 1 H), 2.60–2.54 (m, 2 H), 2.14 (q, J = 8.8 Hz, 1 H), 2.07–2.00 (m, 3 H), 1.76–1.54 (m, 2 H), 1.47–1.23 (m, 18 H), 1.08–1.02 (m, 2 H) ppm; ^{13}C NMR (100 MHz, $CDCl_3$) δ 174.01, 172.48, 168.59, 161.61, 155.84, 152.31, 141.06, 139.09, 136.14, 134.39, 132.66, 129.16, 120.43, 118.81, 114.66, 106.03, 80.05, 76.19, 60.64, 56.05, 53.09, 52.56, 41.86, 35.44, 34.41, 33.90, 32.46, 31.39, 28.99, 28.89, 28.46, 25.44, 23.80, 6.67, 6.27 ppm; HRMS (ESI) *m/z*: $[M + H]^+$ calcd for $C_{37}H_{50}ClN_6O_9S$, 789.3043; found 789.3030.

***tert*-Butyl ((*S*)-1-((2*S*,4*R*)-4-((3-chloro-7-methoxyquinoxalin-2-yl)oxy)-2-(((1*R*,2*S*)-1-(((1-methylcyclopropyl)sulfonyl)carbamoyl)-2-vinylcyclopropyl)carbamoyl)pyrrolidin-1-yl)-1-oxonon-8-en-2-yl)carbamate (17c).**

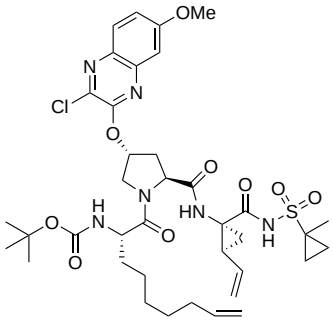

The same procedure was used as described above for compound **16b**. Ester **12c** (1.80 g, 3.0 mmol) was treated with $LiOH.H_2O$ to afford acid **13c**, which was coupled with amine salt **15** (1.0 g, 3.6 mmol) using DIEA (2.0 mL, 12.1 mmol) and HATU (1.70 g, 4.5 mmol) to provide the bis-olefin compound **17c** (1.85 g, 77%) as a white solid. ^{1}H NMR (500 MHz, $CDCl_3$) δ 10.01 (s, 1 H), 7.82 (d, J = 9.0 Hz, 1 H), 7.26–7.23 (m, 1 H), 7.17 (d, J = 2.5 Hz, 1 H), 7.02 (s, 1 H), 5.87 (br s, 1 H), 5.82–5.74 (m 2 H), 5.36 (d, J = 8.8 Hz, 1 H), 5.28 (d, J = 17.0 Hz, 1 H), 5.15 (d, J = 11.2 Hz, 1 H), 5.00–4.96 (m, 1 H), 4.94–4.91 (m, 1 H), 4.53 (t, J = 8.4 Hz, 1 H), 4.37–4.32 (m, 1 H), 4.24 (d, J = 11.5 Hz, 1 H), 4.03 (dd, J = 12.0, 4.0 Hz, 1 H), 3.96 (s, 3 H), 2.61–2.53 (m, 2 H), 2.12 (q, J = 8.8 Hz, 1 H), 2.05–2.00 (m, 3 H), 1.74–1.58 (m, 4 H), 1.50 (s, 3 H), 1.47–1.24 (m, 16 H), 0.92–0.86 (m, 1 H), 0.85–0.80 (m, 1 H); ^{13}C NMR (125 MHz, $CDCl_3$) δ 173.74, 172.32, 167.42, 161.39, 155.68, 152.09, 140.85, 138.88, 135.93, 134.20, 132.59, 128.95, 120.19, 118.57, 114.41, 105.83, 79.79, 75.95, 60.39, 55.83, 52.86, 52.40, 41.79, 36.59,

35.21, 34.16, 33.65, 32.30, 28.73, 28.69, 28.27, 25.34, 23.44, 18.41, 14.24, 13.39 ppm; HRMS (ESI) *m/z*: $[M + H]^+$ calcd for $C_{38}H_{52}ClN_6O_9S$, 803.3200; found 803.3194.

***tert*-Butyl ((*S*)-1-((2*S*,4*R*)-2-(((1*R*,2*S*)-1-((cyclopropylsulfonyl)carbamoyl)-2-vinylcyclopropyl)carbamoyl)-4-((3-isopropyl-7-methoxyquinoxalin-2-yl)oxy)pyrrolidin-1-yl)-1-oxonon-8-en-2-yl)carbamate (16e).**

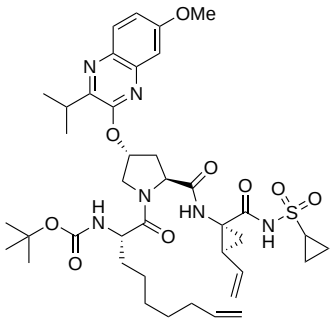

The same procedure was used as described above for compound **16b**. Ester **12e** (2.0 g, 3.3 mmol) was treated with $LiOH.H_2O$ to afford acid **13e**, which was coupled with amine salt **14** (1.20 g, 4.5 mmol) using DIEA (2.25 mL, 13.6 mmol) and HATU (1.90 g, 5.0 mmol) to provide the bis-olefin compound **16e** (1.85 g, 70%) as a white solid. ^{1}H NMR (400 MHz, $CDCl_3$) δ 10.25 (s, 1 H), 7.85 (d, *J* = 8.8 Hz, 1 H), 7.19 (dd, *J* = 8.8, 2.8 Hz, 1 H), 7.12 (d, *J* = 2.8 Hz, 1 H), 7.01 (s, 1 H), 5.92 (br s, 1 H), 5.84–5.73 (m, 2 H), 5.34 (d, *J* = 8.8 Hz, 1 H), 5.27 (d, *J* = 17.2 Hz, 1 H), 5.14 (d, *J* = 11.6 Hz, 1 H), 5.01–4.89 (m, 2 H), 4.48 (t, *J* = 8.4 Hz, 1 H), 4.40–4.33 (m, 1 H), 4.18 (d, *J* = 11.6 Hz, 1 H), 4.02 (dd, *J* = 11.6, 7.2 Hz, 1 H), 3.93 (s, 3 H), 3.40–3.33 (m, 1 H), 2.96–2.90 (m, 1 H), 2.56–2.52 (m, 2 H), 2.12 (q, *J* = 8.8 Hz, 1 H), 2.06–1.99 (m, 3 H), 1.75–1.54 (m, 2 H), 1.46–1.23 (m, 24 H), 1.07–1.02 (m, 2 H) ppm; ^{13}C NMR (100 MHz, $CDCl_3$) δ 173.80, 172.33, 168.47, 160.28, 155.64, 154.23, 151.76, 140.49, 138.84, 134.43, 132.48, 129.41, 118.68, 118.54, 114.43, 105.76, 79.75, 74.33, 60.39, 55.67, 53.21, 52.38, 41.58, 35.22, 34.24, 33.65, 32.17, 31.15, 30.63, 28.75, 28.65, 28.23, 25.22, 23.59, 20.61, 20.41, 6.45, 6.02 ppm; HRMS (ESI) *m/z*: $[M + H]^+$ calcd for $C_{40}H_{57}N_6O_9S$, 797.3902; found 797.3906.

***tert*-Butyl ((*S*)-1-((2*S*,4*R*)-4-((3-isopropyl-7-methoxyquinoxalin-2-yl)oxy)-2-(((1*R*,2*S*)-1-(((1-methylcyclopropyl)sulfonyl)carbamoyl)-2-vinylcyclopropyl)carbamoyl)pyrrolidin-1-yl)-1-oxonon-8-en-2-yl)carbamate (17e).**

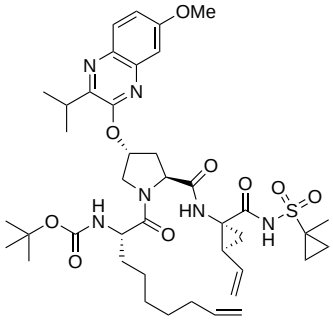

The same procedure was used as described above for compound **16b**. Ester **12e** (2.0 g, 3.3 mmol) was treated with $LiOH.H_2O$ to afford acid **13e**, which was coupled with amine salt **15** (1.27 g, 4.5 mmol) using DIEA (2.25 mL, 13.6 mmol) and HATU (1.90 g, 5.0 mmol) to provide the bis-olefin compound **17e** (2.0 g, 75%) as a white solid. ^{1}H NMR (400 MHz, $CDCl_3$) δ 10.03 (s, 1 H), 7.85 (d, J = 9.2 Hz, 1 H), 7.19 (dd, J = 9.2, 2.8 Hz, 1 H), 7.12 (d, J = 2.8 Hz, 1 H), 7.03 (s, 1 H), 5.92 (br s, 1 H), 5.84–5.73 (m, 2 H), 5.36 (d, J = 8.8 Hz, 1 H), 5.27 (d, J = 17.2 Hz, 1 H), 5.14 (d, J = 10.8 Hz, 1 H), 5.01–4.89 (m, 2 H), 4.47 (t, J = 7.6 Hz, 1 H), 4.40–4.33 (m, 1 H), 4.15 (d, J = 11.6 Hz, 1 H), 4.02 (dd, J = 11.6, 4.0 Hz, 1 H), 3.94 (s, 3 H), 3.40–3.33 (m, 1 H), 2.57–2.52 (m, 2 H), 2.12 (q, J = 8.4 Hz, 1 H), 2.05–1.99 (m, 3 H), 1.76–1.58 (m, 4 H), 1.49 (s, 3 H), 1.45–1.20 (m, 22 H), 0.92–0.87 (m, 1H), 0.85–0.79 (m, 1 H) ppm; ^{13}C NMR (100 MHz, $CDCl_3$) δ 173 .79, 172.38, 167.50, 160.28, 155.71, 154.23, 151.76, 140.49, 138.85, 134.43, 132.61, 129.42, 118.69, 118.54, 114.41, 105.76, 79.72, 74.32, 60.40, 55.68, 53.19, 52.47, 41.71, 36.56, 35.24, 34.22, 33.64, 32.18, 30.61, 28.70, 28.67, 28.25, 25.35, 23.51, 20.63, 20.42, 18.38, 14.26, 13.31; HRMS (ESI) *m/z*: $[M + H]^+$ calcd for $C_{41}H_{59}N_6O_9S$, 811.4059; found 811.4043.

***tert*-Butyl ((*S*)-1-((2*S*,4*R*)-2-(((1*R*,2*S*)-1-((cyclopropylsulfonyl)carbamoyl)-2-vinylcyclopropyl)carbamoyl)-4-((3-(thiophen-2-yl)quinoxalin-2-yl)oxy)pyrrolidin-1-yl)-1-oxonon-8-en-2-yl)carbamate (16f).**

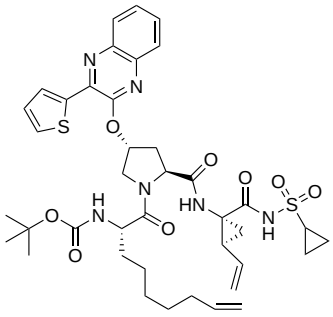

The same procedure was used as described above for compound **16b**. Ester **12f** (1.85 g, 3.0 mmol) was treated with $LiOH.H_2O$ to afford acid **13f**, which was coupled with amine salt **14** (0.96 g, 3.6 mmol) using DIEA (2.0 mL, 12.1 mmol) and HATU (1.70 g, 4.5 mmol) to provide the bis-olefin compound **16f** (1.60 g, 66%) as a white solid. ^{1}H NMR (400 MHz, $CDCl_3$) δ 10.23 (s, 1 H), 8.10 (d, J =

3.2 Hz, 1 H), 8.01 (dd, *J* = 8.0, 1.2 Hz, 1 H), 7.79 (dd, *J* = 8.8, 1.6 Hz, 1 H), 7.65–7.56 (m, 2H), 7.53 (d, *J* = 5.2 Hz, 1 H), 7.17 (dd, *J* = 4.8, 4.0 Hz, 1 H), 7.11 (s, 1 H), 6.08 (br s, 1 H), 5.83–5.73 (m, 2 H), 5.35 (d, *J* = 8.8 Hz, 1 H), 5.26 (dd, *J* = 16.8, 1.2 Hz, 1 H), 5.13 (dd, *J* = 10.4, 1.2 Hz, 1 H), 5.01–4.90 (m, 2 H), 4.54 (t, *J* = 8.8 Hz, 1 H), 4.46–4.39 (m, 1 H), 4.34 (d, *J* = 12.4 Hz, 1 H), 4.07 (dd, *J* = 12.0, 3.6 Hz, 1 H), 2.95–2.87 (m, 1 H), 2.68–2.56 (m, 2 H), 2.10 (q , *J* = 8.8 Hz, 1 H), 2.05–1.98 (m, 3 H), 1.75–1.55 (m, 2 H), 1.45–1.16 (m, 18 H), 1.06–0.99 (m, 2 H) ppm; ^{13}C NMR (100 MHz, $CDCl_3$) *δ* 173.83, 172.34, 168.51, 155.70, 152.05, 140.39, 139.17, 138.93, 138.86, 138.72, 132.47, 130.46, 130.35, 129.56, 128.57, 128.13, 127.54, 126.72, 118.54, 114.44, 79.73, 75.39, 60.32, 53.23, 52.51, 41.57, 35.14, 34.10, 33.66, 31.99, 31.14, 28.75, 28.67, 28.26, 25.34, 23.56, 6.46, 6.03 ppm; HRMS (ESI) *m/z*: $[M + H]^+$ calcd for $C_{40}H_{51}N_6O_8S_2$, 807.3204; found 807.3214.

***tert*-Butyl ((*S*)-1-((2*S*,4*R*)-2-(((1*R*,2*S*)-1-((cyclopropylsulfonyl)carbamoyl)-2-vinylcyclopropyl)carbamoyl)-4-((3-ethylquinoxalin-2-yl)oxy)pyrrolidin-1-yl)-1-oxonon-8-en-2-yl)carbamate (16g).**

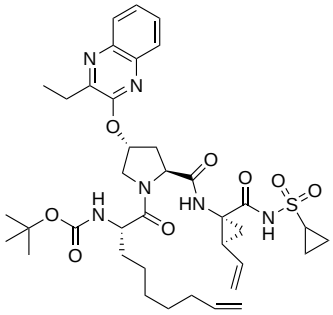

The same procedure was used as described above for compound **16b**. Ester **12g** (1.95 g, 3.5 mmol) was treated with $LiOH.H_2O$ to afford acid **13g**, which was coupled with amine salt **14** (1.10 g, 4.1 mmol) using DIEA (2.30 mL, 14.0 mmol) and HATU (2.0 g, 5.3 mmol) to provide the bis-olefin compound **16g** (2.0 g, 76%) as a white solid. ^{1}H NMR (400 MHz, $CDCl_3$) *δ* 10.24 (s, 1 H), 7.96 (d, *J* = 8.4 Hz, 1 H), 7.78 (d, *J* = 8.0 Hz, 1 H), 7.63–7.53 (m, 2 H), 7.05 (s, 1 H), 5.93 (br s, 1H), 5.85–5.73 (m, 2 H), 5.35 (d, *J* = 8.4 Hz, 1 H), 5.27 (d, *J* = 17.2 Hz, 1 H), 5.14 (d, *J* = 10.8 Hz, 1 H), 5.00–4.90 (m, 2 H), 4.48 (t, *J* = 8.0 Hz, 1 H), 4.37–4.32 (m, 1 H), 4.20 (d, *J* = 12.0 Hz, 1 H), 4.03 (dd, *J* = 12.0, 4.0 Hz, 1 H), 2.96–2.89 (m, 3 H), 2.57–2.52 (m, 2 H), 2.12 (q, *J* = 8.8 Hz, 1 H), 2.05–1.99 (m, 2 H), 1.75–1.54 (m, 2 H), 1.46–1.17 (m, 22 H), 1.08–1.02 (m, 2 H) ppm; ^{13}C NMR (100 MHz, $CDCl_3$) *δ* 173.81, 172.33, 168.51, 155.64, 154.33, 151.84, 139.16, 138.91, 138.84, 132.48, 129.11, 128.31, 126.92, 126.86, 118.54, 114.44, 79.74, 74.56, 60.33, 53.16, 52.35, 41.56, 35.22, 34.18, 33.65, 32.14, 31.13, 28.74, 28.65, 28.23, 26.73, 25.24, 23.62, 11.42, 6.47, 6.00 ppm; HRMS (ESI) *m/z*: $[M + H]^+$ calcd for $C_{38}H_{53}N_6O_8S$, 753.3640; found 753.3636.

tert-Butyl ((2*R*,6*S*,13a*S*,14a*R*,16a*S*,*Z*)-14a-((cyclopropylsulfonyl)carbamoyl)-2-((7-methoxy-3-methylquinoxalin-2-yl)oxy)-5,16-dioxo-1,2,3,5,6,7,8,9,10,11,13a,14,14a,15,16,16a-hexadecahydrocyclopropa[*e*]pyrrolo[1,2-*a*][1,4]diazacyclopentadecin-6-yl)carbamate (18b).

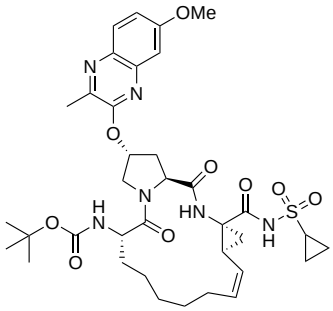

A degassed solution of bis-olefin **16b** (1.57 g, 2.0 mmol) in 1,2-DCE (310 mL) was heated to 50 °C under argon, then Zhan 1b catalyst (0.150 g, 0.20 mmol) was added in two portions over 10 min. The resulting reaction mixture was heated to 70 °C and stirred for 6 h. The reaction mixture was cooled to room temperature and solvents were evaporated under reduced pressure. The residue was purified by flash chromatography using 50–90% EtOAc/hexanes as the eluent to yield the P1–P3 macrocyclic product **18b** (0.67 g, 45%) as an off-white solid. ^{1}H NMR (400 MHz, $CDCl_3$) δ 10.28 (s, 1 H), 7.80 (d, J = 9.6 Hz, 1 H), 7.19–7.16 (m, 2 H), 6.88 (s, 1 H), 5.89 (br s, 1 H), 5.69 (q, J = 9.2 Hz, 1 H), 5.12 (d, J = 8.0 Hz, 1 H), 4.97 (t, J = 9.2 Hz, 1 H), 4.61 (t, J = 8.0 Hz, 1 H), 4.51 (d, J = 12.0 Hz, 1 H), 4.28–4.22 (m, 1 H), 4.01 (dd, J = 11.6, 4.0 Hz, 1 H), 3.94 (s, 3 H), 2.94–2.86 (m, 1 H), 2.70–2.48 (m, 6 H), 2.31 (q, J = 8.4 Hz, 1 H), 1.94–1.68 (m, 2 H), 1.60–1.22 (m, 19 H), 1.16–1.06 (m, 2 H), 0.95–0.89 (m, 1 H) ppm; ^{13}C NMR (100 MHz, $CDCl_3$) δ 177.14, 173.33, 168.0, 160.31, 155.32, 155.03, 144.49, 141.01, 136.30, 134.24, 128.68, 124.47, 118.90, 105.97, 79.85, 74.84, 59.44, 55.72, 53.06, 51.96, 44.57, 34.58, 32.72, 31.02, 29.73, 28.15, 27.10, 27.05, 26.01, 22.18, 20.96, 19.73, 6.67, 6.12 ppm; HRMS (ESI) *m/z*: $[M + H]^+$ calcd for $C_{36}H_{49}N_6O_9S$, 741.3276; found 741.3255. Anal. RP-HPLC: t_R 12.71 min, purity 99%.

tert-Butyl ((2*R*,6*S*,13a*S*,14a*R*,16a*S*,*Z*)-2-((7-methoxy-3-methylquinoxalin-2-yl)oxy)-14a-(((1-methylcyclopropyl)sulfonyl)carbamoyl)-5,16-dioxo-1,2,3,5,6,7,8,9,10,11,13a,14,14a,15,16,16a-hexadecahydrocyclopropa[*e*]pyrrolo[1,2-*a*][1,4]diazacyclopentadecin-6-yl)carbamate (19b).

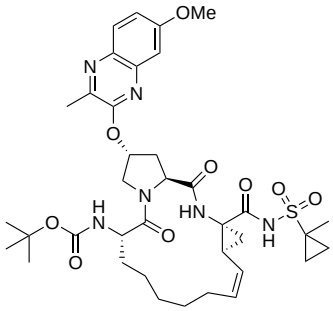

The same procedure was used as described above for compound **18b**. Bis-olefin **17b** (1.50 g, 1.9 mmol) was treated with Zhan 1b catalyst (0.150 g, 0.20 mmol) in 1,2-DCE (300 mL) to provide the P1–P3 macrocyclic compound **19b** (1.0 g, 70%) as an off-white solid. ^{1}H NMR (400 MHz, $CDCl_3$) δ 10.16 (s, 1 H), 7.82 (d, J = 9.2 Hz, 1 H), 7.19–7.16 (m, 2 H), 6.92 (s, 1 H), 5.88 (br s, 1 H), 5.69 (q, J = 9.2 Hz, 1 H), 5.12 (d, J = 7.6 Hz, 1 H), 4.99 (t, J = 8.8 Hz, 1 H), 4.61 (t, J = 8.0 Hz, 1 H), 4.51 (d, J = 11.2 Hz, 1 H), 4.28–4.22 (m, 1 H), 4.03 (dd, J = 11.2, 4.0 Hz, 1 H), 3.95 (s, 3 H), 2.70–2.50 (m, 6 H), 2.31 (q, J = 8.8 Hz, 1 H), 1.92–1.66 (m, 4 H), 1.60–1.20 (m, 21 H), 0.85–0.78 (m, 2 H) ppm; ^{13}C NMR (100 MHz, $CDCl_3$) δ 177.16, 173.33, 166.94, 160.33, 155.32, 155.04, 144.46, 141.03, 134.20, 136.25, 128.66, 124.89, 118.93, 105.98, 79.85, 74.88, 59.46, 55.72, 53.08, 51.97, 44.73, 36.43, 34.61, 32.72, 29.65, 28.15, 27.06, 26.07, 22.21, 20.96, 19.71, 18.17, 14.51, 12.51 ppm; HRMS (ESI) *m/z*: $[M + H]^+$ calcd for $C_{37}H_{51}N_6O_9S$, 755.3433; found 755.3404. Anal. HPLC: t_R 13.57 min, purity 99%.

***tert*-Butyl ((2*R*,6*S*,13a*S*,14a*R*,16a*S*,*Z*)-2-((3-chloro-7-methoxyquinoxalin-2-yl)oxy)-14a-((cyclopropylsulfonyl)carbamoyl)-5,16-dioxo-1,2,3,5,6,7,8,9,10,11,13a,14,14a,15,16,16a-hexadecahydrocyclopropa[*e*]pyrrolo[1,2-*a*][1,4]diazacyclopentadecin-6-yl)carbamate (18c).**

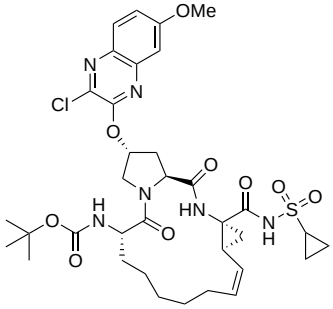

The same procedure was used as described above for compound **18b**. Bis-olefin **16c** (1.50 g, 1.9 mmol) was treated with Zhan 1b catalyst (0.150 g, 0.20 mmol) in 1,2-DCE (300 mL) to provide the P1–P3 macrocyclic compound **18c** (0.73 g, 50%) as an off-white solid. ^{1}H NMR (400 MHz, $CDCl_3$) δ 10.30 (s, 1 H), 7.78 (d, J = 9.6 Hz, 1 H), 7.25–7.20 (m, 2 H), 7.00 (s, 1 H), 5.86 (s, 1 H), 5.68 (q, J = 9.2 Hz, 1 H), 5.19 (d, J = 7.6 Hz, 1 H), 4.95 (t, J = 9.2 Hz, 1 H), 4.65 (t, J = 8.0 Hz, 1

H), 4.59 (d, *J* = 11.6 Hz, 1 H), 4.26–4.22 (m, 1 H), 4.03 (dd, *J* = 11.6, 4.0 Hz, 1 H), 3.95 (s, 3 H), 2.94–2.87 (m, 1 H), 2.68–2.51 (m, 3 H), 2.31 (q, *J* = 8.8 Hz, 1 H), 1.94–1.74 (m, 2 H), 1.60–1.20 (m, 19 H), 1.17–1.04 (m, 2 H), 0.96–0.89 (m, 1 H) ppm; ^{13}C NMR (100 MHz, $CDCl_3$) *δ* 177.32, 173.48, 168.24, 161.52, 155.30, 152.45, 141.15, 136.53, 136.25, 134.26, 129.02, 124.71, 120.31, 106.06, 80.14, 76.38, 59.71, 56.08, 52.90, 52.15, 44.80, 34.73, 32.85, 31.28, 29.88, 28.38, 27.36, 27.31, 26.29, 22.46, 21.13, 6.90, 6.35 ppm. HRMS (ESI) *m/z*: $[M + H]^+$ calcd for $C_{35}H_{46}ClN_6O_9S$, 761.2730; found 761.2706. Anal. HPLC: t_R 14.28 min, purity 96%.

***tert*-Butyl ((2*R*,6*S*,13a*S*,14a*R*,16a*S*,*Z*)-2-((3-chloro-7-methoxyquinoxalin-2-yl)oxy)-14a-(((1-methylcyclopropyl)sulfonyl)carbamoyl)-5,16-dioxo-1,2,3,5,6,7,8,9,10,11,13a,14,14a,15,16,16a-hexadecahydrocyclopropa[*e*]pyrrolo[1,2-*a*][1,4]diazacyclopentadecin-6-yl)carbamate (19c).**

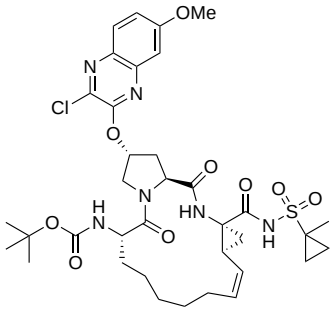

The same procedure was used as described above for compound **18b**. Bis-olefin **17c** (1.20 g, 1.5 mmol) was treated with Zhan 1b catalyst (0.150 g, 0.20 mmol) in 1,2-DCE (300 mL) to provide the P1–P3 macrocyclic compound **19c** (1.0 g, 86%) as an off-white solid. ^{1}H NMR (400 MHz, $CDCl_3$) *δ* 10.20 (s, 1 H), 7.78 (d, *J* = 10.0 Hz, 1 H), 7.23–7.20 (m, 2 H), 7.07 (s, 1 H), 5.85 (br s, 1 H), 5.67 (q, *J* = 8.4 Hz, 1 H), 5.25 (d, *J* = 7.2 Hz, 1 H), 4.96 (t, *J* = 9.2 Hz, 1 H), 4.67–4.58 (m, 2 H), 4.28–4.22 (m, 1 H), 4.04 (dd, *J* = 11.2, 3.2 Hz, 1 H), 3.96 (s, 3 H), 2.68–2.62 (m, 2 H), 2.60–2.50 (m, 1 H), 2.33 (q, *J* = 8.0 Hz, 1 H), 1.91–1.72 (m, 4 H), 1.60–1.20 (m, 21 H), 0.84–0.78 (m, 2 H) ppm; ^{13}C NMR (100 MHz, $CDCl_3$) *δ* 177.18, 173.18, 167.07, 161.27, 155.06, 152.21, 140.92, 136.27, 135.99, 134.0, 128.76, 124.88, 120.09, 105.81, 79.90, 76.21, 59.51, 55.85, 52.69, 51.89, 44.70, 36.41, 34.54, 32.57, 29.48, 28.25, 28.15, 27.11, 26.15, 22.22, 20.83, 18.17, 14.51, 12.50 ppm; HRMS (ESI) *m/z*: $[M + H]^+$ calcd for $C_{36}H_{48}ClN_6O_9S$, 775.2887; found 775.2870. Anal. HPLC: t_R 14.69 min, purity 97%.

***tert*-Butyl ((2*R*,6*S*,13a*S*,14a*R*,16a*S*,*Z*)-14a-((cyclopropylsulfonyl)carbamoyl)-2-((3-isopropyl-7-methoxyquinoxalin-2-yl)oxy)-5,16-dioxo-1,2,3,5,6,7,8,9,10,11,13a,14,14a,15,16,16a-hexadecahydrocyclopropa[*e*]pyrrolo[1,2-*a*][1,4]diazacyclopentadecin-6-yl)carbamate (18e).**

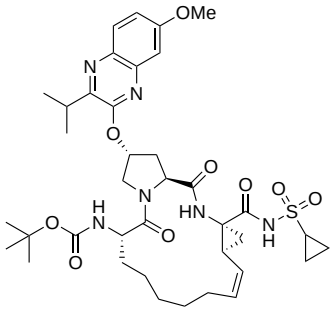

The same procedure was used as described above for compound **18b**. Bis-olefin **16e** (1.80 g, 2.3 mmol) was treated with Zhan 1b catalyst (0.150 g, 0.20 mmol) in 1,2-DCE (350 mL) to provide the P1–P3 macrocyclic compound **18e** (0.95 g, 58%) as an off-white solid. ^{1}H NMR (400 MHz, $CDCl_3$) δ 10.28 (s, 1 H), 7.83 (d, *J* = 9.6 Hz 1 H), 7.20–7.15 (m, 2 H), 6.94 (s, 1 H), 5.91 (s, 1 H), 5.70 (q, *J* = 8.4 Hz, 1 H), 5.20 (d, *J* = 8.0 Hz, 1 H), 4.97 (t, *J* = 8.8 Hz, 1 H), 4.58 (t, *J* = 8.0 Hz, 1 H), 4.46 (d, *J* = 12.0 Hz, 1 H), 4.33–4.26 (m, 1 H), 4.03 (dd, *J* = 12.0, 4.4 Hz, 1 H), 3.94 (s, 3 H), 3.41–3.33 (m, 1 H), 2.93–2.86 (m, 1 H), 2.66–2.50 (m, 3 H), 2.34 (q, *J* = 8.8 Hz, 1 H), 1.93–1.74 (m, 2 H), 1.60–1.05, m, 27 H), 0.95–0.88 (m, 1 H) ppm; ^{13}C NMR (100 MHz, $CDCl_3$) δ 177.22, 173.13, 168.13, 160.22, 154.96, 154.36, 151.82, 140.61, 136.32, 134.31, 129.28, 124.45, 118.61, 105.79, 79.81, 74.55, 59.47, 55.71, 53.12, 51.86, 44.52, 34.74, 32.91, 31.00, 30.58, 29.65, 28.18, 27.16, 27.11, 26.12, 22.14, 20.89, 20.51, 20.42, 6.67, 6.10 ppm; HRMS (ESI) *m/z*: $[M + H]^+$ calcd for $C_{38}H_{53}N_6O_9S$, 769.3589; found 769.3565. Anal. HPLC: t_R 15.82 min, purity 98%.

***tert*-Butyl ((2*R*,6*S*,13a*S*,14a*R*,16a*S*,*Z*)-2-((3-isopropyl-7-methoxyquinoxalin-2-yl)oxy)-14a-(((1-methylcyclopropyl)sulfonyl)carbamoyl)-5,16-dioxo-1,2,3,5,6,7,8,9,10,11,13a,14,14a,15,16,16a-hexadecahydrocyclopropa[*e*]pyrrolo[1,2-*a*][1,4]diazacyclopentadecin-6-yl)carbamate (19e).**

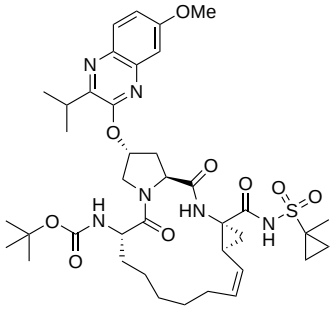

The same procedure was used as described above for compound **18b**. Bis-olefin **17e** (1.90 g, 2.3 mmol) was treated with Zhan 1b catalyst (0.20 g, 0.27 mmol) in 1,2-DCE (350 mL) to provide the P1–P3 macrocyclic compound **19e** (1.1 g, 60%) as an off-white solid. ^{1}H NMR (400 MHz, $CDCl_3$) δ 10.15 (s, 1 H), 7.83 (d, *J* = 9.6 Hz, 1 H), 7.19–7.15 (m, 2 H), 6.95 (s, 1 H), 5.91 (s, 1 H), 5.70 (q, *J* = 8.4 Hz, 1

H), 5.19 (d, *J* = 8.0 Hz, 1 H), 4.99 (t, *J* = 9.6 Hz, 1 H), 4.57 (t, *J* = 8.0 Hz, 1 H), 4.47 (d, *J* = 11.6 Hz, 1 H), 4.34–4.27 (m, 1 H), 4.06 (dd, *J* = 11.2, 4.0 Hz, 1 H), 3.94 (s, 3 H), 3.41–3.34 (m, 1 H), 2.68–2.48 (m, 3 H), 2.34 (q, *J* = 8.4 Hz, 1 H), 1.93–1.70 (m, 4 H), 1.62–1.17 (m, 27 H), 0.84–0.78 (m, 2 H) ppm; ^{13}C NMR (100 MHz, $CDCl_3$) *δ* 177.19, 173.14, 167.04, 160.24, 154.96, 154.36, 151.79, 140.62, 136.25, 134.28, 129.25, 124.88, 118.64, 105.81, 79.81, 74.61, 59.49, 55.71, 53.15, 51.87, 44.68, 36.43, 34.75, 32.91, 30.59, 29.59, 28.17, 27.14, 26.17, 22.18, 20.91, 20.50, 20.42, 18.17, 14.50, 12.49 ppm; HRMS (ESI) *m/z*: $[M + H]^+$ calcd for $C_{39}H_{55}N_6O_9S$, 783.3746; found 783.3722. Anal. HPLC: t_R 16.46 min, purity 98%.

***tert*-Butyl ((2*R*,6*S*,13a*S*,14a*R*,16a*S*,*Z*)-14a-((cyclopropylsulfonyl)carbamoyl)-5,16-dioxo-2-((3-(thiophen-2-yl)quinoxalin-2-yl)oxy)-1,2,3,5,6,7,8,9,10,11,13a,14,14a,15,16,16a-hexadecahydrocyclopropa[*e*]pyrrolo[1,2-*a*][1,4]diazacyclopentadecin-6-yl)carbamate (18f).**

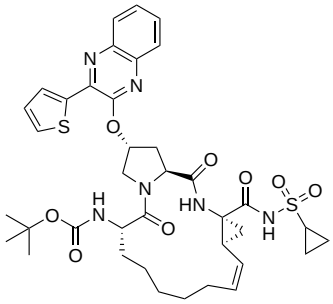

The same procedure was used as described above for compound **18b**. Bis-olefin **16f** (0.60 g, 0.7 mmol) was treated with Zhan 1b catalyst (0.10 g, 0.13 mmol) in 1,2-DCE (200 mL) to provide the P1–P3 macrocyclic compound **18f** (0.35 g, 61%) as an off-white solid. ^{1}H NMR (400 MHz, $CDCl_3$) *δ* 10.28 (s, 1 H), 8.08 (d, *J* = 3.2 Hz, 1 H), 7.99 (d, *J* = 7.2 Hz, 1 H), 7.83 (dd, *J* = 8.4, 1.2 Hz, 1 H), 7.65–7.55 (m, 2 H), 7.49 (d, *J* = 4.4 Hz, 1 H), 7.14 (t, *J* = 4.0 Hz, 1 H), 6.96 (s, 1 H), 6.08 (br s, 1 H), 5.66 (q, *J* = 9.2 Hz, 1 H), 5.16 (d, *J* = 8.4 Hz, 1 H), 4.95 (t, *J* = 10.0 Hz, 1 H), 4.69 (t, *J* = 8.0 Hz, 1 H), 4.63 (d, *J* = 12.4 Hz, 1 H), 4.34–4.27 (m, 1 H), 4.08 (dd, *J* = 12.0, 4.0 Hz, 1 H), 2.94–2.86 (m, 1 H), 2.76–2.69 (m, 2 H), 2.58–2.48 (m, 1 H), 2.29 (q, *J* = 8.4 Hz, 1 H), 1.92–1.74 (m, 2 H), 1.64–1.04 (m, 20 H), 0.96–0.88 (m, 1 H) ppm; ^{13}C NMR (100 MHz, $CDCl_3$) *δ* 177.19, 173.43, 168.20, 155.16, 152.45, 140.65, 139.81, 139.10, 139.07, 136.53, 130.53, 130.33, 129.72, 128.72, 128.30, 127.60, 127.07, 124.72, 80.06, 75.73, 59.75, 53.41, 52.21, 44.79, 34.84, 33.13, 31.27, 29.96, 28.30, 27.41, 27.23, 26.21, 22.54, 21.17, 6.93, 6.37 ppm; HRMS (ESI) *m/z*: $[M + H]^+$ calcd for $C_{38}H_{47}N_6O_8S_2$, 779.2891; found 779.2873. Anal. HPLC: t_R 15.96 min, purity 97%.

***tert*-Butyl ((2*R*,6*S*,13a*S*,14a*R*,16a*S*,*Z*)-14a-((cyclopropylsulfonyl)carbamoyl)-2-((3-ethylquinoxalin-2-yl)oxy)-5,16-dioxo-1,2,3,5,6,7,8,9,10,11,13a,14,14a,15,16,16a-**

hexadecahydrocyclopropa[*e*]pyrrolo[1,2-*a*][1,4]diazacyclopentadecin-6-yl)carbamate (18g).

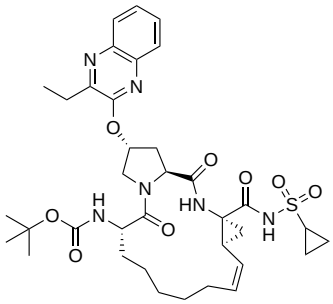

The same procedure was used as described above for compound **18b**. Bis-olefin **16g** (1.80 g, 2.4 mmol) was treated with Zhan 1b catalyst (0.20 g, 0.30 mmol) in 1,2-DCE (350 mL) to provide the P1–P3 macrocyclic compound **18g** (1.05 g, 60%) as an off-white solid. ^{1}H NMR (400 MHz, $CDCl_3$) δ 10.32 (s, 1 H), 7.94 (d, J = 8.0 Hz, 1 H), 7.80 (dd, J = 8.0. 1.2 Hz 1 H), 7.62–7.51 (m, 2 H), 7.02 (s, 1 H), 5.91 (br s, 1 H), 5.67 (q, J = 8.4 Hz, 1 H), 5.19 (d, J = 7.6 Hz, 1 H), 4.95 (t, J = 9.2 Hz, 1 H), 4.61 (t, J = 8.0 Hz, 1 H), 4.51 (d, J = 11.6 Hz, 1 H), 4.27–22 (m, 1 H), 4.03 (dd, J = 11.2, 3.6 Hz, 1 H), 2.94–2.85 (m, 3 H), 2.65–2.52 (m, 3 H), 2.32 (q, J = 8.4 Hz, 1 H), 1.91–1.76 (m, 2 H), 1.56–1.20 (m, 20 H), 1.15–1.04 (m, 4 H), 0.93–0.87 (m, 1 H) ppm; ^{13}C NMR (400 MHz, $CDCl_3$) δ 177.23, 173.20, 168.17, 154.96, 154.48, 152.00, 139.29, 138.81, 136.32, 128.98, 128.20, 126.95, 126.68, 124.50, 79.77, 74.79, 59.46, 53.16, 51.91, 44.57, 34.64, 32.81, 30.99, 29.66, 28.13, 27.09, 26.68, 26.06, 22.14, 20.94, 11.31, 6.66, 6.10 ppm; HRMS (ESI) *m/z*: $[M + H]^+$ calcd for $C_{36}H_{49}N_6O_8S$, 725.3327; found 725.3301. Anal. HPLC: t_R 14.40 min, purity 99%.

Cyclopentyl ((2*R*,6*S*,13a*S*,14a*R*,16a*S*,*Z*)-14a-((cyclopropylsulfonyl)carbamoyl)-2-((7-methoxy-3-methylquinoxalin-2-yl)oxy)-5,16-dioxo-1,2,3,5,6,7,8,9,10,11,13a,14,14a,15,16,16a-hexadecahydrocyclopropa[*e*]pyrrolo[1,2-*a*][1,4]diazacyclopentadecin-6-yl)carbamate (22b).

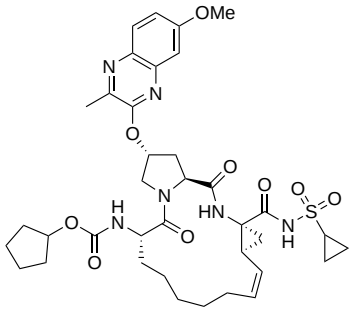

Compound **18b** (0.32 g, 0.43 mmol) was treated with a solution of 4 N HCl in 1,4-dioxane (10 mL). The reaction mixture was stirred at room temperature for 3 h, and then concentrated under reduced pressure, and the residue was dried under

high vacuum. The off-white solid was triturated with diethyl ether (3 × 10 mL) and dried under high vacuum to yield the amine salt **20b** (0.29 g, 100%) as a white powder.

A solution of the above amine salt **20b** (0.29 g, 0.43 mmol) in anhydrous CH_3CN (13 mL) was treated with DIEA (0.28 mL, 1.7 mmol) and *N*-(cyclopentyloxycarbonyloxy)-succinimide (0.108 g, 0.48 mmol). The reaction mixture was stirred at room temperature for 36 h, then concentrated under reduced pressure and dried under high vacuum. The residue was purified by flash chromatography using 50–90% EtOAc/hexanes as the eluent to provide the target compound **22b** (0.29 g, 90%) as a white solid. ^{1}H NMR (400 MHz, $CDCl_3$) δ 10.29 (s, 1 H), 7.79 (d, J = 9.6 Hz, 1 H), 7.20–7.16 (m, 2 H), 6.98 (s, 1 H), 5.91 (br s, 1 H), 5.68 (q, J = 8.8 Hz, 1 H), 5.24 (d, J = 8.0 Hz, 1 H), 4.96 (t, J = 8.8 Hz, 1 H), 4.88–4.84 (br s, 1 H), 4.62 (t, J = 7.6 Hz, 1 H), 4.42 (d, J = 11.6 Hz, 1 H), 4.33–4.27 (m, 1 H), 4.04 (dd, J = 11.6, 4.0 Hz, 1 H), 3.94 (s, 3 H), 2.94–2.86 (m, 1 H), 2.69–2.48 (m, 5 H), 2.29 (q, J = 8.4 Hz, 1 H), 1.93–1.23 (m, 21 H), 1.17–1.05 (m, 2 H), 0.96–0.87 (m, 1 H) ppm; ^{13}C NMR (100 MHz, $CDCl_3$) δ 177.18, 173.03, 168.05, 160.22, 155.69, 155.32, 144.67, 140.95, 136.25, 134.26, 128.85, 124.44, 118.79, 105.97, 77.89, 74.63, 59.45, 55.72, 53.02, 52.20, 44.51, 34.55, 32.72, 32.65, 32.59, 31.02, 29.74, 27.21, 27.03, 26.04, 23.60, 23.57, 22.15, 20.90, 19.86, 6.67, 6.12 ppm; HRMS (ESI) *m/z*: calcd for $C_{37}H_{49}N_6O_9S$ $[M + H]^+$ 753.3276; found 753.3252. Anal. HPLC: t_R 13.05 min, purity 99%.

Cyclopentyl ((2*R*,6*S*,13a*S*,14a*R*,16a*S*,*Z*)-2-((7-methoxy-3-methylquinoxalin-2-yl)oxy)-14a-(((1-methylcyclopropyl)sulfonyl)carbamoyl)-5,16-dioxo-1,2,3,5,6,7,8,9,10,11,13a,14,14a,15,16,16a-hexadecahydrocyclopropa[*e*]pyrrolo[1,2-*a*][1,4]diazacyclopentadecin-6-yl)carbamate (23b).

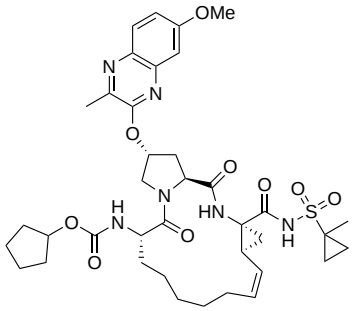

The same procedure was used as described above for compound **22b**. Compound **19b** (0.44 g, 0.58 mmol) was treated 4 N HCl in 1,4-dioxane (10 mL) to yield the amine salt **21b**, which was treated with DIEA (0.38 mL, 2.3 mmol) and *N*-(cyclopentyloxycarbonyloxy)-succinimide (0.15 g, 0.66 mmol) to provide the target compound **23b** (0.32 g, 72%) as a white solid. ^{1}H NMR (400 MHz, $CDCl_3$) δ 10.17 (s, 1 H), 7.79 (d, J = 10.0 Hz, 1 H), 7.20–7.16 (m, 2 H), 6.96 (s, 1 H), 5.91 (br s, 1 H), 5.69 (q, J = 8.8 Hz, 1 H), 5.25 (d, J = 8.0 Hz, 1 H), 4.98 (t, J = 9.6 Hz, 1 H), 4.88–4.83 (m, 1 H), 4.61 (t, J = 8.0 Hz, 1 H), 4.43 (d, J = 11.2 Hz, 1

H), 4.34–4.27 (m, 1 H), 4.05 (dd, *J* = 10.8, 4.0 Hz, 1 H), 3.94 (s, 3 H), 2.70–2.48 (m, 5 H), 2.30 (q, *J* = 8.8 Hz, 1 H), 1.93–1.23 (m, 25 H), 0.85–0.78 (m, 2 H) ppm; ^{13}C NMR (100 MHz, $CDCl_3$) *δ* 177.20, 173.01, 167.0, 160.22, 155.68, 155.31, 144.67, 140.96, 136.21, 134.27, 128.85, 124.86, 118.79, 105.98, 77.89, 74.67, 59.48, 55.72, 53.05, 52.20, 44.67, 36.43, 34.58, 32.72, 32.65, 32.57, 29.64, 27.17, 27.04, 26.09, 23.59, 23.57, 22.18, 20.91, 19.85, 18.17, 14.49, 12.51 ppm; HRMS (ESI) *m/z*: calcd for $C_{38}H_{51}N_6O_9S$ $[M + H]^+$ 767.3433; found 767.3408. Anal. HPLC: t_R 13.88 min, purity 98%.

Cyclopentyl ((2*R*,6*S*,13a*S*,14a*R*,16a*S*,*Z*)-2-((3-chloro-7-methoxyquinoxalin-2-yl)oxy)-14a-((cyclopropylsulfonyl)carbamoyl)-5,16-dioxo-1,2,3,5,6,7,8,9,10,11,13a,14,14a,15,16,16a-hexadecahydrocyclopropa[*e*]pyrrolo[1,2-*a*][1,4]diazacyclopentadecin-6-yl)carbamate (22c).

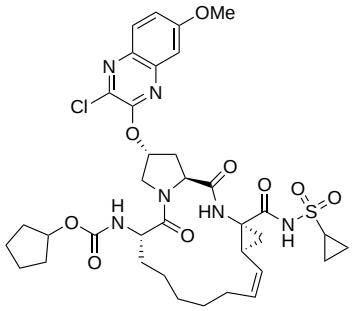

The same procedure was used as described above for compound **22b**. Compound **18c** (0.40 g, 0.53 mmol) was treated 4 N HCl in 1,4-dioxane (10 mL) to yield the amine salt **20c**, which was treated with DIEA (0.35 mL, 2.1 mmol) and *N*-(cyclopentyloxycarbonyloxy)-succinimide (0.15 g, 0.66 mmol) to provide the target compound **22c** (0.34 g, 83%) as a white solid. ^{1}H NMR (500 MHz, $CDCl_3$) *δ* 10.30 (s, 1 H), 7.79 (d, *J* = 9.0 Hz, 1 H), 7.23–7.20 (m, 2 H), 7.11 (s, 1 H), 5.89 (br s, 1 H), 5.68 (q, *J* = 9.0 Hz, 1 H), 5.30 (d, *J* = 8.0 Hz, 1 H), 4.96 (t, *J* = 9.0 Hz, 1 H), 4.84–4.80 (m, 1 H), 4.67 (t, *J* = 7.6 Hz, 1 H), 4.51 (d, *J* = 11.4 Hz, 1 H), 4.29 (t, *J* = 7.6 Hz, 1 H), 4.04 (dd, *J* = 11.0, 3.5 Hz, 1 H), 3.95 (s, 3 H), 2.93–2.87 (m, 1 H), 2.71–2.47 (m, 3 H), 2.30 (q, *J* = 8.5 Hz, 1 H), 1.95–1.20 (m, 20 H), 1.16–1.04 (m, 2 H), 0.95–0.87 (m, 1 H) ppm; ^{13}C NMR (125 MHz, $CDCl_3$) *δ* 177.11, 173.01, 168.06, 161.31, 155.75, 152.29, 140.95, 136.22, 136.18, 134.08, 128.77, 124.49, 120.08, 105.88, 77.98, 76.05, 59.48, 55.86, 52.62, 52.19, 44.53, 34.43, 32.70, 32.62, 32.47, 31.07, 29.70, 27.23, 27.06, 26.06, 23.59, 23.57, 22.25, 20.85, 6.67, 6.12 ppm; HRMS (ESI) *m/z*: calcd for $C_{36}H_{46}ClN_6O_9S$ $[M + H]^+$ 773.2730; found 773.2714. Anal. HPLC: t_R 14.35 min, purity 96%.

Cyclopentyl ((2*R*,6*S*,13a*S*,14a*R*,16a*S*,*Z*)-2-((3-chloro-7-methoxyquinoxalin-2-yl)oxy)-14a-(((1-methylcyclopropyl)sulfonyl)carbamoyl)-5,16-dioxo-1,2,3,5,6,7,8,9,10,11,13a,14,14a,15,16,16a-hexadecahydrocyclopropa[*e*]pyrrolo[1,2-*a*][1,4]diazacyclopentadecin-6-yl)carbamate (23c).

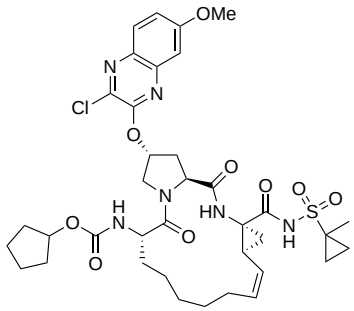

The same procedure was used as described above for compound **22b**. Compound **19c** (0.50 g, 0.64 mmol) was treated 4 N HCl in 1,4-dioxane (10 mL) to yield the amine salt **21c**, which was treated with DIEA (0.43 mL, 2.6 mmol) and *N*-(cyclopentyloxycarbonyloxy)-succinimide (0.20 g, 0.88 mmol) to provide the target compound **23c** (0.46 g, 91%) as a white solid.^{1}H NMR (400 MHz, $CDCl_3$) δ 10.22 (s, 1 H), 7.78 (d, J = 10.0 Hz, 1 H), 7.23–7.20 (m, 2 H), 7.16 (s, 1 H), 5.87 (br s, 1 H), 5.66 (q, J = 8.4 Hz, 1 H), 5.39 (d, J = 7.2 Hz, 1 H), 4.95 (t, J = 9.6 Hz, 1 H), 4.84–4.80 (m, 1 H), 4.65 (t, J = 8.0 Hz, 1 H), 4.53 (d, J = 8.4 Hz, 1 H), 4.32–4.26 (m, 1 H), 4.04 (dd, J = 12.0, 4.0 Hz, 1 H), 3.95 (s, 3 H), 2.67–2.46 (m, 3 H), 2.30 (q, J = 8.4 Hz, 1 H), 1.90–1.23 (m, 24 H), 0.84–0.78 (m, 2 H) ppm; ^{13}C NMR (100 MHz, $CDCl_3$) δ 177.18, 172.93, 167.03, 161.26, 155.73, 152.26, 140.93, 136.22, 136.16, 134.04, 128.73, 124.86, 120.08, 105.84, 77.96, 76.06, 59.52, 55.85, 52.61, 52.14, 44.68, 36.42, 34.45, 32.69, 32.60, 32.40, 29.54, 27.14, 27.07, 26.12, 23.58, 23.55, 22.23, 20.85, 18.17, 14.50, 12.52 ppm; HRMS (ESI) *m/z*: calcd for $C_{37}H_{48}ClN_6O_9S$ $[M + H]^+$ 787.2887; found 787.2872. Anal. HPLC: t_R 15.11 min, purity 99%.

Cyclopentyl ((2*R*,6*S*,13a*S*,14a*R*,16a*S*,*Z*)-14a-((cyclopropylsulfonyl)carbamoyl)-2-((3-isopropyl-7-methoxyquinoxalin-2-yl)oxy)-5,16-dioxo-1,2,3,5,6,7,8,9,10,11,13a,14,14a,15,16,16a-hexadecahydrocyclopropa[*e*]pyrrolo[1,2-*a*][1,4]diazacyclopentadecin-6-yl)carbamate (22e).

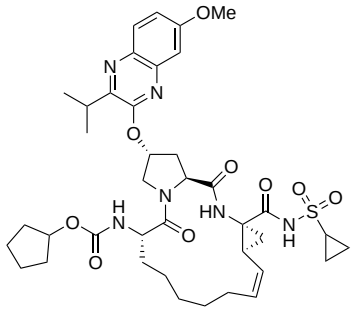

The same procedure was used as described above for compound **22b**. Compound **18e** (0.45 g, 0.58 mmol) was treated 4 N HCl in 1,4-dioxane (10 mL) to yield the amine salt **20e**, which was treated with DIEA (0.40 mL, 2.4 mmol) and *N*-(cyclopentyloxycarbonyloxy)-succinimide (0.15 g, 0.66 mmol) to provide

the target compound **22e** (0.40 g, 88%) as a white solid. ^{1}H NMR (400 MHz, $CDCl_3$) δ 10.29 (s, 1 H), 7.84 (d, J = 8.8 Hz 1 H), 7.20–7.16 (m, 2 H), 6.94 (s, 1 H), 5.93 (br s, 1 H), 5.70 (q, J = 8.4 Hz, 1 H), 5.28 (d, J = 8.0 Hz 1 H), 4.97 (t, J = 8.8 Hz, 1 H), 4.87–4.82 (m, 1 H), 4.59 (t, J = 7.2 Hz, 1 H), 4.44 (d, J = 11.2 Hz, 1 H), 4.36–4.30 (m, 1 H), 4.04 (dd, J = 11.6, 7.6 Hz, 1 H), 3.94 (s, 3 H), 3.42–3.34 (m, 1 H), 2.93–2.86 (m, 1 H), 2.70–2.48 (m, 3 H), 2.32 (q, J = 8.4 Hz, 1 H), 1.94–1.21 (m, 26 H), 1.16–1.05 (m, 2 H), 0.96–0.88 (m, 1 H) ppm; ^{13}C NMR (100 MHz, $CDCl_3$) δ 177.20, 172.97, 168.08, 160.25, 155.60, 154.40, 151.82, 140.65, 136.27, 134.23, 129.18, 124.47, 118.65, 105.81, 77.81, 74.46, 59.49, 55.70, 53.06, 52.13, 44.52, 34.63, 32.73, 32.57, 31.01, 30.63, 29.68, 27.17, 27.06, 26.08, 23.56, 22.17, 20.91, 20.48, 20.43, 6.65, 6.10 ppm; HRMS (ESI) *m/z*: calcd for $C_{39}H_{53}N_6O_9S$ $[M + H]^+$ 781.3589; found 781.3569. Anal. HPLC: t_R 16.03 min, purity 98%.

Cyclopentyl ((2*R*,6*S*,13a*S*,14a*R*,16a*S*,*Z*)-2-((3-isopropyl-7-methoxyquinoxalin-2-yl)oxy)-14a-(((1-methylcyclopropyl)sulfonyl)carbamoyl)-5,16-dioxo-1,2,3,5,6,7,8,9,10,11,13a,14,14a,15,16,16a-hexadecahydrocyclopropa[*e*]pyrrolo[1,2-*a*][1,4]diazacyclopentadecin-6-yl)carbamate (23e).

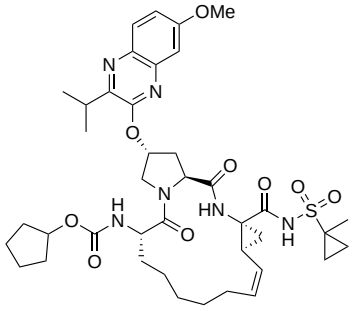

The same procedure was used as described above for compound **22b**. Compound **19e** (0.45 g, 0.57 mmol) was treated 4 N HCl in 1,4-dioxane (10 mL) to yield the amine salt **21e**, which was treated with DIEA (0.40 mL, 2.4 mmol) and *N*-(cyclopentyloxycarbonyloxy)-succinimide (0.15 g, 0.66 mmol) to provide the target compound **23e** (0.40 g, 88%) as a white solid. ^{1}H NMR (400 MHz, $CDCl_3$) δ 10.16 (s, 1 H), 7.85 (d, J = 8.8 Hz, 1 H), 7.21–7.16 (m, 2 H), 6.90 (s, 1 H), 5.93 (br s, 1 H), 5.71 (q, J = 8.4 Hz, 1 H), 5.25 (d, J = 8.0 Hz 1 H), 4.99 (t, J = 8.8 Hz, 1 H), 4.86–4.82 (m, 1 H), 4.58 (t, J = 8.0 Hz, 1 H), 4.46 (d, J = 11.2 Hz, 1 H), 4.36–4.29 (m, 1 H), 4.05 (dd, J = 11.2, 3.6 Hz, 1 H), 3.94 (s, 3 H), 3.42–3.34 (m, 1 H), 2.72–2.48 (m, 3 H), 2.32 (q, J = 8.4 Hz, 1 H), 1.94–1.21 (m, 30 H), 0.86–0.78 (m, 2 H) ppm; ^{13}C NMR (100 MHz, $CDCl_3$) δ 177.24, 172.94, 167.04, 160.25, 155.60, 154.40, 151.81, 140.67, 136.23, 134.21, 129.17, 124.89, 118.66, 105.83, 77.80, 74.52, 59.53, 55.71, 53.08, 52.13, 44.68, 36.43, 34.65, 32.72, 32.56, 30.63, 29.59, 27.14, 27.08, 26.14, 23.55, 22.19, 20.92, 20.47, 20.44,

18.17, 14.49, 12.47 ppm; HRMS (ESI) *m/z*: calcd for $C_{40}H_{55}N_6O_9S$ $[M + H]^+$ 795.3746; found 795.3723. Anal. HPLC: t_R 16.71 min, purity 99%.

Cyclopentyl ((2*R*,6*S*,13a*S*,14a*R*,16a*S*,*Z*)-14a-((cyclopropylsulfonyl)carbamoyl)-5,16-dioxo-2-((3-(thiophen-2-yl)quinoxalin-2-yl)oxy)-1,2,3,5,6,7,8,9,10,11,13a,14,14a,15,16,16a-hexadecahydrocyclopropa[*e*]pyrrolo[1,2-*a*][1,4]diazacyclopentadecin-6-yl)carbamate (22f).

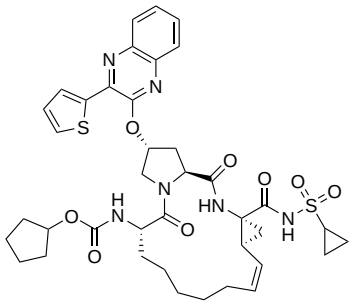

The same procedure was used as described above for compound **22b**. Compound **18f** (0.40 g, 0.51 mmol) was treated 4 N HCl in 1,4-dioxane (10 mL) to yield the amine salt **20f**, which was treated with DIEA (0.35 mL, 2.1 mmol) and *N*-(cyclopentyloxycarbonyloxy)-succinimide (0.15 g, 0.66 mmol) to provide the target compound **22f** (0.38 g, 94%) as an off-white solid. ^{1}H NMR (500 MHz, $CDCl_3$) δ 10.25 (s, 1 H), 8.08 (s, 1 H), 8.00 (d, J = 8.0 Hz, 1 H), 7.83 (d, J = 8.0 Hz, 1 H) 7.65–7.56 (m, 2 H), 7.47 (d, J = 4.0 Hz, 1 H), 7.12 (t, J = 4.0 Hz, 1 H), 6.93 (s, 1 H), 6.11 (br s, 1 H), 5.66 (q, J = 8.8 Hz, 1 H), 5.25 (d, J = 8.0 Hz, 1 H), 4.95 (t, J = 9.0 Hz, 1 H), 4.80–4.75 (m, 1 H), 4.68–4.61 (m, 2 H), 4.37 (t, J = 9.0 Hz, 1 H), 4.08 (d, J = 11.2 Hz, 1 H), 2.92–2.85 (m, 1 H), 2.75–2.69 (m, 2 H), 2.57–2.49 (m, 1 H), 2.29 (q, J = 8.6 Hz, 1 H), 1.88–1.22 (m, 23 H), 1.17–1.05 (m, 2 H), 0.94–0.87 (m, 1 H) ppm; ^{13}C NMR (125 MHz, $CDCl_3$) δ 176.98, 173.11, 167.92, 155.68, 152.27, 139.71, 138.90, 138.85, 136.28, 130.44, 130.04, 129.51, 128.48, 128.08, 127.40, 126.84, 124.47, 77.90, 75.50, 59.51, 53.24, 52.26, 44.57, 34.61, 32.89, 32.78, 32.48, 31.06, 29.74, 27.19, 27.01, 26.01, 23.58, 22.29, 20.94, 6.68, 6.14 ppm; HRMS (ESI) *m/z*: calcd for $C_{39}H_{47}N_6O_8S_2$ $[M + H]^+$ 791.2891; found 791.2872. Anal. HPLC: t_R 16.39 min, purity 99%.

Cyclopentyl ((2*R*,6*S*,13a*S*,14a*R*,16a*S*,*Z*)-14a-((cyclopropylsulfonyl)carbamoyl)-2-((3-ethylquinoxalin-2-yl)oxy)-5,16-dioxo-1,2,3,5,6,7,8,9,10,11,13a,14,14a,15,16,16a-hexadecahydrocyclopropa[*e*]pyrrolo[1,2-*a*][1,4]diazacyclopentadecin-6-yl)carbamate (22g).

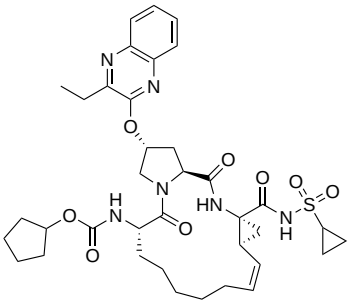

The same procedure was used as described above for compound **22b**. Compound **18g** (0.50 g, 0.69 mmol) was treated 4 N HCl in 1,4-dioxane (10 mL) to yield the amine salt **20g**, which was treated with DIEA (0.46 mL, 2.8 mmol) and *N*-(cyclopentyloxycarbonyloxy)-succinimide (0.18 g, 0.79 mmol) to provide the target compound **22g** (0.42 g, 83%) as a white solid. ^{1}H NMR (400 MHz, $CDCl_3$) δ 10.31 (s, 1 H), 7.95 (d, J = 8.0 Hz, 1 H), 7.81 (d, J = 8.0 Hz, 1 H), 7.63–7.52 (m, 2 H), 7.00 (s, 1 H), 5.94 (br s, 1 H), 5.69 (q, J = 8.4 Hz, 1 H), 5.26 (d, J = 8.0 Hz, 1 H), 4.96 (t, J = 9.6 Hz, 1 H), 4.83–4.78 (m, 1 H), 4.62 (t, J = 8.0 Hz, 1 H), 4.46 (d, J = 12.0 Hz, 1 H), 4.32–4.25 (m, 1 H), 4.04 (dd, J = 11.6, 3.6 Hz, 1 H), 2.95–2.85 (m, 3 H), 2.66–2.50 (m, 3 H), 2.30 (q, J = 8.8 Hz, 1 H), 1.93–1.05 (m, 25 H), 0.95–0.88 (m, 1 H) ppm; ^{13}C NMR (400 MHz, $CDCl_3$) δ 177.18, 173.05, 168.10, 155.62, 154.51, 152.11, 139.30, 138.85, 136.29, 128.99, 128.18, 126.96, 126.72, 124.50, 77.82, 74.68, 59.46, 53.12, 52.20, 44.55, 34.56, 32.69, 32.57, 31.00, 29.70, 27.12, 27.03, 26.74, 26.02, 23.55, 22.17, 20.94, 11.37, 6.66, 6.11 ppm; HRMS (ESI) *m/z*: calcd for $C_{37}H_{49}N_6O_8S$ $[M + H]^+$ 737.3327; found 737.3306. Anal. HPLC: t_R 14.64 min, purity 99%.

Synthesis of Intermediates and Linear Final Compounds

1-(*tert*-Butyl) 2-methyl (2*S*,4*R*)-4-((3-ethyl-7-methoxyquinoxalin-2-yl)oxy)pyrrolidine-1,2-dicarboxylate (4a).

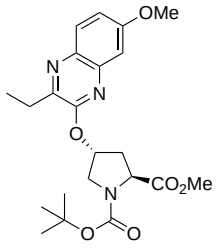

A solution of 3-ethyl-7-methoxyquinoxalin-2(1*H*)-one (3.0 g, 14.7 mmol) in anhydrous NMP (45 mL) was treated with Cs_2CO_3 (7.40 g, 22.7 mmol). After stirring the reaction mixture at room temperature for 15 min, brosylated *cis*-hydroxyproline derivative 1-(*tert*-butyl) 2-methyl (2*S*,4*S*)-4-(((4-bromophenyl)sulfonyl)oxy)pyrrolidine-1,2-dicarboxylate (6.20 g, 13.3 mmol) was added in one portion. The reaction mixture was heated to 55 °C, stirred for 4 h, and then another portion of brosylated *cis*-hydroxyproline derivative (0.48 g, 1.0 mmol) was added. The resulting reaction mixture was stirred at 55 °C for additional 2 h, cooled to room temperature, quenched with aqueous 1 N HCl solution (150 mL), and extracted with EtOAc (300 mL). The organic fraction was washed successively with saturated aqueous $NaHCO_3$ and NaCl (150 mL each), dried (Na_2SO_4), filtered, and evaporated under reduced pressure. The residue was purified by flash column chromatography using 15–30% EtOAc/hexanes as the eluent to provide **4a** (5.50 g, 87%) as a white foamy solid. ^{1}H NMR (400 MHz, $CDCl_3$) (mixture of rotamers, major rotamer) δ 7.85 (d, J = 9.0 Hz, 1 H), 7.18 (m, 1H), 7.11 (d, J = 2.8 Hz, 1 H), 5.73 (br s, 1 H), 4.47 (t, J = 8.0 Hz, 1 H), 3.98–3.86 (m, 5 H), 3.78 (s, 3 H), 2.92 (q, J = 7.2 Hz, 2 H), 2.68–2.60 (m, 1 H), 2.43–2.36 (m, 1 H), 1.43 (s, 9 H), 1.31 (t, J = 7.2 Hz, 3 H) ppm; ^{13}C NMR (100 MHz, $CDCl_3$) δ 173.56, 160.59, 155.38, 154.02, 148.95, 141.26, 134.12, 129.07, 119.02, 106.11, 80.76, 73.81, 58.43, 55.93, 52.73, 52.40, 36.88, 28.47, 26.68, 11.97 ppm; HRMS (ESI) *m/z*: $[M + H]^+$ calcd for $C_{22}H_{30}N_3O_6$, 432.2129; found 432.2135.

1-(*tert*-Butyl) 2-methyl (2*S*,4*R*)-4-((7-methoxy-3-methylquinoxalin-2-yl)oxy)pyrrolidine-1,2-dicarboxylate (4b).

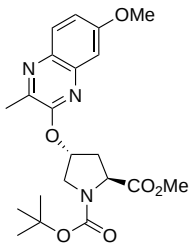

The same procedure was used as described above for compound **4a**. 7-Methoxy-3-methylquinoxalin-2(1*H*)-one (6.2 g, 32.6 mmol) in NMP (100 mL) was treated with Cs_2CO_3 (16.0 g, 49.0 mmol) and activated *cis*-hydroxyproline derivative (15.0 g, 32.3 mmol) to provide **4b** (10.0 g, 74%) as a white foamy solid. ^{1}H NMR (500 MHz, $CDCl_3$) (mixture of rotamers, major rotamer) δ 7.80 (d, J = 9.0 Hz, 1 H), 7.17 (dd, J = 9.0, 3.0 Hz, 1 H), 7.11 (d, J = 2.5 Hz, 1 H), 5.71 (br s, 1 H), 4.48 (t, J = 8.0 Hz, 1 H), 3.99–3.91 (m, 4 H), 3.87 (d, J = 12.5 Hz, 1H), 3.78 (s, 3 H), 2.67–2.58 (m, 1 H), 2.56 (s, 3 H), 2.43–2.37 (m, 1 H), 1.43 (s, 9 H) ppm; ^{13}C NMR (125 MHz, $CDCl_3$) δ 173.36, 160.24, 155.51, 153.81, 144.60, 141.04, 134.22, 128.95, 118.63, 105.95, 80.54, 73.59, 58.20, 55.68, 52.48, 52.20, 36.70, 28.26, 19.93 ppm; HRMS (ESI) *m/z*: $[M + H]^+$ calcd for $C_{21}H_{28}N_3O_6$, 418.1973; found 418.1976.

1-(*tert*-Butyl) 2-methyl (2*S*,4*R*)-4-((3-isopropyl-7-methoxyquinoxalin-2-yl)oxy)pyrrolidine-1,2-dicarboxylate (4c).

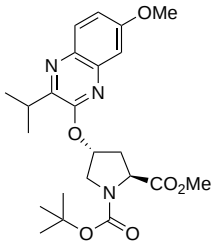

The same procedure was used as described above for compound **4a**. 3-Isopropyl-7-methoxyquinoxalin-2(1*H*)-one (4.0 g, 18.3 mmol) in NMP (65 mL) was treated with Cs_2CO_3 (9.0 g, 27.6 mmol) and activated *cis*-hydroxyproline derivative (8.30 g, 17.9 mmol) to provide **4c** (7.30 g, 90%) as a colorless gummy solid. ^{1}H NMR (500 MHz, $CDCl_3$) (mixture of rotamers, major rotamer) δ 7.83 (d, J = 8.0 Hz, 1 H), 7.16 (d, J = 8.4 Hz, 1 H), 7.10 (s, 1 H) 5.74 (br s, 1 H), 4.48 (t, J = 7.5 Hz, 1 H), 3.92–3.87 (m, 5 H), 3.78 (s, 3 H), 3.41–3.36 (m, 1 H), 2.68–2.59 (m, 1 H), 2.42–2.35 (m, 1 H), 1.43 (s, 9 H), 1.31 (t, J = 7.0 Hz, 6 H) ppm; ^{13}C NMR (125 MHz, $CDCl_3$) δ 173.37, 160.19, 154.62, 153.82, 152.00, 140.68, 134.31, 129.39, 118.41, 105.80, 80.49, 73.36, 58.28, 55.67, 52.58, 52.19, 36.68, 30.81, 28.25, 20.43, 20.38 ppm; HRMS (ESI) *m/z*: $[M + H]^+$ calcd for $C_{23}H_{32}N_3O_6$, 446.2286; found 446.2287.

1-(*tert*-butyl) 2-methyl (2*S*,4*R*)-4-((3-chloro-7-methoxyquinoxalin-2-yl)oxy)pyrrolidine-1,2-dicarboxylate (4d).

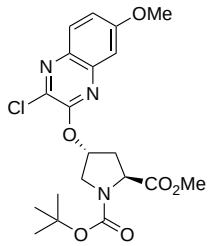

The same procedure was used as described above for compound **4a**. 3-Chloro-7-methoxyquinoxalin-2(1*H*)-one (4.0 g, 19.0 mmol) in NMP (60 mL) was treated with Cs_2CO_3 (9.30 g, 28.6 mmol) and activated *cis*-hydroxyproline derivative (8.40 g, 18.1 mmol) to provide **4d** (6.30 g, 76%) as an off-white foamy solid. ^{1}H NMR (400 MHz, $CDCl_3$) (mixture of rotamers, major rotamer) δ 7.80 (d, J = 8.8 Hz, 1 H), 7.21 (dd, J = 8.8, 2.8 Hz, 1 H), 7.12 (d, J = 2.8 Hz, 1 H), 5.69 (br s, 1 H), 4.52 (t, J = 7.6 Hz, 1 H), 4.0–3.94 (s, 4 H), 3.88 (d, J = 12.8 Hz, 1 H), 3.78 (s, 3 H), 2.72–2.62 (m, 1 H), 2.45–2.37 (m, 1 H), 1.43 (s, 9 H) ppm; ^{13}C NMR (400 MHz, $CDCl_3$) δ 173.32, 162.35, 153.84, 152.48, 141.03, 136.11, 134.06, 129.97, 119.95, 105.83, 80.60, 75.02, 58.10, 55.81, 52.36 , 52.10, 36.64, 28.27 ppm; HRMS (ESI) *m/z*: $[M + H]^+$ calcd for $C_{20}H_{25}ClN_3O_6$, 438.1426; found 438.1438.

1-(*tert*-Butyl) 2-methyl (2*S*,4*R*)-4-((7-methoxy-3-(trifluoromethyl)quinoxalin-2-yl)oxy)pyrrolidine-1,2-dicarboxylate (4e).

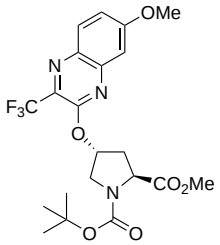

The same procedure was used as described above for compound **4a**. 7-Methoxy-3-(trifluoromethyl)quinoxalin-2(1*H*)-one (4.76 g, 19.5 mmol) in anhydrous NMP (65 mL) was treated with Cs_2CO_3 (9.80 g, 30.0 mmol) and activated *cis*-hydroxyproline derivative (9.0 g, 19.4 mmol) to provide **4e** (6.50 g, 71%) as a pale yellow foamy solid. ^{1}H NMR (500 MHz, $CDCl_3$) (mixture of rotamers, major rotamer) δ 7.77 (d, J = 9.0 Hz, 1 H), 7.48–7.43 (m, 2 H), 5.76 (br s, 1 H), 4.50 (t, J = 8.0 Hz, 1 H), 3.97–3.91 (m, 5 H), 3.78 (s, 3 H), 2.69–2.64 (m, 1 H), 2.41–2.34 (m, 1 H), 1.42 (s, 9 H) ppm; ^{13}C NMR (125 MHz, $CDCl_3$) δ 173.43, 159.58, 153.98, 152.11, 138.39, 137.22, 127.99, 125.73, 120.70 (q, J = 273.4 Hz), 107.64, 80.69, 74.62, 58.27, 56.02, 52.32, 52.11, 36.70, 28.34 ppm; ^{19}F NMR (470 MHz, $CDCl_3$); −67.73 ppm; HRMS (ESI) *m/z*: $[M + H]^+$ calcd for $C_{21}H_{25}F_3N_3O_6$, 472.1690; found 472.1689.

Methyl (2*S*,4*R*)-1-((*S*)-2-((*tert*-butoxycarbonyl)amino)-3,3-dimethylbutanoyl)-4-((3-ethyl-7-methoxyquinoxalin-2-yl)oxy)pyrrolidine-2-carboxylate (6a).

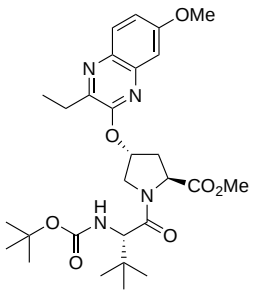

A solution of P2 intermediate **4a** (2.75 g, 6.4 mmol) in anhydrous CH_2Cl_2 (20 mL) was treated with a solution of 4 N HCl in 1,4-dioxane (20 mL). After stirring the reaction mixture at room temperature for 3 h, solvents were evaporated under reduced pressure, and the residue was dried under high vacuum. The pale yellow solid was triturated with diethyl ether (20 mL), filtered and washed with diethyl ether diethyl ether (3 × 5 mL) to yield the amine salt **5a** (2.30 g, 98%) as an off-white powder.

A mixture of amine salt **5a** (1.15 g, 3.1 mmol) and Boc-Tle-OH (0.88 g, 3.8 mmol) in anhydrous DMF (20 mL) was treated with DIEA (2.52 mL, 15.2 mmol) and HATU (2.17 g, 5.7 mmol). The resulting reaction mixture was stirred at room temperature for 4 h, then diluted with EtOAc (150 mL), and washed successively with aqueous 0.5 N HCl, saturated aqueous $NaHCO_3$, and saturated aqueous NaCl (75 mL each). The organic portion was dried (Na_2SO_4), filtered, and evaporated under reduced pressure. The residue was purified by flash chromatography using 25–30% EtOAc/hexanes as the eluent to provide **6a** (1.45 g, 85%) as a white foamy solid. ^{1}H NMR (400 MHz, $CDCl_3$) (mixture of rotamers, major rotamer) δ 7.87 (d, J = 9.2 Hz, 1 H), 7.19 (dd, J = 8.8, 2.8 Hz, 1 H), 7.13 (d, J = 2.8 Hz, 1 H), 5.86 (br s, 1 H), 5.18 (d, J = 9.2 Hz, 1 H), 4.73 (t, J = 8.4 Hz, 1 H), 4.27–4.22 (m, 2 H), 4.11–4.04 (m, 1 H), 3.94 (s, 3 H), 3.78 (s, 3 H), 2.87 (q, J = 7.2 Hz, 2 H), 2.71–2.65 (m, 1 H), 2.39–2.31 (m, 1 H), 1.33 (s, 9 H), 1.27 (t, J = 7.2 Hz, 3 H), 1.05 (s, 9 H) ppm; ^{13}C NMR (100 MHz, $CDCl_3$) δ 172.50, 171.60, 160.57, 155.92, 155.11, 149.02, 141.11, 134.13, 129.13, 118.99, 106.20, 79.79, 74.37, 58.76, 58.19, 55.92, 53.92, 52.57, 35.85, 35.23, 28.43, 26.50, 11.85 ppm; HRMS (ESI) *m/z*: $[M + Na]^+$ calcd for $C_{28}H_{41}N_4O_7$, 545.2970; found 545.2973.

Methyl (2*S*,4*R*)-1-((*S*)-2-((*tert*-butoxycarbonyl)amino)-3,3-dimethylbutanoyl)-4-((7-methoxy-3-methylquinoxalin-2-yl)oxy)pyrrolidine-2-carboxylate (6b).

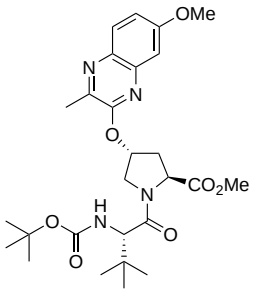

The same procedure was used as described above for compound **6a**. Compound **4b** (3.60 g, 8.6 mmol) was treated with 4 N HCl (25 mL) to afford the amine salt **5b** (3.0 g, 8.5 mmol), which was coupled with Boc-Tle-OH (2.40 g, 10.4 mmol) using DIEA (7.0 mL, 42.4 mmol) and HATU (5.65 g, 14.8 mmol) to provide **6b** (3.50 g, 78%) as a white foamy solid. ^{1}H NMR (500 MHz, $CDCl_3$) (mixture of rotamers, major rotamer) δ 7.80 (d, J = 9.0 Hz, 1 H), 7.18 (dd, J = 9.0, 2.5 Hz, 1 H), 7.12 (d, J = 3.0 Hz, 1 H), 5.84 (br s, 1 H), 5.18 (d, J = 9.5 Hz, 1 H), 4.75 (t, J = 8.5 Hz, 1 H), 4.27–4.22 (m, 2 H), 4.07 (dd, J = 11.5, 4.5 Hz, 1 H), 3.94 (s, 3 H),

3.77 (s, 3 H), 2.70–2.65 (m, 1 H), 2.52 (s, 3 H), 2.38–2.32 (m, 1 H), 1.34 (s, 9 H), 1.05 (s, 9 H) ppm; ^{13}C NMR (125 MHz, $CDCl_3$) δ 172.42, 171.57, 160.36, 155.87, 155.39, 144.86, 141.05, 134.51, 129.15, 118.76, 106.19, 79.71, 74.30, 58.70, 58.03, 55.79, 53.81, 52.48, 35.70, 35.15, 28.36, 26.42, 19.97 ppm; HRMS (ESI) *m/z*: $[M + H]^+$ calcd for $C_{27}H_{39}N_4O_7$, 531.2813; found 531.2807.

Methyl (2*S*,4*R*)-1-((*S*)-2-((*tert*-butoxycarbonyl)amino)-3,3-dimethylbutanoyl)-4-((3-isopropyl-7-methoxyquinoxalin-2-yl)oxy)pyrrolidine-2-carboxylate (6c).

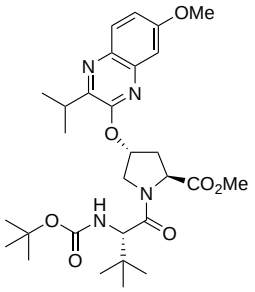

The same procedure was used as described above for compound **6a**. Compound **4c** (1.30 g, 2.92 mmol) was treated with 4 N HCl (12 mL) to afford the amine salt **5c** (1.05 g, 2.75 mmol), which was coupled with Boc-Tle-OH (0.83 g, 3.60 mmol) using DIEA (2.38 mL, 14.4 mmol) and HATU (1.85 g, 4.86 mmol) to provide **6c** (1.30 g, 85%) as a white foamy solid. ^{1}H NMR (500 MHz, $CDCl_3$) (mixture of rotamers, major rotamer) δ 7.83 (d, J = 9.0 Hz, 1 H), 7.17 (dd, J = 9.0, 3.0 Hz, 1 H), 7.11 (d, J = 3.0 Hz, 1 H), 5.88 (br s, 1 H), 5.20 (d, J = 9.5 Hz, 1 H), 4.72 (t, J = 8.5 Hz, 1 H), 4.26–4.21 (m, 2 H), 4.07 (dd, J = 11.5, 4.0 Hz, 1 H), 3.94 (s, 3 H), 3.77 (s, 3 H), 3.39–3.33 (m, 1 H), 2.71–2.65 (m, 1 H), 2.38–2.32 (m, 1 H), 1.33 (s, 9 H), 1.28 (t, J = 7.0 Hz, 6 H), 1.05 (s, 9 H) ppm; ^{13}C NMR (125 MHz, $CDCl_3$) δ 172.41, 171.45, 160.33, 155.77, 154.47, 152.19, 140.67, 134.59, 129.56, 118.57, 106.01, 79.64, 74.04, 58.66, 58.14, 55.78, 53.91, 52.46, 35.88, 35.16, 30.80, 28.36, 26.40, 20.61, 20.52 ppm; HRMS (ESI) *m/z*: $[M + H]^+$ calcd for $C_{29}H_{43}N_4O_7$, 559.3126; found 559.3112.

Methyl (2*S*,4*R*)-1-((*S*)-2-((*tert*-butoxycarbonyl)amino)-3,3-dimethylbutanoyl)-4-((3-chloro-7-methoxyquinoxalin-2-yl)oxy)pyrrolidine-2-carboxylate (6d).

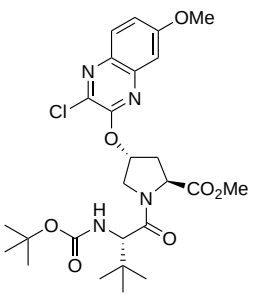

The same procedure was used as described above for compound **6a**. Compound **4d** (1.05 g, 2.40 mmol) was treated with 4 N HCl (10 mL) to afford the amine salt **5d** (0.89 g, 2.40 mmol), which was coupled with Boc-Tle-OH (0.66 g, 2.86 mmol) using DIEA (1.90 mL, 11.5 mmol) and HATU (1.41 g, 3.72 mmol) to provide **6d** (1.0 g, 76%) as an off-white foamy solid. ^{1}H NMR (500 MHz, $CDCl_3$) (mixture of rotamers, major rotamer) δ 7.81 (d, J = 9.0 Hz, 1 H), 7.22 (dd, J = 9.0, 2.5 Hz, 1 H), 7.15 (d, J = 3.0 Hz, 1 H), 5.81 (br s, 1 H), 5.21 (d, J = 10.0 Hz, 1 H), 4.79 (t, J = 8.5 Hz, 1 H), 4.31 (d, J = 12.0 Hz, 1 H), 4.21 (d, J = 10.0 Hz, 1 H), 4.09 (dd, J = 11.5, 4.0 Hz, 1 H), 3.96 (s, 3 H), 3.78 (s, 3 H), 2.74–2.68 (m, 1 H), 2.40–2.34 (m, 1 H), 1.32 (s, 9 H), 1.04 (s, 9 H) ppm; ^{13}C NMR (125 MHz, $CDCl_3$) δ 172.36, 171.54, 161.40, 155.87, 152.36, 140.99, 136.27, 134.26, 129.05, 120.05, 106.05, 79.77, 75.69, 58.63, 58.02, 55.92, 53.43, 52.50, 35.74, 34.98, 28.36, 26.40 ppm; HRMS (ESI) *m/z*: $[M + H]^+$ calcd for $C_{26}H_{36}ClN_4O_7$, 551.2267; found 551.2257.

Methyl (2*S*,4*R*)-1-((*S*)-2-((*tert*-butoxycarbonyl)amino)-3,3-dimethylbutanoyl)-4-((7-methoxy-3-(trifluoromethyl)quinoxalin-2-yl)oxy)pyrrolidine-2-carboxylate (6e).

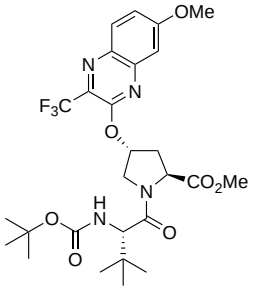

The same procedure was used as described above for compound **6a**. Compound **4e** (1.30 g, 2.76 mmol) was treated with 4 N HCl (10 mL) to afford the amine salt **5e** (1.10 g, 2.70 mmol), which was coupled with Boc-Tle-OH (0.81 g, 3.50 mmol) using DIEA (2.30 mL, 14.0 mmol) and HATU (2.0 g, 5.25 mmol) to provide **6e** (1.50 g, 95%) as a pale yellow foamy solid. ^{1}H NMR (500 MHz, $CDCl_3$) (mixture of rotamers, major rotamer) δ 7.78 (d, J = 9.0 Hz, 1 H), 7.47 (dd, J = 9.5, 3.0 Hz, 1 H), 7.43 (d, J = 2.5 Hz, 1 H), 5.87 (br s, 1 H), 5.22 (d, J = 9.5 Hz, 1 H), 4.74 (t, J = 8.5 Hz, 1 H), 4.27 (d, J = 12.0 Hz, 1 H), 4.20 (d, J = 9.5 Hz, 1 H), 4.11–4.07 (m, 1 H), 3.94 (s, 3 H), 3.77 (s, 3 H), 2.71–2.66 (m, 1 H), 2.38–2.32 (m, 1 H), 1.30 (s, 9 H), 1.03 (s, 9 H) ppm; ^{13}C NMR (125 MHz, $CDCl_3$) δ 172.36, 171.47, 159.64, 155.84, 151.89, 138.51, 137.09, 134.59 (q, J = 35.9 Hz), 128.04, 125.73, 120.69 (d, J = 273.8 Hz), 107.65, 79.69, 75.05, 58.58, 57.92, 56.03, 53.47, 52.49, 35.75, 34.97, 28.26, 26.37 ppm; ^{19}F NMR (470 MHz, $CDCl_3$); −67.84 ppm; HRMS (ESI) *m/z*: $[M + H]^+$ calcd for $C_{27}H_{36}F_3N_4O_7Na$, 585.2531; found 585.2516.

***tert*-Butyl ((*S*)-1-((2*S*,4*R*)-2-(((1*R*,2*S*)-1-((cyclopropylsulfonyl)carbamoyl)-2-vinylcyclopropyl)carbamoyl)-4-((3-ethyl-7-methoxyquinoxalin-2-yl)oxy)pyrrolidin-1-yl)-3,3-dimethyl-1-oxobutan-2-yl)carbamate (3). Et-tBu-H**

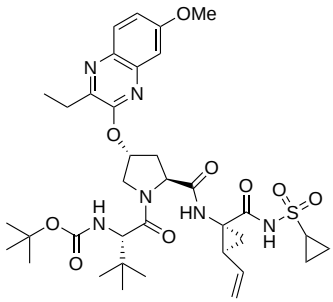

A solution of P2–P3 intermediate **6a** (1.80 g, 3.31 mmol) in THF-H_2O mixture (1:1, 50 mL) was treated with LiOH.H_2O (0.46 g, 11.0 mmol). The resulting reaction mixture was stirred at room temperature for 24 h. The reaction mixture was cooled to ~5 °C, acidified to a pH of 2.0 by slow addition of aqueous 0.50 N HCl (~ 75 mL), and extracted with EtOAc (2 × 150 mL). The organic portions were washed separately with saturated aqueous NaCl (75 ml), dried (Na_2SO_4), filtered, and evaporated under reduced pressure. The gummy residue was dissolved in $CHCl_3$ (20 mL), concentrated under reduced pressure, and the residue was dried under high vacuum overnight to yield the acid **7a** (1.75 g, 100%) as a white foamy solid.

A mixture of acid **7a** (0.88 g, 1.64 mmol) and P1–P1' amine salt **8** (0.48 g, 1.80 mmol) in anhydrous DMF (15 mL) was treated with DIEA (1.10 mL, 6.60 mmol) and HATU (0.94 g, 2.46 mmol). The resulting reaction mixture was stirred at room temperature for 2 h, then diluted with EtOAc (100 mL) and washed successively with aqueous 0.5 N HCl, saturated aqueous $NaHCO_3$, and saturated aqueous NaCl (50 mL each). The organic portion was dried (Na_2SO_4), filtered, and evaporated under reduced pressure. The residue was purified by flash chromatography using 50–80% EtOAc/hexanes as the eluent to provide compound **3** (0.95 g, 78%) as a white solid. ^{1}H NMR (400 MHz, $CDCl_3$) δ 10.08 (s, 1 H), 7.84 (d, J = 9.2 Hz, 1 H), 7.20–7.14 (m, 2 H), 7.07 (s, 1 H), 5.90 (br s, 1 H), 5.79–5.72 (m, 1 H), 5.28–5.22 (m, 2 H), 5.15 (d, J = 10.4 Hz, 1 H), 4.48 (t, J = 8.4 Hz, 1 H), 4.30 (d, J = 12.0 Hz, 1 H), 4.24 (d, J = 9.6 Hz, 1 H), 4.03 (dd, J = 11.6, 3.2 Hz, 1 H), 3.94 (s, 3 H), 2.94–2.83 (m, 3 H), 2.56–2.52 (m, 2 H), 2.12 (q, J = 8.4 Hz, 1 H), 1.97 (dd, J = 8.0, 6.0 Hz, 1 H), 1.48 (dd, J = 9.2, 5.6 Hz, 1 H), 1.40–1.22 (m, 13 H), 1.10–0.96 (m, 12 H) ppm; ^{13}C NMR (100 MHz, $CDCl_3$) δ 173.05, 172.77, 168.64, 160.56, 155.87, 154.99, 148.86, 141.05, 134.51, 132.76, 129.32, 119.01, 118.85, 106.19, 80.06, 74.37, 60.09, 58.96, 55.92, 54.51, 42.05, 38.85, 35.81, 35.75, 34.51, 31.49, 28.43, 26.71, 22.63, 11.84, 6.50, 6.45 ppm; HRMS (ESI) m/z: $[M + H]^+$ calcd for $C_{36}H_{51}N_6O_9S$, 743.3433; found 743.3431.

***tert*-Butyl ((*S*)-1-((2*S*,4*R*)-2-(((1*R*,2*S*)-1-((cyclopropylsulfonyl)carbamoyl)-2-vinylcyclopropyl)carbamoyl)-4-((7-methoxy-3-methylquinoxalin-2-yl)oxy)pyrrolidin-1-yl)-3,3-dimethyl-1-oxobutan-2-yl)carbamate (10b). Me-tBu-H**

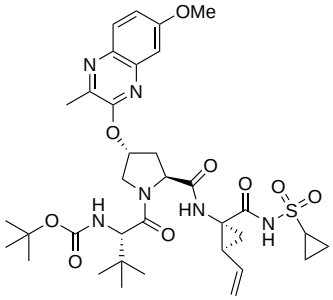

The same procedure was used as described above for compound **3**. Ester **6b** (1.30 g, 2.45 mmol) was treated with $LiOH.H_2O$ (0.36 g, 8.60 mmol) to afford acid **7b** (1.25 g, 2.42 mmol). A portion of acid **7b** (0.62 g, 1.20 mmol) was reacted with amine salt **8** (0.40 g, 1.50 mmol) using DIEA (0.80 mL, 4.84 mmol) and HATU (0.70 g, 1.84 mmol) to provide compound **10b** (0.64 g, 74%) as a white solid. ^{1}H NMR (400 MHz, $CDCl_3$) δ 10.08 (s, 1 H), 7.79 (d, J = 9.2 Hz, 1 H), 7.18 (dd, J = 8.8, 2.4 Hz, 1 H), 7.13 (d, J = 2.8 Hz, 2 H), 5.86 (br s, 1 H), 5.80–5.71 (m, 1 H), 5.28–5.23 (m, 2 H), 5.13 (d, J = 10.8 Hz, 1 H), 4.51 (t, J = 8.4 Hz, 1 H), 4.30 (d, J = 11.6 Hz, 1 H), 4.24 (d, J = 9.2 Hz, 1 H), 4.03 (dd, J = 12.0, 4.0 Hz, 1 H), 3.94 (s, 3 H), 2.93–2.86 (m, 1 H), 2.56–2.50 (m, 5 H), 2.11 (q, J = 9.2 Hz, 1 H), 1.95 (dd, J = 8.0, 6.0 Hz, 1 H), 1.49–1.43 (m, 2 H), 1.33 (s, 9 H), 1.07–0.97 (m, 12 H) ppm; ^{13}C NMR (100 MHz, $CDCl_3$) δ 172.89, 172.49, 168.48, 160.25, 155.67, 155.12, 144.48, 140.89, 134.31, 132.51, 128.94, 118.78, 118.64, 106.0, 79.84, 74.25, 59.79, 58.72, 55.68, 54.23, 41.83, 35.55, 35.42, 34.21, 31.23, 28.22, 26.48, 22.32, 19.81, 6.27, 6.22 ppm; HRMS (ESI) *m/z*: $[M + H]^+$ calcd for $C_{35}H_{49}N_6O_9S$, 729.3276; found 729.3283.

***tert*-Butyl ((*S*)-1-((2*S*,4*R*)-2-(((1*R*,2*S*)-1-((cyclopropylsulfonyl)carbamoyl)-2-vinylcyclopropyl)carbamoyl)-4-((3-isopropyl-7-methoxyquinoxalin-2-yl)oxy)pyrrolidin-1-yl)-3,3-dimethyl-1-oxobutan-2-yl)carbamate (10c). i-Pr-tBu-H**

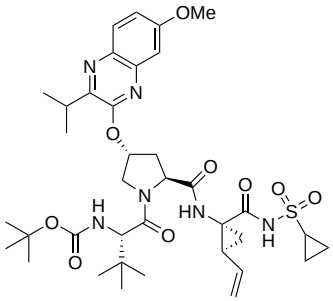

The same procedure was used as described above for compound **3**. Ester **6c** (2.25 g, 4.03 mmol) was treated with $LiOH.H_2O$ (0.68 g, 16.1 mmol) to afford acid **7c** (2.15 g, 3.95 mmol). A portion of acid **7c** (1.0 g, 1.84 mmol) was coupled with amine salt **8** (0.60 g, 2.25 mmol) using DIEA (1.25 mL, 7.40 mmol) and HATU (1.0 g, 2.63 mmol) to provide compound **10c** (1.25 g, 90%) as a white solid. ^{1}H

NMR (400 MHz, $CDCl_3$) δ 10.11 (s, 1 H), 7.83 (d, J = 9.2 Hz, 1 H), 7.18 (dd, J = 8.8, 2.4 Hz, 1 H), 7.12 (d, J = 2.8 Hz, 1 H), 7.02 (s, 1 H), 5.91 (br s, 1 H), 5.82–5.73 (m, 1 H), 5.28–5.23 (m, 2 H), 5.14 (d, J = 10.4 Hz, 1 H), 4.46 (t, J = 8.4 Hz, 1 H), 4.29–4.22 (m, 2 H), 4.06 (dd, J = 11.6, 4.0 Hz, 1 H), 3.94 (s, 3 H), 3.37–3.30 (m, 1 H), 2.94–2.87 (m, 1 H), 2.57–2.49 (m, 2 H), 2.12 (q, J = 8.4 Hz, 1 H), 1.96 (dd, J = 8.4, 6.0 Hz, 1 H), 1.48 (dd, J = 9.6, 6.0 Hz, 1 H), 1.40–1.20 (m, 15 H), 1.05–0.95 (m, 12 H) ppm; ^{13}C NMR (100 MHz, $CDCl_3$) δ 172.79, 172.42, 168.52, 160.23, 155.60, 154.19, 151.78, 140.52, 134.42, 132.55, 129.37, 118.61, 105.81, 79.78, 74.02, 59.97, 58.68, 55.68, 54.34, 41.75, 35.70, 35.57, 34.37, 31.25, 30.67, 28.21, 26.47, 22.57, 20.51, 20.44, 6.29, 6.21 ppm; HRMS (ESI) m/z: $[M + H]^+$ calcd for $C_{37}H_{53}N_6O_9S$, 757.3589; found 757.3588.

tert-Butyl ((_S_)-1-((2_S_,4_R_)-4-((3-chloro-7-methoxyquinoxalin-2-yl)oxy)-2-(((1_R_,2_S_)-1-((cyclopropylsulfonyl)carbamoyl)-2-vinylcyclopropyl)carbamoyl)pyrrolidin-1-yl)-3,3-dimethyl-1-oxobutan-2-yl)carbamate (10d). Cl-tBu-H

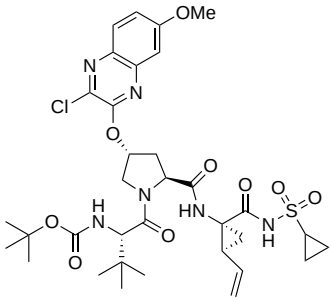

The same procedure was used as described above for compound **3**. Ester **6d** (2.0 g, 3.63 mmol) was treated with $LiOH.H_2O$ (0.60 g, 14.3 mmol) to afford acid **7d** (1.90 g, 3.54 mmol). A portion of acid **7d** (0.92 g, 1.71 mmol) was coupled with amine salt **8** (0.50 g, 1.88 mmol) using DIEA (1.15 mL, 6.96 mmol) and HATU (0.95 g, 2.50 mmol) to provide compound **10d** (1.0 g, 78%) as a white solid. ^{1}H NMR (400 MHz, $CDCl_3$) δ 10.07 (s, 1 H), 7.81 (d, J = 8.8 Hz, 1 H), 7.26–7.22 (1 H), 7.18 (d, J = 2.4 Hz, 1 H), 7.04 (s, 1 H), 5.87 (br s, 1 H), 5.81–5.74 (m, 1 H), 5.29–5.20 (m, 2 H), 5.14 (d, J = 10.4 Hz, 1 H), 4.55 (t, J = 8.4 Hz, 1 H), 4.37 (d, J = 11.6 Hz, 1 H), 4.21 (d, J = 9.6 Hz, 1 H), 4.05 (dd, J = 12.0, 3.6 Hz, 1 H), 3.96 (s, 3 H), 2.93–2.88 (m, 1 H), 2.57 (dd, J = 7.6, 2.8 Hz, 2 H), 2.12 (q, J = 8.8 Hz, 1 H), 1.98 (dd, J = 7.6, 6.0 Hz, 1 H), 1.48 (dd, J = 9.6, 6.0, 1 H), 1.38–1.34 (m, 2 H), 1.31 (s, 9 H), 1.09–0.98 (m, 11 H) ppm; ^{13}C NMR (100 MHz, $CDCl_3$) δ 172.94, 172.63, 168.57, 161.46, 155.82, 152.21, 141.01, 136.09, 134.25, 132.65, 129.00, 120.22, 118.77, 106.05, 80.04, 75.77, 60.55, 59.97, 58.85, 54.01, 42.01, 35.69, 35.53, 34.36, 31.39, 28.34, 26.60, 22.46, 6.40, 6.35 ppm; HRMS (ESI) m/z: $[M + H]^+$ calcd for $C_{34}H_{46}ClN_6O_9S$, 749.2730; found 749.2736.

tert-Butyl ((_S_)-1-((2_S_,4_R_)-2-(((1_R_,2_S_)-1-((cyclopropylsulfonyl)carbamoyl)-2-vinylcyclopropyl)carbamoyl)-4-((7-methoxy-3-(trifluoromethyl)quinoxalin-2-

yl)oxy)pyrrolidin-1-yl)-3,3-dimethyl-1-oxobutan-2-yl)carbamate (10e). CF3-tBu-H

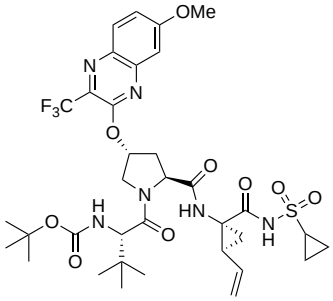

The same procedure was used as described above for compound **3**. Ester **6e** (1.60 g, 2.74 mmol) was treated with $LiOH.H_2O$ (0.40 g, 9.53 mmol) to afford acid **7e** (1.56 g, 2.74 mmol). A portion of acid **7e** (0.78 g, 1.37 mmol) was coupled with amine salt **8** (0.45 g, 1.69 mmol) using DIEA (0.95 mL, 5.75 mmol) and HATU (0.85 g, 2.24 mmol) to provide compound **10e** (0.80 g, 75%) as an off-white solid. ^{1}H NMR (400 MHz, $CDCl_3$) δ 10.09 (s, 1 H), 7.80 (d, J = 8.8 Hz, 1 H), 7.48 (dd, J = 8.8, 2.8 Hz, 1 H), 7.42 (d, J = 2.8 Hz, 1 H), 7.15 (s, 1 H), 5.92 (br s, 1 H), 5.81–5.72 (m, 1 H), 5.29–5.23 (m, 2 H), 5.14 (d, J = 11.2 Hz, 1 H), 4.50 (t, J = 8.8 Hz, 1 H), 4.32 (d, J = 12.0 Hz, 1 H), 4.19 (d, J = 9.6 Hz, 1 H), 4.04 (dd, J = 12.4, 4.0 Hz, 1 H), 3.94 (s, 3 H), 2.93–2.87 (m, 1 H), 2.53 (dd, J = 8.8, 2.8 Hz, 2 H), 2.13 (q, J = 8.4 Hz, 1 H), 1.96 (dd, J = 8.4, 6.0 Hz, 1 H), 1.48 (dd, J = 9.6, 6.0 Hz, 1 H), 1.36–1.32 (m, 2 H), 1.28 (s, 9 H), 1.05–0.96 (m, 11 H) ppm; ^{13}C NMR (100 MHz, $CDCl_3$) δ 172.74, 172.37, 168.52, 159.38, 155.61, 151.59, 138.37, 136.95, 134.24 (q, J = 35.8 Hz), 132.54, 127.97, 125.70, 120.57 (d, J = 273.6 Hz), 118.60, 106.42, 79.76, 75.0, 59.79, 58.60, 55.90, 53.93, 41.79, 35.57, 35.45, 34.27, 31.24, 28.11, 26.43, 22.45, 6.26, 6.19 ppm; HRMS (ESI) *m/z*: $[M + H]^+$ calcd for $C_{35}H_{46}F_3N_6O_9S$, 783.2994; found 783.3000.

***tert*-Butyl ((*S*)-1-((2*S*,4*R*)-4-((3-ethyl-7-methoxyquinoxalin-2-yl)oxy)-2-(((1*R*,2*S*)-1-(((1-methylcyclopropyl)sulfonyl)carbamoyl)-2-vinylcyclopropyl)carbamoyl)pyrrolidin-1-yl)-3,3-dimethyl-1-oxobutan-2-yl)carbamate (11a). Et-tBu-Me**

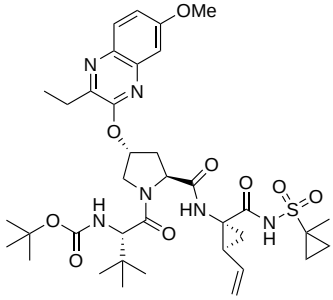

The same procedure was used as described above for compound **3**. Acid **7a** (0.73 g, 1.38 mmol) was coupled with amine salt **9** (0.45 g, 1.60 mmol) using

DIEA (0.95 mL, 5.75 mmol) and HATU (0.85 g, 2.24 mmol) to provide compound **11a** (0.80 g, 77%) as a white solid. ^{1}H NMR (500 MHz, $CDCl_3$) δ 9.80 (s, 1 H), 7.83 (d, *J* = 9.0 Hz, 1 H), 7.20–7.15 (m, 3 H), 5.89 (br s, 1 H), 5.72–5.64 (m, 1 H), 5.28 (d, *J* = 17.0 Hz, 1 H), 5.21 (d, *J* = 9.5 Hz, 1 H), 5.15 (d, *J* = 10.0 Hz, 1 H), 4.57 (t, *J* = 8.0 Hz, 1 H), 4.31 (d, *J* = 12.0 Hz, 1 H), 4.24 (d, *J* = 9.5 Hz, 1 H), 4.02 (dd, *J* = 12.0, 4.0 Hz, 1 H), 3.95 (s, 3 H), 2.86 (q, *J* = 7.5 Hz, 2 H), 2.67–2.61 (m, 1 H), 2.57–2.52 (m, 1 H), 2.11 (q, *J* = 8.5 Hz, 1 H), 1.94 (dd, *J* = 8.0, 6.0 Hz, 1 H), 1.73–1.68 (m, 1 H), 1.64–1.60 (m, 1 H), 1.50 (s, 3 H), 1.39 (dd, *J* = 9.0, 6.5 Hz, 1 H), 1.33 (s, 9 H), 1.27 (t, *J* = 7.5 Hz, 3 H), 1.03 (s, 9 H), 0.90–0.81 (m, 2 H) ppm; ^{13}C NMR (125 MHz, $CDCl_3$) δ 173.56, 172.86, 167.24, 160.42, 155.77, 154.92, 148.85, 140.95, 134.54, 132.74, 129.28, 118.89, 118.84, 106.14, 79.98, 74.18, 59.64, 58.95, 55.83, 54.36, 42.55, 36.69, 35.58, 35.06, 34.16, 28.34, 26.60, 21.42, 18.54, 14.17, 13.66, 11.70 ppm; HRMS (ESI) *m/z*: $[M + H]^+$ calcd for $C_{37}H_{53}N_6O_9S$, 757.3589; found 757.3587.

tert-Butyl ((*S*)-1-((2*S*,4*R*)-4-((7-methoxy-3-methylquinoxalin-2-yl)oxy)-2-(((1*R*,2*S*)-1-(((1-methylcyclopropyl)sulfonyl)carbamoyl)-2-vinylcyclopropyl)carbamoyl)pyrrolidin-1-yl)-3,3-dimethyl-1-oxobutan-2-yl)carbamate (11b). Me-tBu-Me

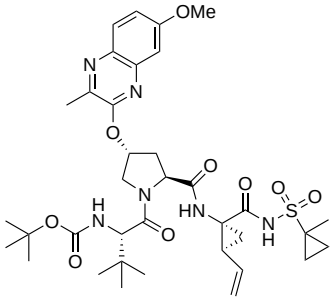

The same procedure was used as described above for compound **3**. Acid **7b** (0.62 g, 1.20 mmol) was coupled with amine salt **9** (0.40 g, 1.43 mmol) using DIEA (0.80 mL, 4.84 mmol) and HATU (0.70 g, 1.84 mmol) to provide compound **11b** (0.70 g, 79%) as a white solid. ^{1}H NMR (400 MHz, $CDCl_3$) δ 9.80 (s, 1 H), 7.80 (d, *J* = 9.2 Hz, 1 H), 7.23 (s, 1 H), 7.20–7.14 (m, 2 H), 5.86 (br s, 1 H), 5.72–5.63 (m, 1 H), 5.29–5.21 (m, 2 H), 5.15 (d, *J* = 10.0 Hz, 1 H), 4.60 (t, *J* = 8.4 Hz, 1 H), 4.32 (d, *J* = 11.2 Hz, 1 H), 4.23 (d, *J* = 9.2 Hz, 1 H), 4.01 (dd, *J* = 11.6, 3.6 Hz, 1 H), 3.94 (s, 3 H), 2.69–2.61 (m, 1 H), 2.57–2.50 (m, 4 H), 2.10 (q, *J* = 8.4 Hz, 1 H), 1.93 (dd, *J* = 8.0, 5.6 Hz, 1 H), 1.73–1.67 (m, 1 H), 1.63–1.59 (m, 1 H), 1.50 (s, 3 H), 1.37 (dd, *J* = 9.6, 6.0 Hz, 1 H), 1.33 (s, 9 H), 1.02 (s, 9 H), 0.88–0.81 (m, 2 H) ppm; ^{13}C NMR (100 MHz, $CDCl_3$) δ 173.67, 172.99, 167.35, 160.48, 155.89, 155.39, 144.74, 141.14, 134.57, 132.82, 129.19, 119.0, 106.25, 80.10, 74.40, 59.69, 59.04, 55.92, 54.41, 42.64, 36.74, 35.61, 35.12, 34.14, 28.45, 26.71, 21.44, 20.08, 18.62, 14.26, 13.72 ppm; HRMS (ESI) *m/z*: $[M + H]^+$ calcd for $C_{36}H_{51}N_6O_9S$, 743.3433; found 743.3428.

***tert*-Butyl ((*S*)-1-((2*S*,4*R*)-4-((3-isopropyl-7-methoxyquinoxalin-2-yl)oxy)-2-(((1*R*,2*S*)-1-(((1-methylcyclopropyl)sulfonyl)carbamoyl)-2-vinylcyclopropyl)carbamoyl)pyrrolidin-1-yl)-3,3-dimethyl-1-oxobutan-2-yl)carbamate (11c). i-Pr-tBu-Me**

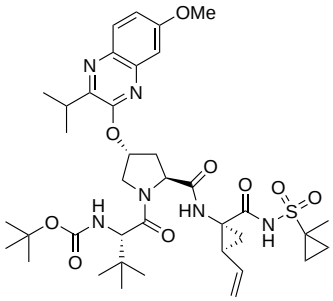

The same procedure was used as described above for compound **3**. Acid **7c** (1.0 g, 1.84 mmol) was coupled with amine salt **9** (0.67 g, 2.39 mmol) using DIEA (1.25 mL, 7.56 mmol) and HATU (1.0 g, 2.63 mmol) to provide compound **11c** (1.20 g, 85%) as a white solid. ^{1}H NMR (400 MHz, $CDCl_3$) δ 9.85 (s, 1 H), 7.83 (d, J = 9.2 Hz, 1 H), 7.18–7.12 (m, 3 H), 5.89 (br s, 1 H), 5.73–5.64 (m, 1 H), 5.30–5.24 (m, 2 H), 5.15 (d, J = 10.4 Hz, 1 H), 4.53 (t, J = 8.4 Hz, 1 H), 4.30–4.21 (m, 2 H), 4.04 (dd, J = 12.0, 4.0 Hz, 1 H), 3.94 (s, 3 H), 3.38–3.29 (m, 1 H), 2.60–2.50 (m, 2 H), 2.13 (q, J = 8.4 Hz, 1 H), 1.93 (dd, J = 8.0, 6.0 Hz, 1 H), 1.73–1.53 (m, 2 H), 1.50 (s, 3 H), 1.44–1.17 (m, 16 H), 1.02 (s, 9 H), 0.90–0.80 (m, 2 H) ppm; ^{13}C NMR (100 MHz, $CDCl_3$) δ 173.45, 172.52, 167.27, 160.22, 155.58, 154.23, 151.78, 140.54, 134.40, 132.63, 129.36, 118.73, 118.59, 105.83, 79.78, 73.98, 59.60, 58.75, 55.68, 54.28, 42.32, 36.52, 35.59, 34.96, 34.20, 30.65, 28.21, 26.45, 21.47, 20.49, 20.45, 18.39, 13.97, 13.56 ppm; HRMS (ESI) *m/z*: $[M + H]^+$ calcd for $C_{38}H_{55}N_6O_9S$, 771.3746; found 771.3735.

***tert*-Butyl ((*S*)-1-((2*S*,4*R*)-4-((3-chloro-7-methoxyquinoxalin-2-yl)oxy)-2-(((1*R*,2*S*)-1-(((1-methylcyclopropyl)sulfonyl)carbamoyl)-2-vinylcyclopropyl)carbamoyl)pyrrolidin-1-yl)-3,3-dimethyl-1-oxobutan-2-yl)carbamate (11d). Cl-tBu-Me**

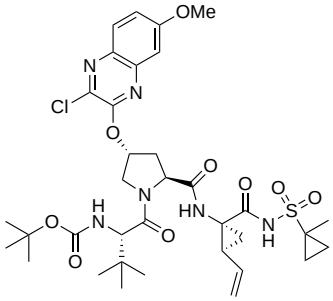

The same procedure was used as described above for compound **3**. Acid **7d** (0.92 g, 1.71 mmol) was coupled with amine salt **9** (0.53 g, 1.88 mmol) using DIEA (1.15 mL, 6.96 mmol) and HATU (0.95 g, 2.50 mmol) to provide compound

11d (1.0 g, 77%) as a white solid. ^{1}H NMR (400 MHz, $CDCl_3$) δ 9.83 (s, 1 H), 7.80 (d, J = 8.8 Hz, 1 H), 7.23 (dd, J = 8.8, 2.8 Hz, 1 H), 7.18 (d, J = 2.4 Hz, 1 H), 5.84 (br s, 1 H), 5.72–5.63 (m, 1 H), 5.27 (d, J = 16.4 Hz, 1 H), 5.23 (d, J = 9.2 Hz, 1 H), 5.15 (d, J = 10.4 Hz, 1 H), 4.62 (t, J = 8.0 Hz, 1 H), 4.38 (d, J = 12.0 Hz, 1 H), 4.21 (d, J = 9.6 Hz, 1 H), 4.03 (dd, J = 11.6, 4.4 Hz, 1 H), 3.96 (s, 3 H), 2.64–2.54 (m, 2 H), 2.13 (q, J = 8.8 Hz, 1 H), 1.94 (dd, J = 8.0, 6.0 Hz, 1 H), 1.75–1.58 (m, 2 H), 1.50 (s, 3 H), 1.44–1.38 (m, 1 H), 1.31 (s, 9 H), 1.02 (s, 9 H), 0.88–0.80 (m, 2 H) ppm; ^{13}C NMR (100 MHz, $CDCl_3$) δ 173.35, 172.64, 167.17, 161.29, 155.66, 152.08, 140.87, 135.95, 134.08, 132.60, 128.85, 120.08, 118.75, 105.89, 79.91, 75.56, 59.53, 58.73, 55.82, 53.80, 42.38, 36.50, 35.43, 34.89, 33.98, 28.21, 26.44, 21.32, 18.40, 13.99, 13.52 ppm; HRMS (ESI) *m/z*: $[M + H]^+$ calcd for $C_{35}H_{48}ClN_6O_9S$, 763.2887; found 763.2878.

tert-Butyl ((*S*)-1-((2*S*,4*R*)-4-((7-methoxy-3-(trifluoromethyl)quinoxalin-2-yl)oxy)-2-(((1*R*,2*S*)-1-(((1-methylcyclopropyl)sulfonyl)carbamoyl)-2-vinylcyclopropyl)carbamoyl)pyrrolidin-1-yl)-3,3-dimethyl-1-oxobutan-2-yl)carbamate (11e). CF3-tBu-Me

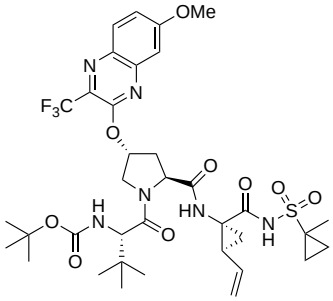

The same procedure was used as described above for compound **3**. Acid **7e** (0.78 g, 1.37 mmol) was coupled with amine salt **9** (0.48 g, 1.71 mmol) using DIEA (0.95 mL, 5.75 mmol) and HATU (0.85 g, 2.24 mmol) to provide compound **11e** (0.82 g, 75%) as an off-white solid. ^{1}H NMR (400 MHz, $CDCl_3$) δ 9.80 (s, 1 H), 7.81 (d, J = 8.8 Hz, 1 H), 7.48 (dd, J = 8.8, 2.8 Hz, 1 H), 7.43 (d, J = 2.8 Hz, 1 H), 7.25 (s, 1 H), 5.92 (br s, 1 H), 5.73–5.64 (m, 1 H), 5.28 (d, J = 17.2 Hz, 1 H), 5.20 (d, J = 9.6 Hz, 1 H), 5.15 (d, J = 10.8 Hz, 1 H), 4.56 (t, J = 8.4 Hz, 1 H), 4.34 (d, J = 12.0 Hz, 1 H), 4.18 (d, J = 9.6 Hz, 1 H), 4.0 (dd, J = 11.6, 3.6 Hz, 1 H), 3.94 (s, 3 H), 2.64–2.51 (m, 2 H), 2.13 (q, J = 8.4 Hz, 1 H), 1.95 (dd, J = 8.0, 6.0 Hz, 1 H), 1.73–1.60 (m, 2 H), 1.59 (s, 3 H), 1.43–1.38 (m, 11 H), 1.28 (s, 9 H), 0.89–0.80 (m, 2 H) ppm; ^{13}C NMR (100 MHz, $CDCl_3$) δ 173.53, 172.82, 167.41, 159.76, 155.80, 151.85, 138.61, 137.20, 134.48 (q, J = 35.9 Hz), 132.86, 128.21, 125.90, 120.81 (d, J = 274.0 Hz), 118.96, 107.68, 80.0, 75.16, 59.69, 58.90, 56.13, 54.12, 42.60, 36.75, 35.69, 35.17, 34.28, 28.34, 26.65, 21.66, 18.65, 13.79, 13.44 ppm; HRMS (ESI) *m/z*: $[M + H]^+$ calcd for $C_{36}H_{48}F_3N_6O_9S$, 797.3150; found 797.3146.

Cyclopentyl ((*S*)-1-((2*S*,4*R*)-2-(((1*R*,2*S*)-1-((cyclopropylsulfonyl)carbamoyl)-2-vinylcyclopropyl)carbamoyl)-4-((3-ethyl-7-methoxyquinoxalin-2-

yl)oxy)pyrrolidin-1-yl)-3,3-dimethyl-1-oxobutan-2-yl)carbamate (14a). Et-Cyp-H

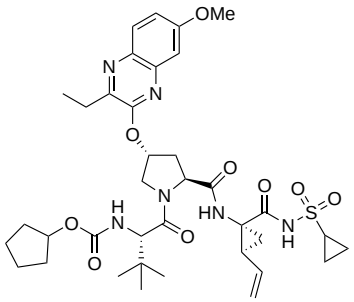

Compound **3** (0.40 g, 0.54 mmol) was treated with a solution of 4 N HCl in 1,4-dioxane (10 mL). After stirring the reaction mixture at room temperature for 3 h, solvents were evaporated under reduced pressure. The residue was triturated with diethyl ether (3 × 10 mL) and dried to yield the amine salt **12a** (0.37 g, 100%) as a white powder.

A solution of the above amine salt **12a** (0.37 g, 0.54 mmol) in anhydrous CH_3CN (15 mL) was treated with DIEA (0.37 mL, 2.24 mmol) and *N*-(cyclopentyloxycarbonyloxy)-succinimide (0.15 g, 0.66 mmol). The reaction mixture was stirred at room temperature for 36 h, then concentrated under reduced pressure and dried under high vacuum. The residue was purified by flash chromatography using 50–90% EtOAc/hexanes as the eluent to provide the target compound **14a** (0.36 g, 88%) as a white solid. ^{1}H NMR (400 MHz, $CDCl_3$) δ 10.03 (s, 1 H), 7.83 (d, J = 9.0 Hz, 1 H), 7.19 (dd, J = 9.0, 2.8 Hz, 1 H), 7.14 (d, J = 2.5 Hz, 2 H), 5.90 (br s, 1 H), 5.80–5.73 (m, 1 H), 5.33–5.24 (m, 2 H), 5.15 (d, J = 10.6 Hz, 1 H), 4.90–4.86 (m, 1 H), 4.51 (t, J = 8.6 Hz, 1 H), 4.32–4.26 (m, 2 H), 4.05 (dd, J = 11.6, 3.6 Hz, 1 H), 3.94 (s, 3 H), 2.93–2.84 (m, 3 H), 2.57–2.53 (m, 1 H), 2.12 (q, J = 8.4 Hz, 1 H), 1.96 (dd, J = 8.0, 6.0 Hz, 1 H), 1.76–1.45 (m, 8 H), 1.30–1.14 (m, 5 H), 1.08–0.98 (m, 11 H) ppm; ^{13}C NMR (100 MHz, $CDCl_3$) δ 172.93, 172.61, 168.54, 160.41, 156.49, 154.92, 148.91, 140.92, 134.60, 132.66, 129.31, 118.81, 106.13, 78.06, 74.17, 60.02, 59.22, 55.82, 54.40, 41.96, 35.68, 35.61, 34.38, 32.92, 32.71, 32.53, 31.41, 26.61, 23.80, 22.53, 11.72, 6.40, 6.17 ppm; HRMS (ESI) *m/z*: $[M + H]^+$ calcd for $C_{37}H_{51}N_6O_9S$, 755.3433; found 755.3429.

Cyclopentyl ((*S*)-1-((2*S*,4*R*)-2-(((1*R*,2*S*)-1-((cyclopropylsulfonyl)carbamoyl)-2-vinylcyclopropyl)carbamoyl)-4-((7-methoxy-3-methylquinoxalin-2-yl)oxy)pyrrolidin-1-yl)-3,3-dimethyl-1-oxobutan-2-yl)carbamate (14b). Me-Cyp-H

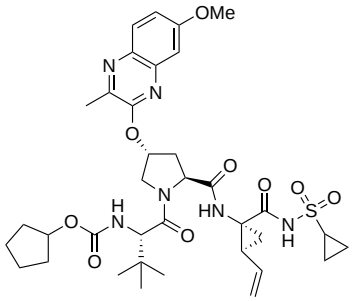

The same procedure was used as described above for compound **14a**. Compound **10b** (0.31 g, 0.42 mmol) was treated with 4 N HCl in 1,4-dioxane (10 mL) to yield the amine salt **12b**, which was treated with DIEA (0.30 mL, 1.82 mmol) and *N*-(cyclopentyloxycarbonyloxy)-succinimide (0.12 g, 0.53 mmol) to provide the target compound **14b** (0.26 g, 84%) as a white solid. ^{1}H NMR (400 MHz, $CDCl_3$) δ 10.05 (s, 1 H), 7.80 (d, J = 8.8 Hz, 1 H), 7.19 (dd, J = 9.2, 2.8 Hz, 1 H), 7.14 (d, J = 2.8 Hz, 1 H), 7.08 (s, 1 H), 5.88 (br s, 1 H), 5.81–5.72 (m, 1 H), 5.34 (d, J = 9.6 Hz, 1 H), 5.26 (d, J = 17.2 Hz, 1 H), 5.15 (d, J = 10.0 Hz, 1 H), 4.92–4.87 (m, 1 H), 4.52 (t, J = 8.0 Hz, 1 H), 4.32–4.25 (m, 2 H), 4.05 (dd, J = 11.2, 4.0 Hz, 1 H), 3.94 (s, 3 H), 2.94–2.87 (m, 1 H), 2.57–2.51 (m, 5 H), 2.11 (q, J = 8.4 Hz, 1 H), 1.97 (dd, J = 7.6, 5.6 Hz, 1 H), 1.78–1.45 (m, 8 H), 1.38–1.32 (m, 2 H), 1.08–0.98 (s, 11 H) ppm; ^{13}C NMR (100 MHz, $CDCl_3$) δ 172.73, 172.46, 168.40, 160.26, 156.40, 155.16, 144.55, 140.89, 134.35, 132.48, 128.95, 118.80, 118.69, 106.0, 77.94, 74.16, 59.87, 59.05, 55.69, 54.20, 41.79, 35.57, 35.50, 34.17, 32.78, 32.60, 31.24, 26.47, 23.68, 22.41, 19.84, 6.28, 6.22 ppm; HRMS (ESI) *m/z*: $[M + H]^+$ calcd for $C_{36}H_{49}N_6O_9S$, 741.3276; found 741.3275.

Cyclopentyl ((*S*)-1-((2*S*,4*R*)-2-(((1*R*,2*S*)-1-((cyclopropylsulfonyl)carbamoyl)-2-vinylcyclopropyl)carbamoyl)-4-((3-isopropyl-7-methoxyquinoxalin-2-yl)oxy)pyrrolidin-1-yl)-3,3-dimethyl-1-oxobutan-2-yl)carbamate (14c). i-Pr-Cyp-H

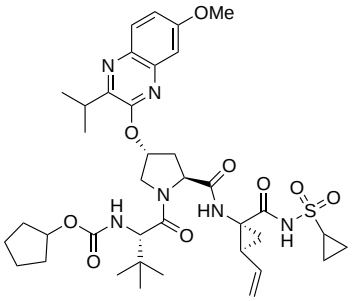

The same procedure was used as described above for compound **14a**. Compound **10c** (0.50 g, 0.66 mmol) was treated with 4 N HCl in 1,4-dioxane (10 mL) to yield the amine salt **12c**, which was treated with DIEA (0.44 mL, 2.66 mmol) and *N*-(cyclopentyloxycarbonyloxy)-succinimide (0.16 g, 0.70 mmol) to provide the target compound **14c** (0.48 g, 95%) as a white solid. ^{1}H NMR (400

MHz, $CDCl_3$) δ 10.07 (s, 1 H), 7.83 (d, *J* = 9.2 Hz, 1 H), 7.19–7.12 (m, 3 H), 5.91 (br s, 1 H), 5.80–5.72 (m, 1 H), 5.38 (d, *J* = 9.6 Hz, 1 H), 5.26 (d, *J* = 17.2 Hz, 1 H), 5.13 (d, *J* = 10.4 Hz, 1 H), 4.90–4.86 (m, 1 H), 4.48 (t, *J* = 8.8 Hz, 1 H), 4.32–4.27 (m, 2 H), 4.06 (dd, *J* = 12.0, 4.0 Hz, 1 H), 3.94 (s, 3 H), 3.38–3.32 (m, 1 H), 2.93–2.87 (m, 1 H), 2.55–2.51 (m, 2 H), 2.12 (q, *J* = 8.8 Hz, 1 H), 1.96 (dd, *J* = 8.4, 6.0 Hz, 1 H), 1.78–1.47 (m, 7 H), 1.40–1.23 (m, 9 H), 1.07–0.97 (m, 11 H) ppm; ^{13}C NMR (100 MHz, $CDCl_3$) δ 172.81, 172.34, 168.52, 160.22, 156.33, 154.23, 151.80, 140.53, 134.43, 132.54, 129.36, 118.59, 105.82, 77.86, 73.99, 59.92, 59.02, 55.67, 54.31, 41.77, 35.64, 35.51, 34.33, 32.78, 32.56, 31.24, 30.65, 26.48, 26.18, 23.66, 22.50, 20.50, 20.46, 6.29, 6.20 ppm; HRMS (ESI) *m/z*: $[M + H]^+$ calcd for $C_{38}H_{53}N_6O_9S$, 769.3589; found 769.3587.

Cyclopentyl ((*S*)-1-((2*S*,4*R*)-4-((3-chloro-7-methoxyquinoxalin-2-yl)oxy)-2-(((1*R*,2*S*)-1-((cyclopropylsulfonyl)carbamoyl)-2-vinylcyclopropyl)carbamoyl)pyrrolidin-1-yl)-3,3-dimethyl-1-oxobutan-2-yl)carbamate (14d). Cl-Cyp-H

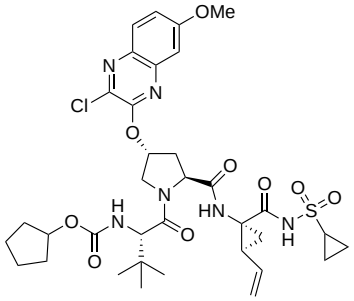

The same procedure was used as described above for compound **14a**. Compound **10d** (0.50 g, 0.67 mmol) was treated with 4 N HCl in 1,4-dioxane (10 mL) to yield the amine salt **12d**, which was treated with DIEA (0.45 mL, 2.72 mmol) and *N*-(cyclopentyloxycarbonyloxy)-succinimide (0.16 g, 0.70 mmol) to provide the target compound **14d** (0.46 g, 90%) as a white solid. ^{1}H NMR (400 MHz, $CDCl_3$) δ 10.03 (s, 1 H), 7.81 (d, *J* = 9.0 Hz, 1 H), 7.23 (dd, *J* = 9.0, 3.0 Hz, 1 H), 7.18 (d, *J* = 3.0 Hz, 1 H), 7.14 (br s, 1 H), 5.86 (br s, 1 H), 5.78–5.72 (m, 1 H), 5.33 (d, *J* = 8.4 Hz, 1 H), 5.27 (d, *J* = 17.0 Hz, 1 H), 5.15 (d, *J* = 10.6 Hz, 1 H), 4.88–4.85 (m, 1 H), 4.58 (t, *J* = 8.4 Hz, 1 H), 4.38 (d, *J* = 12.0 Hz, 1 H), 4.23 (d, *J* = 10.0 Hz, 1 H), 4.04 (dd, *J* = 11.6, 3.6 Hz, 1 H), 3.96 (s, 3 H), 2.92–2.88 (m, 1 H), 2.57 (dd, *J* = 8.0, 2.4 Hz, 2 H), 2.12 (q, *J* = 8.6 Hz, 1 H), 1.97 (dd, *J* = 7.6, 6.0 Hz, 1 H), 1.75–1.43 (m, 8 H), 1.37–1.30 (m, 2 H), 1.08–0.96 (m, 11 H) ppm; ^{13}C NMR (100 MHz, $CDCl_3$) δ 172.86, 172.61, 168.53, 161.47, 156.58, 152.27, 141.03, 136.25, 134.30, 132.63, 129.01, 120.21, 118.81, 106.07, 78.16, 75.68, 59.99, 59.17, 55.95, 53.93, 42.04, 35.64, 35.50, 34.26, 32.92, 32.72, 31.40, 26.60, 23.82, 22.40, 6.40, 6.35 ppm; HRMS (ESI) *m/z*: $[M + H]^+$ calcd for $C_{35}H_{46}ClN_6O_9S$, 761.2730; found 761.2730.

Cyclopentyl ((*S*)-1-((2*S*,4*R*)-2-(((1*R*,2*S*)-1-((cyclopropylsulfonyl)carbamoyl)-2-vinylcyclopropyl)carbamoyl)-4-((7-methoxy-3-(trifluoromethyl)quinoxalin-

2-yl)oxy)pyrrolidin-1-yl)-3,3-dimethyl-1-oxobutan-2-yl)carbamate (14e). CF3-Cyp-H

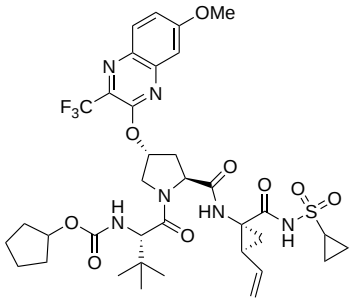

The same procedure was used as described above for compound **14a**. Compound **10e** (0.40 g, 0.51 mmol) was treated with 4 N HCl in 1,4-dioxane (10 mL) to yield the amine salt **12e**, which was treated with DIEA (0.35 mL, 2.10 mmol) and *N*-(cyclopentyloxycarbonyloxy)-succinimide (0.13 g, 0.57 mmol) to provide the target compound **14e** (0.35 g, 86%) as an off-white solid. ^{1}H NMR (400 MHz, $CDCl_3$) δ 10.05 (s, 1 H), 7.81 (d, J = 9.2 Hz, 1 H), 7.48 (dd, J = 9.2, 2.8 Hz, 1 H), 7.43 (d, J = 2.8 Hz, 1 H), 7.18 (s, 1 H), 5.93 (br s, 1 H), 5.81–5.72 (m, 1 H), 5.32–5.25 (m, 2 H), 5.15 (d, J = 11.2 Hz, 1 H), 4.81–4.77 (m, 1 H), 4.53 (t, J = 8.4 Hz, 1 H), 4.35 (d, J = 12.0 Hz, 1 H), 4.19 (d, J = 9.6 Hz, 1 H), 4.02 (dd, J = 12.0, 4.0 Hz, 1 H), 3.94 (s, 3 H), 2.94–2.88 (m, 1 H), 2.56–2.52 (m, 2 H), 2.13 (q, J = 8.4 Hz, 1 H), 1.97 (dd, J = 7.6, 5.6 Hz, 1 H), 1.74–1.33 (m, 11 H), 1.25–1.0 (m, 11 H) ppm; ^{13}C NMR (100 MHz, $CDCl_3$) δ 172.69, 172.39, 168.42, 159.54, 156.34, 151.65, 138.40, 136.96, 134.34 (q, J = 35.8 Hz), 132.50, 127.96, 125.67, 120.60 (d, J = 273.6 Hz), 118.66, 107.42, 77.82, 74.94, 59.77, 58.92, 55.90, 53.87, 41.82, 35.47, 35.43, 34.16, 32.75, 32.42, 31.24, 26.41, 23.67, 23.62, 22.37, 6.26, 6.20 ppm; HRMS (ESI) *m/z*: $[M + H]^+$ calcd for $C_{36}H_{46}F_3N_6O_9S$, 795.2994; found 795.2996.

Cyclopentyl ((*S*)-1-((2*S*,4*R*)-4-((3-ethyl-7-methoxyquinoxalin-2-yl)oxy)-2-(((1*R*,2*S*)-1-(((1-methylcyclopropyl)sulfonyl)carbamoyl)-2-vinylcyclopropyl)carbamoyl)pyrrolidin-1-yl)-3,3-dimethyl-1-oxobutan-2-yl)carbamate (15a). Et-Cyp-Me

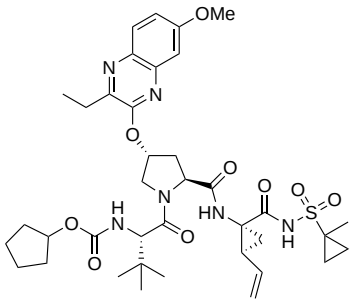

The same procedure was used as described above for compound **14a**. Compound **11a** (0.35 g, 0.46 mmol) was treated with 4 N HCl in 1,4-dioxane (10

mL) to yield the amine salt **13a**, which was treated with DIEA (0.31 mL, 1.94 mmol) and *N*-(cyclopentyloxycarbonyloxy)-succinimide (0.13 g, 0.57 mmol) to provide the target compound **15a** (0.34 g, 96%) as a white solid. ^{1}H NMR (500 MHz, $CDCl_3$) δ 9.77 (s, 1 H), 7.83 (d, *J* = 9.0 Hz, 1 H), 7.19 (dd, *J* = 9.0, 2.5 Hz, 1 H), 7.15 (d, *J* = 2.5 Hz, 1 H), 5.89 (br s, 1 H), 5.72–5.64 (m, 1 H), 5.33–5.25 (m, 2 H), 5.15 (d, *J* = 10.5 Hz, 1 H), 4.87 (m, 1 H), 4.58 (t, *J* = 8.0 Hz, 1 H), 4.33 (d, *J* = 12.0 Hz, 1 H), 4.27 (d, *J* = 10.0 Hz, 1 H), 4.02 (dd, *J* = 12.0, 4.0 Hz, 1 H), 3.95 (s, 3 H), 2.86 (q, *J* = 7.5 Hz, 2 H), 2.67–2.62 (m, 1 H), 2.56–2.51 (m, 1 H), 2.11 (q, *J* = 8.5 Hz, 1 H), 1.93 (dd, *J* = 8.0, 6.5 Hz, 1 H), 1.77–1.05 (m, 13 H), 1.38 (dd, *J* = 9.0, 6.0 Hz, 1 H), 1.27 (t, *J* = 7.5 Hz, 3 H), 1.03 (s, 9 H), 0.90–0.80 (m, 2 H) ppm; ^{13}C NMR (125 MHz, $CDCl_3$) δ 173.55, 172.78, 167.25, 160.40, 156.48, 154.95, 148.92, 140.95, 134.60, 132.73, 129.30, 118.90, 118.79, 106.15, 78.07, 74.10, 59.64, 59.25, 55.82, 54.31, 42.55, 36.68, 35.54, 35.01, 34.10, 32.93, 32.71, 26.59, 23.80, 18.54, 14.15, 11.70 ppm; HRMS (ESI) *m/z*: $[M + H]^+$ calcd for $C_{38}H_{53}N_6O_9S$, 769.3589; found 769.3584.

Cyclopentyl ((*S*)-1-((2*S*,4*R*)-4-((7-methoxy-3-methylquinoxalin-2-yl)oxy)-2-(((1*R*,2*S*)-1-(((1-methylcyclopropyl)sulfonyl)carbamoyl)-2-vinylcyclopropyl)carbamoyl)pyrrolidin-1-yl)-3,3-dimethyl-1-oxobutan-2-yl)carbamate (15b). Me-Cyp-Me

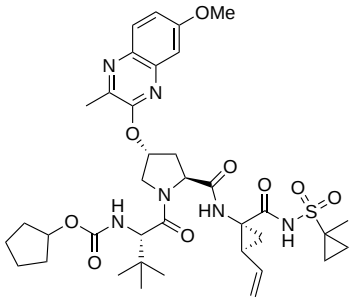

The same procedure was used as described above for compound **14a**. Compound **11b** (0.40 g, 0.54 mmol) was treated with 4 N HCl in 1,4-dioxane (10 mL) to yield the amine salt **13b**, which was treated with DIEA (0.36 mL, 2.18 mmol) and *N*-(cyclopentyloxycarbonyloxy)-succinimide (0.14 g, 0.62 mmol) to provide the target compound **15b** (0.34 g, 96%) as a white solid. ^{1}H NMR (400 MHz, $CDCl_3$) δ 9.77 (s, 1 H), 7.80 (d, *J* = 9.0 Hz, 1 H), 7.32 (s, 1 H), 7.19–7.14 (m, 2 H), 5.87 (br s, 1 H), 5.71–5.64 (m, 1 H), 5.38 (d, *J* = 9.6 Hz, 1 H), 5.27 (d, *J* = 17.0 Hz, 1 H), 5.15 (d, *J* = 10.6 Hz, 1 H), 4.94–4.87 (m, 1 H), 4.61 (t, *J* = 8.0 Hz, 1 H), 4.32 (d, *J* = 11.6 Hz, 1 H), 4.27 (d, *J* = 9.6 Hz, 1 H), 4.03 (dd, *J* = 11.6, 4.0 Hz, 1 H), 3.94 (s, 3 H), 2.70–2.60 (m, 1 H), 2.56–2.50 (m, 4 H), 2.11 (q, *J* = 8.4 Hz, 1 H), 1.92 (dd, *J* = 8.0, 6.0 Hz, 1 H), 1.80–1.49 (m, 12 H), 1.37 (dd, *J* = 9.2, 6.0 Hz, 1 H), 1.02 (s, 9 H), 0.88–0.79 (m, 2 H) ppm; ^{13}C NMR (100 MHz, $CDCl_3$) δ 172.57, 172.73, 167.33, 160.40, 156.55, 155.34, 144.74, 141.06, 134.50, 132.74, 129.08, 118.86, 106.20, 78.07, 74.25, 59.61, 59.26, 55.81, 54.28, 42.50, 36.68, 35.50, 34.97, 34.11, 32.92, 32.75, 26.60, 23.81, 21.41,

19.96, 18.52, 14.05, 13.71 ppm; HRMS (ESI) *m/z*: $[M + H]^+$ calcd for $C_{37}H_{51}N_6O_9S$, 755.3433; found 755.3433.

Cyclopentyl ((*S*)-1-((2*S*,4*R*)-4-((3-isopropyl-7-methoxyquinoxalin-2-yl)oxy)-2-(((1*R*,2*S*)-1-(((1-methylcyclopropyl)sulfonyl)carbamoyl)-2-vinylcyclopropyl)carbamoyl)pyrrolidin-1-yl)-3,3-dimethyl-1-oxobutan-2-yl)carbamate (15c). i-Pr-Cyp-Me

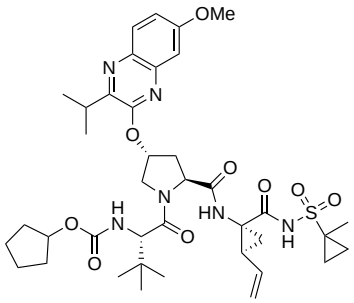

The same procedure was used as described above for compound **14a**. Compound **11c** (0.62 g, 0.80 mmol) was treated with 4 N HCl in 1,4-dioxane (12 mL) to yield the amine salt **13c**, which was treated with DIEA (0.53 mL, 3.20 mmol) and *N*-(cyclopentyloxycarbonyloxy)-succinimide (0.20 g, 0.88 mmol) to provide the target compound **15c** (0.58 g, 93%) as a white solid. ^{1}H NMR (400 MHz, $CDCl_3$) δ 9.83 (s, 1 H), 7.84 (d, J = 9.2 Hz, 1 H), 7.23 (m, 1 H), 7.20–7.13 (m, 2 H), 5.89 (br s, 1 H), 5.73–5.64 (m, 1 H), 5.35 (d, J = 9.2 Hz, 1 H), 5.27 (d, J = 16.4 Hz, 1 H), 5.14 (d, J = 10.4 Hz, 1 H), 4.90–4.84 (m, 1 H), 4.56 (t, J = 8.0 Hz, 1 H), 4.33–4.24 (m, 2 H), 4.04 (dd, J = 12.0, 4.4 Hz, 1 H), 3.94 (s, 3 H), 3.38–3.31 (m, 1 H), 2.67–2.52 (m, 2 H), 2.12 (q, J = 8.0 Hz, 1 H), 1.93 (dd, J = 8.0, 6.0 Hz, 1 H), 1.77–1.50 (m, 12 H), 1.41–1.25 (m, 8 H), 1.02 (s, 9 H), 0.89–0.80 (m, 2 H) ppm; ^{13}C NMR (100 MHz, $CDCl_3$) δ 173.37, 172.52, 167.22, 160.22, 156.29, 154.26, 151.81, 140.55, 134.42, 132.59, 129.35, 118.76, 118.57, 105.84, 77.86, 73.89, 59.55, 59.06, 55.67, 54.22, 42.32, 36.51, 35.51, 34.96, 34.10, 32.80, 32.56, 30.65, 26.44, 23.66, 21.43, 20.50, 20.42, 18.40, 13.95, 13.57 ppm; HRMS (ESI) *m/z*: $[M + H]^+$ calcd for $C_{39}H_{55}N_6O_9S$, 783.3746; found 783.3745.

Cyclopentyl ((*S*)-1-((2*S*,4*R*)-4-((3-chloro-7-methoxyquinoxalin-2-yl)oxy)-2-(((1*R*,2*S*)-1-(((1-methylcyclopropyl)sulfonyl)carbamoyl)-2-vinylcyclopropyl)carbamoyl)pyrrolidin-1-yl)-3,3-dimethyl-1-oxobutan-2-yl)carbamate (15d). Cl-Cyp-Me

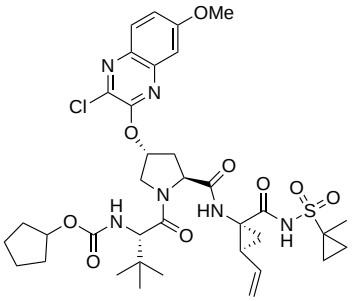

The same procedure was used as described above for compound **14a**. Compound **11d** (0.50 g, 0.65 mmol) was treated with 4 N HCl in 1,4-dioxane (10 mL) to yield the amine salt **13d**, which was treated with DIEA (0.43 mL, 2.60 mmol) and *N*-(cyclopentyloxycarbonyloxy)-succinimide (0.16 g, 0.70 mmol) to provide the target compound **15d** (0.45 g, 89%) as a white solid. ^{1}H NMR (400 MHz, $CDCl_3$) δ 9.79 (s, 1 H), 7.80 (d, J = 8.8 Hz, 1 H), 7.30 (s, 1 H), 7.26–7.21 (m, 2 H), 7.18 (d, J = 2.0 Hz, 1 H), 5.85 (br s, 1 H), 5.73–5.64 (m, 1 H), 5.35 (d, J = 9.2 Hz, 1 H), 5.27 (d, J = 16.8 Hz, 1 H), 5.15 (d, J = 10.8 Hz, 1 H), 4.87–4.84 (m, 1 H), 4.64 (t, J = 7.6 Hz, 1 H), 4.40 (d, J = 11.6 Hz, 1 H), 4.23 (d, J = 10.0 Hz, 1 H), 4.02 (dd, J = 11.6, 4.0 Hz, 1 H), 3.96 (s, 3 H), 2.66–2.54 (m, 2 H), 2.12 (q, J = 8.4 Hz, 1 H), 1.94 (dd, J = 7.6, 6.0 Hz, 1 H), 1.76–1.48 (m, 12 H), 1.39 (dd, J = 9.2, 5.6 Hz, 1 H), 1.01 (s, 9 H), 0.88–0.80 (m, 2 H) ppm; ^{13}C NMR (100 MHz, $CDCl_3$) δ 173.30, 172.60, 167.17, 161.27, 156.42, 152.14, 140.88, 136.12, 134.10, 132.57, 128.82, 120.05, 118.80, 105.89, 78.01, 75.48, 59.53, 59.02, 55.82, 53.74, 42.36, 36.50, 35.34, 34.86, 33.90, 32.78, 32.58, 26.43, 23.70, 21.32, 18.40, 13.95, 13.56 ppm; HRMS (ESI) *m/z*: $[M + H]^+$ calcd for $C_{36}H_{48}ClN_6O_9S$, 775.2887; found 775.2890.

Cyclopentyl ((*S*)-1-((2*S*,4*R*)-4-((7-methoxy-3-(trifluoromethyl)quinoxalin-2-yl)oxy)-2-(((1*R*,2*S*)-1-(((1-methylcyclopropyl)sulfonyl)carbamoyl)-2-vinylcyclopropyl)carbamoyl)pyrrolidin-1-yl)-3,3-dimethyl-1-oxobutan-2-yl)carbamate (15e). CF3-Cyp-Me

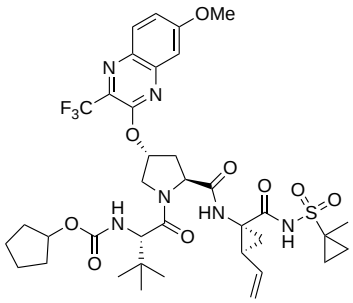

The same procedure was used as described above for compound **14a**. Compound **11e** (0.40 g, 0.50 mmol) was treated with 4 N HCl in 1,4-dioxane (10 mL) to yield the amine salt **13e**, which was treated with DIEA (0.35 mL, 2.10 mmol) and *N*-(cyclopentyloxycarbonyloxy)-succinimide (0.13 g, 0.57 mmol) to provide the target compound **15e** (0.38 g, 94%) as an off-white solid. ^{1}H NMR

(400 MHz, $CDCl_3$) δ 9.79 (s, 1 H), 7.81 (d, J = 9.2 Hz, 1 H), 7.48 (dd, J = 8.8, 2.8 Hz, 1 H), 7.43 (d, J = 2.8 Hz, 1 H), 7.32 (s, 1 H), 5.91 (br s, 1 H), 5.73–5.63 (m, 1 H), 5.30–5.25 (m, 2 H), 5.16 (d, J = 10.8 Hz, 1 H), 4.80–4.75 (m, 1 H), 4.60 (t, J = 7.6 Hz, 1 H), 4.37 (d, J = 12.0 Hz, 1 H), 4.19 (d, J = 9.6 Hz, 1 H), 3.98 (dd, J = 11.6, 3.6 Hz, 1 H), 3.94 (s, 3 H), 2.67–2.51 (m, 2 H), 2.12 (q, J = 8.0 Hz, 1 H), 1.94 (dd, J = 8.0, 6.0 Hz, 1 H), 1.73–1.48 (m, 13 H), 1.38 (dd, J = 9.2, 1.6 Hz, 1 H), 0.99 (s, 9 H), 0.89–0.81 (m, 2 H) ppm; ^{13}C NMR (100 MHz, $CDCl_3$) δ 173.26, 172.60, 167.14, 159.51, 156.31, 151.68, 138.39, 136.96, 134.38 (q, J = 36.0 Hz), 132.58, 127.98, 125.62, 120.60 (d, J = 274.4 Hz), 118.76, 107.42, 77.82, 74.86, 59.41, 58.95, 55.89, 53.79, 42.36, 36.50, 35.30, 34.91, 33.89, 32.76, 32.40, 26.38, 23.66, 23.62, 21.34, 18.40, 13.95, 13.56 ppm; HRMS (ESI) *m/z*: $[M + H]^+$ calcd for $C_{37}H_{48}F_3N_6O_9S$, 809.3150; found 809.3157.

References

1. World Health Organization (WHO). Hepatitis C, Fact Sheet (Updated October 2017): http://www.who.int/mediacentre/factsheets/fs164/en/. (Accessed January 24, 2018).
2. Lauer, G. M.; Walker, B. D. Hepatitis C virus infection. *N. Engl. J. Med.* **2001,** 345, 41–52.
3. Hoofnagle, J. H. Course and outcome of hepatitis C. *Hepatology* **2002,** 36, S21-9.
4. Sharma, S. D. Hepatitis C virus: molecular biology & current therapeutic options. *Indian J. Med. Res.* **2010,** 131, 17–34.
5. Heffernan, A.; Barber, E.; Cook, N. A.; Gomaa, A. I.; Harley, Y. X.; Jones, C. R.; Lim, A. G.; Mohamed, Z.; Nayagam, S.; Ndow, G. In *Aiming at the Global Elimination of Viral Hepatitis: Challenges Along the Care Continuum*, Open Forum Infectious Diseases, 2017; Oxford University Press US: 2017; p ofx252.
6. Gower, E.; Estes, C.; Blach, S.; Razavi-Shearer, K.; Razavi, H. Global epidemiology and genotype distribution of the hepatitis C virus infection. *J. Hepatol.* **2014,** 61, S45–S57.
7. Messina, J. P.; Humphreys, I.; Flaxman, A.; Brown, A.; Cooke, G. S.; Pybus, O. G.; Barnes, E. Global distribution and prevalence of hepatitis C virus genotypes. *Hepatology* **2015,** 61, 77–87.
8. Smith, D. B.; Bukh, J.; Kuiken, C.; Muerhoff, A. S.; Rice, C. M.; Stapleton, J. T.; Simmonds, P. Expanded classification of hepatitis C virus into 7 genotypes and 67 subtypes: updated criteria and genotype assignment web resource. *Hepatology* **2014,** 59, 318–327.
9. Simmonds, P. Genetic diversity and evolution of hepatitis C virus–15 years on. *Journal of General Virology* **2004,** 85, 3173-3188.
10. Mondelli, M. U.; Silini, E. Clinical significance of hepatitis C virus genotypes. *J. Hepatol.* **1999,** 31 Suppl 1, 65–70.
11. Lin, C. HCV NS3-4A serine protease. *Hepatitis C viruses: Genomes and molecular biology* **2006,** 52, 55.
12. Shi, S. T.; Lai, M. M. HCV 5′ and 3′ UTR: when translation meets replication. *Hepatitis C Viruses: Genomes and Molecular Biology* **2006**, 49-87.
13. Friebe, P.; Lohmann, V.; Krieger, N.; Bartenschlager, R. Sequences in the 5′ nontranslated region of hepatitis C virus required for RNA replication. *J. Virol.* **2001,** 75, 12047–12057.
14. Moradpour, D.; Penin, F.; Rice, C. M. Replication of hepatitis C virus. *Nat. Rev. Microbiol.* **2007,** 5, 453–463.
15. Santolini, E.; Migliaccio, G.; La Monica, N. Biosynthesis and biochemical properties of the hepatitis C virus core protein. *J. Virol.* **1994,** 68, 3631–3641.
16. Atoom, A. M.; Taylor, N. G.; Russell, R. S. The elusive function of the hepatitis C virus p7 protein. *Virology* **2014,** 462, 377-387.

17. Scarselli, E.; Ansuini, H.; Cerino, R.; Roccasecca, R. M.; Acali, S.; Filocamo, G.; Traboni, C.; Nicosia, A.; Cortese, R.; Vitelli, A. The human scavenger receptor class B type I is a novel candidate receptor for the hepatitis C virus. *The EMBO journal* **2002,** 21, 5017-5025.
18. Evans, M. J.; von Hahn, T.; Tscherne, D. M.; Syder, A. J.; Panis, M.; Wölk, B.; Hatziioannou, T.; McKeating, J. A.; Bieniasz, P. D.; Rice, C. M. Claudin-1 is a hepatitis C virus co-receptor required for a late step in entry. *Nature* **2007,** 446, 801.
19. Blanchard, E.; Belouzard, S.; Goueslain, L.; Wakita, T.; Dubuisson, J.; Wychowski, C.; Rouille, Y. Hepatitis C virus entry depends on clathrin-mediated endocytosis. *J. Virol.* **2006,** 80, 6964–6972.
20. Major, M. E.; Feinstone, S. M. The molecular virology of hepatitis C. *Hepatology* **1997,** 25, 1527-38.
21. Shi, S.; Lai, M. HCV 5′ and 3′ UTR: when translation meets replication 2006. *Hepatitis C Viruses: Genomes and Molecular Biology.* **2006**, 1–46.
22. Guidelines for the screening, care and treatment of persons with chronic hepatitis C infection. Updated version, April 2016. http://www.who.int/hepatitis/publications/hepatitis-c-guidelines-2016/en/ (Accessed November 28, 2017).
23. Asselah, T.; Boyer, N.; Saadoun, D.; Martinot-Peignoux, M.; Marcellin, P. Direct-acting antivirals for the treatment of hepatitis C virus infection: optimizing current IFN-free treatment and future perspectives. *Liver Int.* **2016,** 36, 47–57.
24. Fensterl, V.; Sen, G. C. Interferons and viral infections. *Biofactors* **2009,** 35, 14–20.
25. Murray, P. R.; Rosenthal, K. S.; Pfaller, M. A. *Medical microbiology*. Elsevier Health Sciences: 2015.
26. Ghany, M. G.; Strader, D. B.; Thomas, D. L.; Seeff, L. B. Diagnosis, management, and treatment of hepatitis C: An update. *Hepatology* **2009,** 49, 1335–1374.
27. Fried, M. W. Side effects of therapy of hepatitis C and their management. *Hepatology* **2002,** 36, S237–S244.
28. Butt, A. A.; McGinnis, K. A.; Skanderson, M.; Justice, A. C. Hepatitis C treatment completion rates in routine clinical care. *Liver Int.* **2009,** 30, 240–250.
29. Grillot, A.-L.; Farmer, L. J.; Rao, B. G.; Taylor, W. P.; Weisberg, I. S.; Jacobson, I. M.; Perni, R. B.; Kwong, A. D. Discovery and Development of Telaprevir. In *Antiviral Drugs*, John Wiley & Sons, Inc.: 2011; pp 207–224.
30. Lin, C.; Kwong, A. D.; Perni, R. B. Discovery and development of VX-950, a novel, covalent, and reversible inhibitor of hepatitis C virus NS3.4A serine protease. *Infect Disord Drug Targets* **2006,** 6, 3–16.
31. Poordad, F.; McCone, J.; Bacon, B. R.; Bruno, S.; Manns, M. P.; Sulkowski, M. S.; Jacobson, I. M.; Reddy, K. R.; Goodman, Z. D.; Boparai, N.; DiNubile, M. J.; Sniukiene, V.; Brass, C. A.; Albrecht, J. K.; Bronowicki, J.-P. Boceprevir for untreated chronic HCV genotype 1 infection. *N. Engl. J. Med.* **2011,** 364, 1195–1206.

32. Sherman, K. E.; Flamm, S. L.; Afdhal, N. H.; Nelson, D. R.; Sulkowski, M. S.; Everson, G. T.; Fried, M. W.; Adler, M.; Reesink, H. W.; Martin, M. Response-guided telaprevir combination treatment for hepatitis C virus infection. *N. Engl. J. Med.* **2011,** 365, 1014–1024.
33. Zeuzem, S.; Andreone, P.; Pol, S.; Lawitz, E.; Diago, M.; Roberts, S.; Focaccia, R.; Younossi, Z.; Foster, G. R.; Horban, A.; Ferenci, P.; Nevens, F.; MÃ¼llhaupt, B.; Pockros, P.; Terg, R.; Shouval, D.; van Hoek, B.; Weiland, O.; Van Heeswijk, R.; De Meyer, S.; Luo, D.; Boogaerts, G.; Polo, R.; Picchio, G.; Beumont, M. Telaprevir for retreatment of HCV infection. *N. Engl. J. Med.* **2011,** 364, 2417–2428.
34. Jacobson, I. M.; McHutchison, J. G.; Dusheiko, G.; Di Bisceglie, A. M.; Reddy, K. R.; Bzowej, N. H.; Marcellin, P.; Muir, A. J.; Ferenci, P.; Flisiak, R. Telaprevir for previously untreated chronic hepatitis C virus infection. *N. Engl. J. Med.* **2011,** 364, 2405–2416.
35. Vierling, J. M.; Davis, M.; Flamm, S.; Gordon, S. C.; Lawitz, E.; Yoshida, E. M.; Galati, J.; Luketic, V.; McCone, J.; Jacobson, I. Boceprevir for chronic HCV genotype 1 infection in patients with prior treatment failure to peginterferon/ribavirin, including prior null response. *J. Hepatol.* **2014,** 60, 748–756.
36. Bacon, B. R.; Gordon, S. C.; Lawitz, E.; Marcellin, P.; Vierling, J. M.; Zeuzem, S.; Poordad, F.; Goodman, Z. D.; Sings, H. L.; Boparai, N.; Burroughs, M.; Brass, C. A.; Albrecht, J. K.; Esteban, R. Boceprevir for previously treated chronic HCV genotype 1 infection. *N. Engl. J. Med.* **2011,** 364, 1207–1217.
37. Kwo, P. Y.; Lawitz, E. J.; McCone, J.; Schiff, E. R.; Vierling, J. M.; Pound, D.; Davis, M. N.; Galati, J. S.; Gordon, S. C.; Ravendhran, N.; Rossaro, L.; Anderson, F. H.; Jacobson, I. M.; Rubin, R.; Koury, K.; Pedicone, L. D.; Brass, C. A.; Chaudhri, E.; Albrecht, J. K. Efficacy of boceprevir, an NS3 protease inhibitor, in combination with peginterferon alfa-2b and ribavirin in treatment-naive patients with genotype 1 hepatitis C infection (SPRINT-1): an open-label, randomised, multicentre phase 2 trial. *Lancet* **2010,** 376, 705–716.
38. Kelleher, T. B.; Afdhal, N. H. Management of the side effects of peg-interferon and ribavirin used for treatment of chronic hepatitis C virus infection. (February 02, 2017.).
39. Afdhal, N.; Reddy, K. R.; Nelson, D. R.; Lawitz, E.; Gordon, S. C.; Schiff, E.; Nahass, R.; Ghalib, R.; Gitlin, N.; Herring, R.; Lalezari, J.; Younes, Z. H.; Pockros, P. J.; Di Bisceglie, A. M.; Arora, S.; Subramanian, G. M.; Zhu, Y.; Dvory-Sobol, H.; Yang, J. C.; Pang, P. S.; Symonds, W. T.; McHutchison, J. G.; Muir, A. J.; Sulkowski, M.; Kwo, P. Ledipasvir and sofosbuvir for previously treated HCV genotype 1 infection. *N. Engl. J. Med.* **2014,** 370, 1483–1493.
40. Ferenci, P.; Bernstein, D.; Lalezari, J.; Cohen, D.; Luo, Y.; Cooper, C.; Tam, E.; Marinho, R. T.; Tsai, N.; Nyberg, A.; Box, T. D.; Younes, Z.; Enayati, P.; Green, S.; Baruch, Y.; Bhandari, B. R.; Caruntu, F. A.; Sepe, T.; Chulanov, V.; Janczewska, E.; Rizzardini, G.; Gervain, J.; Planas, R.; Moreno, C.; Hassanein, T.; Xie, W.; King, M.; Podsadecki, T.; Reddy, K. R. ABT-450/r–ombitasvir and

dasabuvir with or without ribavirin for HCV. *N. Engl. J. Med.* **2014,** 370, 1983–1992.
41. Lawitz, E.; Gane, E.; Pearlman, B.; Tam, E.; Ghesquiere, W.; Guyader, D.; Alric, L.; Bronowicki, J.-P.; Lester, L.; Sievert, W.; Ghalib, R.; Balart, L.; Sund, F.; Lagging, M.; Dutko, F.; Shaughnessy, M.; Hwang, P.; Howe, A. Y. M.; Wahl, J.; Robertson, M.; Barr, E.; Haber, B. Efficacy and safety of 12 weeks versus 18 weeks of treatment with grazoprevir (MK-5172) and elbasvir (MK-8742) with or without ribavirin for hepatitis C virus genotype 1 infection in previously untreated patients with cirrhosis and patients with previous null response with or without cirrhosis (C-WORTHY): a randomised, open-label phase 2 trial. *Lancet* **2014,** 385, 1075–1086
42. Everson, G. T.; Towner, W. J.; Davis, M. N.; Wyles, D. L.; Nahass, R. G.; Thuluvath, P. J.; Etzkorn, K.; Hinestrosa, F.; Tong, M.; Rabinovitz, M.; McNally, J.; Brainard, D. M.; Han, L.; Doehle, B.; McHutchison, J. G.; Morgan, T.; Chung, R. T.; Tran, T. T. Sofosbuvir with velpatasvir in treatment-naive noncirrhotic patients with genotype 1 to 6 hepatitis C virus infection: a randomized trial. *Ann. Intern. Med.* **2015,** 163, 818–826.
43. Bourliere, M.; Gordon, S. C.; Flamm, S. L.; Cooper, C. L.; Ramji, A.; Tong, M.; Ravendhran, N.; Vierling, J. M.; Tran, T. T.; Pianko, S.; Bansal, M. B.; de Ledinghen, V.; Hyland, R. H.; Stamm, L. M.; Dvory-Sobol, H.; Svarovskaia, E.; Zhang, J.; Huang, K. C.; Subramanian, G. M.; Brainard, D. M.; McHutchison, J. G.; Verna, E. C.; Buggisch, P.; Landis, C. S.; Younes, Z. H.; Curry, M. P.; Strasser, S. I.; Schiff, E. R.; Reddy, K. R.; Manns, M. P.; Kowdley, K. V.; Zeuzem, S.; Polaris; Investigators, P.-. Sofosbuvir, Velpatasvir, and Voxilaprevir for Previously Treated HCV Infection. *N. Engl. J. Med.* **2017,** 376, 2134–2146.
44. Gane, E.; Poordad, F.; Wang, S.; Asatryan, A.; Kwo, P. Y.; Lalezari, J.; Wyles, D. L.; Hassanein, T.; Aguilar, H.; Maliakkal, B.; Liu, R.; Lin, C. W.; Ng, T. I.; Kort, J.; Mensa, F. J. High Efficacy of ABT-493 and ABT-530 Treatment in Patients With HCV Genotype 1 or 3 Infection and Compensated Cirrhosis. *Gastroenterology* **2016,** 151, 651–659.
45. Lawitz, E. J.; O'Riordan, W. D.; Asatryan, A.; Freilich, B. L.; Box, T. D.; Overcash, J. S.; Lovell, S.; Ng, T. I.; Liu, W.; Campbell, A.; Lin, C. W.; Yao, B.; Kort, J. Potent antiviral activities of the direct-acting antivirals ABT-493 and ABT-530 with three-day monotherapy for hepatitis C virus genotype 1 infection. *Antimicrob. Agents Chemother.* **2015,** 60, 1546–1555.
46. Bhatia, H. K.; Singh, H.; Grewal, N.; Natt, N. K. Sofosbuvir: a novel treatment option for chronic hepatitis C infection. *J. Pharmacol. Pharmacother.* **2014,** 5, 278.
47. Tomei, L.; Altamura, S.; Bartholomew, L.; Biroccio, A.; Ceccacci, A.; Pacini, L.; Narjes, F.; Gennari, N.; Bisbocci, M.; Incitti, I. Mechanism of action and antiviral activity of benzimidazole-based allosteric inhibitors of the hepatitis C virus RNA-dependent RNA polymerase. *J. Virol.* **2003,** 77, 13225–13231.
48. Tomei, L.; Altamura, S.; Bartholomew, L.; Bisbocci, M.; Bailey, C.; Bosserman, M.; Cellucci, A.; Forte, E.; Incitti, I.; Orsatti, L. Characterization of the

inhibition of hepatitis C virus RNA replication by nonnucleosides. *J. Virol.* **2004,** 78, 938–946.
49. Guedj, J.; Dahari, H.; Rong, L.; Sansone, N. D.; Nettles, R. E.; Cotler, S. J.; Layden, T. J.; Uprichard, S. L.; Perelson, A. S. Modeling shows that the NS5A inhibitor daclatasvir has two modes of action and yields a shorter estimate of the hepatitis C virus half-life. *Proc. Natl. Acad. Sci. U. S. A.* **2013,** 110, 3991–3996.
50. Zeuzem, S. Treatment Options in Hepatitis C: The Current State of the Art. *Dtsch. Arztebl. Int.* **2017,** 114, 11–21.
51. Ng, T. I.; Tripathi, R.; Reisch, T.; Lu, L.; Middleton, T.; Hopkins, T. A.; Pithawalla, R.; Irvin, M.; Dekhtyar, T.; Krishnan, P.; Schnell, G.; Beyer, J.; McDaniel, K. F.; Ma, J.; Wang, G.; Jiang, L. J.; Or, Y. S.; Kempf, D.; Pilot-Matias, T.; Collins, C. In Vitro Antiviral Activity and Resistance Profile of the Next-Generation Hepatitis C Virus NS3/4A Protease Inhibitor Glecaprevir. *Antimicrob. Agents Chemother.* **2017**.
52. Kwo, P. Y.; Poordad, F.; Asatryan, A.; Wang, S.; Wyles, D. L.; Hassanein, T.; Felizarta, F.; Sulkowski, M. S.; Gane, E.; Maliakkal, B.; Overcash, J. S.; Gordon, S. C.; Muir, A. J.; Aguilar, H.; Agarwal, K.; Dore, G. J.; Lin, C. W.; Liu, R.; Lovell, S. S.; Ng, T. I.; Kort, J.; Mensa, F. J. Glecaprevir and pibrentasvir yield high response rates in patients with HCV genotype 1-6 without cirrhosis. *J. Hepatol.* **2017,** 67, 263–271.
53. Yao, N.; Reichert, P.; Taremi, S. S.; Prosise, W. W.; Weber, P. C. Molecular views of viral polyprotein processing revealed by the crystal structure of the hepatitis C virus bifunctional protease-helicase. *Structure* **1999,** 7, 1353–1363.
54. Landro, J. A.; Raybuck, S. A.; Luong, Y. P. C.; O'Malley, E. T.; Harbeson, S. L.; Morgenstern, K. A.; Rao, G.; Livingston, D. J. Mechanistic role of an NS4A peptide cofactor with the truncated NS3 protease of hepatitis C virus: elucidation of the NS4A stimulatory effect via kinetic analysis and inhibitor mapping. *Biochemistry* **1997,** 36, 9340–9348.
55. Li, K.; Foy, E.; Ferreon, J. C.; Nakamura, M.; Ferreon, A. C.; Ikeda, M.; Ray, S. C.; Gale, M., Jr.; Lemon, S. M. Immune evasion by hepatitis C virus NS3/4A protease-mediated cleavage of the Toll-like receptor 3 adaptor protein TRIF. *Proc. Natl. Acad. Sci. U. S. A.* **2005,** 102, 2992–2997.
56. Foy, E.; Li, K.; Sumpter, R., Jr.; Loo, Y. M.; Johnson, C. L.; Wang, C.; Fish, P. M.; Yoneyama, M.; Fujita, T.; Lemon, S. M.; Gale, M., Jr. Control of antiviral defenses through hepatitis C virus disruption of retinoic acid-inducible gene-I signaling. *Proc. Natl. Acad. Sci. U. S. A.* **2005,** 102, 2986–2991.
57. Aydin, C.; Mukherjee, S.; Hanson, A. M.; Frick, D. N.; Schiffer, C. A. The interdomain interface in bifunctional enzyme protein 3/4A (NS3/4A) regulates protease and helicase activities. *Protein Sci.* **2013,** 22, 1786–1798.
58. Lam, A. M.; Keeney, D.; Eckert, P. Q.; Frick, D. N. Hepatitis C virus NS3 ATPases/helicases from different genotypes exhibit variations in enzymatic properties. *J. Virol.* **2003,** 77, 3950–3961.

59. Frick, D. N.; Rypma, R. S.; Lam, A. M.; Gu, B. The nonstructural protein 3 protease/helicase requires an intact protease domain to unwind duplex RNA efficiently. *J. Biol. Chem.* **2004,** 279, 1269–1280.
60. Love, R. A.; Parge, H. E.; Wickersham, J. A.; Hostomsky, Z.; Habuka, N.; Moomaw, E. W.; Adachi, T.; Hostomska, Z. The crystal structure of hepatitis C virus NS3 proteinase reveals a trypsin-like fold and a structural zinc binding site. *Cell* **1996,** 87, 331–342.
61. Kim, J. L.; Morgenstern, K. A.; Lin, C.; Fox, T.; Dwyer, M. D.; Landro, J. A.; Chambers, S. P.; Markland, W.; Lepre, C. A.; O'Malley, E. T.; Harbeson, S. L.; Rice, C. M.; Murcko, M. A.; Caron, P. R.; Thomson, J. A. Crystal structure of the hepatitis C virus NS3 protease domain complexed with a synthetic NS4A cofactor peptide. *Cell* **1996,** 87, 343–355.
62. Barbato, G.; Cicero, D.; Nardi, M. The solution structure of the N-terminal proteinase domain of the hepatitis C virus (HCV) NS3 protein provides new insights into its activation and catalytic mechanism. *J. Mol. Biol.* **1999,** 289, 371–384.
63. Llinas-Brunet, M.; Bailey, M.; Fazal, G.; Goulet, S.; Halmos, T.; Laplante, S.; Maurice, R.; Poirier, M.; Poupart, M. A.; Thibeault, D.; Wernic, D.; Lamarre, D. Peptide-based inhibitors of the hepatitis C virus serine protease. *Bioorg. Med. Chem. Lett.* **1998,** 8, 1713-1718.
64. Steinkuhler, C.; Biasiol, G.; Brunetti, M.; Urbani, A.; Koch, U.; Cortese, R.; Pessi, A.; De Francesco, R. Product inhibition of the hepatitis C virus NS3 protease. *Biochemistry* **1998,** 37, 8899–8905.
65. Ingallinella, P.; Altamura, S.; Bianchi, E.; Taliani, M.; Ingenito, R.; Cortese, R.; De Francesco, R.; Steinkuhler, C.; Pessi, A. Potent peptide inhibitors of human hepatitis C virus NS3 protease are obtained by optimizing the cleavage products. *Biochemistry* **1998,** 37, 8906-14.
66. Ingallinella, P.; Bianchi, E.; Ingenito, R.; Koch, U.; Steinkuhler, C.; Altamura, S.; Pessi, A. Optimization of the P'-Region of Peptide Inhibitors of Hepatitis C Virus NS3/4A Protease. *Biochemistry* **2000,** 39, 12898-12906.
67. Llinas-Brunet, M.; Bailey, M.; Fazal, G.; Ghiro, E.; Gorys, V.; Goulet, S.; Halmos, T.; Maurice, R.; Poirier, M.; Poupart, M.-A. Highly potent and selective peptide-based inhibitors of the hepatitis C virus serine protease: towards smaller inhibitors. *Bioorganic Med. Chem. Lett.* **2000,** 10, 2267–2270.
68. Llinas-Brunet, M.; Bailey, M. D.; Bolger, G.; Brochu, C.; Faucher, A.-M.; Ferland, J. M.; Garneau, M.; Ghiro, E.; Gorys, V.; Grand-Maître, C.; Halmos, T.; Lapeyre-Paquette, N.; Liard, F.; Poirier, M.; Rhéaume, M.; Tsantrizos, Y. S.; Lamarre, D. Structure–activity study on a novel series of macrocyclic inhibitors of the hepatitis C virus NS3 protease leading to the discovery of BILN 2061. *J. Med. Chem.* **2004,** 47, 1605–1608.
69. Lamarre, D.; Anderson, P. C.; Bailey, M.; Beaulieu, P.; Bolger, G.; Bonneau, P.; Bos, M.; Cameron, D. R.; Cartier, M.; Cordingley, M. G.; Faucher, A. M.; Goudreau, N.; Kawai, S. H.; Kukolj, G.; Lagace, L.; LaPlante, S. R.; Narjes, H.; Poupart, M. A.; Rancourt, J.; Sentjens, R. E.; St George, R.;

Simoneau, B.; Steinmann, G.; Thibeault, D.; Tsantrizos, Y. S.; Weldon, S. M.; Yong, C. L.; Llinas-Brunet, M. An NS3 protease inhibitor with antiviral effects in humans infected with hepatitis C virus. *Nature* **2003,** 426, 186–189.

70. Arasappan, A.; Njoroge, F. G.; Chen, K. X.; Venkatraman, S.; Parekh, T. N.; Gu, H.; Pichardo, J.; Butkiewicz, N.; Prongay, A.; Madison, V.; Girijavallabhan, V. P2-P4 macrocyclic inhibitors of hepatitis C virus NS3-4A serine protease. *Bioorg. Med. Chem. Lett.* **2006,** 16, 3960–3965.

71. Bogen, S.; Arasappan, A.; Pan, W.; Ruan, S.; Padilla, A.; Saksena, A. K.; Girijavallabhan, V.; Njoroge, F. G. Hepatitis C virus NS3-4A serine protease inhibitors: SAR of new P1 derivatives of SCH 503034. *Bioorganic Med. Chem. Lett.* **2008,** 18, 4219–4223.

72. Arasappan, A.; Njoroge, F. G.; Chan, T. Y.; Bennett, F.; Bogen, S. L.; Chen, K.; Gu, H.; Hong, L.; Jao, E.; Liu, Y. T.; Lovey, R. G.; Parekh, T.; Pike, R. E.; Pinto, P.; Santhanam, B.; Venkatraman, S.; Vaccaro, H.; Wang, H.; Yang, X.; Zhu, Z.; McKittrick, B.; Saksena, A. K.; Girijavallabhan, V.; Pichardo, J.; Butkiewicz, N.; Ingram, R.; Malcolm, B.; Prongay, A.; Yao, N.; Marten, B.; Madison, V.; Kemp, S.; Levy, O.; Lim-Wilby, M.; Tamura, S.; Ganguly, A. K. Hepatitis C virus NS3-4A serine protease inhibitors: SAR of P'2 moiety with improved potency. *Bioorg. Med. Chem. Lett.* **2005,** 15, 4180–4184.

73. Malancona, S.; Colarusso, S.; Ontoria, J. M.; Marchetti, A.; Poma, M.; Stansfield, I.; Laufer, R.; Di Marco, A.; Taliani, M.; Verdirame, M.; Gonzalez-Paz, O.; Matassa, V. G.; Narjes, F. SAR and pharmacokinetic studies on phenethylamide inhibitors of the hepatitis C virus NS3/NS4A serine protease. *Bioorganic Med. Chem. Lett.* **2004,** 14, 4575–4579.

74. Nilsson, M.; Belfrage, A. K.; Lindstrom, S.; Wahling, H.; Lindquist, C.; Ayesa, S.; Kahnberg, P.; Pelcman, M.; Benkestock, K.; Agback, T.; Vrang, L.; Terelius, Y.; Wikstrom, K.; Hamelink, E.; Rydergard, C.; Edlund, M.; Eneroth, A.; Raboisson, P.; Lin, T. I.; de Kock, H.; Wigerinck, P.; Simmen, K.; Samuelsson, B.; Rosenquist, S. Synthesis and SAR of potent inhibitors of the hepatitis C virus NS3/4A protease: exploration of P2 quinazoline substituents. *Bioorganic Med. Chem. Lett.* **2010,** 20, 4004–4011.

75. Venkatraman, S.; Velazquez, F.; Wu, W.; Blackman, M.; Chen, K. X.; Bogen, S.; Nair, L.; Tong, X.; Chase, R.; Hart, A.; Agrawal, S.; Pichardo, J.; Prongay, A.; Cheng, K. C.; Girijavallabhan, V.; Piwinski, J.; Shih, N. Y.; Njoroge, F. G. Discovery and structure-activity relationship of P1-P3 ketoamide derived macrocyclic inhibitors of hepatitis C virus NS3 protease. *J. Med. Chem.* **2009,** 52, 336–346.

76. Raboisson, P.; de Kock, H.; Rosenquist, A.; Nilsson, M.; Salvador-Oden, L.; Lin, T. I.; Roue, N.; Ivanov, V.; Wahling, H.; Wickstrom, K.; Hamelink, E.; Edlund, M.; Vrang, L.; Vendeville, S.; Van de Vreken, W.; McGowan, D.; Tahri, A.; Hu, L.; Boutton, C.; Lenz, O.; Delouvroy, F.; Pille, G.; Surleraux, D.; Wigerinck, P.; Samuelsson, B.; Simmen, K. Structure-activity relationship study on a novel series of cyclopentane-containing macrocyclic inhibitors of the

hepatitis C virus NS3/4A protease leading to the discovery of TMC435350. *Bioorganic Med. Chem. Lett.* **2008,** 18, 4853–4858.
77. Perni, R. B.; Pitlik, J.; Britt, S. D.; Court, J. J.; Courtney, L. F.; Deininger, D. D.; Farmer, L. J.; Gates, C. A.; Harbeson, S. L.; Levin, R. B.; Lin, C.; Lin, K.; Moon, Y. C.; Luong, Y. P.; O'Malley, E. T.; Rao, B. G.; Thomson, J. A.; Tung, R. D.; Van Drie, J. H.; Wei, Y. Inhibitors of hepatitis C virus NS3.4A protease 2. Warhead SAR and optimization. *Bioorganic Med. Chem. Lett.* **2004,** 14, 1441–1446.
78. Susser, S.; Welsch, C.; Wang, Y.; Zettler, M.; Domingues, F. S.; Karey, U.; Hughes, E.; Ralston, R.; Tong, X.; Herrmann, E.; Zeuzem, S.; Sarrazin, C. Characterization of resistance to the protease inhibitor boceprevir in hepatitis C virus-infected patients. *Hepatology* **2009,** 50, 1709–1718.
79. Susser, S.; Forestier, N.; Welker, M. W.; Vermehren, J.; Karey, U.; Zeuzem, S.; Sarrazin, C. Detection of resistant variants in the hepatitis C virus NS3 protease gene by clonal sequencing at long-term follow-up in patients treated with boceprevir. *J. Hepatol.* **2009,** 50, S7.
80. LaPlante, S. R.; Nar, H.; Lemke, C. T.; Jakalian, A.; Aubry, N.; Kawai, S. H. Ligand bioactive conformation plays a critical role in the design of drugs that target the hepatitis C virus NS3 protease. *J. Med. Chem.* **2013,** 57, 1777–1789.
81. Scola, P. M.; Sun, L.-Q.; Wang, A. X.; Chen, J.; Sin, N.; Venables, B. L.; Sit, S.-Y.; Chen, Y.; Cocuzza, A.; Bilder, D. M.; D'Andrea, S. V.; Zheng, B.; Hewawasam, P.; Tu, Y.; Friborg, J.; Falk, P.; Hernandez, D.; Levine, S.; Chen, C.; Yu, F.; Sheaffer, A. K.; Zhai, G.; Barry, D.; Knipe, J. O.; Han, Y.-H.; Schartman, R.; Donoso, M.; Mosure, K.; Sinz, M. W.; Zvyaga, T.; Good, A. C.; Rajamani, R.; Kish, K.; Tredup, J.; Klei, H. E.; Gao, Q.; Mueller, L.; Colonno, R. J.; Grasela, D. M.; Adams, S. P.; Loy, J.; Levesque, P. C.; Sun, H.; Shi, H.; Sun, L.; Warner, W.; Li, D.; Zhu, J.; Meanwell, N. A.; McPhee, F. The discovery of asunaprevir (BMS-650032), an orally efficacious NS3 protease inhibitor for the treatment of hepatitis C virus infection. *J. Med. Chem.* **2014,** 57, 1730–1752.
82. Agarwal, A.; Zhang, B.; Olek, E.; Robison, H.; Robarge, L.; Deshpande, M. Rapid and sharp decline in HCV upon monotherapy with NS3 protease inhibitor, ACH-1625. *Antivir. Ther.* **2012,** 17, 1533–1539.
83. Lemke, C. T.; Goudreau, N.; Zhao, S.; Hucke, O.; Thibeault, D.; Llinàs-Brunet, M.; White, P. W. Combined X-ray, NMR, and kinetic analyses reveal uncommon binding characteristics of the hepatitis C virus NS3-NS4A protease inhibitor BI 201335. *J. Biol. Chem.* **2011,** 286, 11434–11443.
84. Japan approves first all-oral, interferon- and ribavirin-free hepatitis C treatment, daklinza® (daclatasvir) and sunvepra® (asunaprevir) dual regimen. (February 02, 2017.).
85. Rosenquist, Å.; Samuelsson, B.; Johansson, P.-O.; Cummings, M. D.; Lenz, O.; Raboisson, P.; Simmen, K.; Vendeville, S.; de Kock, H.; Nilsson, M.; Horvath, A.; Kalmeijer, R.; de la Rosa, G.; Beumont-Mauviel, M. Discovery and development of simeprevir (TMC435), a HCV NS3/4A protease inhibitor. *J. Med. Chem.* **2014,** 57, 1673–1693.

86. Jiang, Y.; Andrews, S. W.; Condroski, K. R.; Buckman, B.; Serebryany, V.; Wenglowsky, S.; Kennedy, A. L.; Madduru, M. R.; Wang, B.; Lyon, M.; Doherty, G. A.; Woodard, B. T.; Lemieux, C.; Do, M. G.; Zhang, H.; Ballard, J.; Vigers, G.; Brandhuber, B. J.; Stengel, P.; Josey, J. A.; Beigelman, L.; Blatt, L.; Seiwert, S. D. Discovery of Danoprevir (ITMN-191/R7227), a Highly Selective and Potent Inhibitor of Hepatitis C Virus (HCV) NS3/4A Protease. *J. Med. Chem.* **2013,** 57, 1753–1769.
87. OLYSIO™ (simeprevir) receives FDA approval for combination treatment of chronic hepatitis C. (February 02, 2017).
88. McCauley, J. A.; McIntyre, C. J.; Rudd, M. T.; Nguyen, K. T.; Romano, J. J.; Butcher, J. W.; Gilbert, K. F.; Bush, K. J.; Holloway, M. K.; Swestock, J.; Wan, B. L.; Carroll, S. S.; DiMuzio, J. M.; Graham, D. J.; Ludmerer, S. W.; Mao, S. S.; Stahlhut, M. W.; Fandozzi, C. M.; Trainor, N.; Olsen, D. B.; Vacca, J. P.; Liverton, N. J. Discovery of vaniprevir (MK-7009), a macrocyclic hepatitis C virus NS3/4a protease inhibitor. *J. Med. Chem.* **2010,** 53, 2443–2463.
89. Romano, K. P.; Ali, A.; Aydin, C.; Soumana, D.; Özen, A.; Deveau, L. M.; Silver, C.; Cao, H.; Newton, A.; Petropoulos, C. J.; Huang, W.; Schiffer, C. A. The molecular basis of drug resistance against hepatitis C virus NS3/4A protease inhibitors. *PLoS Pathog.* **2012,** 8, e1002832.
90. Romano, K. P.; Ali, A.; Royer, W. E.; Schiffer, C. A. Drug resistance against HCV NS3/4A inhibitors is defined by the balance of substrate recognition versus inhibitor binding. *Proc. Natl. Acad. Sci. U. S. A.* **2010,** 107, 20986–20991.
91. Pilot-Matias, T.; Tripathi, R.; Cohen, D.; Gaultier, I.; Dekhtyar, T.; Lu, L.; Reisch, T.; Irvin, M.; Hopkins, T.; Pithawalla, R.; Middleton, T.; Ng, T.; McDaniel, K.; Or, Y. S.; Menon, R.; Kempf, D.; Molla, A.; Collins, C. In vitro and in vivo antiviral activity and resistance profile of the hepatitis C virus NS3/4A protease inhibitor ABT-450. *Antimicrob. Agents Chemother.* **2015,** 59, 988–997.
92. Lontok, E.; Harrington, P.; Howe, A.; Kieffer, T.; Lennerstrand, J.; Lenz, O.; McPhee, F.; Mo, H.; Parkin, N.; Pilot-Matias, T.; Miller, V. Hepatitis C virus drug resistance-associated substitutions: state of the art summary. *Hepatology* **2015,** 62, 1623–1632.
93. Kumada, H.; Chayama, K.; Rodrigues, L.; Suzuki, F.; Ikeda, K.; Toyoda, H.; Sato, K.; Karino, Y.; Matsuzaki, Y.; Kioka, K. Randomized phase 3 trial of ombitasvir/paritaprevir/ritonavir for hepatitis C virus genotype 1b–infected Japanese patients with or without cirrhosis. *Hepatology* **2015,** 62, 1037–1046.
94. Krishnan, P.; Schnell, G.; Tripathi, R.; Beyer, J.; Reisch, T.; Zhang, X.; Setze, C.; Rodrigues, L., Jr.; Burroughs, M.; Redman, R.; Chayama, K.; Kumada, H.; Collins, C.; Pilot-Matias, T. Analysis of Hepatitis C Virus Genotype 1b Resistance Variants in Japanese Patients Treated with Paritaprevir-Ritonavir and Ombitasvir. *Antimicrob. Agents Chemother.* **2016,** 60, 1106–13.
95. Carroll, S.; McCauley, J.; Ludmerer, S.; Harper, S.; Summa, V.; Rowley, M.; Rudd, M.; Coleman, P.; Liverton, N.; Butcher, J.; McIntyre, C.; Romano, J.; Bush, K.; Ferrara, M.; Crescenzi, B.; Petrocchi, A.; Difilippo, M.; Burlein, C.; Dimuzio, J.; Graham, D.; McHale, C.; Stahlhut, M.; Gates, A.; Fandozzi, C.;

Trainor, N.; Hazuda, D.; Vacca, J.; Olsen, D. MK-5172: A novel HCV NS3/4A protease inhibitor with potent activity against known resistance mutants. *J. Hepatol.* **2010,** 52, S17.
96. Summa, V.; Ludmerer, S. W.; McCauley, J. A.; Fandozzi, C.; Burlein, C.; Claudio, G.; Coleman, P. J.; DiMuzio, J. M.; Ferrara, M.; Di Filippo, M.; Gates, A. T.; Graham, D. J.; Harper, S.; Hazuda, D. J.; McHale, C.; Monteagudo, E.; Pucci, V.; Rowley, M.; Rudd, M. T.; Soriano, A.; Stahlhut, M. W.; Vacca, J. P.; Olsen, D. B.; Liverton, N. J.; Carroll, S. S. MK-5172, a selective inhibitor of hepatitis C virus NS3/4a protease with broad activity across genotypes and resistant variants. *Antimicrob. Agents Chemother.* **2012,** 56, 4161–4167.
97. Guo, Z.; Black, S.; Hu, Y.; McMonagle, P.; Ingravallo, P.; Chase, R.; Curry, S.; Asante-Appiah, E. Unraveling the structural basis of grazoprevir potency against clinically relevant substitutions in hepatitis C virus NS3/4A protease from genotype 1a. *J. Biol. Chem.* **2017,** 292, 6202–6212.
98. Gane, E.; Ben Ari, Z.; Mollison, L.; Zuckerman, E.; Bruck, R.; Baruch, Y.; Howe, A. Y.; Wahl, J.; Bhanja, S.; Hwang, P.; Zhao, Y.; Robertson, M. N. Efficacy and safety of grazoprevir + ribavirin for 12 or 24 weeks in treatment-naive patients with hepatitis C virus genotype 1 infection. *J. Viral Hepat.* **2016,** 23, 789–797.
99. U.S. food and drug administration approves gilead's vosevi™ (sofosbuvir/velpatasvir/voxilaprevir) for re-treatment of adults with chronic hepatitis C virus. (February 02, 2017).
100. AbbVie receives U.S. FDA approval of MAVYRET™ (glecaprevir/pibrentasvir) for the treatment of chronic hepatitis C in all major genotypes (GT 1-6) in as short as 8 weeks. (February 02, 2017).
101. Romano, K. P.; Laine, J. M.; Deveau, L. M.; Cao, H.; Massi, F.; Schiffer, C. A. Molecular mechanisms of viral and host cell substrate recognition by hepatitis C virus NS3/4A protease. *J. Virol.* **2011,** 85, 6106–6116.
102. Prabu-Jeyabalan, M.; Nalivaika, E.; Schiffer, C. A. Substrate shape determines specificity of recognition for HIV-1 protease: analysis of crystal structures of six substrate complexes. *Structure* **2002,** 10, 369–381.
103. Sesmero, E.; Thorpe, I. F. Using the hepatitis C virus RNA-dependent RNA polymerase as a model to understand viral polymerase structure, function and dynamics. *Viruses* **2015,** 7, 3974–3994.
104. Lawitz, E.; Gaultier, I.; Poordad, F.; Cohen, D. E.; Menon, R.; Larsen, L. M.; Podsadecki, T. J.; Bernstein, B. Initial antiviral activity of the HCV NS3 protease inhibitor ABT-450 when given with low dose ritonavir as 3-day monotherapy: preliminary results of study M11-602 in genotype-1 (GT1) HCV-infected treatment-naive subjects. *Hepatology* **2010,** 52, 1202A.
105. Lawitz, E.; Yang, J. C.; Stamm, L. M.; Taylor, J. G.; Cheng, G.; Brainard, D. M.; Miller, M. D.; Mo, H.; Dvory-Sobol, H. Characterization of HCV resistance from a 3-day monotherapy study of voxilaprevir, a novel pangenotypic NS3/4A protease inhibitor. *Antivir. Ther.* **2017**.

106. Ali, A.; Aydin, C.; Gildemeister, R.; Romano, K. P.; Cao, H.; Özen, A.; Soumana, D.; Newton, A.; Petropoulos, C. J.; Huang, W.; Schiffer, C. A. Evaluating the role of macrocycles in the susceptibility of hepatitis C virus NS3/4A protease inhibitors to drug resistance. *ACS Chem. Biol.* **2013,** 8, 1469–1478.
107. Pawlotsky, J. M. Hepatitis C virus resistance to direct-acting antiviral drugs in interferon-free regimens. *Gastroenterology* **2016,** 151, 70–86.
108. Soumana, D. I.; Kurt Yilmaz, N.; Ali, A.; Prachanronarong, K. L.; Schiffer, C. A. Molecular and dynamic mechanism underlying drug resistance in genotype 3 hepatitis C NS3/4A protease. *J. Am. Chem. Soc.* **2016,** 138, 11850–11859.
109. O'Meara, J. A.; Lemke, C. T.; Godbout, C.; Kukolj, G.; Lagacé, L.; Moreau, B.; Thibeault, D.; White, P. W.; Llinàs-Brunet, M. Molecular mechanism by which a potent hepatitis C virus NS3-NS4A protease inhibitor overcomes emergence of resistance. *J. Biol. Chem.* **2013,** 288, 5673–5681.
110. Trozzi, C.; Bartholomew, L.; Ceccacci, A.; Biasiol, G.; Pacini, L.; Altamura, S.; Narjes, F.; Muraglia, E.; Paonessa, G.; Koch, U. In vitro selection and characterization of hepatitis C virus serine protease variants resistant to an active-site peptide inhibitor. *J. Virol.* **2003,** 77, 3669–3679.
111. Soumana, D. I.; Kurt Yilmaz, N.; Prachanronarong, K. L.; Aydin, C.; Ali, A.; Schiffer, C. A. Structural and thermodynamic effects of macrocyclization in HCV NS3/4A inhibitor MK-5172. *ACS Chem. Biol.* **2016,** 11, 900–909.
112. Zeuzem, S.; Jacobson, I. M.; Baykal, T.; Marinho, R. T.; Poordad, F.; Bourliere, M.; Sulkowski, M. S.; Wedemeyer, H.; Tam, E.; Desmond, P.; Jensen, D. M.; Di Bisceglie, A. M.; Varunok, P.; Hassanein, T.; Xiong, J.; Pilot-Matias, T.; DaSilva-Tillmann, B.; Larsen, L.; Podsadecki, T.; Bernstein, B. Retreatment of HCV with ABT-450/r-ombitasvir and dasabuvir with ribavirin. *N. Engl. J. Med.* **2014,** 370, 1604–1614.
113. Ghany, M. G.; Nelson, D. R.; Strader, D. B.; Thomas, D. L.; Seeff, L. B. An update on treatment of genotype 1 chronic hepatitis C virus infection: 2011 practice guideline by the American Association for the Study of Liver Diseases. *Hepatology* **2011,** 54, 1433–1444.
114. Fried, M. W.; Shiffman, M. L.; Reddy, K. R.; Smith, C.; Marinos, G.; Goncales, F. L., Jr.; Haussinger, D.; Diago, M.; Carosi, G.; Dhumeaux, D.; Craxi, A.; Lin, A.; Hoffman, J.; Yu, J. Peginterferon alfa-2a plus ribavirin for chronic hepatitis C virus infection. *N. Engl. J. Med.* **2002,** 347, 975–982.
115. Falade-Nwulia, O.; Suarez-Cuervo, C.; Nelson, D. R.; Fried, M. W.; Segal, J. B.; Sulkowski, M. S. Oral Direct-Acting Agent Therapy for Hepatitis C Virus Infection: A Systematic Review. *Ann. Intern. Med.* **2017,** 166, 637–648.
116. Sarrazin, C.; Zeuzem, S. Resistance to direct antiviral agents in patients with hepatitis C virus infection. *Gastroenterology* **2010,** 138, 447–462.
117. Rong, L.; Dahari, H.; Ribeiro, R. M.; Perelson, A. S. Rapid emergence of protease inhibitor resistance in hepatitis C virus. *Sci. Transl. Med.* **2010,** 2, 30ra32.

118. Poordad, F.; Felizarta, F.; Asatryan, A.; Sulkowski, M. S.; Reindollar, R. W.; Landis, C. S.; Gordon, S. C.; Flamm, S. L.; Fried, M. W.; Bernstein, D. E.; Lin, C. W.; Liu, R.; Lovell, S. S.; Ng, T. I.; Kort, J.; Mensa, F. J. Glecaprevir and pibrentasvir for 12 weeks for hepatitis C virus genotype 1 infection and prior direct-acting antiviral treatment. *Hepatology* **2017,** 66, 389-397.
119. Sulkowski, M.; Hezode, C.; Gerstoft, J.; Vierling, J. M.; Mallolas, J.; Pol, S.; Kugelmas, M.; Murillo, A.; Weis, N.; Nahass, R.; Shibolet, O.; Serfaty, L.; Bourliere, M.; DeJesus, E.; Zuckerman, E.; Dutko, F.; Shaughnessy, M.; Hwang, P.; Howe, A. Y.; Wahl, J.; Robertson, M.; Barr, E.; Haber, B. Efficacy and safety of 8 weeks versus 12 weeks of treatment with grazoprevir (MK-5172) and elbasvir (MK-8742) with or without ribavirin in patients with hepatitis C virus genotype 1 mono-infection and HIV/hepatitis C virus co-infection (C-WORTHY): a randomised, open-label phase 2 trial. *Lancet* **2015,** 385, 1087–1097.
120. Harper, S.; McCauley, J. A.; Rudd, M. T.; Ferrara, M.; DiFilippo, M.; Crescenzi, B.; Koch, U.; Petrocchi, A.; Holloway, M. K.; Butcher, J. W.; Romano, J. J.; Bush, K. J.; Gilbert, K. F.; McIntyre, C. J.; Nguyen, K. T.; Nizi, E.; Carroll, S. S.; Ludmerer, S. W.; Burlein, C.; DiMuzio, J. M.; Graham, D. J.; McHale, C. M.; Stahlhut, M. W.; Olsen, D. B.; Monteagudo, E.; Cianetti, S.; Giuliano, C.; Pucci, V.; Trainor, N.; Fandozzi, C. M.; Rowley, M.; Coleman, P. J.; Vacca, J. P.; Summa, V.; Liverton, N. J. Discovery of MK-5172, a macrocyclic hepatitis C virus NS3/4a protease inhibitor. *ACS Med. Chem. Lett.* **2012,** 3, 332–336.
121. Rodriguez-Torres, M.; Glass, S.; Hill, J.; Freilich, B.; Hassman, D.; Di Bisceglie, A. M.; Taylor, J. G.; Kirby, B. J.; Dvory-Sobol, H.; Yang, J. C.; An, D.; Stamm, L. M.; Brainard, D. M.; Kim, S.; Krefetz, D.; Smith, W.; Marbury, T.; Lawitz, E. GS-9857 in patients with chronic hepatitis C virus genotype 1-4 infection: a randomized, double-blind, dose-ranging phase 1 study. *J. Viral. Hepat.* **2016,** 23, 614–622.
122. Chan, K.; Yu, M.; Peng, B.; Corsa, A.; Worth, A.; Gong, R.; Xu, S.; Chen, X.; Appleby, T. C.; Taylor, J.; Delaney, W. E.; Cheng, G. In vitro efficacy and resistance profiling of protease inhibitors against a novel HCV genotype 3a replicon. In *International Workshop on HIV & Hepatitis Virus Drug Resistance and Curative Strategies*, Toronto, ON, Canada, 2013.
123. Soumana, D. I.; Ali, A.; Schiffer, C. A. Structural analysis of asunaprevir resistance in HCV NS3/4A protease. *ACS Chem. Biol.* **2014,** 9, 2485–2490.
124. Matthew, A. N.; Zephyr, J.; Hill, C. J.; Jahangir, M.; Newton, A.; Petropoulos, C. J.; Huang, W.; Kurt-Yilmaz, N.; Schiffer, C. A.; Ali, A. Hepatitis C Virus NS3/4A Protease Inhibitors Incorporating Flexible P2 Quinoxalines Target Drug Resistant Viral Variants. *J. Med. Chem.* **2017,** 60, 5699–5716.
125. Horovitz, A. Double-mutant cycles: a powerful tool for analyzing protein structure and function. *Fold Des.* **1996,** 1, R121–126.
126. Yilmaz, N. K.; Swanstrom, R.; Schiffer, C. A. Improving viral protease inhibitors to counter drug resistance. *Trends in microbiology* **2016,** 24, 547-557.
127. Ragland, D. A.; Nalivaika, E. A.; Nalam, M. N. L.; Prachanronarong, K. L.; Cao, H.; Bandaranayake, R. M.; Cai, Y.; Kurt-Yilmaz, N.; Schiffer, C. A. Drug

Resistance Conferred by Mutations Outside the Active Site through Alterations in the Dynamic and Structural Ensemble of HIV-1 Protease. *J. Am. Chem. Soc.* **2014,** 136, 11956–11963.
128. Wittekind, M.; Weinheirner, S.; Zhang, Y.; Goldfarb, V. Modified forms of hepatitis C NS3 protease for facilitating inhibitor screening and structural studies of protease-inhibitor complexes. US Patent 6333186, August 8, 2002.
129. Liu, Y.; Kati, W.; Chen, C. M.; Tripathi, R.; Molla, A.; Kohlbrenner, W. Use of a fluorescence plate reader for measuring kinetic parameters with inner filter effect correction. *Anal. Biochem.* **1999,** 267, 331–335.
130. Sarkar, G.; Sommer, S. S. The "megaprimer" method of site-directed mutagenesis. *Biotechniques* **1990,** 8, 404–407.
131. Otwinowski, Z.; Minor, W. Processing of X-ray diffraction data collected in oscillation mode. *Methods Enzymol.* **1997,** 276, 307–326.
132. McCoy, A. J.; Grosse-Kunstleve, R. W.; Adams, P. D.; Winn, M. D.; Storoni, L. C.; Read, R. J. Phaser crystallographic software. *J. Appl. Crystallogr.* **2007,** 40, 658–674.
133. Emsley, P.; Cowtan, K. Coot: model-building tools for molecular graphics. *Acta Crystallogr. D Biol. Crystallogr.* **2004,** 60, 2126–2132.
134. Adams, P. D.; Afonine, P. V.; Bunkoczi, G.; Chen, V. B.; Davis, I. W.; Echols, N.; Headd, J. J.; Hung, L.-W.; Kapral, G. J.; Grosse-Kunstleve, R. W.; McCoy, A. J.; Moriarty, N. W.; Oeffner, R.; Read, R. J.; Richardson, D. C.; Richardson, J. S.; Terwilliger, T. C.; Zwart, P. H. PHENIX: a comprehensive Python-based system for macromolecular structure solution. *Acta Crystallogr. D Biol. Crystallogr.* **2010,** 66, 213–221.
135. Davis, I. W.; Leaver-Fay, A.; Chen, V. B.; Block, J. N.; Kapral, G. J.; Wang, X.; Murray, L. W.; Arendall, W. B.; Snoeyink, J.; Richardson, J. S.; Richardson, D. C. MolProbity: all-atom contacts and structure validation for proteins and nucleic acids. *Nucl. Acids Res.* **2007,** 35, W375–W383.
136. Brunger, A. T. Free R value: a novel statistical quantity for assessing the accuracy of crystal structures. *Nature* **1992,** 355, 472–475.
137. *PyMOL: The PyMOL Molecular Graphics System, Version 1.8, Schrödinger, LLC.*
138. *Schrödinger Release 2017-4: Prime, Schrödinger, LLC, New York, NY, 2017.*
139. Sastry, G. M.; Adzhigirey, M.; Day, T.; Annabhimoju, R.; Sherman, W. Protein and ligand preparation: parameters, protocols, and influence on virtual screening enrichments. *J Comput Aided Mol Des* **2013,** 27, 221-34.
140. Jacobson, M. P.; Friesner, R. A.; Xiang, Z.; Honig, B. On the role of the crystal environment in determining protein side-chain conformations. *J Mol Biol* **2002,** 320, 597-608.
141. Olsson, M. H.; Søndergaard, C. R.; Rostkowski, M.; Jensen, J. H. PROPKA3: consistent treatment of internal and surface residues in empirical p K a predictions. *Journal of chemical theory and computation* **2011,** 7, 525-537.

142. Søndergaard, C. R.; Olsson, M. H.; Rostkowski, M.; Jensen, J. H. Improved treatment of ligands and coupling effects in empirical calculation and rationalization of p K a values. *Journal of Chemical Theory and Computation* **2011,** 7, 2284-2295.
143. Banks, J. L.; Beard, H. S.; Cao, Y.; Cho, A. E.; Damm, W.; Farid, R.; Felts, A. K.; Halgren, T. A.; Mainz, D. T.; Maple, J. R. Integrated modeling program, applied chemical theory (IMPACT). *Journal of computational chemistry* **2005,** 26, 1752-1780.
144. Bowers, K. J.; Chow, E.; Xu, H.; Dror, R. O.; Eastwood, M. P.; Gregerson, B. A.; Klepeis, J. L.; Kolossvary, I.; Moraes, M. A.; Sacerdoti, F. D.; Salmon, J. K.; Shan, Y.; Shaw, D. E. In *Scalable Algorithms for Molecular Dynamics Simulations on Commodity Clusters*, Proceedings of the ACM/IEEE Conference on Supercomputing (SC06), Tampa, Florida, United States, November 11, 2017, Tampa, Florida, United States.
145. Harder, E.; Damm, W.; Maple, J.; Wu, C.; Reboul, M.; Xiang, J. Y.; Wang, L.; Lupyan, D.; Dahlgren, M. K.; Knight, J. L. OPLS3: a force field providing broad coverage of drug-like small molecules and proteins. *Journal of chemical theory and computation* **2015,** 12, 281-296.
146. Jorgensen, W. L.; Chandrasekhar, J.; Madura, J. D.; Impey, R. W.; Klein, M. L. Comparison of simple potential functions for simulating liquid water. *The Journal of chemical physics* **1983,** 79, 926-935.
147. Essmann, U.; Perera, L.; Berkowitz, M. L.; Darden, T.; Lee, H.; Pedersen, L. G. A Smooth Particle Mesh Ewald Method. *Journal of Chemical Physics* **1995,** 103, 8577-8593.
148. Tuckerman, M.; Berne, B. J.; Martyna, G. J. Reversible multiple time scale molecular dynamics. *The Journal of chemical physics* **1992,** 97, 1990-2001.
149. Lange, O. F.; Grubmuller, H. Generalized correlation for biomolecular dynamics. *Proteins* **2006,** 62, 1053–1061.
150. Hajarizadeh, B.; Grebely, J.; Dore, G. J. Epidemiology and natural history of HCV infection. *Nat. Rev. Gastroenterol. Hepatol.* **2013,** 10, 553–562.
151. Razavi, H.; Waked, I.; Sarrazin, C.; Myers, R. P.; Idilman, R.; Calinas, F.; Vogel, W.; Mendes Correa, M. C.; Hezode, C.; Lazaro, P.; Akarca, U.; Aleman, S.; Balik, I.; Berg, T.; Bihl, F.; Bilodeau, M.; Blasco, A. J.; Brandao Mello, C. E.; Bruggmann, P.; Buti, M.; Calleja, J. L.; Cheinquer, H.; Christensen, P. B.; Clausen, M.; Coelho, H. S.; Cramp, M. E.; Dore, G. J.; Doss, W.; Duberg, A. S.; El-Sayed, M. H.; Ergor, G.; Esmat, G.; Falconer, K.; Felix, J.; Ferraz, M. L.; Ferreira, P. R.; Frankova, S.; Garcia-Samaniego, J.; Gerstoft, J.; Giria, J. A.; Goncales, F. L., Jr.; Gower, E.; Gschwantler, M.; Guimaraes Pessoa, M.; Hindman, S. J.; Hofer, H.; Husa, P.; Kaberg, M.; Kaita, K. D.; Kautz, A.; Kaymakoglu, S.; Krajden, M.; Krarup, H.; Laleman, W.; Lavanchy, D.; Marinho, R. T.; Marotta, P.; Mauss, S.; Moreno, C.; Murphy, K.; Negro, F.; Nemecek, V.; Ormeci, N.; Ovrehus, A. L.; Parkes, J.; Pasini, K.; Peltekian, K. M.; Ramji, A.; Reis, N.; Roberts, S. K.; Rosenberg, W. M.; Roudot-Thoraval, F.; Ryder, S. D.; Sarmento-Castro, R.; Semela, D.; Sherman, M.; Shiha, G. E.; Sievert, W.; Sperl,

J.; Starkel, P.; Stauber, R. E.; Thompson, A. J.; Urbanek, P.; Van Damme, P.; van Thiel, I.; Van Vlierberghe, H.; Vandijck, D.; Wedemeyer, H.; Weis, N.; Wiegand, J.; Yosry, A.; Zekry, A.; Cornberg, M.; Mullhaupt, B.; Estes, C. The present and future disease burden of hepatitis C virus (HCV) infection with today's treatment paradigm. *J. Viral. Hepat.* **2014,** 21 Suppl 1, 34–59.

152. Afdhal, N.; Zeuzem, S.; Kwo, P.; Chojkier, M.; Gitlin, N.; Puoti, M.; Romero-Gomez, M.; Zarski, J.-P.; Agarwal, K.; Buggisch, P.; Foster, G. R.; Bräu, N.; Buti, M.; Jacobson, I. M.; Subramanian, G. M.; Ding, X.; Mo, H.; Yang, J. C.; Pang, P. S.; Symonds, W. T.; McHutchison, J. G.; Muir, A. J.; Mangia, A.; Marcellin, P. Ledipasvir and sofosbuvir for untreated HCV genotype 1 infection. *N. Engl. J. Med.* **2014,** 370, 1889–1898.

153. Meanwell, N. A. 2015 Philip S. Portoghese Medicinal Chemistry Lectureship. Curing hepatitis C virus infection with direct-acting antiviral agents: the arc of a medicinal chemistry triumph. *J. Med. Chem.* **2016,** 59, 7311–7351.

154. McCauley, J. A.; Rudd, M. T. Hepatitis C virus NS3/4a protease inhibitors. *Curr. Opin. Pharmacol.* **2016,** 30, 84–92.

155. Kwong, A. D.; Kauffman, R. S.; Hurter, P.; Mueller, P. Discovery and development of telaprevir: an NS3-4A protease inhibitor for treating genotype 1 chronic hepatitis C virus. *Nat. Biotech.* **2011,** 29, 993–1003.

156. Venkatraman, S.; Bogen, S. L.; Arasappan, A.; Bennett, F.; Chen, K.; Jao, E.; Liu, Y.-T.; Lovey, R.; Hendrata, S.; Huang, Y.; Pan, W.; Parekh, T.; Pinto, P.; Popov, V.; Pike, R.; Ruan, S.; Santhanam, B.; Vibulbhan, B.; Wu, W.; Yang, W.; Kong, J.; Liang, X.; Wong, J.; Liu, R.; Butkiewicz, N.; Chase, R.; Hart, A.; Agrawal, S.; Ingravallo, P.; Pichardo, J.; Kong, R.; Baroudy, B.; Malcolm, B.; Guo, Z.; Prongay, A.; Madison, V.; Broske, L.; Cui, X.; Cheng, K.-C.; Hsieh, Y.; Brisson, J.-M.; Prelusky, D.; Korfmacher, W.; White, R.; Bogdanowich-Knipp, S.; Pavlovsky, A.; Bradley, P.; Saksena, A. K.; Ganguly, A.; Piwinski, J.; Girijavallabhan, V.; Njoroge, F. G. Discovery of (1R,5S)-N-[3-amino-1-(cyclobutylmethyl)-2,3-dioxopropyl]- 3-[2(S)-[[[(1,1-dimethylethyl)amino]carbonyl]amino]-3,3-dimethyl-1-oxobutyl]- 6,6-dimethyl-3-azabicyclo[3.1.0]hexan-2(S)-carboxamide (SCH 503034), a selective, potent, orally bioavailable hepatitis C virus NS3 protease inhibitor: a potential therapeutic agent for the treatment of hepatitis C infection. *J. Med. Chem.* **2006,** 49, 6074–6086.

157. Tsantrizos, Y. S.; Bolger, G.; Bonneau, P.; Cameron, D. R.; Goudreau, N.; Kukolj, G.; LaPlante, S. R.; Llinas-Brunet, M.; Nar, H.; Lamarre, D. Macrocyclic inhibitors of the NS3 protease as potential therapeutic agents of hepatitis C virus infection. *Angew. Chem. Int. Ed. Engl.* **2003,** 42, 1356–1360.

158. Kieffer, T. L.; George, S. Resistance to hepatitis C virus protease inhibitors. *Curr. Opin. Virol.* **2014,** 8, 16–21.

159. King, N. M.; Prabu-Jeyabalan, M.; Nalivaika, E. A.; Schiffer, C. A. Combating susceptibility to drug resistance: lessons from HIV-1 protease. *Chem. Biol.* **2004,** 11, 1333–1338.

160. Özen, A.; Sherman, W.; Schiffer, C. A. Improving the resistance profile of hepatitis C NS3/4A inhibitors: dynamic substrate envelope guided design. *J. Chem. Theory Comput.* **2013,** 9, 5693–5705.
161. Kurt Yilmaz, N.; Swanstrom, R.; Schiffer, C. A. Improving viral protease inhibitors to counter drug resistance. *Trends Microbiol.* **2016,** 24, 547–557.
162. Wang, X. A.; Sun, L.-Q.; Sit, S.-Y.; Sin, N.; Scola, P. M.; Hewawasam, P.; Good, A., C.; Chen, Y.; Campbell, A. Hepatitis C Virus Inhibitors. US Patent 6995174, 2006.
163. Rudd, M. T.; Butcher, J. W.; Nguyen, K. T.; McIntyre, C. J.; Romano, J. J.; Gilbert, K. F.; Bush, K. J.; Liverton, N. J.; Holloway, M. K.; Harper, S.; Ferrara, M.; DiFilippo, M.; Summa, V.; Swestock, J.; Fritzen, J.; Carroll, S. S.; Burlein, C.; DiMuzio, J. M.; Gates, A.; Graham, D. J.; Huang, Q.; McClain, S.; McHale, C.; Stahlhut, M. W.; Black, S.; Chase, R.; Soriano, A.; Fandozzi, C. M.; Taylor, A.; Trainor, N.; Olsen, D. B.; Coleman, P. J.; Ludmerer, S. W.; McCauley, J. A. P2-quinazolinones and bis-macrocycles as new templates for next-generation hepatitis C virus NS3/4a protease inhibitors: discovery of MK-2748 and MK-6325. *ChemMedChem* **2015,** 10, 727–735.
164. Vendeville, S.; Nilsson, M.; de Kock, H.; Lin, T. I.; Antonov, D.; Classon, B.; Ayesa, S.; Ivanov, V.; Johansson, P. O.; Kahnberg, P.; Eneroth, A.; Wikstrom, K.; Vrang, L.; Edlund, M.; Lindstrom, S.; Van de Vreken, W.; McGowan, D.; Tahri, A.; Hu, L.; Lenz, O.; Delouvroy, F.; Van Dooren, M.; Kindermans, N.; Surleraux, D.; Wigerinck, P.; Rosenquist, A.; Samuelsson, B.; Simmen, K.; Raboisson, P. Discovery of novel, potent and bioavailable proline-urea based macrocyclic HCV NS3/4A protease inhibitors. *Bioorg. Med. Chem. Lett.* **2008,** 18, 6189–6193.
165. Moreau, B.; O'Meara, J. A.; Bordeleau, J.; Garneau, M.; Godbout, C.; Gorys, V.; Leblanc, M.; Villemure, E.; White, P. W.; Llinàs-Brunet, M. Discovery of hepatitis C virus NS3-4A protease inhibitors with improved barrier to resistance and favorable liver distribution. *J. Med. Chem.* **2014,** 57, 1770–1776.
166. Gillis, E. P.; Bowsher, M. S.; McPhee, F.; Jenkins, S.; Wang, Y.-K.; Scola, P. M.; Meanwell, N. A. In *In Abstract of Papers, 2nd Generation HCV protease inhibitors: Part 2, optimization of P2**, 250th ACS National Meeting & Exposition, Boston, MA, United States, August 16–20, 2015, Boston, MA, United States, pp pp MEDI-240.
167. Meanwell, N. A. Synopsis of some recent tactical application of bioisosteres in drug design. *J. Med. Chem.* **2011,** 54, 2529–2591.
168. Or, Y. S.; Moore, J. D.; Liu, D.; Sun, Y.; Gai, Y.; Tang, D.; Niu, D.; Xu, G.; Wang, Z. Quinoxalinyl Macrocyclic Hepatitis C Virus Serine Protease Inhibitors. PCT Int. Appl. WO 2008/002924, January 03, 2008.
169. Sun, L.-Q.; Mull, E.; Gillis, E. P.; Bowsher, M. S.; Zhao, Q.; Renduchintala, V. K.; Sarkunam, K.; Nagalakshmi, P.; Babu, P. V. K. S.; Scola, P. M. Hepatitis C Virus Inhibitors. PCT Int. Appl. WO 2014/062196, April 24, 2014.
170. Schrödinger. Schrödinger Release 2017-1; Schrödinger, LLC, New York, NY, United States: 2017.

171. Dultz, G.; Graubard, B. I.; Martin, P.; Welker, M.-W.; Vermehren, J.; Zeuzem, S.; McGlynn, K. A.; Welzel, T. M. Liver transplantation for chronic hepatitis C virus infection in the United States 2002–2014: An analysis of the UNOS/OPTN registry. *PloS One* **2017,** 12, 1–18.
172. Martell, M.; Esteban, J. I.; Quer, J.; Genesca, J.; Weiner, A.; Esteban, R.; Guardia, J.; Gomez, J. Hepatitis C virus (HCV) circulates as a population of different but closely related genomes: quasispecies nature of HCV genome distribution. *J. Virol.* **1992,** 66, 3225–3229.
173. Paolucci, S.; Baldanti, F.; Campanini, G.; Zavattoni, M.; Cattaneo, E.; Dossena, L.; Gerna, G. Analysis of HIV drug-resistant quasispecies in plasma, peripheral blood mononuclear cells and viral isolates from treatment-naive and HAART patients. *J. Med. Virol.* **2001,** 65, 207–217.
174. Bartenschlager, R.; Ahlborn-Laake, L.; Mous, J.; Jacobsen, H. Kinetic and structural analyses of hepatitis C virus polyprotein processing. *J. Virol.* **1994,** 68, 5045–5055.
175. Nalam, M. N.; Ali, A.; Altman, M. D.; Reddy, G. S.; Chellappan, S.; Kairys, V.; Ozen, A.; Cao, H.; Gilson, M. K.; Tidor, B.; Rana, T. M.; Schiffer, C. A. Evaluating the substrate-envelope hypothesis: structural analysis of novel HIV-1 protease inhibitors designed to be robust against drug resistance. *J. Virol.* **2010,** 84, 5368–5378.
176. Bogen, S. L.; Arasappan, A.; Velazquez, F.; Blackman, M.; Huelgas, R.; Pan, W.; Siegel, E.; Nair, L. G.; Venkatraman, S.; Guo, Z. Discovery of potent sulfonamide P4-capped ketoamide second generation inhibitors of hepatitis C virus NS3 serine protease with favorable pharmacokinetic profiles in preclinical species. *Bioorganic Med. Chem.* **2010,** 18, 1854–1865.
177. Bogen, S. L.; Pan, W.; Ruan, S.; Nair, L. G.; Arasappan, A.; Bennett, F.; Chen, K. X.; Jao, E.; Venkatraman, S.; Vibulbhan, B. Toward the back-up of boceprevir (SCH 503034): discovery of new extended P4-capped ketoamide inhibitors of hepatitis C virus NS3 serine protease with improved potency and pharmacokinetic profiles. *J. Med. Chem.* **2009,** 52, 3679–3688.
178. Pennington, L. D.; Moustakas, D. T. The necessary nitrogen atom: A versatile high-impact design element for multiparameter optimization. *J. Med. Chem.* **2017,** 60, 3552–3579.
179. Shen, Y.; Altman, M. D.; Ali, A.; Nalam, M. N. L.; Cao, H.; Rana, T. M.; Schiffer, C. A.; Tidor, B. Testing the substrate-envelope hypothesis with designed pairs of compounds. *ACS Chem. Biol.* **2013,** 8, 2433–2441.
180. Chellappan, S.; Kiran Kumar Reddy, G. S.; Ali, A.; Nalam, M. N.; Anjum, S. G.; Cao, H.; Kairys, V.; Fernandes, M. X.; Altman, M. D.; Tidor, B.; Rana, T. M.; Schiffer, C. A.; Gilson, M. K. Design of mutation-resistant HIV protease inhibitors with the substrate envelope hypothesis. *Chem. Biol. Drug Des.* **2007,** 69, 298–313.
181. Altman, M. D.; Ali, A.; Reddy, G. S.; Nalam, M. N.; Anjum, S. G.; Cao, H.; Chellappan, S.; Kairys, V.; Fernandes, M. X.; Gilson, M. K.; Schiffer, C. A.; Rana, T. M.; Tidor, B. HIV-1 protease inhibitors from inverse design in the substrate

envelope exhibit subnanomolar binding to drug-resistant variants. *J. Am. Chem. Soc.* **2008,** 130, 6099–6113.
182. Reddy, G. S.; Ali, A.; Nalam, M. N.; Anjum, S. G.; Cao, H.; Nathans, R. S.; Schiffer, C. A.; Rana, T. M. Design and synthesis of HIV-1 protease inhibitors incorporating oxazolidinones as P2/P2' ligands in pseudosymmetric dipeptide isosteres. *J. Med. Chem.* **2007,** 50, 4316–4328.
183. Nalam, M. N.; Ali, A.; Reddy, G. S.; Cao, H.; Anjum, S. G.; Altman, M. D.; Yilmaz, N. K.; Tidor, B.; Rana, T. M.; Schiffer, C. A. Substrate envelope-designed potent HIV-1 protease inhibitors to avoid drug resistance. *Chem. Biol.* **2013,** 20, 1116–1124.
184. Ali, A.; Reddy, G. S. K. K.; Nalam, M. N. L.; Anjum, S. G.; Cao, H.; Schiffer, C. A.; Rana, T. M. Structure-based design, synthesis, and structure–activity relationship studies of HIV-1 protease inhibitors incorporating phenyloxazolidinones. *J. Med. Chem.* **2010,** 53, 7699–7708.
185. Cheng, Y. Single-particle cryo-EM at crystallographic resolution. *Cell* **2015,** 161, 450–457.
186. Khoshouei, M.; Radjainia, M.; Baumeister, W.; Danev, R. Cryo-EM structure of haemoglobin at 3.2 Å determined with the Volta phase plate. *Nat. Commun.* **2017,** 8, 16099.
187. Merk, A.; Bartesaghi, A.; Banerjee, S.; Falconieri, V.; Rao, P.; Davis, M. I.; Pragani, R.; Boxer, M. B.; Earl, L. A.; Milne, J. L. Breaking cryo-EM resolution barriers to facilitate drug discovery. *Cell* **2016,** 165, 1698–1707.
188. Danev, R.; Tegunov, D.; Baumeister, W. Using the Volta phase plate with defocus for cryo-EM single particle analysis. *Elife* **2017,** 6.
189. Glaeser, R. M. How good can cryo-EM become? *Nat. Methods* **2015,** 13, 28.
190. Wu, S.; Avila-Sakar, A.; Kim, J.; Booth, D. S.; Greenberg, C. H.; Rossi, A.; Liao, M.; Li, X.; Alian, A.; Griner, S. L. Fabs enable single particle cryoEM studies of small proteins. *Structure* **2012,** 20, 582–592.
191. Borgnia, M. J.; Banerjee, S.; Merk, A.; Matthies, D.; Bartesaghi, A.; Rao, P.; Pierson, J.; Earl, L. A.; Falconieri, V.; Subramaniam, S. Using cryo-EM to map small ligands on dynamic metabolic enzymes: studies with glutamate dehydrogenase. *Mol. Pharmacol* **2016,** 89, 645–651.
192. Beran, R. K.; Pyle, A. M. Hepatitis C viral NS3-4A protease activity is enhanced by the NS3 helicase. *J. Biol. Chem.* **2008,** 283, 29929–29937.
193. Bae, A.; Sun, S.-C.; Qi, X.; Chen, X.; Ku, K.; Worth, A.; Wong, K. A.; Harris, J.; Miller, M. D.; Mo, H. Susceptibility of treatment-naive hepatitis C Virus (HCV) clinical isolates to HCV protease inhibitors. *Antimicrob. Agents Chemother.* **2010,** 54, 5288–5297.
194. Saalau-Bethell, S. M.; Woodhead, A. J.; Chessari, G.; Carr, M. G.; Coyle, J.; Graham, B.; Hiscock, S. D.; Murray, C. W.; Pathuri, P.; Rich, S. J.; Richardson, C. J.; Williams, P. A.; Jhoti, H. Discovery of an allosteric mechanism for the regulation of HCV NS3 protein function. *Nat. Chem. Biol.* **2012,** 8, 920–925.

195. Ndjomou, J.; Corby, M. J.; Sweeney, N. L.; Hanson, A. M.; Aydin, C.; Ali, A.; Schiffer, C. A.; Li, K.; Frankowski, K. J.; Schoenen, F. J. Simultaneously targeting the NS3 protease and helicase activities for more effective hepatitis C virus therapy. *ACS Chem. Biol.* **2015,** 10, 1887–1896.
196. World Health Organization (WHO). Dengue and Severe Dengue, Fact Sheet No 117 (March 2014): http://www.who.int/mediacentre/factsheets/fs117/en/. Accessed January 2015. (January 2015).
197. World Health Organization (WHO). West Nile Virus, Fact Sheet No 354 (July 2011): http://www.who.int/mediacentre/factsheets/fs354/en/. Accessed November 2014.
198. World Health Organization (WHO). Yellow Fever, Fact Sheet No 100 (March 2014): http://www.who.int/mediacentre/factsheets/fs100/en/. Accessed November 2014.
199. Yin, Z.; Patel, S. J.; Wang, W.-L.; Chan, W.-L.; Ranga Rao, K. R.; Wang, G.; Ngew, X.; Patel, V.; Beer, D.; Knox, J. E.; Ma, N. L.; Ehrhardt, C.; Lim, S. P.; Vasudevan, S. G.; Keller, T. H. Peptide inhibitors of dengue virus NS3 protease. Part 2: SAR study of tetrapeptide aldehyde inhibitors. *Bioorg. Med. Chem. Lett.* **2006,** 16, 40–43.
200. Yildiz, M.; Ghosh, S.; Bell, J. A.; Sherman, W.; Hardy, J. A. Allosteric Inhibition of the NS2B-NS3 Protease from Dengue Virus. *ACS Chem. Biol.* **2013,** 8, 2744–2752.
201. Lee, H.; Ren, J.; Nocadello, S.; Rice, A. J.; Ojeda, I.; Light, S.; Minasov, G.; Vargas, J.; Nagarathnam, D.; Anderson, W. F. Identification of novel small molecule inhibitors against NS2B/NS3 serine protease from Zika virus. *Antiviral Res.* **2017,** 139, 49–58.
202. Loehr, K.; Knox, J. E.; Phong, W. Y.; Ma, N. L.; Yin, Z.; Sampath, A.; Patel, S. J.; Wang, W.-L.; Chan, W.-L.; Rao, K. R. Yellow fever virus NS3 protease: peptide-inhibition studies. *J. Gen. Virol.* **2007,** 88, 2223–2227.
203. Lin, K.-H.; Ali, A.; Rusere, L.; Soumana, D. I.; Yilmaz, N. K.; Schiffer, C. A. Dengue virus NS2B/NS3 protease inhibitors exploiting the prime side. *J. Virol.* **2017,** 91, e00045–17.
204. Yang, C.-C.; Hu, H.-S.; Wu, R.-H.; Wu, S.-H.; Lee, S.-J.; Jiaang, W.-T.; Chern, J.-H.; Huang, Z.-S.; Wu, H.-N.; Chang, C.-M. A novel dengue virus inhibitor, BP13944, discovered by high-throughput screening with dengue virus replicon cells selects for resistance in the viral NS2B/NS3 protease. *Antimicrob. Agents Chemother.* **2014,** 58, 110–119.